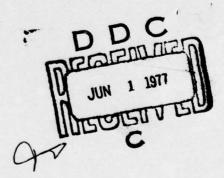RADC-TR-77-153
Final Technical Report
April 1977

WIDEBAND HOLOGRAPHIC DIGITAL RECORDING AND REPRODUCTION

Harris Corporation/ESD

Approved for public release; distribution unlimited.

Sponsored by
Defense Advanced Research Projects Agency (DoD)
ARPA Order No. 2322

The views and conclusions contained in this document are those of the
authors and should not be interpreted as necessarily representing the
official policies, either expressed or implied, of the Defense
Advanced Research Projects Agency or the U. S. Government.

**ROME AIR DEVELOPMENT CENTER
AIR FORCE SYSTEMS COMMAND
GRIFFISS AIR FORCE BASE, NEW YORK 13441**

This report has been reviewed by the RADC Information Office (OI) and is releasable to the National Technical Information Service (NTIS). At NTIS it will be releasable to the general public, including foreign nations.

This report has been reviewed and approved for publication.

APPROVED: *Albert A. Jamberdino*

ALBERT A. JAMBERDINO
Project Engineer

Do not return this copy. Retain or destroy.

MISSION
of
Rome Air Development Center

RADC plans and conducts research, exploratory and advanced development programs in command, control, and communications (C^3) activities, and in the C^3 areas of information sciences and intelligence. The principal technical mission areas are communications, electromagnetic guidance and control, surveillance of ground and aerospace objects, intelligence data collection and handling, information system technology, ionospheric propagation, solid state sciences, microwave physics and electronic reliability, maintainability and compatibility.

WIDEBAND HOLOGRAPHIC DIGITAL RECORDING AND REPRODUCTION

Andrew M. Bardos
George S. Moore
Richard H. Nelson
Lynda M. Ralston
Michael W. Shareck
Curt A. Shuman
Ron J. Straayer
Tom E. Wisnewski

D D C
JUN 1 1977

Approved for public release;
distribution unlimited.

REPORT DOCUMENTATION PAGE		READ INSTRUCTIONS BEFORE COMPLETING FORM
1. REPORT NUMBER RADC-TR-77-153	2. GOVT ACCESSION NO.	3. RECIPIENT'S CATALOG NUMBER
4. TITLE (and Subtitle) WIDEBAND HOLOGRAPHIC DIGITAL RECORDING AND REPRODUCTION		5. TYPE OF REPORT & PERIOD COVERED Final Technical Report. Jan 73 - Nov 76.
		6. PERFORMING ORG. REPORT NUMBER N/A
7. AUTHOR(s) (see reverse)		8. CONTRACT OR GRANT NUMBER(s) F30602-73-C-0155
9. PERFORMING ORGANIZATION NAME AND ADDRESS Harris Corporation/Electronic Systems Division P. O. Box 37 Melbourne FL 32901		10. PROGRAM ELEMENT, PROJECT, TASK AREA & WORK UNIT NUMBERS 63208F 23220001
11. CONTROLLING OFFICE NAME AND ADDRESS Defense Advanced Research Projects Agency 1400 Wilson Blvd Arlington VA 22209		12. REPORT DATE April 1977
		13. NUMBER OF PAGES 361
14. MONITORING AGENCY NAME & ADDRESS(if different from Controlling Office) Rome Air Development Center (IRAP) Griffiss AFB NY 13441		15. SECURITY CLASS. (of this report) UNCLASSIFIED
		15a. DECLASSIFICATION/DOWNGRADING SCHEDULE N/A

16. DISTRIBUTION STATEMENT (of this Report)

Approved for public release; distribution unlimited.

17. DISTRIBUTION STATEMENT (of the abstract entered in Block 20, if different from Report)

Same

Andrew M. Bardos, George S. Moore, Richard H. Nelson, Lynda M. Ralston Michael W. Shareck

18. SUPPLEMENTARY NOTES

RADC Project Engineer:
Albert A. Jamberdino (IRAP)

19. KEY WORDS (Continue on reverse side if necessary and identify by block number)

Recording Devices
Intelligence
Laser Recorders
Holography

20. ABSTRACT (Continue on reverse side if necessary and identify by block number)

Techniques were investigated to apply the concept of holography to the problems of wideband digital recording and reproduction. The feasibility of recording at rates up to 2 Gb/s and playback at both full-record and reduced speeds was theoretically and experimentally considered. The program was a multi-phased effort including the design, development and experimental evaluation of two Exploratory Development Models (EDMs): the Phase I EDM demonstrated recording at 400 Mb/s and playback at 40 Mb/s, and was used to guide design trade-offs for Phase II; the Phase II EDM demonstrated recording at 600 Mb/s playback

DD FORM 1 JAN 73 1473   EDITION OF 1 NOV 65 IS OBSOLETE

cont.

$$> \frac{1}{1,000,000}$$

at full-record and 0 to 1 time expanded rates with bit-error-rates ~~better~~ better than 10^{-6}. Both full-system operational testing and parametric evaluation on a component basis were performed.

This report describes design and performance data at both the system and the subsystem levels for the Phase II hardware. Also a part of this program was the development of conceptual designs for potential multi-gigabit recorders. These designs are presented, along with system and subsystem level trade-offs between the various concepts, and recommendations for subsequent development. Overall, this program has made available a new, high-speed, high-capacity information storage approach offering significant advantages over more conventional recording techniques.

Block 7.

Andrew M. Bardos, George S. Moore, Richard H. Nelson, Lynda M. Ralston, Michael W. Shareck, Curt A. Shuman, Ron J. Straayer, Tom E. Wisnewski

TABLE OF CONTENTS

TABLE OF CONTENTS (Continued)

LIST OF ILLUSTRATIONS

LIST OF ILLUSTRATIONS (Continued)

LIST OF ILLUSTRATIONS (Continued)

LIST OF ILLUSTRATIONS (Continued)

LIST OF TABLES

LIST OF TABLES (Continued)

List of Abbreviations

AO	acousto-optic
AOBD	AO beam deflector
AOD	AO device
AOM	AO modulator
AOMA	AOM array
AOPC	AO page composer
AR	anti-reflection
ATWL	acoustic travelling-wave lens
BCH	Bose-Chauduri-Hocquenghem
BER	bit-error rate
BOF	beginning of film
CCD	charge-coupled device
CW	continuous wave
DC	direct current
DCP	decentering plate
DE	diffraction efficiency
ECC	error correction coding
EDM	exploratory development model
EOF	end of film
FET	field-effect transistor
Gb/s	gigabits per second
ID	identification
LAOPC	linear AOPC
LED	light-emitting diode
LID	latent image decay
MAOPC	matrix AOPC
MAX	maximum
Mb/s	megabits per second

List of Abbreviations (Continued)

MIN	minimum
MLCD	mode-locked, cavity-dumped
NRP	non-return to peak
NRZ	non-return to zero
PC	printed circuit
PF	profile
PMT	photomultiplier tube
PLL	phase-locked loop
PN	pseudorandom noise
RCD	record
RD	read
RF	radio frequency
RLC	resistance-inductance-capacitance
RP	return to peak
RZ	return to zero
SNR	signal-to-noise ratio
STL	spinner-transform lens
WBR	wideband recorder

SECTION I

PROGRAM SUMMARY

Continuing advances in the technologies supporting wideband communications and information handling are leading to extremely high-rate digital data systems. We anticipate that operation of these systems will require wideband recording capabilities significantly exceeding the performance of current digital data handling equipment. Although much effort has gone into the development of electron-beam, laser-beam and high density magnetic-tape recorders, currently reported results show that the capabilities of these technologies fall far short of expected data rates. Even with further development, parallel operation of two or more such recorders will be required to handle digital data at rates of 300 to 1,000 Mb/s or more. For some mission requirements, parallel operation of multiple recorders may be undesirable due to problems associated with reconstituting bit-to-bit time integrity between machine outputs during playback.

Holographic recording techniques, however, can provide the capability of high-rate, high-capacity recording on single film reels with low-error-rate readout at both full-record and reduced speeds. During the program documented in this report we addressed the anticipated requirements of gigabit record rates for periods up to 20 minutes, both full-speed and 10-to-1 time expanded playback rates, and 10^{-6} bit error rates.

This report covers work accomplished under the Wideband Holographic Digital Recorder and Reproducer (Contract Number F30602-73-C-0155), for the Rome Air Development Center and the Advanced Research Projects Agency. The objectives of the program included:

1. The design, fabrication and demonstration of a wideband recorder Exploratory Development Model (EDM) using holographic techniques;

2. A parametric evaluation on a component basis of the subsystems of the EDM;

3.   The conceptual design and trade-off analysis of alternative approaches to realizing a 2 Gb/s record capability.

Development of the EDM was undertaken in two phases, exploiting our technology investigations described in the Final Report of an earlier effort completed under Rome Air Development Center Contract Number F30602-71-C-0365. The primary goals of the Phase I EDM were to demonstrate 400 Mb/s recording and 40 Mb/s readout. These goals were extended for the Phase II EDM (Figure 1-1) to demonstrate 600 Mb/s recording, and both full-speed and reduced-speed readout with error rates better than 10^{-6}.

At the inception of Phase I, several major components of the system required development; the selection of an adequate recording film was also required. Some of the high-risk developments included: a multichannel optical modulator; a scanner-lens sub-system; a film transport; a readout photodetector array. Each of these subsystems, along with supporting optics and data handling electronics, were successfully designed, fabricated and integrated into a demonstrable recorder and reader. With this EDM, 400 Mb/s recording and 40 Mb/s readout was achieved. The system bit-error-rate performance was evaluated to determine the performance-limiting components and subsystems. Film processing and handling, along with laser-scanner focal variations were the principal causes of readout data errors.

The technical objectives for Phase II of the program included: an increase in record speed to 600 Mb/s; real-time playback of the recordings; and a readout bit-error-rate of less than 10^{-6}. The Phase II EDM was realized by almost completely rebuilding the Phase I system (excluding the scanner lenses).

Following the successful demonstration of the Phase II EDM early in 1976, system testing was conducted and extensive performance data were collected. In this report we describe the design of the system and present the system performance data gathered. Design and performance data at both system and subsystem levels are presented

for the Phase II hardware. References are made to Phase I only when required for complete appreciation of the technology development.

The system description, presented in Section II of this report, includes discussions of: 1) the implementation approach, with functional descriptions of major subsystems; 2) the format of the recorded film; 3) the formatting of the digital data into signals used in the recording and readout processes; 4) the recorder and reader electro-optical subsystem configurations; 5) the techniques used to achieve synchronization of the data during readout; and 6) a synopsis of the built-in system operability characteristics and diagnostic capabilities. The system description is followed by detailed discussions of the design and implementation of each major subsystem addressed during this development. Section II concludes with a comprehensive presentation of the system and subsystem tests that were conducted and the experimental results. Included are the parametric evaluations performed to determine the impact of subsystem parameters on overall system performance.

In Section III we present considerations relative to the implementation of future operational systems and summarize conceptual designs synthesized for multi-gigabit recorders. Section III concludes with system and subsystem level trade-offs between the various concepts and our recommendations for subsequent development.

This and related programs have significantly extended the limits of several technologies. These developments and their relevance to wideband recording are discussed in Section IV.

Conclusions and recommendations are given in Section V. While the EDM developed and tested under this program was not intended to be a finished product, it has demonstrated that optical techniques for high-rate, high-capacity digital data recording and playback are viable. We have demonstrated recording at 600 Mb/s using a single film transport at effective information packing densities that are about five times greater than those demonstrated by high-speed (e.g., 80 Mb/s) magnetic tape recorders. Thus,

a production version of the EDM would provide the recording speed capability of nearly eight 80 Mb/s tape recorders with all of the data stored on a single high-density reel. Playback of the data is readily achieved without the need for phase-locking multiple tape transports. Furthermore, using the EDM we have demonstrated that playback may be conducted at a broad range of playback speeds (e.g., from full speed to a ten-fold time expansion) and may be repeated a large number of times (e.g., 200) from the same film with little degradation of data integrity. We feel that with these demonstrations and the multigigabit technology investigations and design studies, Harris Corporation is now in a position to responsibly reply to requests for wideband digital recording systems capable of recording and playback at speeds up to 2 Gb/s.

SECTION II

RECORDER DEVELOPMENT

2.1 SYSTEM DESCRIPTION

The Wideband Recorder (WBR) Phase II Exploratory Development Model (EDM) can be described from several points of view. In Paragraph 2.2 we view the system as a cooperative collection of several sophisticated electrical, electro-optical, and electro-mechanical subsystems, each with its own critical design and performance parameters, and each making a contribution to the state of the art in its own area. Before concentrating on the individual subsystems, however, we present the key features of the system as a whole. We include general introductions to the system, and specific information about those subsystems that determine the overall operational characteristics of the Wideband Recorder/Reproducer System.

We begin with a general description of the EDM approach and the functioning recorder/reproducer system that resulted. Then, in more detail, we discuss holographic recording and the format of the recorded data. Other subjects include: the electronics which generate and format the data for recording; the optical system block diagrams, and the associated light budgets; the acousto-optic devices which provide conversion from time-varying electrical signals to time-varying optical signals; the electronic circuits which synchronize the recovery of the data during the reproduction process; and the optical, electrical, and mechanical features of the system which enhance its operability and diagnostic capabilities.

2.1.1 System Overview

2.1.1.1 System Approach

The Exploratory Development Model (EDM) implementation is a significant extension of fundamental laser line-scanning technology. Two improvements in the

fundamental techniques make possible the high-rate, high-capacity data recording and retrieval. First, the line scanner is augmented by a multichannel optical modulator specifically developed for this application. With this modulator, high-rate digital data to be recorded on film can be demultiplexed into several lower-rate data channels, each of which is clocked into the optical system in parallel. The high-speed requirements of the system are thereby placed on the input electronics subsystem and the dynamics of opto-mechanisms (e.g., light modulators, deflectors and film drive) are reduced. Second, holographic techniques are used to improve the performance of the EDM during data recovery. By simultaneously recording a linear array of data bits (i.e., one bit from each of the input channels) into a one-dimensional Fourier transform hologram we can significantly enhance the readout performance during high-speed data recovery. The spatial invariance property and the relatively large dimension of the hologram (in one direction) significantly relaxes the degree of accuracy necessary to sequentially address and read out the data by a scanning laser beam. A measure of redundancy, with associated immunity to recording medium imperfections such as film scratches and emulsion defects due to handling and processing, is provided by the holograms. Because data from each input channel is recorded and subsequently reconstructed simultaneously, skew between readout channels is eliminated – an advantage over high-density, longitudinal magnetic tape recordings.

The EDM approach uses photographic film in a reel format as the recording medium to enable sustained recording of high-speed data. Figure 2-1 shows the format of the data as recorded on the film. Holograms are recorded across the film (with the long dimension of each hologram in the direction of film motion) in rows that are on 1 mm centers, of which distance 0.8 mm is devoted to hologram length and 0.2 mm to interrow guardbands. Each hologram is about 0.016 mm wide and, since each hologram contains 128 data bits, the average packing density is 800 kilobits per square centimeter.

Figure 2-2 depicts the configuration of the holographic recorder and shows the data handling subsystems. A laser is used for recording and readout illumination.

250-FOOT ROLL

INTERFERENCE FRINGES

35 mm

26.0 mm

16 μm

16 μm

HOLOGRAM

0.2 mm

0.8 mm

89444—80
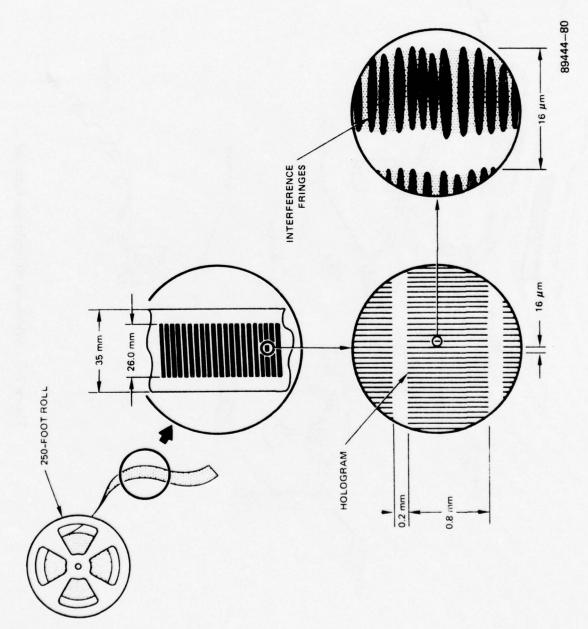
Figure 2-1. Holographic Storage Format
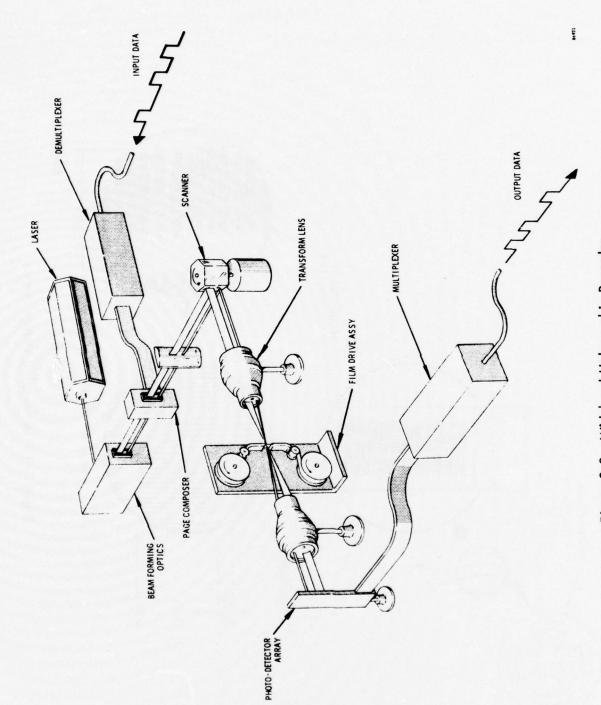
Figure 2-2. Wideband Holographic Recorder

INPUT DATA

DEMULTIPLEXER

LASER

SCANNER

TRANSFORM LENS

BEAM FORMING
OPTICS

PAGE COMPOSER

FILM DRIVE ASSY

MULTIPLEXER

OUTPUT DATA

PHOTO-DETECTOR
ARRAY

Beam-forming optics split and shape the laser beam into a signal beam and a reference beam. As the signal beam passes through the page composer (i.e., multichannel, optical modulator) the demultiplexed and electronically buffered data is converted from the electrical domain to the optical domain so that a multichannel, spatial, data pattern results. The Fourier transform of this data pattern is produced optically and raster-scanned onto the continuously moving film by the scanner. At the film plane, the reference beam is added to the spatially-modulated signal beam to record the data as a Fourier transform hologram.

After a given amount of data is recorded, the exposed film is removed from the film transport, processed using conventional techniques, and remounted on the transport for retrieval. During readout, the holograms are illuminated by the reference beam to reconstruct an image of the original data at a photodetector array. The data is then electronically determined and can be multiplexed into the original data stream.

2.1.1.2   System Functional Description

With this overview, we now consider the holographic optical system in more detail, using Figure 2-3 which depicts a functional system diagram of the present WBR. In this figure, we have simplified certain subsystems, but all of the operational features can be seen. We now briefly describe the key components and their functions and locations in the system; in the following sections we describe the major components and subsystems in more detail.

Since the WBR System is a holographic system, a laser provides the source of coherent light required. The beam-forming optics block represents those components that separate the beam into signal and reference beams. The signal beam is formed into a line source of light, since it is needed to illuminate a one-dimensional, multichannel page composer.
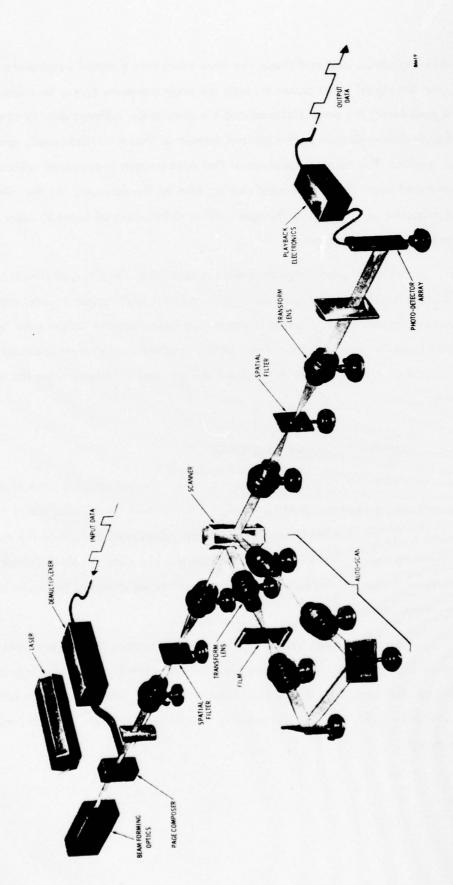
Figure 2-3. Wideband Holographic Recorder/Reproducer

The formatting of high-rate data into 128 parallel channels, and the modulation of the data in those channels onto the optical signal beam are accomplished by the demultiplexer and the page composer. The demultiplexer (the feasibility of which was demonstrated in an earlier phase of this program) converts the high-rate, serial bit stream to 128 low-rate parallel bit streams. These bit streams are modulated onto RF carriers and sent to the page composer, which is a linear array of 128 acousto-optic elements. The electrical energy is converted to acoustic waves within a glass crystal, so that when the light passes through the crystal, it is modulated by the acoustic waves to produce 128 optical data channels.

The next step is to produce the Fourier transform of the optical bit pattern at a spatial filter plane, where the reference and signal beams are brought together. Optical noise is removed at this stage, and the beam size is adjusted as required. To record the hologram, the light distribution at the spatial filter plane is imaged to the film by way of a multifaceted spinning mirror (the scanner). As the film is transported through the film plane, the beam scans laterally across it, recording rows of holograms.

After the film is developed, it is replaced in its original position and is illuminated by the reference beam. The holographically diffracted data is then conducted back to the spinning mirror in an "autoscan" arrangement. After its second reflection on the moving mirror, the data no longer has an angular scanning motion and can, therefore, be successfully imaged onto a stationary detector. The next steps in the readout process are the removal of optical noise at a second spatial filter plane and the imaging of the data onto an array of photodetectors by means of an array of fiber-optic elements (not shown in the figure).

Finally, threshold decisions are made on the detected signals and the resulting binary data is sent to verification circuitry to check on the fidelity of the readout process. Remultiplexing of the data for playback in a single full-rate bit stream, while not implemented in the present system, would be done at this point.
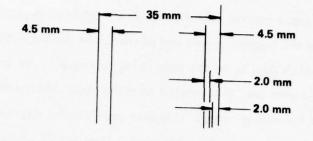
2.1.2   Recording Format

We use a scanning process to distribute the data to be recorded across the width of the film. In conjunction with the temporal modulations imposed on the optical beams, this scanning produces on the film a particular structure of data-bearing holograms and other auxiliary marks. Knowledge of this structure is essential to an understanding of the operation of the Phase II system.

Details of how we implement the scanning process are covered in later sections. Here we will present the features of the recorded scan structure, including the holograms and the additional information recorded to facilitate the readout process. We also briefly describe the holographic process, some of its advantages, and the way in which its properties are utilized in the WBR system.

2.1.2.1   Geometric Allocation

Figure 2-4 shows the details of the space allocation on the film to the various recorded signals. The hologram area occupies the central 26 mm of the 35 mm film. The hologram rows, approximately 1 mm in height, are slightly skewed due to the motion of the film during recording. Adjacent to the hologram recording area, along one side of the film, two additional tracks are recorded. The outermost track (called the marker or sync track) is an uninterrupted 50 percent duty cycle track, with one marker for every row of holograms. This marker track is used during the readout process to derive a sync signal which can be compared to the sync signal of the scanner and phase locked to it, thus assuring the proper positional relationship of the hologram row and the beam which scans it. The inner auxiliary track, called the ID Track, is recorded out of phase with the Marker Track, so that the same writing beam can be used for both. The ID Track records an identification pattern for each block of 40 rows. The ID pattern assigned to each block consists of four binary coded decimal digits enclosed within two additional marks which indicate the beginning and end of each group. This 4-digit capacity gives the EDM the ability to code and identify individual rows within up to 1200 feet of film.
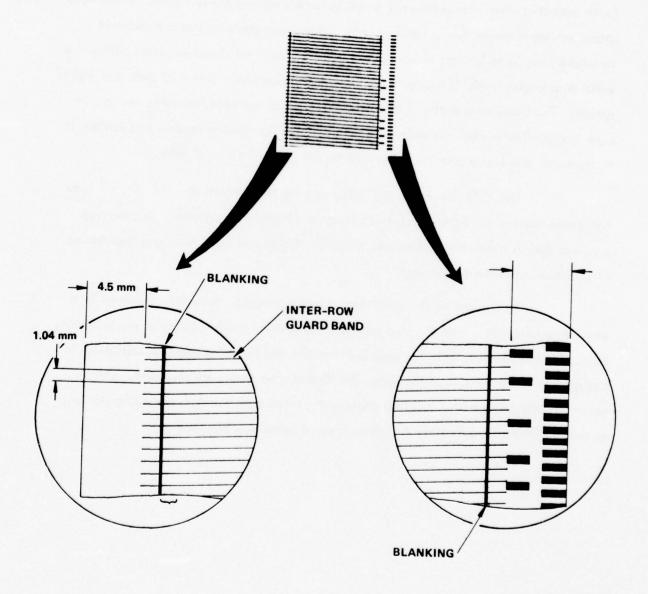
Figure 2-4. Recording Format

The expanded views of Figures 2-4B and 2-4C give the details of the recording format at the beginning and end of scan. At the beginning of a scan spurious data is recorded which duplicates the data being recorded at the end of the previous scan. This spurious data area is separated from the valid portion of the scan by a 17-hologram-wide "blanking" area. This area provides the necessary relaxation of the lateral tracking tolerance of the film transport. Then the 24 checkerboard holograms (with data that alternates between 1 and 0 in each channel) are recorded. These holograms provide a means during readout for the recovered clock and data dependent threshold circuits to become operationally ready. The final signal recorded before the valid data begins is the "frame sync," a series of seven nonholographic dark and light spaces. The frame sync pattern causes the intensity of the beam scanning the row to vary in a particular way just before the data is to start. During readout this pattern is recognized, and frame sync thus provided for the upcoming row of data.

The 1512 data-carrying holograms are then recorded. The 16 μm × 1 mm holograms overlap in the long direction by approximately 15 percent. This overlap provides dark row-to-row guardbands which facilitate row separation and suppression of film base noise during readout.
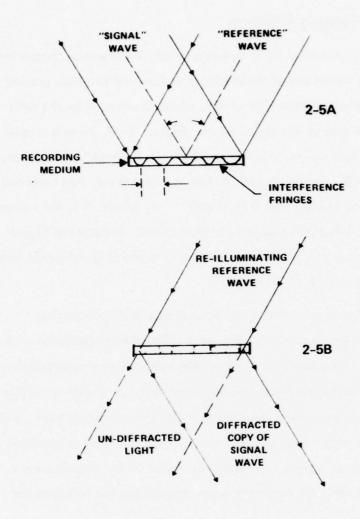
At the end of the valid data, blanking is again recorded, followed by a small area of spurious data which duplicates the data at the beginning of the following scan. During readout, only the area between the two blanking tracks is utilized. In the space beyond the end of the scan, the ID and sync tracks are recorded. This recording takes place at a location slightly displaced from the data recording station, so that a different, separately modulated record beam may be used.

2.1.2.2   Holography and Frequency Allocation

When two mutually coherent light beams overlap, interference fringes are formed. Holographic recording makes use of these fringes to form a diffraction grating in a recording medium such as photographic film which, when illuminated by the reference beam, will diffract a duplicate of the signal beam. Figure 2-5A shows a simple example of this process. Two light waves, arbitrarily labeled "reference" and "signal," strike a recording medium at an θ. In the recording medium, fringes are then recorded, whose spatial period "d" is related to the angle θ by $d \sin\theta = \lambda$, where λ is the wavelength of the light being used. When the hologram is illuminated, as shown in Figure 2-5B, the diffracted light is similar in direction and intensity to the original signal wave. This is the basis for holographic storage of information.

For a proper choice of recording medium and associated parameters, holography can be modeled as a linear process. Therefore, the effects associated with the presence of multiple signal beams are given by the principle of linear superposition. Specifically, if several signal waves are present during recording, each with a slightly different angle θ, then each will independently interfere with the reference wave, and the recorded fringe pattern will be a linear superposition of the individual (sinusoidal) fringe patterns of the various signal waves. Furthermore, signal beams present during recording will be reconstructed when the reference wave illuminates the hologram for readout.

The only additional precondition for this linear recording is that the phase of any given channel be randomly related to the phase of the other channels. This will prevent an intensity buildup at the central or "dc" point where all the sinusoids have a simultaneous maximum, which would exceed the film's linear range. In the WBR system this "phase randomization" is accomplished by electronically varying the phase of the RF signals which drive the AOPC channels, causing a corresponding variation of the phase of the optical channels. The dc energy is thus distributed over the entire

"SIGNAL" WAVE   "REFERENCE" WAVE

2-5A

RECORDING MEDIUM

INTERFERENCE FRINGES

RE-ILLUMINATING REFERENCE WAVE

2-5B

UN-DIFFRACTED LIGHT

DIFFRACTED COPY OF SIGNAL WAVE

2-5C

AMPLITUDE

128 DATA CHANNELS

B

REFERENCE BEAM

A

0   313   625   SPATIAL FREQUENCY (CYCLES/MM)

89444-25
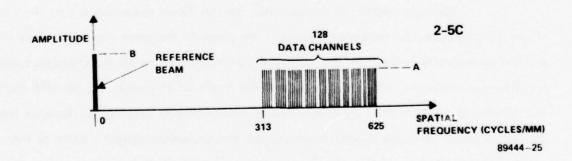
Figure 2-5. Holographic Recording

hologram, and the overall intensity fluctuations are kept small enough to remain within the linear dynamic range of the film.

The holograms recorded by the WBR Phase II EDM are of this multichannel nature. Figure 2-5C shows the spatial frequency allocation of the data recorded in each hologram. There are 128 signal waves, whose incidence angles correspond to spatial frequencies in the band between 313 and 625 cycles/mm, recorded per hologram. In practice, some of the signal waves have zero-amplitude, i.e., are not present, since they represent "0" bits. The amplitudes of the signal waves (when they represent "1" bits) are set at a uniform level "A." The proper strength for the reference beam, "B," can be chosen such that the "K-ratio,"

$$K = \frac{B}{128 \cdot <A>}$$

is consistent with minimum optical noise degradation of the holographically reconstructed data.

It is important to note that holographic data storage results in a distributed storage effect. Since each "1" or "0" bit is represented by a sinusoidal fringe pattern which extends across the entire hologram, damage to a small portion of the hologram does not eradicate the data of any specific signal wave, but merely reduces the signal-to-noise ratio of all signal waves by a small amount. In a discrete storage scheme, damage to 1/128th of a hologram would eliminate one entire bit of information. With the holographically distributed storage, each bit (signal wave) would lose about 1 percent of its energy, but all 128 bits would be detected successfully. Thus, a certain measure of redundancy and noise immunity is gained from the distributed storage effect of holographic recording.

2.1.3   Signal Formatting

The electronic control circuits which coordinate the operation of the Phase II system, in addition to handling the digital data pulses which represent the user data to be recorded, must also provide various kinds of housekeeping signals during the recording process, and retrieve them during readout. Examples of this include the means

for recovering a readout clock signal, the means for recovering the signals which provide scan-start information, and the means for providing a smooth transition from one scan to the next.

Acousto-optic modulators provide the means by which these temporal signals are impressed on the optical beams. The operating characteristics and specific applications of these devices are discussed in detail in Paragraph 2.1.4.3. In this paragraph they simply may be considered to be devices whose optical output is proportional to the RF input signal.

Since the WBR Phase II system is an Exploratory Development Model, it must both provide its own simulated data, and verify the integrity of that data when it is retrieved by the readout process. Also, since a major system goal is high-integrity readout, error correction coding has been implemented, with corresponding decoding equipment for use during playback.

In this section we describe the structure of the information recorded in each scan of holograms. The sequence and interrelationships of the acousto-optic devices which provide the beam modulation is also given. The generation of the simulated data (actually a known digital sequence) and the nature of the error correction code is then delineated. This is followed by brief sections on the circuits which implement the coding for recording and process the coded data during playback.

2.1.3.1   Recorder Overhead and Signal Shapes

A scan or row of holograms is produced by the deflection of the signal and reference beams across the film by a facet of the spinner. A scan consists of 1560 system clock periods. Data is not recorded during all 1560 clock periods, since some overhead functions must occupy a part of the scan period. The four resulting regions are illustrated in Figure 2-6.
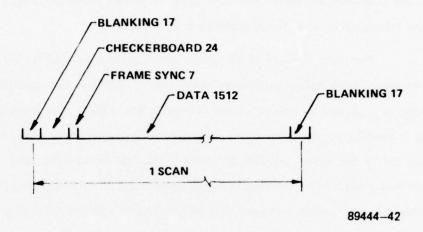
Figure 2-6. Functional Regions of Recorded Scan

The spinner facets are over-illuminated so that as one facet completes a scan, the next facet is beginning the next scan. This near-100 percent duty-cycle illumination, the film transport lateral position repeatability, and the spinner phase-lock tolerance, require a blanking region at the beginning and end of each scan. This region is recorded on the film as a very dense region achieved by operating the reference beam at a much higher level than is used to record holograms. In the Phase II system, the overhead allocated to blanking is 17 system clock periods, primarily to relax the tolerance on the film transport's lateral tracking.

The next interval of 24 system clock periods is used for bit sync and threshold recovery. Each hologram is separated from its neighbor by a guardband; this guardband is produced by operating the reference beam for a short time at the same level as is used to generate the blanking region. During readout, the reference beam is modulated by the dense guardbands between the less dense holograms. This signal is detected and processed to develop bit sync as described in Paragraph 2.1.5.2. The data present in each page composer channel during this period alternates between 1 and 0 (a checkerboard pattern). Each channel has the same pattern or its complement; therefore, only half the channels are active for any given hologram. The next region of seven system clock periods is used to record information for frame sync recovery. A special pattern (1100101) is recorded by allowing the density of selected holograms to become very low. This density level is achieved by extinguishing the reference beam for positions in the pattern corresponding to a "1."

The remaining 1512 system clock periods are used to record data holograms. These holograms are also separated by guardbands for continued bit sync recovery. Figure 2-7 illustrates the acousto-optic modulators (AOMs) used to temporally modulate the various beams in the Wideband system. The first AOM is referred to as the Parabola AOM. It is operated in the loss modulation mode to correct for reference beam intensity variations due to the scanning process. As more RF power is applied to this device, more energy is diffracted from the transmitted beam. The RF drive signal to this device for a single scan is shown in Figure 2-8.
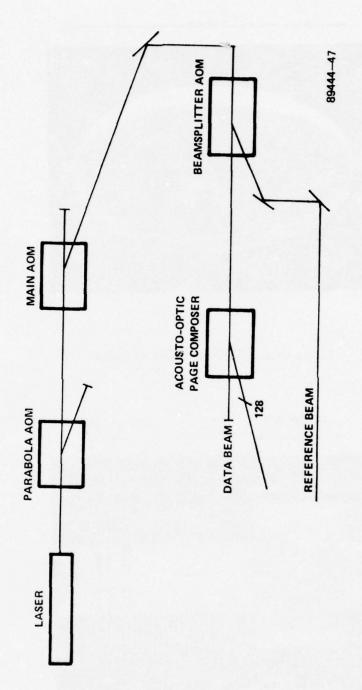
Figure 2-7. Acousto-Optic Devices in WBR System

LASER

PARABOLA AOM

MAIN AOM

ACOUSTO-OPTIC
PAGE COMPOSER

BEAMSPLITTER AOM

DATA BEAM

128

REFERENCE BEAM

89444—47
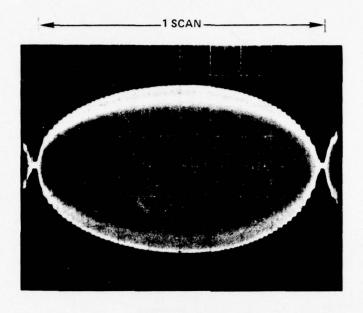
Figure 2-8.   Parabola AOM RF Drive

89444-76
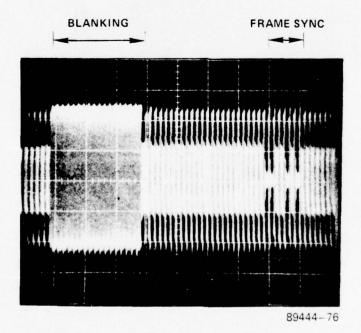
Figure 2-9.   Main AOM RF Drive

The next AOM in the system is the Main AOM. The light diffracted from this device is used to generate both the signal and reference beams. The primary function of the Main AOM is to temporally modulate the reference beam during recording to generate the Blanking region, the hologram-to-hologram guardbands, and the Frame Sync region. The intensity of the diffracted beam is approximately proportional to the applied RF power. Figure 2-9 illustrates the RF drive signal applied to the Main AOM during the region from end-of-scan through Blanking, Checkerboard, Frame Sync, and data holograms in the beginning of the following scan. There are three levels of RF drive used by the Main AOM: Guardband, Hologram, and Off. In recording data holograms or checkerboards, the RF drive alternates between the hologram level and the guardband level. During Blanking, the Main AOM operates at the guardband level. The Frame Sync region is generated by turning the Main AOM off during certain periods in order to produce clear regions on the film. During readout, the reference beam illuminates these clear regions and is detected by the same detector used to recover bit sync. This signal is processed to develop frame sync for the scan as described in Paragraph 2.1.5.3.

The temporally modulated beam from the Main AOM then enters the beam-splitter AOM. This is a CW-drive device used to split the main beam into the signal and reference beams; an acousto-optic beamsplitter is required to compensate for the Doppler shift of the acousto-optic page composer (AOPC). The diffracted beam is downshifted in frequency by an amount equal to the frequency of the applied RF drive. This frequency-shifted diffracted beam becomes the reference beam.

The transmitted beam is modulated by the AOPC to become the signal beam. Four functions are performed by the RF drive electronics to properly excite the AOPC: parabola correction, RZ data chop, phase randomization, and data modulation. A functional diagram of the AOPC drive system is shown in Figure 2-10. The Master Oscillator Output enters the parabola modulator to generate additional correction in the signal beam for intensity variations arising from the scanning process. The parabola
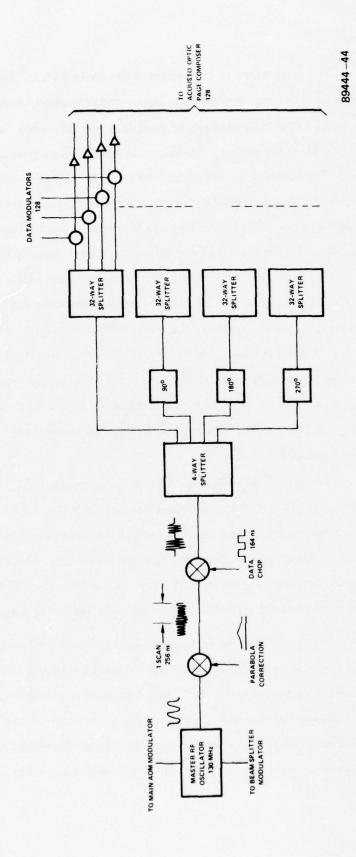
Figure 2-10. AOPC Drive Electronic – Functional Diagram

89444 –44

2-20
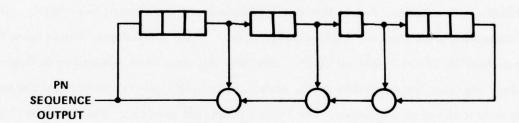
correction is followed by a chopping modulator to provide for return-to-zero (RZ) data modulation. The output is then split and phase-shifted into four quadrature phases. These assure proper "phase randomization" of the recorded data, as described in Paragraph 2.1.2.2, and are required for any system implementation. Each of these phases then feeds 32 of the 128 data modulators. Finally, these digitally modulated signals are used to drive the AOPC.

2.1.3.2   Data Generation

In the Exploratory Development Model, 32 pseudorandom data sources are utilized to provide data sequences for the acousto-optic page composer (AOPC). The pseudorandom sequences are of length 511. The same sequence is used for each data source, but each starts at a different point in the sequence. The sequence has every possible 9-bit pattern excluding nine consecutive 0's. Data of this nature may be validly utilized as a test source since, in an operational system, the input data stream would be multiplied (exclusive ORed) with a pseudorandom noise (PN) sequence to randomize the input data. For example, this operation will take a string of 0's or 1's and produce either the PN sequence or its complement. Recovery of the original data on readout is accomplished by simply postmultiplying (exclusive ORing) of the recorded data with the same PN sequence.

The test data for the Exploratory Development Model is generated by the 9-bit pseudorandom noise sequence generator shown in Figure 2-11. This circuit is very similar to a circular shift register with its end-around feedback exclusive ORed with selected taps of the register. The feedback taps are chosen in such a way that the circuit generates a bit sequence which is cyclic of length 2^{N-1}, where N is the number of elements in the feedback shift register. This sequence has no shorter subsequences, and does not contain the sequence of N successive zeros. The sequence may be started at any point by loading the shift register with the 9 bits just prior to the desired starting position in the sequence. Shifted versions of the sequence are generated by using a property of these circuits: the exclusive OR of two shifted versions of the sequence generates the same sequence at another shift relative to the two generating sequences. Since there are 32 data patterns and the sequence is of length 511, the exclusive OR combinations are chosen to yield shifted versions of approximately 16-bit shifted intervals.

Twenty-nine of the data sources are each put into four AOPC modulators, and another data source is put into two other AOPC modulators; this provides 118 of the recorded data channels. The remaining two data sequences are encoded using the error-correction code described in Paragraph 2.1.3.3. These coded sequences drive eight other

2-22

Figure 2-11. Nine-Bit PN Sequence Generator

channels. The two remaining modulators are driven by alternating 1-0 patterns of data, which may be used during testing. These 128 data sources are randomly assigned to the 128 elements of the AOPC and provide simulated user data for system performance evaluation.

2.1.3.3   The Error-Correcting Code

The error-correcting code implemented in the Exploratory Development Model is a 63, 51 BCH code interleaved to depth 4. The basic 63, 51 code uses 12 bits of parity and 51 bits of data to yield a code word of 63 bits. The rate of this code is 51/63 or 81 percent. This code can correct any single- or double-error pattern in the 63-bit block. In addition, due to the specific implementation chosen, the code is capable of correcting some selected triple-error patterns. The triple patterns chosen were the higher probability errors involving bursts. Interleaving, sometimes referred to as time-spreading, improves the capability of the code for burst errors while maintaining the same random error-correction properties. The coding is applied to each of the user data channels, and its 128 parallel encoders and decoders would be utilized in an operational system.

Interleaving is accomplished by the generation and combination of four codewords into a "superblock" of length 252, as shown in Figure 2-12. The basic code can correct a burst of length 3. A burst length of 12 or less occurring in the interleaved code will generate, at most, three errors in each of the four primary codewords and will, therefore, be fully corrected.

The random error capability of this code may be approximated in the region of interest by the equation

$$BER_c = 3100 \times BER_r^3$$

where BER_r is the raw bit error rate, and BER_c is the corrected bit error rate.

```
            a₁  a₂  a₃  a₄  · · ·  a₆₃

FOUR 63,51   b₁  b₂  b₃  b₄  · · ·  b₆₃
BCH CODE
WORDS        c₁  c₂  c₃  c₄  · · ·  c₆₃

             d₁  d₂  d₃  d₄  · · ·  d₆₃

                        INTERLEAVING


a₁ b₁ c₁ d₁ a₂ b₂ c₂ d₂ · · · a₅₁ b₅₁ c₅₁ d₅₁   a₅₂ b₅₂ c₅₂ d₅₂ · · · a₆₃ b₆₃ c₆₃ d₆₃

            204 USER DATA BITS                        48 PARITY BITS

|←——————————— 252 BIT INTERLEAVED "SUPERBLOCK" ———————————→|
```

89444-59
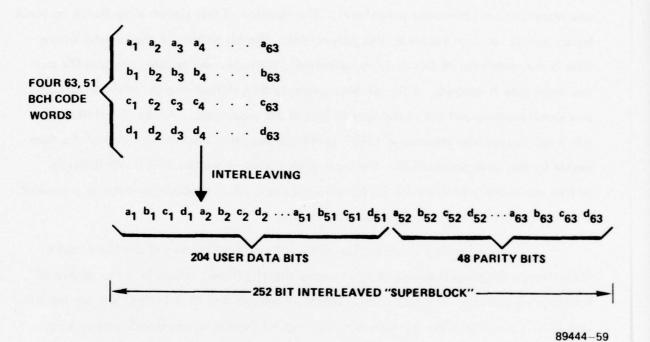
Figure 2-12.   Depth-Four Interleaving

2.1.3.4   Encoder Operation

A functional block diagram of a 51, 63 BCH Encoder is shown in Figure 2-13. The encoder is comprised of 12 D-type flip-flops arranged as a feedback shift register using exclusive OR input taps. The pattern of the taps is specified by the BCH code and represents an 11th-order polynomial. The function of this circuit is to divide an input binary pattern or data vector by this polynomial. The bit pattern in the register at any time is the remainder of this division operation. Initially, the register contains 0's and the input gate is opened. A 51-bit data vector is then shifted into the division circuit and simultaneously put out as the first 51 bits of the codeword. At the completion of this step, the register contains a 12-bit remainder resulting from the division of the data vector by the code polynomial. The input gate is closed and the 12-bit remainder is shifted out as the parity bits of the 63-bit codeword. This process generates a codeword that is an exact multiple of the code polynomial.

Interleaving is accomplished by a slight modification of the basic coder. Each D-type flip-flop is replaced by N sequential flip-flops, where N is the degree of interleaving desired. The operation is identical except that 51 x N data bits are fed in, and 12 x N parity bits are generated by the register forming a superblock codeword of length 63 x N bits. In the Exploratory Development Model, N is 4, yielding a 252-bit superblock.

2.1.3.5.   Decoder Operation

A functional block diagram of a 51, 63 BCH Error-Correcting Decoder is shown in Figure 2-14. The principal elements of the decoder are a syndrome generator, a syndrome look-up table, and a buffer memory. The syndrome generator is nearly identical in construction to the encoder described in Paragraph 2.1.3.4. The conceptual operation of this unit is best described in terms of operations involving binary polynomials. Each 63-bit codeword or code vector represents a 62nd-order polynomial, with each bit representing the coefficient of its particular term in the polynomial. The codeword transmitted is a multiple of the code polynomial. The syndrome generator is a

DATA/PARITY

INPUT DATA

CODEWORD
OUTPUT

D FLIP-FLOP

EXCLUSIVE
OR

89444—45
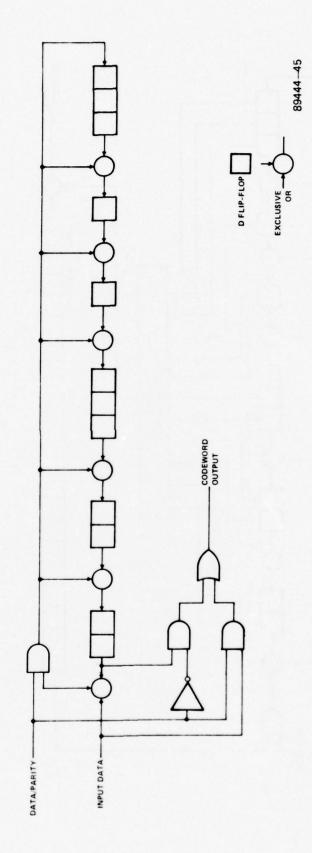
Figure 2-13. 63, 51 BCH Encoder – Functional Diagram

2-27
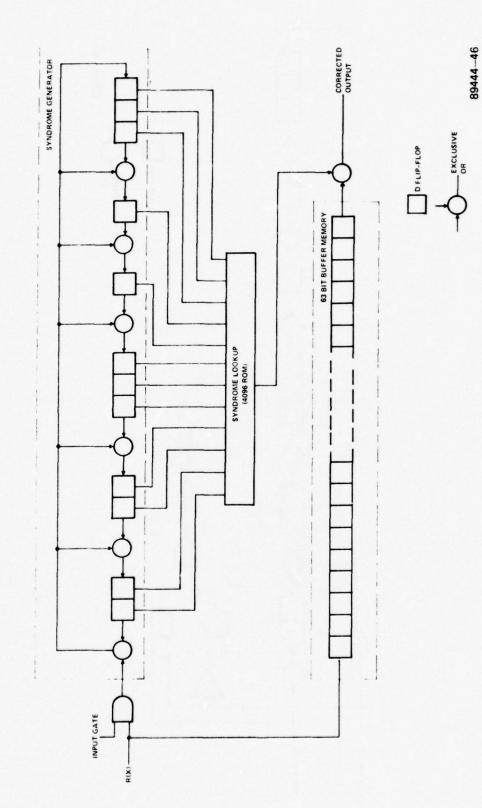
Figure 2-14. 63, 51 BCH Decoder – Functional Diagram

89444–46

division circuit that divides the input bit pattern, or received vector, by the code polynomial. If there were no errors, the remainder, referred to as the syndrome, would be 0. The received vector, R(x), may be considered to be the Modulo-2 sum of the 63-bit code vector, C(x), and a 63-bit error vector, E(x). The received vector is a linear sum of the two polynomials. The syndrome generator divides the received vector by the code polynomial, G(x), yielding a syndrome, S(x), given by:

$$S(x) = R(x) \bmod G(x) = C(x) + E(x) \bmod G(x)$$
$$= C(x) \bmod G(x) + E(x) \bmod G(x) = E(x) \bmod G(x)$$

S(x) is seen to be the sum of the remainder resulting from the division of the transmitted codeword by the code polynomial and the remainder of the error vector divided by the code polynomial. The codeword is a multiple of G(x); therefore, its remainder is 0, leaving the syndrome totally associated with the error polynomial alone. The 51, 63 BCH code is capable of correcting all single and double errors. Single and double errors will have error vectors with one or two nonzero coefficients. The syndrome for every correctable error vector is distinct, and its inspection at this time could yield the error vector that corrupted the data stream. This error polynomial could then be Modulo-2 summed with the received bit stream, effectively cancelling the errors. The implementation of this brute-force decoder would involve a very large syndrome look-up table. In order to avoid a large table, another characteristic of the code polynomial is utilized. The syndrome generator outputs, with the input disconnected, become cyclic with a 63-shift period. Thus, any pattern in the shift register will repeat in the register after 63 shifts. Each shift operation corresponds to the generation of the syndrome associated with an equivalent cyclic shift of the received vector. A normalized error polynomial is defined as one in which the right-most bit is a 1. By using this concept, there is only one single-bit error pattern,

000 001,

and 62 double-bit error patterns,

000 ... 00011,

000 ... 00101,

$$000 \ldots 01001,$$

$$\cdot$$

$$\cdot$$

$$\cdot$$

$$100 \ldots 00001.$$

This requires that only 63 different 12-bit patterns be recognized to detect all the possible shifted versions of the correctable error patterns. This may be accomplished with a 4096 (2^{12}) bit read-only memory.

The total operation of the decoder is as follows: the received vector is shifted simultaneously into the syndrome generator and the 63-bit buffer memory. The input to the syndrome generator is now disconnected. At this point, the first bit of the received vector is about to exit from the buffer memory, and the syndrome corresponds to the error vector in the received vector. If the error vector is correctable and has a 1 as its right-most bit, the syndrome look-up table recognizes the error pattern. This correction bit is exclusive ORed with the bit exiting from the buffer memory, thus effecting the correction of the erroneous bit. If the error vector does not have a 1 in the first bit position, its syndrome is not recognized, and the bit exiting from the output buffer is unchanged. The generator is now shifted to produce the syndrome associated with a single cyclic shift of the error vector. The correction process is now repeated for the second bit of the received vector, which is now exiting from the buffer memory. This procedure continues until the entire received vector has been processed. Several slight modifications to this basic circuit are used in the Exploratory Development Model. Some highly probable triple-error patterns can also be corrected. The syndromes of these patterns are also recognized by the syndrome look-up table. Interleaving is achieved in a manner similar to that used in the encoder. Each D-type flip-flop in the syndrome generator is replaced with four flip-flops, and the buffer memory length is increased to 252 (4 x 63).

Error patterns that contain more than three errors may result in erroneous correction of the received vector. The construction of the basic decoder guarantees that not more than three additional errors will be added in the case of a decoding failure.

2.1.4 Optical System

The electronic circuits described in the previous section provide timing and control information to the various system elements to coordinate the recording and play-back of data. But the actual recording and readout is an optical process, and a complex optical system is required to shape and direct the beams. As we have indicated above, the key elements in the optical system are the acousto-optic devices, which allow the electronic control signals to interact with the optical beams. In this section we describe the optical system on a block diagram level, including all the system components which interact with the optical signals and the light budgets associated with those components. We then provide some of the details of the acousto-optic interaction and the key optical devices it makes possible. We should note that more detailed information about the most complex acousto-optic device, the page composer, is provided in Paragraph 2.2.4.

2.1.4.1 Functional Schematic Description

The sequence of events that takes place in the WBR Phase II EDM will now be described with reference to Figures 2-15 and 2-16, which contain block diagrams of the record (Figure 2-15) and readout (Figure 2-16) processes. In these figures, optical signals are represented by dotted lines, while electronic control and output signals are shown as straight lines. Only the points of interface of the electronic control and output signals are shown, since details of the electronic control system are given in Paragraph 2.2.1. In the following descriptions of the record and readout systems, frequent reference is made to other sections of this report, in which detailed data on the various subsystems are given.

Record System

Elements crucial to the recording system (Figure 2-15) include:

- Laser Light Source - The WBR Phase II EDM uses a CR-12 Argon-Ion laser, supplying 1 to 2 watts at 514.5 nm for the recording process.
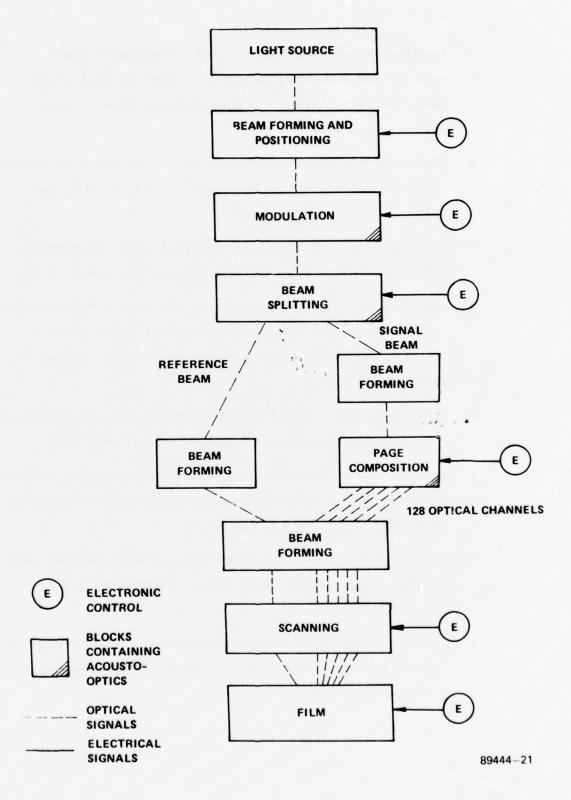
Figure 2-15.   Recording System – Optical Block Diagram

89444–21

- Beam Forming and Positioning – Control systems operate active reflective and decentering optics to compensate for possible laser drift. The beam is prepared for modulation and focused into an acousto-optic device.

- Modulation – Temporal intensity modulation is imposed on the beam by an acousto-optic device (see Paragraphs 2.1.3.1, 2.1.4.3, and 2.2.3.1).

- Beam Splitting – Another acousto-optic device splits the beam into signal and reference beams (see Paragraphs 2.1.4.3 and 2.2.3.1).

- Beam Forming – In both signal and reference beams, additional shaping takes place. The signal beam is shaped into a line source to illuminate the linear acousto-optic page composer (AOPC) (see Paragraph 2.2.3.1).

- Page Composition – The 128-element AOPC modulates the signal beam into 128 optical channels (see Paragraphs 2.2.3.1 and 2.2.4).

- Beam Forming – The reference beam and multiple-channel signal beam are formed into the Fourier transform hologram recording format (see Paragraphs 2.2.3.1 and 2.2.3.3).

- Scanning – A multifaceted spinning mirror images the hologram via a transforming/scanning lens to the film (see Paragraphs 2.2.3.1, 2.2.3.3, and 2.2.5).

- Film – 35mm film on a film transport mechanism is moved through the scanning beam and rows of holograms are recorded (see Paragraphs 2.2.7 and 2.2.10.1).

Readout System

After off-line processing of the film (see Paragraph 2.2.10.2), the film is replaced in the system and readout (Figure 2-16) is done. Key elements are:

- Light Source – As above. Readout power levels average 3 to 4 watts.

- Beam Forming and Positioning – As in record, drift is servoed out. Modulation, signal beam, etc., are unnecessary for readout, so the beam is formatted and sent directly to the scanning system.

- Scanning – The same system as was used to record, now scans only the (readout) reference beam.

- Film – The transport moves the rows of holograms synchronously past the scanning read beam.

- Descanning – Stationary detection of the scanning holographic data is made possible by a second reflection on the multifaceted spinner (see Paragraph 2.2.3.3).

- Beam Forming and Clock and Sync Detector – The undiffracted portion of the reference beam (also descanned) is focused to a detector where the hologram-imposed modulation is used to derive clock and sync signals (see Paragraph 2.1.5).

- Beam Forming and Scaling – The diffracted data is scaled and focused to properly match the data channels to the fiber-optic array elements.

- Fiber-Optic Array – A linear array of fiber-optic elements distributes the optical channels to the photodetectors.

- Photodetector Array – An array of discrete photodetector elements detects the binary data in the individual channels and sends it to thresholding and verification circuitry (Paragraphs 2.2.1 and 2.3.2).

LIGHT SOURCE

BEAM FORMING AND POSITIONING — E

SCANNING — E

FILM — E

DESCANNING

128 OPTICAL CHANNELS

BEAM FORMING

BEAM FORMING AND SCALING

CLOCK AND SYNC DETECTOR

FIBER-OPTIC ARRAY

E

PHOTODETECTOR ARRAY

E

E   ELECTRONICS CONTROL

- - - - -   OPTICAL SIGNALS

————   ELECTRICAL SIGNALS

89444-14
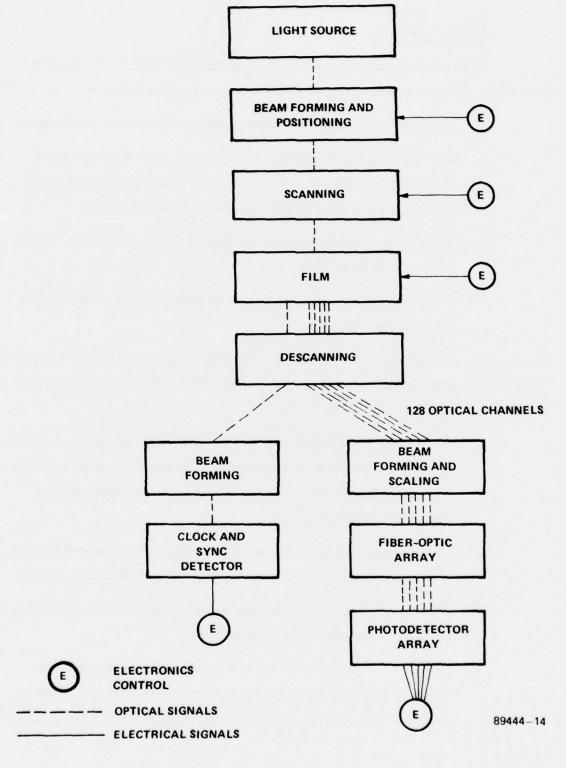
Figure 2-16.   Readout System – Optical Block Diagram

2.1.4.2 Light Budgets

To properly evaluate the total light input power required for the operation of the WBR Phase II EDM, and to provide similar information for the design of future systems, total-system-efficiency data are required. We present first the anticipated efficiencies of the various subsystems (which correspond to the blocks of Figures 2-16 and 2-17), including the number and nature of the components contained in each. Then some achieved efficiencies for certain key areas are presented, with interpretations of their impact on future systems.

Record System Design Values

Table 2-1 shows the predicted transmittance factors for the various blocks of the record system. The key at the bottom of the table details the assumptions made concerning the losses expected at each type of element. These values are representative of what has been achieved in similar systems in the past. Note that the goal for the overall record system efficiency (for the reference beam) is 1.3 percent. Since the power entering the beam splitter will undergo a 3:1 split in favor of the signal beam which illuminates the page composer, we must anticipate an effective efficiency value of around 0.3 percent for the reference beam.

Read System Design Values

Data for the transmittances of the read system are given in Table 2-2. No AOM's are included, since the holograms and guardbands provide their own modulation during the scanning process. The most significant losses in the read path are the over-illumination of apertures required both vertically and horizontally to produce relatively uniform intensity profiles, and the diffraction efficiency of the film. The diffraction efficiency is maintained in the fractional percentage region by using a sufficiently low signal-to-reference ratio. This assures a minimum of signal distortion by keeping the recording well within the linear region of the film's dynamic range. Note that the overall efficiency computed for the read path is 0.005 percent.

Table 2-1. Design Goals for Record System Optical Efficiency

Subsystem Block	Elements Contained	Expected Block Transmittance	Cumulative Total Efficiency
Light Source	Laser	1.00 (by definition)	100%
Beam Forming and Positioning	1 AOM 2 Tilt Plates 6 Mirrors	0.65	65%
Modulation	2 Lenses 1 AOM	0.36	23%
Beamsplitting	2 Lenses 2 Mirrors 1 Tilt Plate 1 AOM	0.34	8.0%
Beam Forming (Reference)	1 Tilt Plate 6 Lenses 1 Mirror	0.71	5.6%
Beam Forming (Reference and Signal)	2 Lenses 1 Baltar 1 Mirror	0.77	4.3%
Scanning	1 Spinner 1 Ferson Lens	0.30	1.3%

NOTE: Component losses used in generating the above table are as follows:

Simple Lenses	4%	Ferson Lens	15%
Mirrors	2%	Spinner	
AOMs	20–60%	Geometrical	65%
Baltar Lenses	15%	Optical	15%

Table 2-2.   Design Goals for Read System Optical Efficiency

Subsystem Block	Elements Contained	Expected Block Transmittance	Cumulative Total Efficiency
Light Source	Laser	1.00 (by definition)	100%
Beam Forming and Positioning	1 AOM 2 Tilt Plates 6 Mirrors 3 Lenses 1 Baltar Lens 1 Slit Aperture	0.27	27%
Scanning	1 Spinner Facet 1 Ferson Lens	0.25	6.8%
Film	Diffraction Efficiency Transmittance	0.003	0.020%
Descanning	3 Ferson Lenses 2 Mirrors 1 Spinner Facet	0.50	0.010%
Beam Forming and Scaling	5 Lenses 2 Mirrors	0.75	0.008%
Channel Distribution	Optical Fiber	0.67	0.005%

System Performance Values

For recordings made on Kodak SO-141 films, experience has shown that a peak power of around 3.4 mW is required. Based upon the system losses detailed in Tables 2-1 and 2-2, this would imply an input power requirement of 1.0 watt. Operation of the WBR Phase II EDM has indicated that this is insufficient. Other possible sources of light loss include: system cleanliness, optical coating consistency, aperture losses not detailed above, and other "implementation losses." The effect of these other losses has been to require approximately 2.0 watts of light at 514.5 nm for recording. Thus, the effective recording system efficiency is about 0.17 percent. Based upon the 0.005 percent read system efficiency given above, the predicted light power for readout is calculated as follows. About 300 nW/channel is the minimum required to provide adequate electronic SNR at the detector; with 128 channels, this becomes 38 μW. For 0.005 percent system efficiency, the implied power requirement is 38 μW/5 x 10^{-5} or 770 mW. Since the sources of optical noise in the system have been found to be of greater significance in computing the optimum SNR, a greater input power to the detectors will be required, and this has been found to be approximately 600 nW/channel. With this new figure, the required input power would be 1.5 W. Finally, the actual "implementation losses" encountered in the readout have been found to bring this power requirement to approximately 3.0 W.

2.1.4.3   Acousto-Optic Devices

Acousto-optic (AO) devices perform several important functions in the WBR Phase II EDM. These functions include (temporal) modulation, beam splitting, and page composition. We now briefly describe the nature of an AO device, and follow the description with specific examples from the system.

An AO device is a block of transparent material (various types of glass, for example) through which we pass the laser beam that we want to modulate or deflect. In the crystal, the light beam encounters the acoustic wave. Devices used in the WBR system operate in the "Bragg" diffraction mode (see Reference 1). This mode produces two main output beams as shown in Figure 2-17. One beam, the undiffracted component, has not interacted with the acoustic wave and is usually discarded. The other beam, the diffracted component, has interacted with the acoustic wave. Temporal modulation of the acoustic wave amplitude can be used to temporally modulate the amplitude of the diffracted light wave. Frequency modulation of the acoustic wave will produce angular variation of the light wave, since the diffraction angle is proportional to the spatial frequency of the acoustic wave. The acoustic wave is introduced into the crystal by means of an electromechanical transducer which is bonded to one face of the crystal, and which in turn is connected to an appropriate source of RF electrical energy and associated control circuits for amplitude or frequency modulation.

Example 1 – Modulation

The transitions in light level which are used to record holograms and guard-bands are produced by passing the beam through an AO modulator. High-rate recording requires that the rise time associated with these transitions be as short as possible. Since the rise time of a change in light level produced by an AOM depends on the propagation time of the acoustic waves through the optical beam, the rise time can be minimized by using a very small light beam. This is achieved in the main light-modulating AOM of WBR by focusing the beam through the AOM, as shown in Figure 2-18.

---

1. Adler, Robert, "Interaction Between Light and Sound," IEEE Spectrum, May 1976.

COLLIMATED
LIGHT INPUT

DIFFRACTED
BEAM

L

h

RF POWER
AMP

ℓ

UNDIFFRACTED
"DC" COMPONENT

88244-3
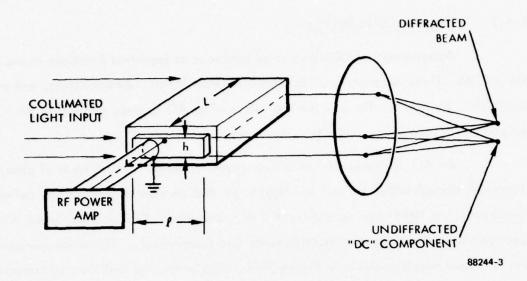
Figure 2-17. Typical Acousto-Optic Beam Deflector or Modulator

DIFFRACTED
BEAM

UNDIFFRACTED
BEAM

TRANSDUCER

L

ACOUSTIC
BEAM

INCIDENT OPTICAL BEAM

86896-8
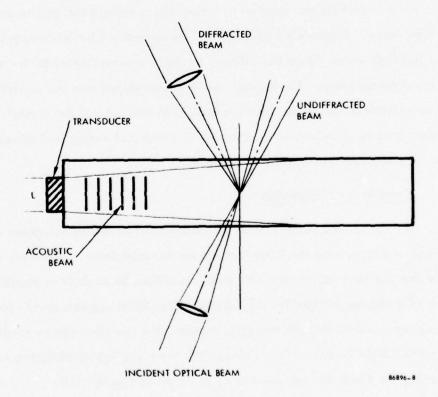
Figure 2-18. Details of Acousto-Optic Interaction

Example 2 – Beam Splitting

To produce the two beams necessary for holographic recording, the WBR Phase II EDM employs an AO beamsplitter. Since the signal to this device is constant, rise time considerations are not important here. However, another characteristic of acousto-optic devices is very significant. That is the fact that, because the light wave interacts with a moving acoustic wave, a Doppler-like frequency shift (equal in magnitude to the RF acoustic frequency) is induced in the diffracted light. Since holographic recording requires complete coherence between reference and signal wave, this frequency shift would ordinarily prevent such recording. This problem is solved in the WBR by using the diffracted, frequency-shifted light as the reference beam, and using the undiffracted light to illuminate another AO device, the page composer. Driven by the same RF source as the beamsplitter, the page composer imparts to the signal beam a frequency shift identical to that of the reference. Thus, coherence is preserved and interference can still take place.

Example 3 – Page Composition

To produce simultaneously many optical channels of data, a multichannel AO device is needed. Except for its multichannel nature, this device is essentially identical to the modulator described in Example 1 above. A simple diagram of the operation of such a device is shown in Figure 2-19. The AO page composer used in the WBR Phase II EDM has 128 channels arranged in a linear array. To minimize signal rise time, the line source of light is focused through the crystal, as Figure 2-19 shows. Further details of the construction and performance characteristics of the page composer will be found in Section 2.2.4.

Additional information on acousto-optic devices may be found in Reference 2.

---

2. Palermo, C. J., R. M. Montgomery, and E. H. Young, Jr., "Applications of Acousto-Optics to Laser Recording," SPIE Symposium Proceedings, San Diego, California, August 1974.

DIFFRACTED LIGHT SHOWING BITS

LIGHT WEAKENED BY DIFFRACTION

UNDIFFRACTED LIGHT

INCIDENT LIGHT

LIGHT SOURCE

TRANSDUCERS
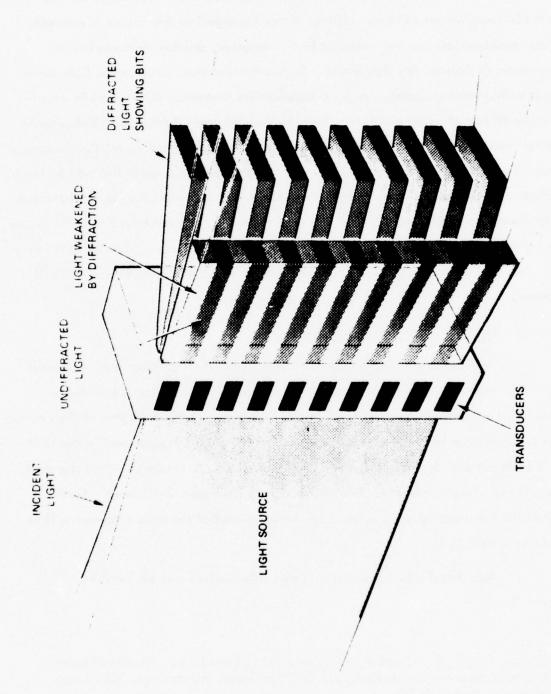
Figure 2-19. Acousto-Optic Page Composer

85569-2

2-44

2.1.5   Readout Synchronization

The timing of the readout process in a system operating at these high data rates is a critical element in achieving high fidelity data reproduction. Multichannel holographic recording brings to this process a distinct advantage, since it permits the recording to be made on a single recording medium. This automatically maintains the temporal integrity of the recorded data, avoiding the resynchronization and skewing problems found in some other recording techniques. The digital nature of the recovered data, furthermore, makes time-base correction a relatively easy process, requiring only a small buffer. Analog recording, on the other hand, places very stringent requirements on the time-base stability of the deflection mechanism.

Nevertheless, careful consideration must be given to methods of synchronizing the various elements of the playback unit, and providing bit-synchronous clock and scan-sync signals as well. For example, the mechanical tolerances associated with the scanning process can be significantly reduced by implementing a bit-sync and scan-sync recovery scheme which reacquires these critical signals on each line being read out.

In previous sections we have seen how several types of timing information are included among the recorded signals. This section will present details of the utilization of these timing marks on the film during playback.

2.1.5.1   Film Transport Synchronization

Readout synchronization of the film transport is required so that the scanned beam strikes the hologram row at the correct position. The synchronization process begins with the recording. A synchronization mark is placed on the margin of the film as each hologram row is recorded. These synchronization marks form a 50 percent duty cycle track. During the off-time of the synchronization marker, another track, the identification marker track, is recorded. The ID marker is used to generate an address for the hologram rows. Both the synchronization and the ID marker tracks are shown in Figure 2-20 in a 1:1 scale. To record the marker tracks, a 15 mW laser, operating at 488.0 nm
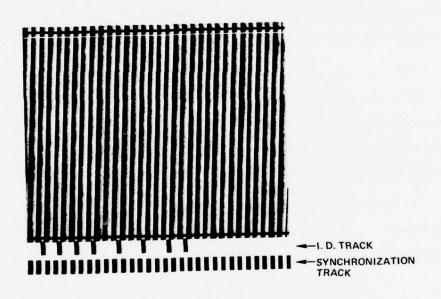
Figure 2-20. Recorded Synchronization and Identification Tracks

is used. The laser beam is modulated and deflected into both synchronization and ID marker tracks. This is accomplished by an acousto-optic modulator, driven by two different frequencies in alternating sequence. The modulated beams are focused to a line at the film plane after passing through a mask. These tracks are detected during readout and the resultant signals are processed by the transport controller and the system control electronics.

For readout, the film is illuminated by an infrared Light Emitting Diode. The illuminated area of the film is focused on a mask containing two rectangular apertures spaced 1/4 marker-cycle apart. The two markers are then focused on a split detector, one for each aperture. The synchronization track is detected by a dc-coupled, two-phase analog detector; the resultant wave forms are triangular in shape. Both phases are digitized so that direction information can be derived. Also, one of the digitized phases is phase-locked to a system input clock by a Type 2 phase-lock servo during system readout. During "Hold" mode operation, the two detected analog phases are position-servoed to two matching phases generated by the "Hold" mode control. Because the synchronization marker spacing can be changed for experimental investigations, the detector optics have a zoom capability.

The ID track detector is a simple interruption detector. It is placed in very close proximity to the synchronization track detector to reduce phase errors. The signal is digitized at the detector and is fed directly to the system control electronics for processing.

2.1.5.2   Bit Sync Recovery

During recording, the reference beam is modulated between the guardband and hologram levels. The guardband level forms a dense region between the holograms. On readout, the reference beam scanning the film is temporally modulated by the density variation, with a strong component at the hologram frequency. Processing of this transmitted reference beam yields hologram sync (bit sync). The reference beam intensity is detected by a photodetector and appears as in Figures 2-21 and 2-22; this
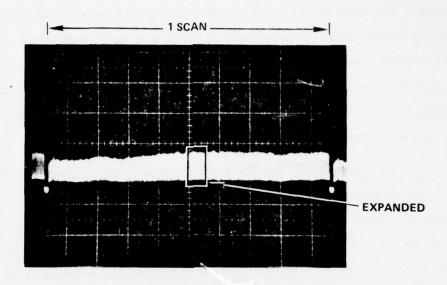
Figure 2-21. Readout Reference Beam Intensity (Full Scan)

89444—73
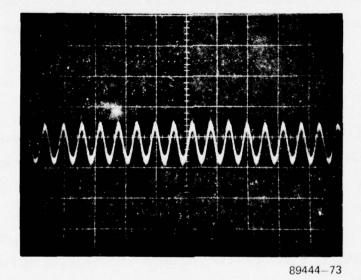
Figure 2-22. Readout Reference Beam Intensity (Expanded)

signal cannot, however, be used directly for clock as it has a dc component and may be corrupted by scratches and imperfections in the film.

The signal is therefore high-pass filtered to remove the dc and hard-limited by a digital comparator, as shown in the block diagram in Figure 2-23; this limiting reduces the energy seen by the narrowband filter due to scratches, etc. This digitized signal is filtered by an RLC passband filter, and is then digitized by a second comparator, yielding bit sync.

The choice of filter Q is a compromise between acquisition time and ability to operate through a temporary loss of the reference signal. The envelope response of the narrowband filter is given by

$$e^{-\alpha t}$$

where

$$\alpha = \frac{\pi F}{Q} \quad ,$$

and F is the nominal bit sync frequency. Loss of the reference beam information is generally assumed to be less than four hologram periods and not greater than 10 hologram periods. Using 1/e points at 10 hologram periods yields a Q of approximately 30. The system presently allocates 24 hologram periods to bit sync and threshold acquisition.

89444-48
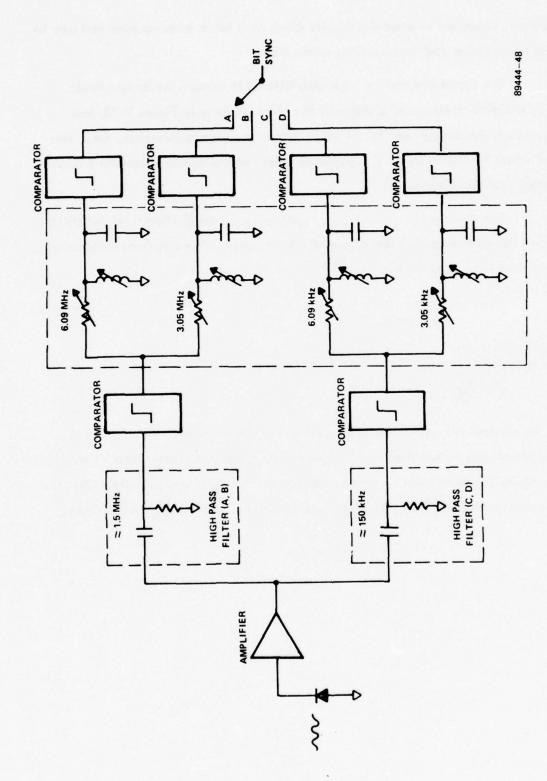
Figure 2-23. Bit Sync Signal Processing

2.1.5.3   Frame Sync Detection

At the beginning of each hologram row, a special frame sync code pattern is recorded. This pattern, 1100101, is realized by turning off the reference beam during the four holograms corresponding to "1" bits in the pattern. The reference beam intensity is shown in Figure 2-24.

Figure 2-25 is the photodetector output obtained during readout. Recovery of the frame sync information is obtained by processing this signal. Figure 2-26 is a functional block diagram of the electronics used to extract frame sync data. The detected signal is first fed into a precision, gated, controlled-attack and controlled-decay peak detector. The signal is gated to allow the peak detector to acquire and track the peaks of the input signal only during the period immediately preceding frame sync. The location of the frame sync is known within the approximately ±6 hologram periods allocated to film transport lateral tolerance. The peak detector uses variable resistor R1 to set the attack time for peak recovery to about 20 holograms to prevent scratches and other noise sources from generating false peak information. When the "threshold acquisition gate" closes, the peak level begins to decay as set by variable resistor R2. This level will decay to near zero by the beginning of the next scan (approximately 1,500 periods later) but is essentially constant over the frame sync portion of the scan immediately following the closure of the threshold acquisition gate. This signal is then amplified by the noninverting amplifier to be used as a threshold for the second comparator. The original detected signal is compared with the threshold to generate the digital frame sync data. The four signals of interest corresponding to the signal points shown in Figure 2-26 are shown in Figure 2-27.

The recognition of the frame sync pattern is accomplished by the correlator shown in Figure 2-28. The digital frame sync data is shifted into the 7-bit shift register using the bit sync clock. The outputs of the shift register are exclusive ORed with the frame sync pattern (1100101) and the results of the comparison are sent into a majority logic gate. Recognition of the pattern occurs when the frame sync pattern or a pattern differing by only 1 bit (0100101, 1000101, 1110101, 1101101, 1100001, 1100111, or 1100100) is occupying the shift register. The frame sync pattern chosen is one of a

FRAME SYNC
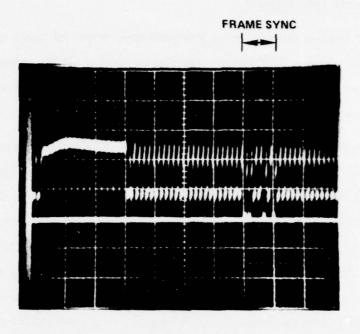
Figure 2-24. Record Reference Beam Intensity (Frame Sync Region)

FRAME SYNC

89444-72
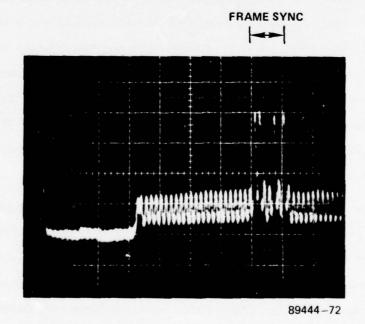
Figure 2-25. Readout Reference Beam Intensity (Frame Sync Region)
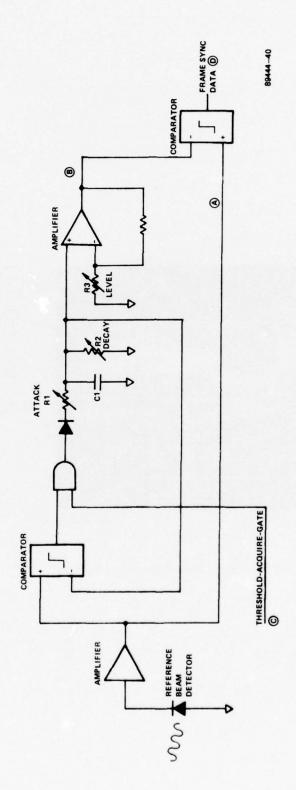
Figure 2-26. Frame Sync Data Processing Electronics

89444-40

89444-75
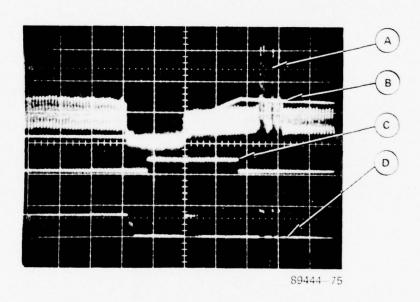
Figure 2-27.   Frame Sync Data Processing Signals

89444—41
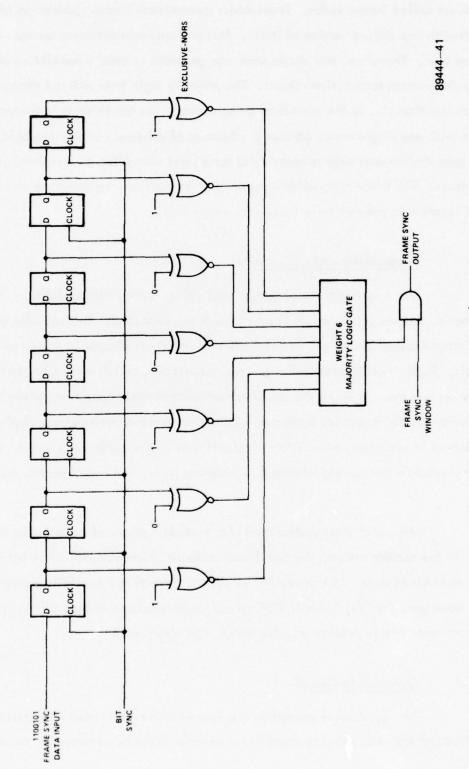
Figure 2-28. Frame Sync Correlator

special set called Barker codes. These codes guarantee minimum correlation of a pattern with any shifted version of itself. This pattern has a maximum autocorrelation level of four. Therefore, any single error can generate at most a correlation of weight five in the pattern recognition circuit. The majority logic gate will not recognize weights less than six, so the correlator always recognizes the frame sync pattern, or the pattern with any single error, correctly. Because of the decay of the threshold, the frame sync digital data only remains valid for a short time after the threshold acquisition gate closes. The frame sync window opens only during this period of time around the known location to prevent false frame sync recoveries.

2.1.6   Operability and Diagnostics

For a system to be of operational value, even in an exploratory development mode, the complexity of its functions must be minimized. This includes both direct simplification of design, and reduction of required operator interface with system controls. Such simplifications have two major functions. First, they simplify the procedures and thus minimize the risk involved in any system operation, permitting the exploratory system to provide maximum information to the experimenters. Second, the inclusion of at least some operability considerations in the exploratory version of a system provides a base of experience on which any later, less experimental, system may draw.

An exploratory system must also provide a means of assessing its performance. In the current system, the significant measure of performance is the bit error rate of the reproduced data. In this section we discuss some of the operability considerations which have gone into the Phase II WBR system, and also some of the techniques with which bit error rate is determined, displayed, and interpreted.

2.1.6.1   Operability Design

The experience gained on the Phase I system indicated that considerable simplification and shortening of operational routines could be obtained by the addition

of a few relatively simple techniques and devices. The additions made to the Phase II system fall into three basic categories:

- Reducing the number of required operations, by making some adjustments automatic or unnecessary;

- Using new techniques or devices to simplify the desirable or unavoidable operations;

- Adding methods of monitoring the status of various elements of the system for possible necessary adjustment.

Specific methods for aligning and operating the EDM system are described in Paragraph 2.3.1 on record and readout procedures. The present discussion will be limited to presenting a few examples of operability improvements in the above three categories as implemented in the WBR Phase II system.

Automating or Eliminating Adjustments

The main feature of the Phase II system which falls into this category is the addition of a beam pointing servo mirror system just after the laser source. This servo system receives feedback from a four-quadrant detector located about 2 meters farther down the optical path. The feedback is used to control a piezoelectrically adjustable mirror, which can thus effectively remove any pointing angle variations in the laser output. This has significantly shortened the time necessary for system alignment.

It should be noted that the laser beam can be affected by thermal drift in two ways: pointing angle and lateral position. The servo system described above is able to remove only the pointing angle drift. Therefore, we can anticipate that significant additional gains in the system stability and alignment time could be made by the closing of an additional servo loop around the remotely adjustable decentering plate units already installed in the system.

Simplifying Necessary Adjustments

Several improvements in the Phase II system fall into this category:

- Beam Imaging Test Fixture. This device permits a magnified image of the light that will form the hologram to be cast on an appropriate screen. This facilitates such alignment procedures as setting slit jaws, reference beam intensity balance, and data beam intensity balance (see Paragraph 2.3.1 for descriptions of the purpose of these alignment procedures).

- Timing Slit Test Fixture. To determine exact overlap between signal and reference beams during alignment, the time of their coincidence in the film plane with this slit is measured. The slit also provides a preliminary signal for use as a stable oscilloscope trigger source.

- Reference and Signal Beam Detection. All alignments involving timing and temporal sequencing are made considerably simpler by PMT detection and oscilloscope display of the two beams. This also allows monitoring of these signals during and after an exposure run.

- Electronic Test Modes. Temporal modulation of the light beams can make some optical power measurements ambiguous. This has been prevented in Phase II by the use of special electronic test modes, which permit the modulation to be stopped while the power measurements and certain alignment procedures are done.

Monitoring System Status

Some of the devices and techniques which permit remote monitoring of critical parameters relating to system performance are:

- Remote Power Measurement. Beam power in the Phase II system can be determined for several critical locations using remotely activated detectors. These two-position detectors move into the beam and send a light-intensity-proportional signal to a display on the electronics

panel. Standard readings characteristic of optimum system alignment have been established for each remote detector.

- AOPC Thermal Sensing. The temperature of the page composer is critical to both crystal safety and optical performance. Thermistors integral to the AOPC (see Paragraph 2.2.4) send temperature information to another front panel display. Transducer temperature is continuously displayed, with heat sink temperature available using a momentary contact switch.

- Film/Spinner Synchronization. The relative phase of read beam and film rows is an important readout parameter. A mirror device which produces an image of the film as it passes through the read station in the air platen makes adjustment of this phase relationship a simple matter.

2.1.6.2   Readout Diagnostics

The analysis electronics section processes the retrieved signals to provide alignment, diagnostic, and performance information. The following signals are processed: ID data, bit sync, frame sync, and digital data.

The ID Data is processed to determine the location of the data being accessed. This information is used to realize partial film readouts, film defect analysis, and other diagnostic procedures.

Bit sync provides the clock for the input of frame sync data and digital data. The final recovery of frame sync is gated by a window function to enhance data analysis. This window, based on the recovery ID data, provides a vertical (along film) gating function. Analysis may be performed on any contiguous block of scans on the film. A subset of this window allows, for example, the inspection of scans recorded by a single spinner facet or the exclusion of all scans made by a single spinner facet for diagnostic purposes.

Two digital data channels are processed by error correction and error analysis sections of the readout electronics. If the data stream present is one of the eight coded channels, the error correcting decoder processes the data before error analysis is performed. The error analysis is performed by two different error detection schemes. In the first, referred to as AF, the analysis is based on a property of PN sequences which allows the next bit to be predicted by processing the previous 9 bits of the sequence; the circuit used is shown in Figure 2-29. One problem encountered with this circuit is that any single error generates a burst of five indicated errors. Also, burst errors, within a length of 9 bits, do not necessarily each generate five indicated errors. Thus, the true error rate is the indicated rate divided by five, but only if the errors are random. The main advantage of this circuit is that the error detector is self-synchronizing and will recover from a bit slip within the following 9 bit times.

2-60

89444—60
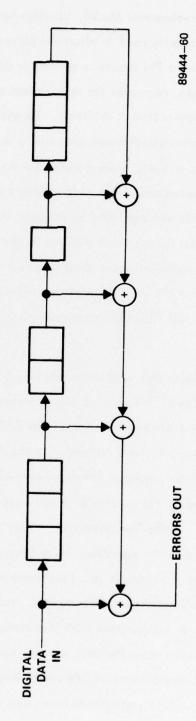
Figure 2-29. "AF" Error Detector

In the Exploratory Development Model, bit slips have been nonexistent, and this error detector has been primarily used to align the second error detection scheme, DD. This scheme, utilizing a PN sequence generator functionally identical to that used to create the recorded data, recreates the data stream and compares the detected data stream with this reconstructed data stream. To perform this task the circuit, shown in Figure 2-30, must be provided with frame sync and a sequence prefix. The prefix properly positions the generator so that, when enabled by the frame sync, the detected and generated data sequences are at the same relative point. Determination of the prefix for an unknown channel is accomplished by using an AF configuration for alignment of the generator. A horizontal (along scan) window on the error analysis circuitry allows the operator to select the beginning and ending location in each scan for error detection. This window, along with the vertical window, allows the operator to select a variety of readouts ranging from full film, full scan analysis to observation of a single hologram.

The errors detected with this system are fed into a bit error rate (BER) counter circuit for numerical display. This counter counts errors and data samples as gated by the vertical and horizontal window functions. The BER displays operate in three modes: Automatic, Semiautomatic, and Manual. In the Automatic mode, the counters operate until a number of data samples (thumbwheel-selected, power-of-10) have been processed. It then displays the number of errors encountered in this sample while analyzing the next sample. In the Semiautomatic mode, the update of the BER display is inhibited until requested by the operator; this allows spot samples to be taken where the data rate divided by the data sample provides too short a time to note each BER reading. The Manual mode allows the operator to start and stop the counter on command. This feature is useful, in conjunction with the windowing functions, for single-scan error analyses. In these cases, the data sample is not an integral power of 10. One diagnostic mode allows measurement of BER based only on "false 1" errors or "false 0" errors. An operability feature implemented provides audio-visual presentation of bit error rate.

89444—61

EXCLUSIVE ON
D-FLIP FLOP
WITH LOAD
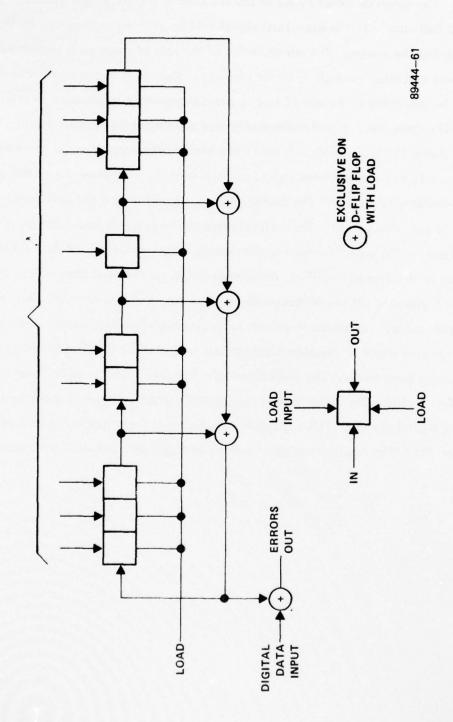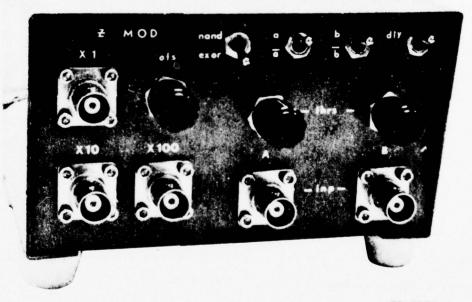
Figure 2-30. "DD" Error Detector

2-63

The errors detected by AF or DD are used to trigger a tone generator and flash an LED indicator. This audio-visual signal may be utilized as feedback by the operator aligning the system. The minimization of the rate of these error signals allows threshold level and other controls to be set properly. The errors to the audio-visual section may be prescaled by powers of four to provide maximum information at any error rate and system rate. Another diagnostic tool developed for readout analysis is the Z-mod unit shown in Figure 2-31; this unit has a high voltage amplifier driver to modulate the Z-axis (i.e., display intensity) of an oscilloscope. A typical use of this unit is a special error-density display. The oscilloscope is aligned so that the horizontal trace corresponds to one scan period. The vertical drive to the scope is modulated by a sawtooth waveform having a period equal to the desired length of the film to be studied. Errors are fed to the Z-mod amplifier, generating points on the oscilloscope face for each error. A polaroid picture of the oscilloscope during a data run records this information for further study. Longitudinal defects or scratches on the film appear on these pictures as vertical streaks. Localized defects are indicated by localized clusters of points, denoting burst errors. The Z-mod unit also has provisions for error correlation analysis. This includes digitizing analog signals and performing logical operations on the resulting digital signals. This capability may be used, for example, to correlate optical noise (from film base scattering or surface damage) with detected data errors.

76−2369

Figure 2-31. 2-MOD Unit

2.2   SUBSYSTEM DESCRIPTION

Now that an overview of the WBR system as a whole has been presented, we will add some details of the operational characteristics of the major subsystems. Many of these subsystems represent significant examples or extensions of the state of the art in their respective areas.

Subsystems to be described in this section include: Control Electronics, Optical System, Page Composer, Multifaceted Spinning Mirror, Transform Lenses, Film Transport, Fiber Optic Signal Distributor, Photodetector Array and the Recording Material and Film Processing.

2.2.1   Control Electronics

Many of the functions of the Control Electronics subsystem have been described in previous sections. However, we include here, for completeness, a *control electronics* block diagram, along with a description of some of the signals which provide coordination between the various aspects of the record and readout processes.

2.2.1.1   Functional Description

A functional block diagram of the control electronics is illustrated in Figure 2-32. The control electronics are responsible for properly synchronizing all elements of the system and for the sequencing of the system during recording.

The spinner is provided with a spinner clock and system sync information. The spinner clock controls the speed of the spinner and is automatically selected by the system rate control. System sync provides a reference signal for properly phasing the spinner facet position; this phasing is required to center the scan on the film. The spinner provides the control electronics with a once-around sync signal. This signal is used in generating the ID data recorded on the film, providing specific information about which of the 40 facets was used to record each scan; this information may be used for diagnostic purposes during system checkout and experiments.
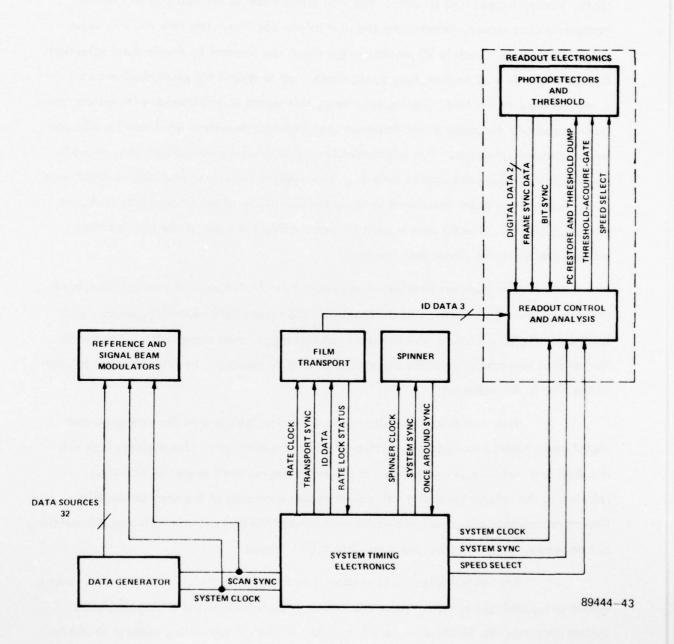
Figure 2-32. Control Electronics – Block Diagram

The film transport is provided with three inputs during recording: rate clock, transport sync, and ID data. The rate clock controls the velocity of the film transport during record, determining the row-to-row spacing. The rate clock is adjustable over an approximately 20 percent range about the nominal by thumbwheel selection. Transport sync is a 50 percent duty cycle clock used to record the phase-lock markers along the edge of the film. During recording, this signal is synchronous with system sync. During readout, the phase of the transport sync (relative to system sync) may be adjusted by thumbwheel selection. This adjustment is used to correct phase offsets introduced by the distance between the marker recording and readout stations; it also allows intentional phase-lock offsets to be introduced to study the sensitivity of bit error rate to transport phase-lock errors. The ID data is used to record along the edge of the film location markers similar to the phase-lock markers.

The transport provides a rate lock status indicator to the control electronics. This signal gives the command to start and stop the actual data recording process, and initializes the ID counter as the transport reaches operational speed. The ID output to the readout electronics provides signals which may be processed to determine the position of the film in the transport.

Two signals are provided to the data simulator and to the reference and signal beam modulation section: system clock and system sync. The system clock sets the data rate, while scan sync initiates the beginning-of-scan sequence at a time relative to the spinner sync that will assure proper centering of the scan on the film. During recording, several acousto-optic modulators (AOM's) are controlled by this section, but on readout only the parabola correction AOM is used.

The readout electronic section is provided with three inputs: system clock, system sync, and system rate. The system clock is used for internal timing purposes. System sync provides information on the location of the spinner during readout to aid in the recovery of bit sync, frame sync, and threshold information. The speed select signal is used to control filter selection for various circuits in the photodetector and sync recovery circuits for the four different readout speeds.

The photodetector-threshold section receives several inputs from the data analysis and readout control section primarily related to spinner position. The dc restoration signal and threshold dump signal reset several circuits during the blanking period between scans. The frame-sync-acquire-gate function is used in frame sync data recovery, as described in Paragraph 2.1.5.3. The photodetector-threshold section provides bit sync, frame sync data, and two digital data streams to the data analysis and readout control section.

2.2.2   Control Panel Descriptions

A fuller understanding of many of the operational routines of the WBR system may be obtained with the aid of additional information about the location and nature of the control functions available to the system's operators. Consistent with the purpose of the Exploratory Development Model (viz., to investigate implementation alternatives and to evaluate performance) many front panel controls were provided. And although they are extremely useful during this phase of the hardware development cycle, many of these controls will be internally implemented or eliminated in subsequent designs. These include recording test modes, error indicators, and controls for a multiplicity of thresholding circuits and data routing options.

In this section we describe in detail the function of each control and readout device on each of the system's key control panels, including all record, readout and diagnostic functions, and the Film Transport Control Unit.

2.2.2.1   System Control Drawer

The System Control Drawer Front Panel is shown in Figure 2-33. The controls are segmented into discrete groups according to function. The Master Clock selection function is located in the bottom left corner of the drawer. The toggle switch allows selection of the internal crystal oscillator (6.09375 MHz) or an external master clock reference. To the right is the system clock rate selector. Position A is the 600 megabit per second (Mb/s) rate, B is the 300 Mb/s rate, C is the 60 Mb/s rate, and D is the 30 Mb/s rate.

75-5539
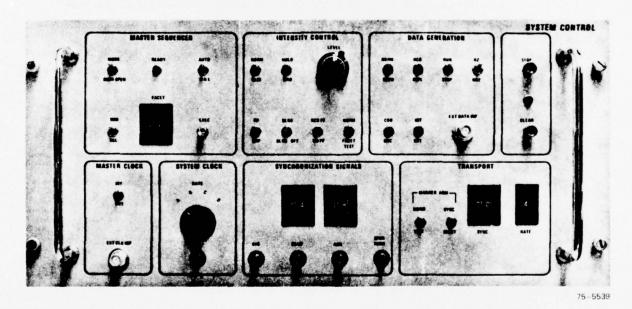
Figure 2-33.   System Control Panel

The next section controls the generation of the primary synchronization signals for the system. The bottom left test point allows monitoring of the system sync (spinner sync). The test point to the immediate right of the system sync test point provides scan sync. The position of scan sync relative to the system sync is controlled by the thumbwheel located above the test point. The thumbwheel provides 60 discretely selectable steps. The next thumbwheel/test point pair controls the generation of auxiliary sync; this signal is provided as a spare and is used extensively as a trigger source for oscilloscopes in the system. A spinner-turn-sync test point is provided at the bottom right of this section; this sync signal occurs once for each full rotation of the spinner.

The bottom right section of the front panel controls the transport functions. The pair of switches selects the mode of the transport marker AOM. The modes, controlled by the left switch, are normal and test. The test mode modulates the AOM continuously. The deflection position of the AOM is selected by the right switch, either SYNC or IDENT. The thumbwheel in the center of this section controls the vertical phasing of the transport during readout and allows the transport to be properly phased with the spinner, centering the readout beam on the row of holograms. The thumbwheel on the right selects the transport rate during record. The eight selectable rate positions allow adjustment of the record velocity over a range of approximately 19 percent about the nominal rate.

The top right section contains the emergency stop controls. Activation of the top pushbutton immediately stops the transport and closes the main system shutter. This state is indicated by the LED indicator in the center of the section and may be cleared by operation of the "clear" pushbutton.

The Data Generation section primarily controls the data generators. The top left switch selects either normal rate data generation or slow data generation. There are two slow generation rates, "two-scan" and "demonstration," selected by the switch to the immediate right. In the two-scan mode, the data presented to the

acousto-optic page composer (AOPC) changes every two scans, providing identical data in all of the holograms of two rows. The demonstration mode slows the data generation rate to a few Hz, allowing a visual demonstration of the AOPC operation. The third switch from the left may be used to stop generation at random points in the pseudo-random (PN) data sequence; this is a test and alignment mode. The top right switch selects return-to-zero (RZ), or chopped, operation of the AOPC, or non-return-to-zero (NRZ); the normal mode is RZ; NRZ is a test and alignment mode. The bottom left switch enables the pair of error correction encoders. The down position selects the uncoded PN sequence. The bottom right switch allows a single external data stream to be inserted via the BNC input at the bottom right of the section; this stream replaces one of the 32 PN sequences generated.

The Intensity Control Section provides mode selection and level control of the main AOM which controls reference beam modulation. The top left switch selects the modes of operation: normal and test. Test mode operates the main AOM continuously in one of the two active levels, hologram or guardband, as selected by the center switch. The test mode allows the intensity of the two different illumination levels to be monitored during record alignment. The potentiometer control sets the hologram level relative to the guardband level.

The bottom left switch selects one of two possible modes of hologram pro-file generation. The return-to-peak (RP) mode places guardbands between each holo-gram. Non-return-to-peak (NRP) provides a continuous hologram level for systems testing and analysis. The second switch selects a test mode that removes the blanking signal at the beginning and end of each scan. The third switch selects the two profiles available for parabola AOM correction, record profile (RCD PF) and read profile (RD PF). The bottom right switch selects a test mode where selected facets may be disabled for spinner test and diagnosis. The facets to be disabled are selected by an array of 40 switches located in the drawer.

The top left section controls the operation of the automatic sequencer. The top right switch selects the mode of the automatic sequencer. The manual mode allows all functions to free run for alignment and test purposes. The automatic position enables the automatic record sequencer. The sequence, initiated by the operation of the execute (EXEC) pushbutton, proceeds as follows. The transport is started, and when it reaches full operating speed, the ID counter is released and the main shutter is opened, allowing data recording. At the end of the film, the sequencer closes the main shutter and issues a full stop command to the transport. The READY indicator in this section indicates that all switches on the system control drawer are in the proper position for a normal recording. The switch at the top left controls the main shutter operation. In the MODE position, the shutter is closed if the system is in the MANUAL mode. When the system is in the AUTOMATIC mode, the shutter is controlled by the automatic sequencer. When the switch is in the SHUTTER OPEN position, the shutter remains open. The bottom left switch and thumbwheel were incorporated for a special test mode used to record single scan test films. This mode was considered unnecessary and not implemented.
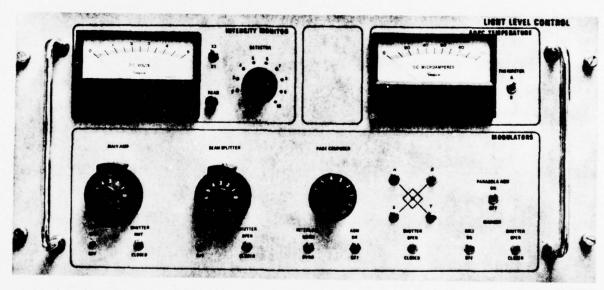
2.2.2.2   Light Level Control Panel

The light level control drawer controls the operation of the modulators in the system and provides for the monitoring of light levels throughout the system.. The front panel is shown in Figure 2-34. The lower left corner of the drawer contains the main AOM and main shutter controls. The left switch enables or disables the operation of the main AOM. The RF attenuator located above this switch controls the RF power delivered to the main AOM. The next switch selects the main shutter mode. In the remote position, the operation of the shutter is controlled by the system control drawer.

To the right of the main AOM and main shutter controls are the controls for the beamsplitter AOM and reference beam shutter. The left switch enables or disables the operation of the beamsplitter AOM and the right switch opens or closes the reference beam shutter. The RF attenuator above the switch controls the RF power to the beamsplitter AOM, allowing adjustment of the ratio of signal-beam-to-reference-beam intensities.

The next group of controls operates the signal beam modulators. The left switch defeats the acousto-optic page composer (AOPC) interlocks. The interlocks operate from the AOPC crystal temperature sensors and airflow detector to prevent inadvertent thermal damage to the AOPC. The next switch enables or disables the operation of the AOPC. The right switch of this group opens and closes the signal beam shutter. The grouping of four switches above the bottom row allows any combination of the four groups of 32 channels to be operated. Each of the groups is driven by one of the four quadrature phases used to provide phase randomized holograms. The normal mode of operation is to have all four groups active, but certain tests are performed with various groupings of the four different phases. The phases are labelled α, β, γ, and δ.

The pair of switches at the right side of the drawer control the marker beam modulators. The left switch enables or disables the operation of the marker beam AOM, and the right switch opens or closes the marker beam shutter. The single switch

2-74

75-5545

Figure 2-34. Light Level Control Panel
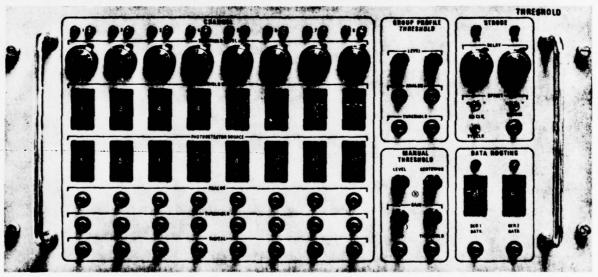
above this pair enables or disables operation of the loss-modulated parabola correction AOM.

The grouping in the top right is the display and selector for the AOPC thermal sensing thermistors. The meter indicates temperature in degrees centigrade. The momentary toggle switch allows either the AOPC transducer temperature or the heat-sink temperature to be monitored

The section in the top left corner of the drawer allows light intensities throughout the system to be monitored. The intensity monitor may be absolutely cali-brated or used as a relative level indicator. Each detector is adjusted by the inclusion of neutral density filters in the detector unit and by potentiometer adjustment internal to the drawer. The toggle switch selects meter sensitivity: times 1 or times 3. The rotary switch chooses the detector to be accessed. The pushbutton activates the sole-noid of the selected detector unit to position the detector in the beam to be monitored.

2.2.2.3 Threshold Drawer Front Panel

The Threshold Drawer processes recovered analog information yielding three digital outputs: bit sync, frame sync data, and digital data. This drawer's front panel is given in Figure 2-35. Bit sync and frame sync data are recovered as described in Paragraph 2.1.5. Bit sync is further processed by the strobe controls in the top right corner of the drawer. These controls allow continuous delay adjustment of the bit synchronous clock to properly center-sample the processed analog data sources. There are two continuous delay modules. One is for system readout rates A and B, the second for system readout rates C and D; LED indicators identify the selected delay module. The appropriate delay line is selected by the system rate control on the System Control drawer. Near each delay line is a horizontal switch which may be used to introduce a π phase offset. The toggle switch in the lower left corner of this section selects either the recovered clock or system clock. System clock is used for certain system alignment modes where the normal recovered clock is not available. The test point allows monitor-ing of the generated strobe. There are no front panel controls for frame sync data recovery.

75—5531

Figure 2-35. Threshold Control Panel

The drawer contains eight processing units or channels to recover digital data. The controls for these eight units occupy the left two-thirds of the drawer. Each unit has a pair of LED indicators, a threshold level potentiometer, a threshold source selector, a photodetector source selector, an analog data test point, an analog threshold test point, and a digital data test point. The LED's indicate which channels are selected for BER analysis. The two thumbwheels in the bottom right of the drawer select the channels to be processed. The digital data from the two selected channels are processed by the dual BER electronics in the readout drawer. The potentiometer adjusts the gain for the threshold level. The threshold source thumbwheel selects one of the four available thresholds for data recovery:

1. Group profile threshold No. 1,

2. Group profile threshold No. 2,

3. Manual threshold,

4. Adaptive threshold.

Each of these threshold techniques is discussed in Paragraph 2.2.9. The photodetector source thumbwheel selects one of the eight photodetectors to be processed by the channel. The analog test point provides the analog data signal. The threshold test point provides the threshold being used to digitize the data. The digital test point provides the digital data recovered by the channel.
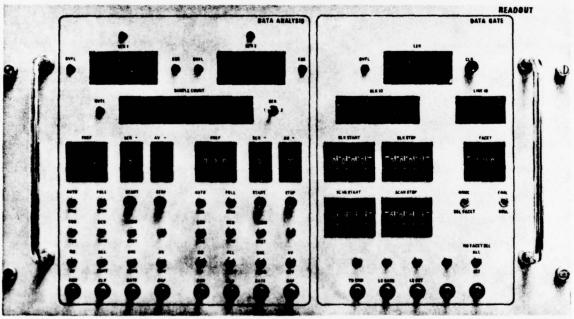
The Group Profile Threshold section controls the generation of the two group profile thresholds described in Paragraph 2.2.9. The Manual Threshold section contains four potentiometers to set the overall gain, the centering, and the left and right gains as described in Paragraph 2.2.9. The test points allow monitoring of the input reference ramp and the generated threshold.

2.2.2.4   Readout Panel

The readout drawer processes and analyzes the recovered digital information it receives from the threshold drawer: bit sync, frame sync data, and digital data. The processed ID data is also displayed. The readout panel is shown in Figure 2-36.

The right side of the drawer is related to generation of the data gates or windows used in readout analysis. The top display presents the line error rate (LER). The LER indicates the number of failures to recover frame sync. The pushbutton is utilized to reset the display. The two displays immediately below the LER display present the processed ID data. This indicates the block (a block is 40 scans) and facet associated with the scan currently being processed. The three thumbwheels below these displays are used in setting the vertical window discussed in Paragraph 2.1.6.2. The block-start and block-stop thumbwheel groups set the inclusive vertical limits for processing. The "facet" thumbwheel group is enabled by the toggle switch below. In the normal position, all scans in the selected blocks are recovered. In the single facet position, all scans associated with the selected facet are either recovered or ignored. Either recovery or rejection mode is selected by the second toggle switch. The far right toggle switch on the bottom row of switches allows scans read out by selected facets to be ignored. The facets are selected by a 40-switch array in the system control drawer. The bottom three test points provide the threshold-dump signal, the frame sync (line sync) gate, and the frame sync (line sync) detect signals. These signals are discussed in Paragraphs 2.1.5.2 and 2.1.5.3. The bottom two thumbwheel groups set the horizontal window function. The thumbwheels determine the first and last holograms of a scan to be analyzed. This allows partial scan analyses to determine error statistics as a function of scan location.

The left half of the drawer contains the controls for the dual BER processor as discussed in Paragraph 2.1.6.2. The top LED's are visual indicators for the audio-visual BER presentation. The top numerical displays indicate the number of errors in a data sample. The LED's to the left of the display indicate when an overflow has occurred. The LED's to the right flash to indicate that a sample has been completed.

2-79

75-5541

Figure 2-36. Readout Control Panel

The display below the error display indicates the number of data samples taken. The toggle switch selects the BER processor to which the display is connected. The thumb-wheels control three functions: prefix selection, sample number selection, and the audiovisual prescale. The prefix thumbwheels allow the three-octal-digit prefix associated with a recovered scan to be selected. The "BER divide" thumbwheel selects the number of samples to be processed by the BER counters; the number of samples is 10^N, where N is the number selected. The "audiovisual prescale" thumbwheel selects the power of four used to prescale errors before presentation on the audiovisual displays. The top row of switches controls the modes of the BER counters. The modes are full automatic, semiautomatic, and manual. The start pushbutton allows updating of the BER display in the semiautomatic mode and clears and starts the counters when in the manual mode. The stop pushbutton stops the counters when in the manual mode. The second row of switches controls the operation of the error correcting decoder. The left switch sets the decoder for coded or uncoded data channels. If the channel is coded, the second switch may be used to inhibit the corrective action; this is useful to observe the correcting power of the decoder. The third switch selects one of two different modes of error correction capability in the decoder: burst and random. Only the random mode was implemented in the present system, and this switch is not used. The fourth switch is a spare.

The bottom row of switches controls the error detection electronics and the audiovisual electronics. The left-most switch selects either DD or AF error detection. The next switch determines whether all errors are counted, or just "false 1" or "false 0" errors are counted. The next switch selects which of the two partial-errors options is enabled. The right-most switch of the group enables or disables the audio-visual display.

The test points at the bottom provide an error signal, a clock, a data gate signal, and an AF-type error signal. The error signal monitors the error detectors, and the clock signal is the bit synchronous clock. The data gate signal indicates the window used for data analysis, and is controlled by the window functions on the right side of the drawer. The AF-type error signal is derived from an AF-type error detector; this detector requires only digital data and bit sync. The operation of this detector is

unaffected by the control settings anywhere on the drawer, thus providing a monitoring point that is useful for the initial alignment of the system.

2.2.2.5   Film Transport Control Panel

The transport subsystem controls are grouped to provide maximum user access. The most frequently used controls are placed on the remote panel. All indicators, and seldom-used controls, are on the transport control panel (Refer to Figure 2-37).

The transport itself has two control switches mounted for easy access when working on the transport. One is a Film Tension Switch which de-energizes the spooling motors and thus relieves film tension. The second is a Power Wind Button. When this button is depressed with film tension off, the take-up spooling motor is energized with moderate power. This control, in conjunction with mechanical fixturing on the transport, provides a means of spooling and unspooling bulk film.

The Remote Panel contains the Mode Selector that is used to select Record, Rewind, Read, and Cycle Modes. The selector is used in conjunction with the Execute and Stop Buttons (also on the Remote Panel). The Hold Mode Control is on this panel and is used to advance the film one hologram row per turn of the Hold Control. The Hold Control is bi-directional. The Slew Control is also on the Remote Panel and provides a bi-directional variable slew of the film. The last control available on the Remote Panel is the Film Tension Switch.

The Main Power Switch is mounted in the lower right corner of the Transport Control Panel. Directly above it is another Film Tension Switch and a Stop Button. The next switch to the left is the Footage Indicator Zero/Preset Switch. This switch is a three-position, center-off, momentary type. In the up position, the counter is set to zero. In the down position, the film footage counter is set to the EOF (end of film) Tab setting. Directly to the left of the Zero/Preset Switch is the Footage Indicator. This indicator is bi-directional and shows the film footage on the take-up spool. Below the Footage Indicator are the film-tab thumbwheel switches. They are, from left to right, the BOF, MIN, MAX, and EOF Tabs. The BOF (beginning of film) Tab sets the
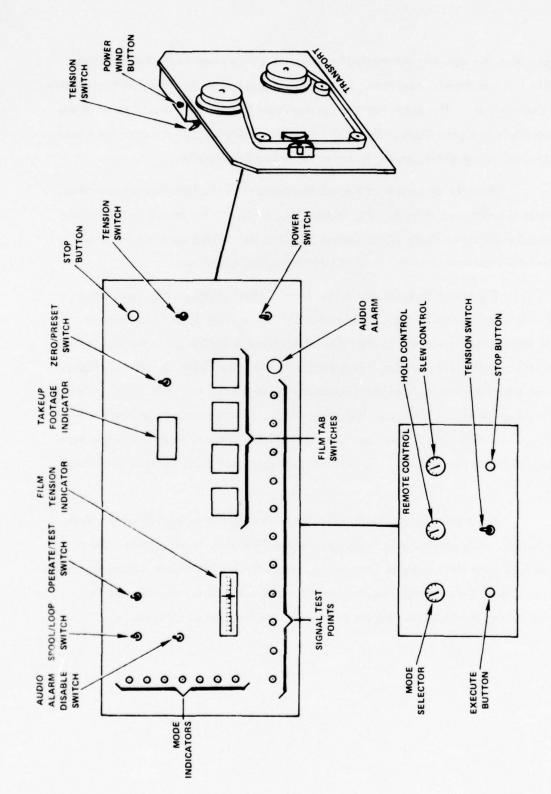
Figure 2-37. Film Transport Control Panel

TENSION SWITCH

POWER WIND BUTTON

TRANSPORT

STOP BUTTON

TENSION SWITCH

POWER SWITCH

ZERO/PRESET SWITCH

TAKEUP FOOTAGE INDICATOR

AUDIO ALARM

HOLD CONTROL

SLEW CONTROL

TENSION SWITCH

STOP BUTTON

FILM TENSION INDICATOR

FILM TAB SWITCHES

REMOTE CONTROL

OPERATE/TEST SWITCH

SPOOL/LOOP SWITCH

AUDIO ALARM DISABLE SWITCH

SIGNAL TEST POINTS

MODE SELECTOR

EXECUTE BUTTON

MODE INDICATORS

point at which the transport automatically executes a Stop when in the Rewind Mode. The MIN Tab sets the minimum footage turn-around point when the transport is operating in the Cycle Mode. The MAX Tab sets the maximum footage turn-around point of the transport while in Cycle Mode. The EOF Tab sets the film footage at which the transport executes a Stop while running in either Record or Read Modes.

Directly to the left of the tab thumbwheels is the Film Tension Indicator. This meter is calibrated in tenths of a pound of film tension. The switch just above the tension indicator is the Audio Alarm Defeat Switch. This switch turns off the Audio Out-of-Lock Indicator when only visual lock indication is desired.

The switch directly above the Alarm Defeat Switch is the Spool/Loop Switch. This switch selects the circuitry necessary for running either film loops or spooled film on the transport. To the right of the Spool/Loop Switch is the Operate/ Test Switch. In the test position, the system's signals are simulated by internal clocks. Thus, the subsystem may be operated independently of the system. A group of indicator lights are located on the left-most side of the panel. The upper-most indicator is the Rate/Phase Lock Indicator. Rate lock is indicated in the Record Mode and phase lock is indicated in the Read Mode. The remaining six indicators show the real-time mode status.

The Audio Out-of-Lock Indicator is located just to the left of the Main Power Switch. This audio indicator beeps whenever the servo is out of rate lock or out of phase lock after the Record or Read modes, respectively, have been executed. Along the lower side of the panel are located several signal test points from which servo performance may be checked. Figure 2-37 shows the location of all controls.

2.2.3 Optical System

In Paragraph 2.1.4 we dealt with the optical system on a block diagram level, with each block containing many optical components which act together to perform the function of the block. Now we provide more detailed information about the contents of those blocks, and expand important areas of the system into optical schematic form.

In this section we provide details of the recording and readout optics, including additional information on the design and performance of the critical autoscan subsystem. The requirements for the scanning Fourier transform lenses which, with the spinner, make up the autoscan subsystem are outlined. Design criteria and implementation considerations for the spinner and the lenses will will be given in Paragraphs 2.2.5 and 2.2.6 respectively.

2.2.3.1 Optical Layout Description

In Paragraph 2.1.4.1 the functional groupings of the WBR Phase II EDM optics were described; we now present a more detailed schematic view of the optical system. Figures 2-38 through 2-40 are restricted to block diagrams, since they describe portions of the system where no relevant spatial structure has been imposed on the beam (although temporal modulation does take place in these sections). Figures 2-41 and 2-42 show the regions of the system where the spatial structure is of interest.

Some elements of the system shown in Figure 2-38 were not previously described. The parabola AOM is used to vary the beam intensity synchronously with the scan across the film. Without this correction, the center of the scan would be brighter than the edges, due to the natural Gaussian profile of the laser beam. With the Parabola AOM's correction, the scanning beam's intensity is kept essentially constant across the scan. Two Decentering plates (2D DCP) are provided to allow full two-dimensional beam translation to compensate for possible drift in the output position of the laser beam. An adjustable iris serves as a repeatable beam position defining aperture and also helps block the diffracted beam from the parabola AOM.
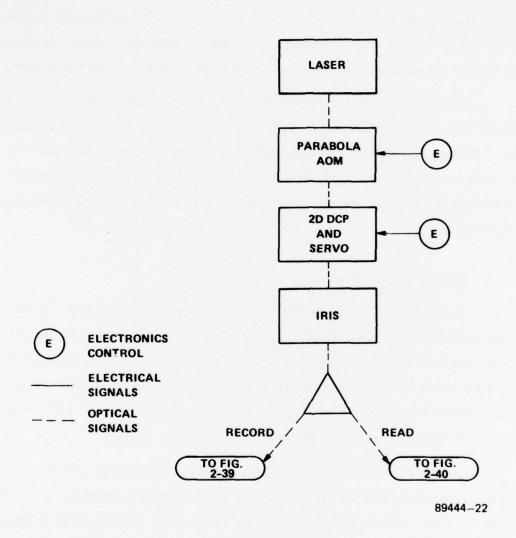
Figure 2-38. Optics Common to Both Recorder and Reader – Block Diagram

For recording, the beam continues along the path shown in Figure 2-39. The modulation and beam splitting blocks have been described in Paragraph 2.1.4. Adjustable decentering plates are then provided in both reference and signal paths, and focusing optics provide near-point-source inputs to the optics of Figure 2-41. Components shown in Figure 2-41 have the following functions:

- Cylinder and Sphere - These elements produce a line source of illumination for the AOPC. As the top view shows, the line of light is focused into the AOPC crystal.

- AOPC - The line of light is modulated into 128 optical channels (see Paragraphs 2.1.4.3 and 2.2.4 for details).

- Sphere and Cylinder - The sphere performs a two-dimensional Fourier transform on the reference and signal beams. The cylinder reimages laterally, producing at the slit a one-dimensional Fourier transform, which will later be imaged to the film.

- Forming Slit - This element is used to set the limits of resolution vertically and horizontally to filter out extraneous optical noise.

- Sphere and Scanning Lens - The light amplitude distribution at the slit is imaged, via the spinner, to the film, where it is recorded as a hologram.

- Spinner - The multifaceted spinning mirror distributes the light across the film. Since two facets are illuminated, 100 percent duty cycle recording can be achieved. More details are in Paragraph 2.2.5.

For readout, the output beam of Figure 2-38 is sent to Figure 2-40, since the modulation functions are unnecessary. The readout beam rejoins the record path at the point marked X in Figure 2-41. Some additional beam expansion optics are used to give it a size appropriate to that point. It then passes through the same scanning optics

FROM FIG.
2-38

BEAM
EXPANSION

SCANNING

FILM

DESCANNING

TO FIG.
2-42

89444–20

Figure 2-40. Readout System Optical Block Diagram

FROM FIG.
2-38

MODULATION

BEAM
SPLITTING

REFERENCE

DCP

FOCUS

SIGNAL

DCP

FOCUS

TO FIG.
2-41
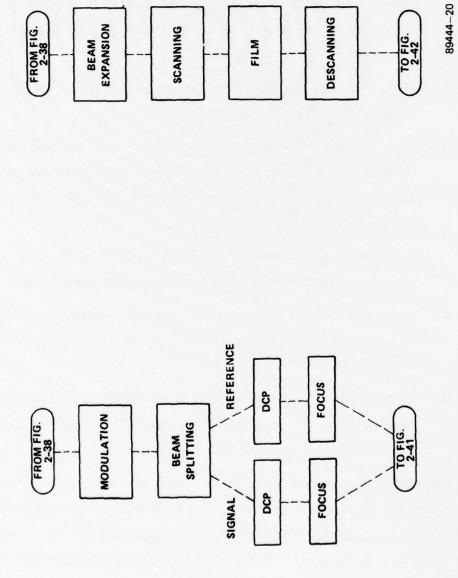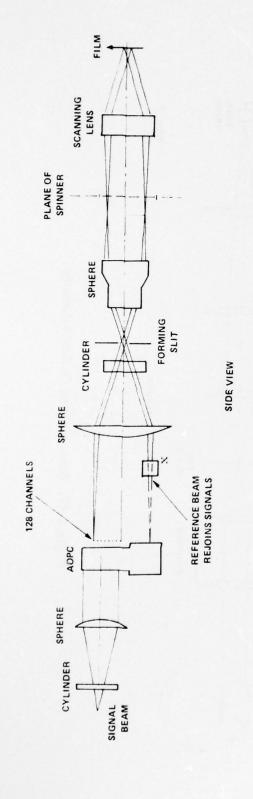
Figure 2-39. Record System Optical Block Diagram
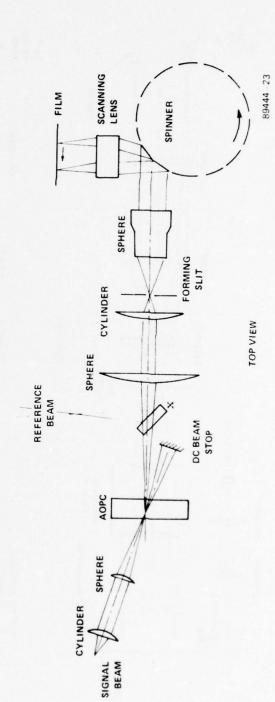
Figure 2-41. Record System Optical Schematic

89444 23
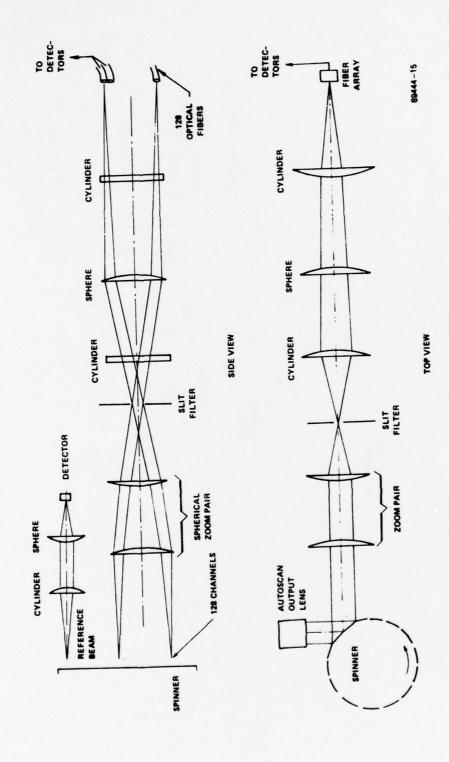
Figure 2-42. Readout System Optical Schematic

89444-15

(as in Figure 2-41) to the film, where a portion of the light is diffracted as data. The data and reference beams then are re-reflected on the spinner by the "autoscan" system described in Paragraph 2.2.3.2. Then the data and reference beams are processed as shown in Figure 2-42.

The undiffracted portion of the beam is picked off just after the spinner and focused to a detector, where it is used to generate readout clock and sync signals (as described in Paragraph 2.1.5).

The data, its center now being defined as the new optical axis, is then processed as follows:

- A spherical zoom pair is used, in combination with a later sphere, to scale the channels vertically, and also to provide channel-to-channel focusing capability (three lenses are needed to provide both capabilities simultaneously).

- A pair of cylinder lenses reimages the lateral dimension of the hologram to fit within the dimension of the optical fibers.

- A filter slit trims away any extraneous optical noise which may be generated in the film base or other optical elements.

- Finally, a fiber optic array intercepts the 128 channels and distributes them for processing by discrete photodetectors.

2.2.3.2   Autoscan

One of the keys to successful data reproduction is the ability to produce a stationary image of the data being scanned out of the film. The unique arrangement of lenses and mirrors that accomplishes this task is called an "autoscan" system, and is shown schematically in Figure 2-43. We will now give a few details of the operation of this subsystem.
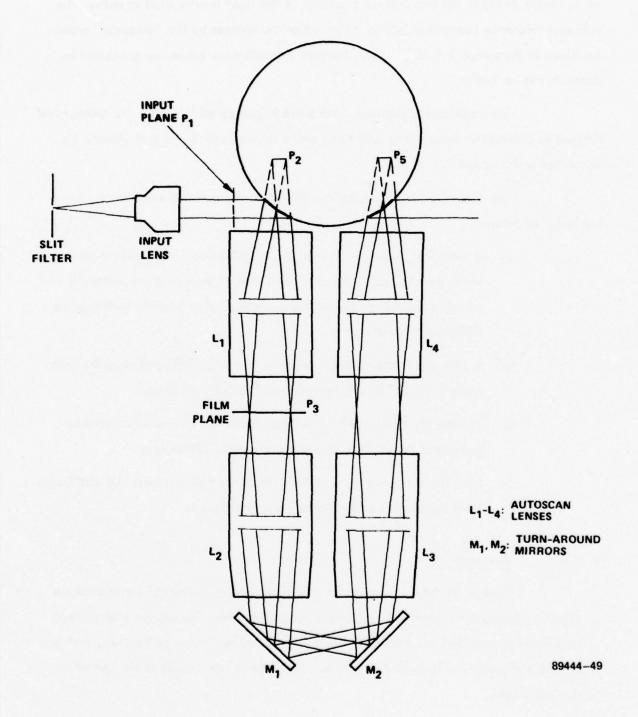
Figure 2-43. Autoscan System

89444-49

2-92

The data input to this subsystem is anamorphic by nature; thus, both the "horizontal" and "vertical" properties of this optical process should be examined. A horizontally collimated line of light illuminates the facets at the input side of the system. As the spinner turns, each facet in turn intercepts the beam and directs it toward the first lens. Due to the offset between the facets and the axis of rotation, the collimated input beams have a virtual pivot point within the spinner head at the plane marked "P_2." By locating plane P_2, the entrance pupil of the system, in the front focal plane of the lens L_1, we ensure a telecentric scan in the rear focal plane, that is, in the film plane, P_3.

Some additional details are significant to the recording process. The over-illumination at the input assures that we can achieve near-100 percent duty cycle recording, since the next facet will be fully illuminated and ready to start its scan by the time the previous scan is completed by the previous facet. Also imporant is the vertical structure of the beam. Since we wish to record true Fourier transform holograms, we need to produce vertically collimated signal and reference beams in the film plane. This is accomplished by making the plane of vertical focus of these beams coincident with the virtual horizontal pivot point within the spinner. In summary, in the film plane we have a horizontally telecentric and vertically collimated scan.

In the readout process, the function of the input components is the same, except of course that the data beams are no longer present. After the reference beam strikes the film, the reference and diffracted data beams continue through the system as shown in the diagram. The result is a one-to-one and upright image of the reference and data beams, located at the output plane of the spinner, P_5. Furthermore, since the system images the input pivot point to the output pivot point, the output facet is always in position to direct the output light parallel to its original direction. The result is a "descanned" beam, which has no residual angular component to its scanning motion. It can, therefore, be collected by the downstream optics into a stationary detector for analysis, after spatial noise is removed at a stationary filter plane.

Specific characteristics of the Lens-Spinner Autoscan System are shown in Table 2-3.

Table 2-3.   Lens-Spinner Autoscan System Data

Transform Lenses

Focal Length	80 mm
Field Size	26 mm
Resolution	7 μm
Focal Depth Tolerance	50 μm
Linearity	F-theta
Distortion	±2%

Multifaceted Spinner

Number of Facets	40
Facet Size (height x width)	1.25 inches x 0.5 inch
Rotational Speed	6,000 r/min
Facet Flatness	±λ/20 p-p
Facet Pointing Accuracy	6 arc seconds p-p
Servo System	Dual Phase Lock

The most critical parameter in the scanner's specifications is the facet flatness, which is required to maintain the tolerance on overall depth of focus during recording. Additional discussion of the Transform Lens requirements is provided in the next paragraph.

A photograph of the autoscan subsystem as implemented in the Phase II EDM is shown in Figure 2-44, including the multi-faceted spinner, the four transform lenses, and the turnaround mirrors.   In the background, the film transport with double-sided air platen and portions of the illumination and readout systems are visible.

75-5534
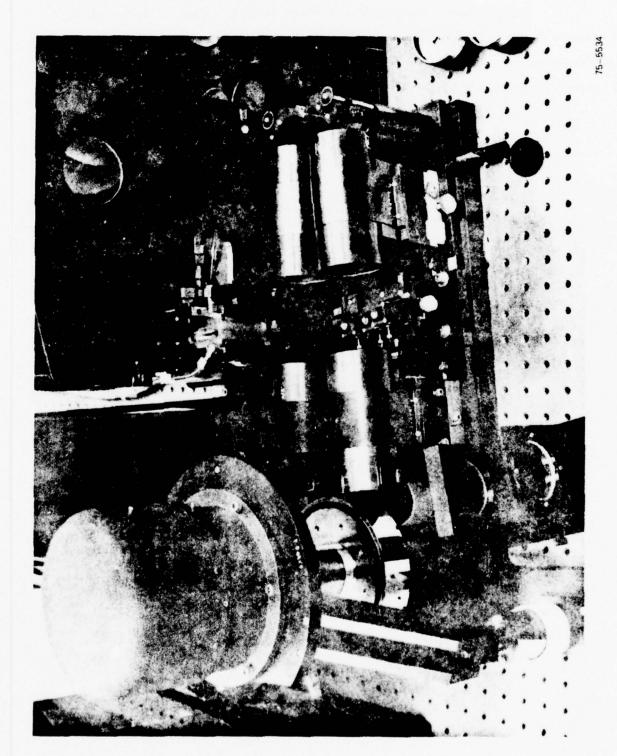
Figure 2-44. Autoscan Subsystem

2.2.3.3   Transform Lens Requirements

The principal requirements of the transform lenses (or "scanner"lenses) are associated with their ability to form the required scanned holographic imagery in the film plane while maintaining good focus and distortion-free registration of the data image as the spinner rotates. Additional constraints arise from the autoscan geometry, film transport space requirements, optical efficiency, and various other system criteria. A list of some of the performance parameters is given in Table 2-4.

The entrance pupil is located at the front focal plane of the first lens; its dimensions are 7.8 mm and 25 mm in the horizontal and vertical directions, respectively. A sequence of temporally and spatially varying coherent input patterns passes through the pupil, covering an 18° field. The scanning properties of the lens can be defined by considering the input pattern to be a single uniphase wavefront, while the data imaging properties can be analyzed by treating the input pattern as an array of incoherent line sources representing the 128 data bits.

As the spinner rotates at a constant speed, the holograms should be deflected in the film plane at a uniform velocity. This will ensure that temporally equispaced (fixed frequency) exposures will yield spatially equispaced holograms. Angular and spatial variations of lens transmissivity and vignetting should be minimized in order to provide uniform recording exposure and readout illumination, without significant bit-to-bit and hologram-to-hologram variations. A flat-field telecentric scan is needed to assure good focus on the film and a subsequent relaying of this field through three more lenses.

The data propagation through four identical scan lenses puts stringent criteria on image distortion and curvature of field. In some instances, there is cancellation of aberrations (distortion, for example) between consecutive lens pairs as long as those aberrations are identical. As a result, unit-to-unit repeatability of lens performance becomes even more important than aberration-free design. This places a very significant burden on good fabrication and testing.

Table 2-4. Scanner Lens Performance Parameters

Transform or Film Plane – Through One Lens

● Hologram recording efficiency	≥ 0.85 (85%)
● Variation in the hologram recording efficiency with bit location	≤ 0.02 (2%)
● Variation in hologram recording efficiency with spinner rotation	≤ 0.02 (2%)
● Hologram spacing error	≤ 0.3 micron (2%)
● Telecentricity error	≤ 1 minute of arc
● Focal depth error	≤ 20 micron

Output Image Plane – Through Four Lenses

● Distortion over entire output image	$\leq 10^{-3}$ (0.1%)
● Bit location error (vertical)	≤ 0.01 mm
● Bit location error (horizontal)	≤ 0.10 mm
● Focal depth error	≤ 3 mm

2.2.3.4   Engineering Considerations

The WBR Phase II EDM is a sophisticated system, containing nearly 100 optical and electro-optical components. The production of an operable and maintainable system of this degree of complexity requires that detailed attention be paid to the physical characteristics of the system, with particular emphasis on those features which have a direct impact on system performance. We will now describe some of these key engineering design features.

Alignment

Both in the initial construction of the system and in its operational routines, proper alignment is critical to system performance. The following areas have received specific design consideration for alignment capability.

- Laser - Because thermal and other effects can produce intensity fluctuations, the laser used in the system uses a light-control servo system that varies the input current to produce a more stable light output.

- Beam Position - The output beam of the laser can also drift in angular and lateral position. Accordingly, adjustable servos are provided to compensate for these drifts (additional details on this are given in Paragraph 2.1.6.1).

- Component Alignment - Detecting and correcting incorrect positions or adjustments of the optical components has been facilitated by the addition of beam-position-defining apertures and irises at various places in the system.

- Page Composer Input - For opto-mechanical reasons (see Paragraph 2.2.4) a wedged-crystal page composer design was used in the Phase II EDM. Attaining the correct light input angle to the AOPC was made easier by the addition of an input-angle adjusting device. This device is aligned only once, during system setup.

- Autoscan – The performance of this subsystem is critical to the readout process. Therefore, many of its components have been provided with alignment aids, including calibration marks and position locks.

Cleaning

Small amplitude or phase particles which occur on the optical surfaces in the early part of the EDM's light path can have serious consequences downstream. The resulting diffraction patterns or phase wedging can interfere with proper hologram formation and readout. To minimize this effect, while still providing a system which can be operable and productive in a laboratory environment, the following features are included.

- Air Filtering – A high-volume filter system removes most of the large particles in the laboratory atmosphere. This also contributes to better film surface preservation.

- Dust Covers – During normal operation, the optical components are covered to prevent exposure to any residual particles in the lab atmosphere. The covers are partially transparent, and access ports are provided for routine maintenance and alignment.

- Accessibility – Mounts for all components are designed to be either fully removable/replaceable with no misalignment, or fully accessible for periodic cleaning as necessary.

- Physical Security – Wherever possible, mounts for optical components are designed to preclude damage from inadvertent fingerprints, scratches, etc.

- Regular Inspection – A schedule of inspection and routine cleaning of component surfaces has been found to provide optimum wavefront quality and light throughput.

Thermal Effects

In several areas of the system, the monitoring and control of temperature variations are of importance, both for preventing damage to critical components and to optimize system stability. These include the following areas.

- AOM's – The single channel Acousto-optic modulators in the WBR system do not receive enough RF electrical energy to cause heating problems. The focused laser beam that enters some of these crystals, however, can be of concern. We have found that no significant problems occur at power densities below about 10^4 W/cm^2; therefore, operation of the WBR Phase II EDM has been constrained to that region. More refractory acoustic materials are available for future consideration.

- Page Composer – The light power entering the AOPC is thermally negligible. Because of its multichannel structure, however, the RF electrical energy input can be as great as 10 W continuous. The resulting thermal gradients are potentially damaging to the crystal, as well as seriously degrading to the optical quality of the throughput. For this reason, the Phase II AOPC has a remote temperature monitor station, thermal overload protection, and provision for forced-air cooling.

- System – The WBR Phase II laboratory is equipped with an air-conditioning system, to provide a thermally stable environment for the laser, electronics power supplies, etc.

Other Considerations

A few other areas of interest in the engineering design of the WBR Phase II EDM will be mentioned:

- Standardization – Wherever possible, physical, mechanical and optical characteristics of the parts and components used in the system

have been chosen to provide maximum interchangability in replace-
ment or maintainance situations.

- AR Coating – To maximize the overall system efficiency, all trans-
  missive optical surfaces have been coated with multilayer antireflec-
  tion coatings; layer thickness is matched to the optical wavelength in
  use.

- Selection and Testing – All purchased optical components used in the
  WBR Phase II system have undergone thorough interferometric testing
  and selection procedures. Several marginally unacceptable compo-
  nents from the Phase I system were eliminated in this way.

2.2.4   Page Composer

An important feature of the Phase II WBR system is its use of a multichannel
recording technique to reduce the effective operating speed of the major system compo-
nents. By converting the 128 channels of digitally modulated RF electronic signals into
128 parallel optical channels, the acousto-optic page composer (AOPC) provides a key
step in this process.

The AOPC provides both modulation and formatting of the data to be
recorded. Paragraph 2.1.4.3 provided some details of the acousto-optic process itself.
In this section we describe the nature, design characteristics, construction features,
and performance of the AOPC used in the Phase II system.

2.2.4.1   Functional Description

Description of the design and mechanical construction of the Phase II
AOPC will be done with the aid of Figure 2-45. In this cutaway drawing, most of
the important physical features can be seen in relationship to the unit as a whole.
Important design considerations for a multichannel AOPC include: maximization of
diffraction efficiency, extinction ratio, bandwidth, and useful aperture; minimization

PC CARD
SUPPORT

CRYSTAL/CARD
EPOXY BOND

GROUND PLANE

TRANSDUCER

136 ELECTRODES

REAR CRYSTAL
SUPPORT

FRONT
CRYSTAL
SUPPORT

COMPRESSION
SCREWS

THERMISTOR

HEAT
SINK

LIGHT
PATH

AIR

AIR

RF COAX
SIGNAL
CABLE

COOLING MANIFOLD
AND THERMISTOR
MOUNT

GROUND
CONNECTION

GROUND PLANE

89444-24
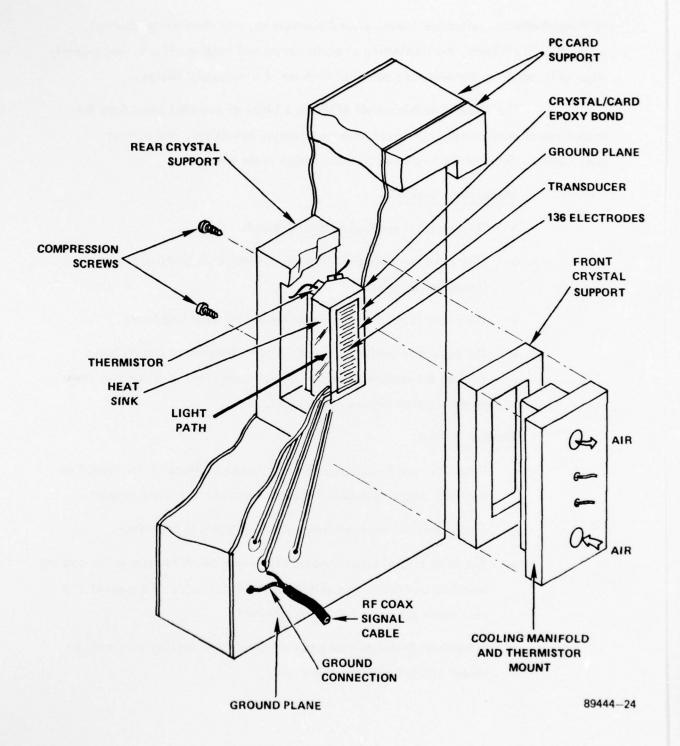
Figure 2-45. AOPC - Cutaway View

of thermal effects, reflection losses, crystal aberrations, and channel-to-channel crosstalk. In addition, the monitoring of performance and heating effects, and properly adjustable mounting hardware are essential features of a successful design.

The Phase II multichannel AOPC is a blend of essential ideas from the disciplines of mechanical, electrical, thermodynamic, acoustical, and optical engineering. Some of the key items in these design areas are:

Mechanical Design

- The crystal is epoxied to the PC board.

- Electrodes are deposited through a metal mask bridging the card/transducer interface.

- The board is edge-supported by the AOPC mounting frame.

- The crystal is held in compression onto the printed circuit board through the rear/front crystal support assembly. This removes stress on the crystal-to-card epoxy bond.

Thermal Design

- Heat sinks are mounted on the rear wedged surface of the crystal to cool the crystal and spread the compressive load of the support.

- Thermistors are mounted integrally with the rear heat sinks.

- The front crystal support mates with a rear block to form an air cooling manifold and protective shield for the electrodes. The support and rear block are of an insulating material.

- Additional thermistors are mounted within the cooling manifold, in direct contact with the transducers.

<u>Electrical Design</u>

- Transducer/PC Board grounding is achieved at the perimeter of the transducer and on the back side of the PC board with two gold-wire bonds.

- The signal-carrying lines on the PC board are stripline designed for 50 Ω nominal impedance.

- The fanout of striplines on the PC board permits direct connection from RF signal carrying coaxial cables to the PC leads.

<u>Acousto-Optical Design</u>

- The rear of the crystal is wedged to disperse the acoustic wave.

- The AOPC crystal itself is wedged to provide clearance between beam path and support structures (see below).

Some additional details of the acousto-optical design are given in Figures 2-46 to 2-48. In those figures, θ_B is the Bragg angle, θ_{in} is the incidence angle, and θ_w is the half-angle of the wedged crystal.

Specifically,

$$\theta_B = \frac{\lambda}{2n\Lambda} = \frac{\lambda f_a}{2n V_a}$$

where λ and Λ are the optical and acoustic wavelengths, respectively, f_a is the drive frequency, V_a is the acoustic velocity, and n is the optical index of refraction. In the case of the Phase II AOPC, we find $\theta_B \cong 5.1$ mr (in glass).

In interacting with a moving acoustic wave in the Bragg cell, the optical beam receives a Doppler frequency shift equal to the acoustic frequency. Figure 2-46 and 2-47 show the two possible Bragg diffraction configurations. In Figure 2-46, the incident optical beam has a motion component parallel to the acoustic wave, causing the optical frequency of the diffracted light to be downshifted by the interaction.
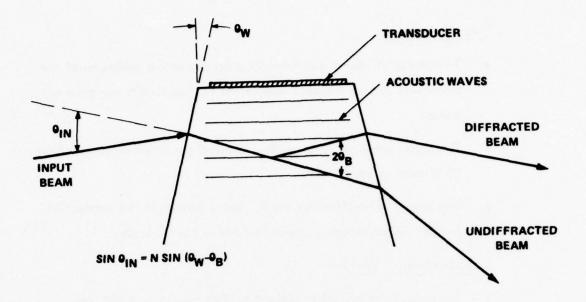
Figure 2-46. AOPC Acoustic Detail - Frequency Downshift

$$\text{SIN } \theta_{IN} = N \text{ SIN } (\theta_W - \theta_B)$$

$$\text{SIN } \theta_{IN} = N \text{ SIN } (\theta_W + \theta_B)$$

89444-13
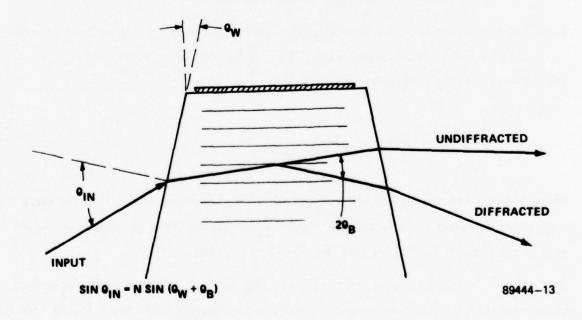
Figure 2-47. AOPC Acoustic Detail - Frequency Upshift
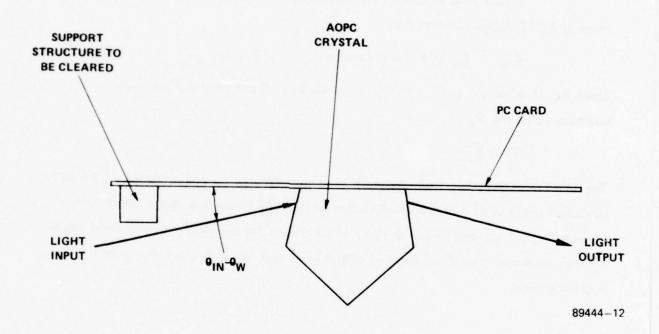
Figure 2-48.   Structure Clearance by Crystal Wedging

Figure 2-47 illustrates the reverse situation. To record holographic interference between a signal beam and a reference beam, their temporal frequencies must be identical. The Phase II system uses an acousto-optic beamsplitter to separate the beams, resulting in a downshifted reference beam frequency. By driving the beamsplitter and AOPC from the same RF source, and by configuring the AOPC in the downshifted mode of Figure 2-47, we ensure that frequency coherence is maintained.

Figure 2-48 illustrates the beam/structure clearance consideration. The Phase II AOPC design requires that

$$\theta_{in} - \theta_w \geq 4^o \text{ for clearance.}$$

Since θ_B is relatively small, $\sin \theta_{in} \cong n \sin \theta_w$. These two relations yield a minimum value for θ_w of

$$\theta_w \geq 6^o .$$

The value selected, $\theta_w = 6^o$, provides structural clearance, and produces a total beam deviation angle of 8°. The beam deviation in the WBR Phase II system is taken care of by inserting a "zig-zag" input device, which offsets the illumination beam input angle by such an amount that the diffracted output beam can continue along the optical recording path.

2.2.4.2   Specifications and Hardware Description

Listing of Specifications

The following table lists the complete specifications for the WBR Phase II
AOPC. One explanatory note is needed. The Phase II unit was fabricated with a greater
wedge angle than necessary.   Therefore, the table below includes both the actual
wedge and deviation angles and the minimum required angles.

Table 2-5. WBR Phase II AOPC Specifications

- Crystal

    Number of Elements (Electrodes)   136

    Electrode Center-To-Center Spacing 250 μm

    Electrode Height   125 μm

    Interaction Length   6 mm

    Material   SF 8 Glass

    Transducer Size   10 mm x 35 mm

- Optical

    Clear Aperture   35 mm x 10 mm

    Optical Wedge (Actual)   15°/Surface

    Optical Wedge (Minimum)   6°/Surface

    Beam Deviation (Actual)   21°

    Beam Deviation (Minimum)   8°

    Coating   MgF for 514.5 nm

    Reflectance after Coating   1.3%/Surface

Table 2-5. WBR Phase II AOPC Specifications (Continued)

- Electrical

RF Carrier Frequency	130 MHz
Card/Cable Interface Impedance	14 Ω
Digital Data Rate	6 M bit/second/channel

- Thermal

Transducer Cooling	Forced Air
Crystal Cooling	Convective
Temperature Sensing	Matched Thermistor Pair

- Performance

Insertion Loss (Including Absorption)	5.3%
Power Reflective Losses (Calculated from Interface Impedance Value)	32%
Diffraction Efficiency (Nominal, 514.5 nm	50%/200 mW

Hardware Description

Most of the physical characteristics of the AOPC unit have been given above, and a schematic view is shown in Figure 2-45. Figures 2-49 through 2-52 show various views of the AOPC as integrated into the Phase II system. Figure 2-49 is a view of the AOPC from the output side, looking back toward the input side. The light aperture can be seen, as well as the lower portion of the crystal itself. Figure 2-50 is a photo of the "rear" or non-PC side of the AOPC unit. In this picture, light travels through the unit from right to left. The pivot at the center by which pitch adjustments of the mount are made can be seen, as well as the yaw or Bragg angle adjustment control at the lower left. Figure 2-51 shows the PC side of the unit, including

76-2365
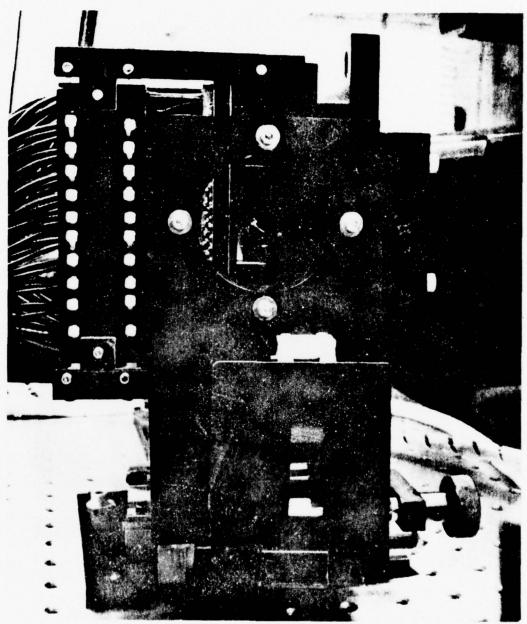
Figure 2-49. AOPC Unit — Optical Output Aperture

76-2364
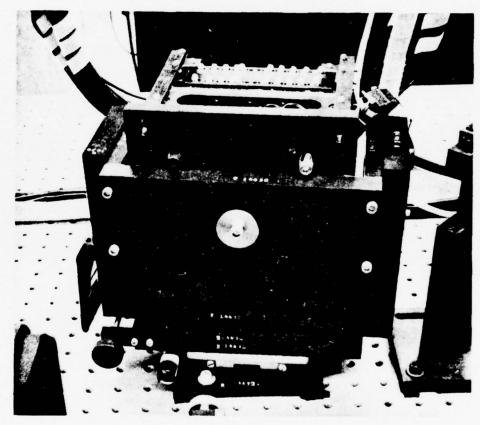
Figure 2-50. AOPC Unit - Rear View

75-5528
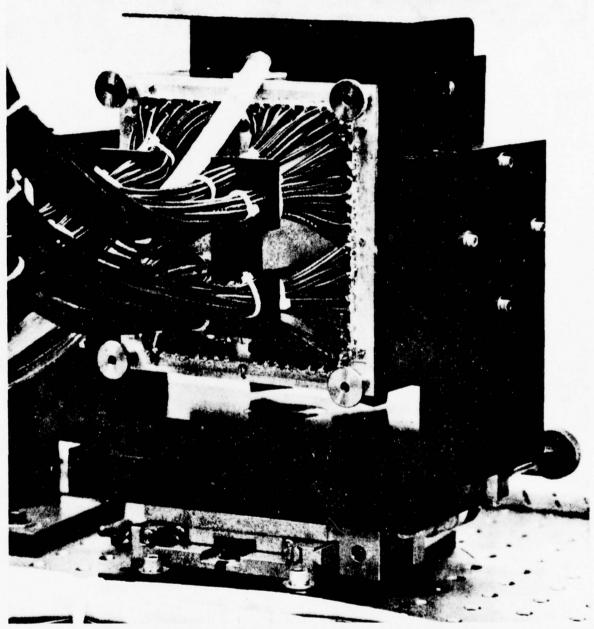
Figure 2-51. AOPC Unit - Connector Side

76-2366
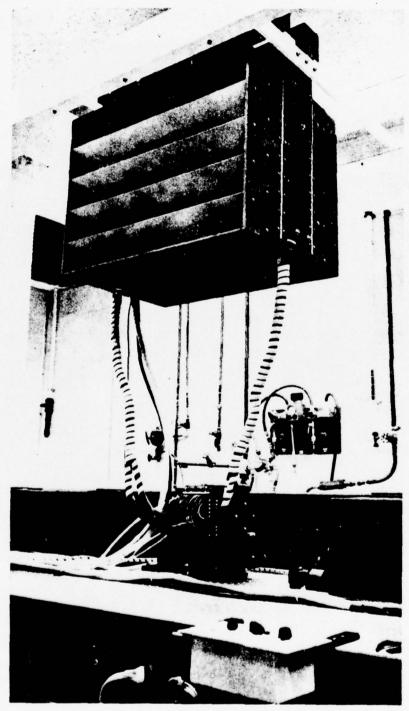
Figure 2-52. AOPC Unit and Drive Module

the RF drive cables, which carry the digital information to each channel. The connector unit through which the cables contact the PC card in this photo is not used on the final Phase II AOPC.

Finally, Figure 2-52 shows a vertical view of the AOPC and its RF drive electronics assembly, which is supported above the system and sends the data to the AOPC via 128 coaxial cables. Also visible in this photo are the cables of the thermistor temperature monitoring system, and hoses which permit the forced air cooling of the transducer portion of the unit.

2.2.5   Spinner

After the AOPC has produced the optical data, and the optical system has transformed it into the proper format for recording, the data and reference beams must be scanned across the width of the moving film. This is done in the Phase II EDM by a multifaceted spinning mirror and scanning lens. Details of the requirements for the Fourier transform scanning lenses will be given in the following section. In this section we describe the specifications and performance of the spinner unit, and some of its important design considerations.

2.2.5.1   Functional Description and Performance

Some of the key Phase II spinner specifications are given in the following table.

Table 2-6. Spinner Specifications

- **Electronic**

Speed (Maximum)	6000 r/min
Dynamic Range	22:1
Encoders	Dual: 40, 2400 bits/turn
Slew Rate (Maximum)	0.05%/sec
Timing Jitter (Maximum)	20 ns
Lock-Up Time	90 seconds
Compatibility	TTL
Clock Loss Response	Unpowered deceleration

- **Optical**

Number of Facets	40
Facet Width	0.434" ±0.004"
Facet Height	1.25" ±0.020"
Facet Figure	1/10 wave
Figure Repeatability	1/16 wave peak-to-peak
Scratch and Dig	60/40
Reflectivity (Minimum)	84%
Reflectivity Uniformity	4% peak-to-peak
Wavelength	514.5 nm
Material	Beryllium
Descan Error (Maximum)	±3 arc seconds
Dynamic Facet Repeatability (Top Speed)	±30 arc seconds
Pyramidal Angle	$0°$ ±30 arc seconds
Facet-to-Axis Angle	±15 arc seconds

Two items in the above table are of particular importance to system performance and deserve further elaboration.

The purpose of the dual-encoder phase lock system is to ensure that the facet normal vector points at the proper location (the beginning of scan) at the same instant that the control electronics begin imposing a new line of data on the optical write beam. This is achieved in two steps. First, the proper rate is achieved by phase-locking the 2400-bit encoder's output to a reference clock provided by the control electronics. Then, the 40-bit encoder's output is compared to a 40-pulse-per-turn reference signal. If they are coincident, the facets are correctly phased to the data. If not, a search procedure is initiated in which the 2400-bit encoder signal slips one bit at a time with respect to its reference signal, until proper facet/data coincidence is achieved. A maximum of 60 such slips, requiring about 90 seconds, is required for this search procedure.

Another critical element of the specification is the facet figure. This couples directly into system performance, since facet flatness is directly related to depth of focus. It can be shown that the approximate relationship between these two parameters is given by

$$\Delta = \frac{2\sqrt{2}\ F^2 \delta}{r^2}$$

where δ is the amount of facet curvature (peak-to-peak) to produce a shift of focal position of Δ; F is the scan lens focal length; and r is the beam diameter across which the curvature δ is measured. Applying the above formula to the Phase II WBR System (F = 75 mm, r = 4 mm), we see that the 16 wave peak-to-peak curvature allowed by the specification corresponds to about a 30 μm focal plane shift. This is chosen as an upper limit, since film curvature and dynamic film positioning must also receive a share of the overall depth-of-focus budget.

Subsystem Testing and Performance

After it was received from the vendor (Speedring Systems Division of Schiller Industries Inc.), the spinner system was tested to determine conformance to specification. Some of the findings include:

Facet-to-Axis Angle Error (all speeds)	±10 arc seconds
Facet Repeatability (high speeds)	±10 arc seconds
Facet Repeatability (low speeds)	±20 arc seconds
Speed Ranges	All operational
Lock-Up Time	60 seconds
Facet Figure	1/15 wave

All other specifications were met. The slight (6 percent) deviation in facet figure is inconsequential.

Some other operational features which add to the spinner system's flexibility and durability include: protection against uncontrolled reaction to loss of external clock signals; shielding against electrical noise sources; physical shielding for mirror surface protection; microadjustable leveling units for accurate alignment and system integration.

An evaluation of the performance of the Phase II spinner indicates that it has been one of the more reliable subunits of the WBR system, with all electronic specifications still being met after operating for approximately 200 hours and 50 hours at low and high speeds, respectively. Figure 2-53 is a photograph of the Phase II spinner unit integrated into the system. The optical head, motor/encoder housing, and micro-adjustable support units are visible. The control unit for the spinner system is located in the main electronics control rack.

76-2368
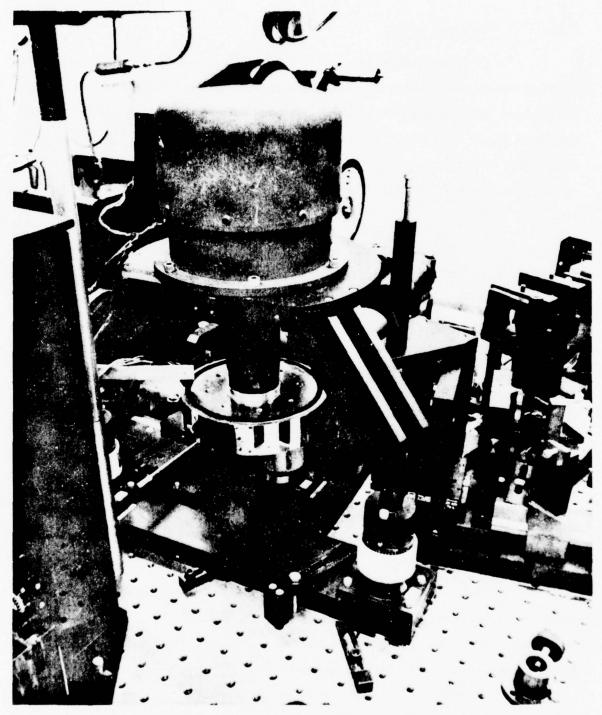
Figure 2-53. Spinner and Drive Unit

2.2.6   Transform Lenses

Of all the optical elements in the Phase II system the most critical are the scanning Fourier transform lenses. In addition to performing a Fourier transform on the 128 channels (and reference beam) which appear at the system input, they must also be capable of producing a linear, distortion-free scan across the full useful recording aperture. Also, for use in the autoscan system which was described in Paragraph 2.2.3.2, not one, but four such lenses must be fabricated to close tolerances and used as a matched set.

In this section we provide information on the methods used to design and specify these critical lenses, and also describe the resulting implementation techniques and achieved performance results.

2.2.6.1   Design Considerations

The four lens assemblies of the autoscan optical system meet a complex set of performance requirements. The first step in the lens design activity was the statement of the functional definition of the required performance in the language of the system designer. The key elements of that first design analysis were: Fourier transforms, diffraction efficiency, scanning and descanning, hologram spacing, diffraction effects, coherent anamorphic input/output, cylindrical wavefront imaging, and configurational constraints. The second step related those requirements to commonly understood optical design and evaluation language.

Historically, laser scanning lenses have been variations of microscope objectives or eye pieces, with the image format proportional to the scan angle. Because of the large scan angles and the high resolution usually required, the clearance between the entrance pupil and the lens is fairly small. Fourier transform lenses, on the other hand, have operated at moderate lens speeds or low numerical apertures, using stationary transform and inverse transform planes; long symmetrical lens designs were used to control phase properties and telecentricity. Our Fourier transform scanning lens combines the qualities of both the scanner and the transform lenses: long pupil distance, image

linearity with scan angle, excellent imagery in both directions, and large apertures and scan angles.

The highly anamorphic nature of the recorder optics increases the complexity of the design task. Holographic information as stored in the WBR system consists of coherent cylindrical wavefronts focusing orthogonally in alternate planes while computer simulation used in lens design assumes plane or spherical wavefronts with pupils and images in alternate planes. The key question can thus be identified as: Can a coherent line source and its resultant cylindrical wavefront be considered equivalent to a set of independent, incoherent point sources, thus making conventional design treatment possible? Such an equivalence is established by replacing the line source-to-orthogonal line transformation problem with a twofold analysis, consisting of point-to-plane and plane-to-point transformations.

First, a conventional "forward" analysis is performed, as illustrated in Figure 2-54. This configuration is considered to be the normal direction of design and evaluation for a lens. The significance of this simulation mode is apparent from the following observation. The data and reference beam input bundle can be considered to be the composite of three effects: an amplitude mask, a phase mask, and a coherent planar illuminating wavefront. The hypothetical amplitude mask, located in the entrance pupil at plane P_2, contains the instantaneous information concerning the time-varying data bits, i.e. logic ones are represented by appropriate transparent areas, while logic zeroes are opaque. The phase mask is a four-level, fixed-pattern phase delay generator that simulates the page composer phase randomization effects. The phase is constant over each data bit area, and varies only by an additive $\pm 90°$ constant between adjacent bits. The illuminating wavefront is swept through a $\pm 9°$ angle corresponding to the deflection generated by one facet of the 40-sided spinner. The "forward" computer design analysis ignores the diffraction effects generated by the two masks and treats only the coherent illuminating plane wave.

P₂

SIDE VIEW

P₃

FILM
PLANE

26.4 mm = f/3

ENTRANCE
PUPIL

7.8 mm = f/10

TOP VIEW

±9° FIELD

89444–82
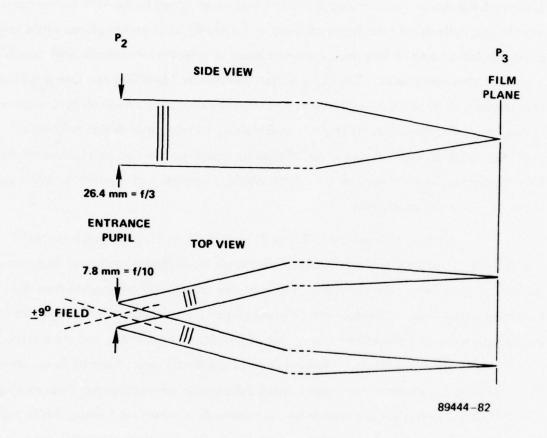
Figure 2-54. Optical Schematic for "Forward" Computer Simulation

The mode parameters defining this configuration are the following:

- Desired effective focal length: 78 ± 3 mm

- Entrance pupil is located at the front focal plane

- Pupil size: 7.8×26.4 mm, i.e. f/10 x f/3

- Object is at infinity (plane wavefront)

- Object subtends $\pm 9°$ in the f/10 direction

- Image plane at the film (back focal plane, P_3)

- Nominal image format: 25 mm, linear with angle (f-theta lens), distortion less than 2%

- Image quality: wavefront in the f/10 direction good to $\lambda/16$ at all scan angles, wavefront errors in the f/3 direction should not exceed $\lambda/5$ per mm

- Front focal length: 50 mm minimum for adequate spinner clearance

- Back focal length: 25 mm minimum to allow film transport clearance

Evaluation in the focal plane provides the most critical data about the recording process: field flatness, image quality, linearity, distortion, effective focal length, and field size.

The second simulation mode, the "reverse" mode, traces light back through the lens. The 0.78 mm by 25 mm hologram recording area now becomes the entrance pupil through which collimated wavefronts are imaged back towards the spinner. In this mode, shown in Figure 2-55, we perform the following checks:

1. To assure good data bit focus on readout: check the phase across the wavefront in the direction associated with the 0.780 mm hologram length; repeat at approximately 1.0 mm increments across the wavefront in the direction associated with the scan. Evaluate at different angles corresponding to various bit locations in the P_2 plane.

SIDE VIEW

0.78 mm = f/100

ENTRANCE
PUPIL

25 mm = f/3.1

TOP VIEW

P$_2$

P$_3$

89444–81
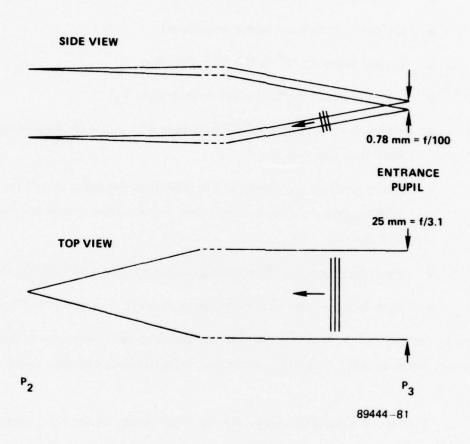
Figure 2-55. Optical Schematic for "Reverse" Computer Simulation

Requirement: ±0.03λ maximum variation across the wavefront aperture associated with the 0.780 mm hologram length.

2. To maintain good telecentricity and to eliminate vignetting: check the phase variation across the wavefront in the direction associated with the scan.

    Requirement: ±1.33λ per mm across the 25 mm scan.

In summary, two major computer simulations are performed: a forward wavefront analysis and a reverse wavefront analysis. On each of these simulations, a complex set of checks is made to ensure full compliance with system requirements. The forward mode controls lens performance characteristics associated primarily with recording, while the reverse mode optimizes the image quality of the retrieved data bits and assures the propagation of the full data package through the four autoscan lenses without vignetting.
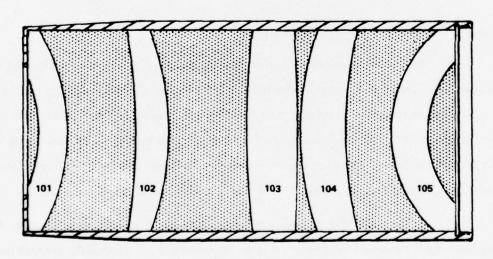
2.2.6.2   Implementation and Performance

An iterative cycle of optimizations and evaluations was performed using both computer simulation modes. The imagery of parallel light through P_2, focusing on P_3, i.e., the image quality criterion of the forward simulation mode is the dominant factor in determining the complexity of the lens. In this mode, relatively large instantaneous f/numbers are used to exacting tolerances. The final Fourier transform scanner lens (Figure 2-56) contains five elements in a nearly symmetrical configuration.

In the past, the optical performance predictions of a sophisticated lens often far exceeded its measured performance after manufacture. To properly predict actual performance of the real lens, to adequately tolerance manufacturing drawings, and to determine if a certain design approach is even feasible to pursue, tolerance analyses are run during optical optimization. If computer predictions indicate sensitivity to index, surfaces, or mechanical placement, modifications are made at the prototype level until satisfactory insensitivity has been achieved.

During the design phase these analyses were performed, indicating that all optical and mechanical requirements can be met, and that the fabrication difficulty

ELEMENT NO.	101	102	103	104	105
RADIUS 1	-40.84	-170.69	249.55	86.54	38.56
THICKNESS	8.25	9.99	14.77	13.85	10.63
RADIUS 2	-55.78	-79.63	-584.02	121.21	30.90
AIR SPACE	19.99	22.33	0.53	13.37	—

GLASS TYPE SF6

Figure 2-56. Scanning Fourier Transform Lens

should not be prohibitive. Due to the complex nature of the requirements and the high confidence level achieved during design, only complete assembly-level testing was performed on each of the four lenses.

The overall results were very satisfactory. Conventional MTF measurements were made and in all cases they showed close correlation with computer predictions. Distortion and focal length measurements showed more variation from lens to lens than anticipated. The effective focal length at the 6° field point varied from 80.7 to 82.2 mm. To accommodate this variation in the autoscan system the lenses had to be selected in pairs having approximately equal magnification. This indicates that much tighter tolerances will need to be specified in a system requiring parts interchangeability. The star test indicated good image formation with only a slight indication of a decentering flaw in one lens. The interferometric test showed good flat field scan performance for all lenses, and good reverse performance, indicating acceptable curvature of field in the bit plane. Transmissivity measurements indicated 96% transmission at 514.5 nm, far exceeding the required 85%.

Testing in the WBR system, while confirming full compliance with design objectives, delineated some areas where further improvement may be necessary.

- The precise matching of focal lengths is not possible without some adjustment (a small vari-focus capability).

- For complete interchangeability it is not sufficient to specify the effective focal length; the principal plane separations also must be equal.

- While 2% distortion is perfectly acceptable as long as it is identical in all lenses, variations in the amount and type of distortion must be tightly controlled.

- A tighter specification is needed for curvature of field in the bit-to-bit direction. The cumulative effects of four lenses currently make that performance rather marginal.

2.2.7 Film Transport

The storage capacity of a recording system is usually related to the surface area of the recording medium. Access to a large surface area, as is required for high speed or high capacity memory systems, requires that the storage medium be transported rapidly past the record/read station. The Phase II WBR is both a high-speed (6×10^8 user bits/second) and, for an EDM, a relatively high capacity (1.2×10^{10} bits) system. It therefore uses a fairly sophisticated film transport system to permit distribution of data along the length of the film in use.

The film transport's key specifications include: the use of 35 mm film in lengths up to 250 feet; a rate-locked recording and phase-locked playback speed of 3.8 m/s; and an air-bearing platen to control the film's focal position. These and other important features of the film transport subsystem are described in this section. Information is also provided about the specifications, mechanical and electromechanical design, servo design, performance achievements, and operational routines of the Phase II transport unit.

2.2.7.1 Performance and Requirements
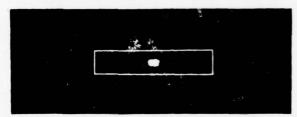
The performance of the servo was measured and is compared with the requirements in Table 2-7. Photographs of actual rate and phase jitter are shown in Figures 2-57 and 2-58, respectively. The photographs in Figure 2-57 are of the 100th pulse after the trigger pulse of the tachometer encoder feedback signal. The horizontal sweep was adjusted so that one centimeter represents 1 percent frequency change in the feedback signal from the tachometer-encoder. The boxes show the maximum allowable rate jitter at the four operating speeds. The photographs in Figure 2-58 are of the feedback synchronization markers after the scope was triggered on the system read clock. The horizontal sweep was adjusted such that 1 centimeter equals 10 percent phase jitter between the input clock and the feedback synchronization markers. The boxes show the maximum allowable phase jitter at the four operating speeds.

Table 2-7. Transport Servo Specifications
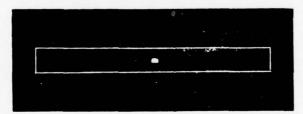
TRANSPORT PARAMETER		HOLD	SLEW	RECORD	REWIND	READ	CYCLE
				MODE OF OPERATION			
CREEP		0	N/S				
JITTER AT SPEEDS	A	±50		$\pm2\%$		$\pm5\%$	±50
	B	±50		$\pm2\%$		$\pm5\%$	$\pm5\%$
	C	±50		$\pm4\%$		$\pm10\%$	$\pm10\%$
	D			$\pm4\%$		$\pm10\%$	$\pm10\%$
ABSOLUTE RATE			$0.001 - 1 \dfrac{M}{SEC}$	$4 \pm0.4 \dfrac{M^*}{rp}$			
LOCKUP TIME		0.5 SEC		1 SEC		2 SEC	2 SEC
REWIND TIME					60 SEC		

*MARKERS/RATE PULSE
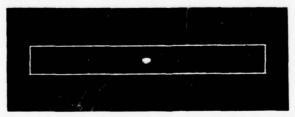
SPEED A (WINDOW ±2%)

SPEED B (WINDOW ±2%)

SPEED C (WINDOW ±4%)
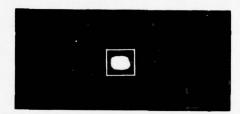
SPEED D (WINDOW ±4%)

Figure 2-57. Film Transport Rate Jitter – Measured Versus Specified

2-130
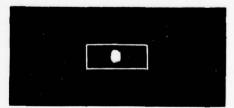
SPEED A (WINDOW ±5%)

SPEED B (WINDOW ±5%)

SPEED C (WINDOW ±10%)

SPEED D (WINDOW ±10%)
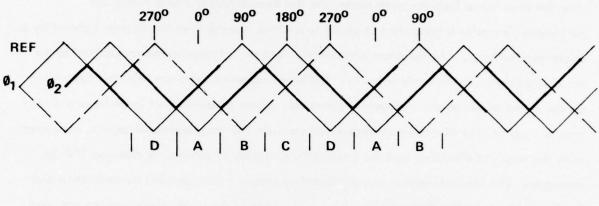
Figure 2-58. Film Transport Phase Jitter – Measured Versus Specified

89444-66

2.2.7.2 Functional Description of Mode Control

The film transport has several modes of operation. When operated in Record, Rewind, Read and Cycle modes, the servo is phase locked. It operates as a rate lock servo while in Slew mode and a position lock servo when in Hold mode. When operated in Hold mode, the two-phase analog marker feedback signal is servoed to a two-phase analog reference signal generated by the Hold Control. The differential voltages between the reference and the feedback of both quadrature phases are derived continuously. These two error voltages are then inverted, making available both the error voltages for the quadrature phases and their complements. One of the four error voltages is selected by a switching scheme as the position error. Phase II of the reference is compared with both Phase I of the reference and its complement. Anytime Phase II is less than both Phase I and its complement, quadrant A is indicated and the Phase I error voltage is selected as the position error. When Phase II is less than Phase I but greater than the Phase I complement, quadrant B is selected. In that case, the Phase II error voltage becomes the position error.

Anytime Phase II is greater than both Phase I and its complement, quadrant C is selected and the inverted Phase I error voltage becomes the position error. When Phase II is greater than Phase I and less than the Phase I complement, quadrant D is indicated and the inverted Phase II error voltage is selected to be the position error. Hysteresis is used at the points of switching to prevent oscillation. Figure 2-59 shows the basic timing and logic diagrams. The position-error voltage is then passed through the Hold mode compensation network and mode selector and is presented to the servo amplifiers.

When the transport is operated in the Slew mode, a rate loop is used. Phase I of the tachometer/encoder is inputted to a frequency-to-voltage converter. The resultant voltage is inverted, providing the rate signal voltage and its complement. A direction command is also derived from Phase I and Phase II of the tachometer/encoder. The direction command selects either the rate signal or its complement to be differentially compared with the Slew control voltage. The resultant rate error voltage is compensated and passed through the mode selector to the servo amplifier.
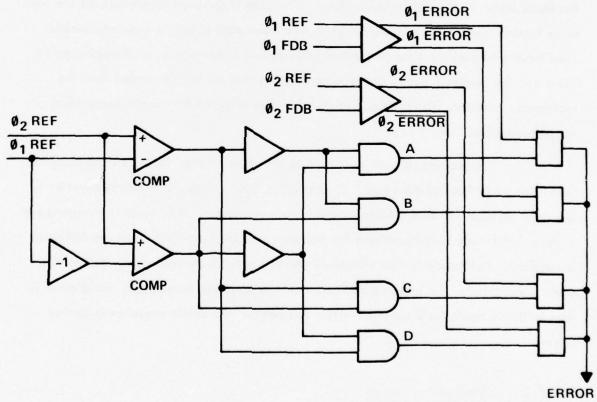
Figure 2-59. Servo Error Sensing Circuits

When the transport is operated in Record, Rewind, Read or Cycle mode, it uses the same servo loop for each mode. In the Record mode, Phase I from the tachometer/encoder is compared in phase to a clock coming from the System Control by a phase-locked loop. The resultant phase-error voltage is compensated and routed to the servo amplifiers via the mode selector. Different compensations are selected depending on the speed at which the transport is operated. Since phase-locked loops have a direction ambiguity, the direction command derived from the tachometer/encoder is compared with the required direction and the transport's direction of rotation is changed if it is improper. The Rewind mode is accomplished by simply interchanging the reference and feedback inputs to the phase-locked loop. The same high-speed compensations are used as in Record, since the transport rewinds at a fixed rate of nearly 4 meters/second. Read mode also uses the same phase-locked loops and compensation as in Record mode; however, the feedback comes from the detected marker on the film rather than the tachometer/encoder. The appropriate signal is also selected for the reference input of the phase-locked loop.

To provide the various inputs to the phase-locked loops, we use a digital data selector in front of the loops. To operate in Cycle mode, it is a simple matter to sequence through the data selector and the mode selector. Cycle mode is a sequence of modes. Read mode is initiated and the transport runs in phase-lock until the MAX tab is satisfied. Hold mode is then initiated. After 2 seconds in Hold mode, the Rewind mode is executed. The transport rewinds until the MIN tab is satisfied. Hold mode is then initiated again for 2 seconds. After this period, the entire sequence is cycled again.

2.2.7.3   Mechanical Design

The mechanical system is a direct spool-to-spool, loopless, continuous motion transport. Figure 2-60 shows the transport's mechanical components' locations. Drive torque is supplied only by the Take-up and Supply Spool Motors. Film Tension is generated by a fixed drive power applied differentially to each spool motor. The Take-up and Supply Spools are precision-machined yet interchangeable. The spooling surface
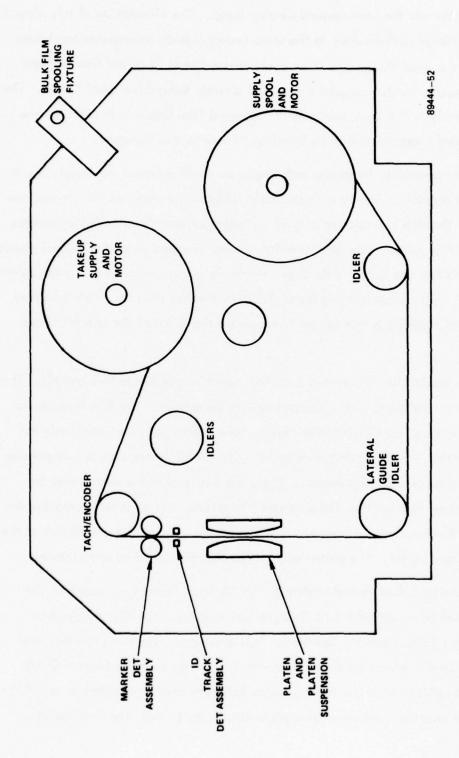
Figure 2-60. Film Transport Mechanical Structure

BULK FILM
SPOOLING
FIXTURE

SUPPLY
AND
MOTOR

SUPPLY
SPOOL
AND
MOTOR

TAKEUP
SUPPLY
AND
MOTOR

IDLER

IDLERS

LATERAL
GUIDE
IDLER

TACH/ENCODER

MARKER
DET
ASSEMBLY

ID
TRACK
DET ASSEMBLY

PLATEN
AND
PLATEN
SUSPENSION

89444-52

is spiral-cut to eliminate the once-around overlap bump. The elimination of this bump is essential to avoid large perturbations to the servo system outside its response bandwidth. The back side of the spool flange is a three cycle encoder used to detect film footage; the reflective detector for this encoder is mounted directly behind the spool flange. The spools attach directly to the drive motor shaft. To spool film from a bulk roll onto the Transport, we added a special Bulk Film Spooling Fixture to the Transport.

The operational threading path begins as the film leaves the Supply Spool and threads under an idler. This idler is specially designed for very low inertia and low rolling friction. The film is supported only at the edges by each idler. This eliminates the possibility of film surface damage. The film is then threaded under the Lateral Guide Idler. This guide idler also supports the film only on the edges. The Lateral guide idler is double flanged, with flange spacing set at 0.002 inch wider than the film's maximum width. The lateral tracking is thus forced to be within the limits of the Lateral Guide Idler.

The guide idler is mounted to a shaft which is adjustable fore and aft. This allows adjustment of the lower film entrance angle to the platen. The film then passes through the double-sided air bearing Film Platen. The Platen gap is set nominally for 0.004 inch wider than the film being transported. The platen is mounted to a suspension system which provides several adjustments. First, the entire platen assembly may be adjusted up and down to align the film gate with the optics. An adjustor is provided for the platen gap. Bi-directional adjustments are available such that the parallelism of the two platen faces may be set. The platen may be opened for inspection and cleaning.

The film is then threaded through the ID Track Detector assembly. The detector is mounted on a translator with 3 degrees of freedom. The film then passes through the Marker Track Detector Assembly. This assembly is fixed and the film must be adjusted to it by the lateral guides. Next, the film passes over the Lateral Guide and Tachometer/Encoder which is a flanged guide idler attached to the shaft of a 1,000-bit encoder. The encoder is mounted on a plate which may be adjusted fore and aft.

This allows adjustment of the upper film entrance angle to the platen. The guide idler supports the film only at the edges. The film is then spooled on the Take-up Spool. This spool is identical to the Supply Spool.
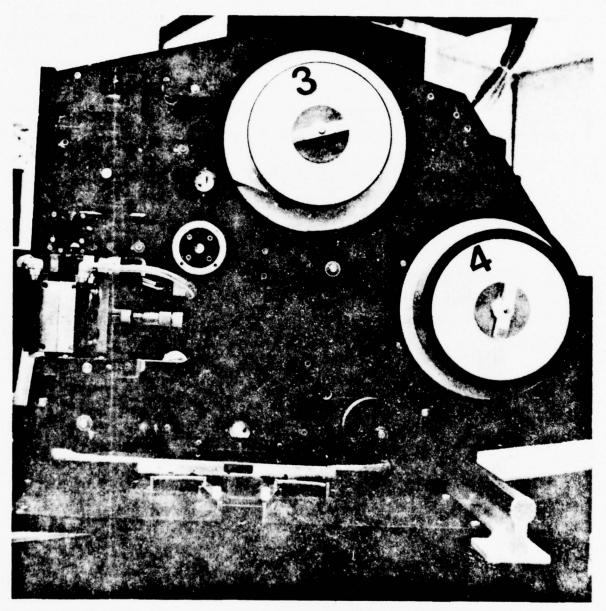
When the transport is operated in the loop mode, extra fixturing is required. The supply spool is replaced with an arm which holds an idler. This arm idler and torque motor provide the necessary loop tension while the Take-up Spool provides the servo drive. Two other idlers present on the Transport are used during loop mode operation. A photograph of the transport as implemented in the Phase II EDM is given in Figure 2-61.

2.2.7.4   Servo Considerations

The film transport subsystem servo is complex; it has three different servo loops. The first is a type-two position loop which is closed while in Hold Mode operation. The second is a type-one rate loop, which is closed while in Slew Mode. The third is a type-two phase loop, which is used during Record, Rewind, and Read Mode operations. The type-two phase loop is the precision servo loop of the system. A detailed description of it follows.

The block diagram in Figure 2-62 shows the servo loop used for speeds of 4.0 and 2.0 meters per second, while Figure 2-63 is for 0.4 and 0.2 meters per second. It can be seen from the block diagrams that the transport is brought up to speed by a heavy fixed drive voltage. The voltage is released just as the transport speed error passes through zero. Also, a cage on the loop integrator is released at this time. This scheme brings the transport speed up very quickly and then hands over to a much lower bandwidth control loop.

The phase loop utilizes a Motorola Phase Locked Loop (PLL). The reference input is from the System Control while the feedback input comes from the tachometer/ encoder or marker. The PLL generates an offset phase/frequency error. Because the PLL generates both phase and frequency error information, this loop can bring the transport

75 5533

Figure 2-61. Film Transport Unit
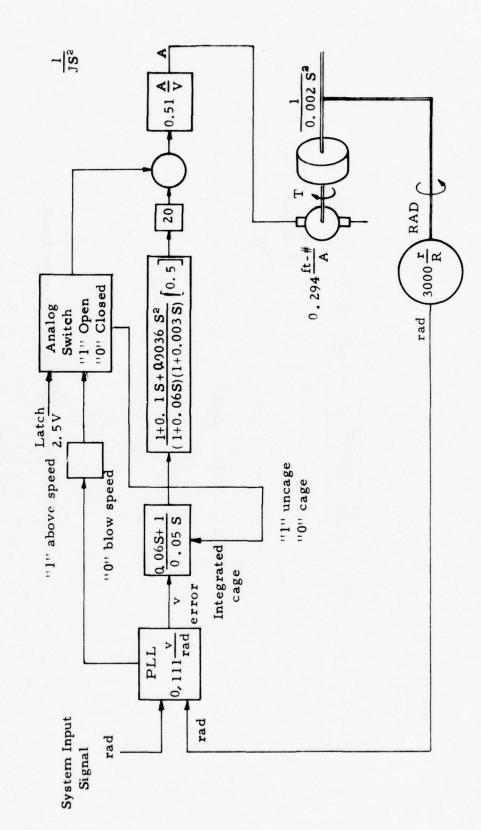
Figure 2-62. Servo Loop Block Diagram – High Speeds
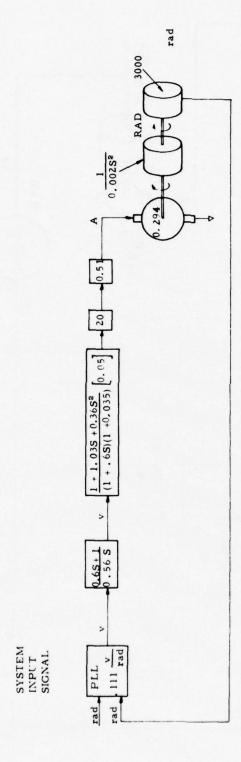
Figure 2-63. Servo Loop Block Diagram – Low Speeds

up to speed from a complete stop. The PLL offset is removed and the gain of the loop is set at the integrator amplifier. The torquer motor supplies a double integration when viscous friction is neglected. This totals a triple integration in the loop; to compensate the triple integration, a complex pair of zeros is used. The compensator also generates two poles, one of which is set to cancel the zero associated with the integrator. The second pole is set well beyond the loop crossover frequency. The compensator/ integrator bandwidth is decreased an order of magnitude between the two higher and the two lower speeds. The frequency crossover points are 1 Hz and 10 Hz for the low and high bandwidths, respectively. The frequency response curves are shown in Figure 2-64.
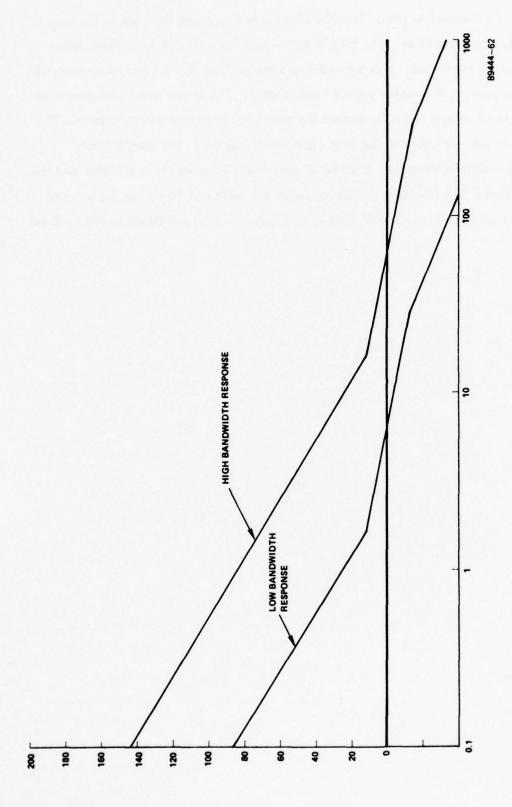
Figure 2-64. Servo Loop Frequency Response

89444-62

2.2.7.5   Film Platen Design

The focal precision of the film is a critical consideration for recording and readout. In the area of the exposure station the film must be constrained to a flat field to within ±20 µm without damaging its surface, even after repeated use. A great variety of factors must be considered, including: variations in the stiffness and curl of the film, the effects of humidity, film tension fluctuations, operability, and frictional effects.

Two basic design alternatives were considered (Figure 2-65). The first is a single-sided air bearing platen that introduces cylindrical curvature (section) into the film, thereby flattening it across its width. Tests of this concept showed essentially scratch-free performance, but inadequate focal precision. The thickness of the supporting air layer is determined by the balance of film tension and air suspension pressure, and therefore it is subject to the fluctuation of those parameters.

The second, and preferred, design utilizes a symmetric double air bearing platen to flatten the film by constraint rather than by section. Both platens are fed by the same air supply, so that pressure changes affect their suspension capabilities equally. This characteristic eliminates focal plane shifting with film tension and air pressure changes. Sandwich platens, however, are more likely to cause scratching because of small film clearances (0.004 inch). Air bearing platens can be self-cleaning, if air velocities and volumes are high enough. Large area platens are more susceptible to scratching than small ones, because for a given flattening force, the air velocities and volumes per unit area would be higher with the smaller platen. Film scratching may take place outside the platen. Therefore, all guides and idlers in the system provide edge support to the film and do not touch the film in the exposure area. The film must be spooled however, and spooling can cause scratching and pitting under certain conditions. Extensive film spooling tests indicate that constant film tensions between 0.4 pounds and 1.2 pounds, coupled with a dust-free environment, caused only minute scratching during hundreds of spooling operations.
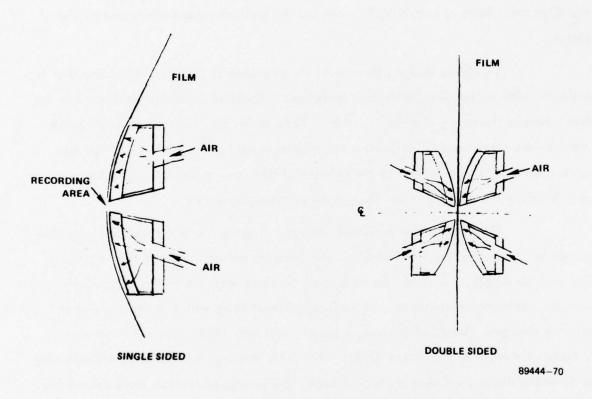
Figure 2-65. Air Bearing Platen Concepts

Film curl is the most significant cause of the observed deviations from flatness. Curl is a result of a differential expansion between the photographic emulsion and the Estar base. At high humidities a mechanical equilibrium exists between the two layers, while at lower relative humidity the emulsion shrinks and causes a predictable film curl. The air platen itself affects the temperature and moisture content of the film. The air has been dehumidified by an air dryer and is cooled by throttling as it comes out of the platen. This cool, dry air tends to shrink the emulsion and curl the film toward the emulsion. When the film is static in the exposure gate, all of the stated curl effects take place. Film curl is reduced by approximately a factor of two when the film is transported. Additional variables are introduced by plastic flow effects (e.g., core set), film tension, temperature changes, and the nonuniform stress patterns caused by the shoulder-support rollers. Even without considering these effects, however, good agreement is found between the actual film deformations and the ones predicted by a simple analytical model based on curl effects alone.

The double air bearing platen exerts a restoring force on any part of the film that deviates from the centerline. Let us assume a linear restoring force, i.e., proportional to the displacement with a negative "spring constant." Considered as a flexible beam, the cross-section of the film in such a restoring force field would obey the differential equation

$$\frac{d^4 y}{dx^4} = -ky.$$

There are four solutions of the type exp (mx), where $m^4 = -k$. The two symmetric solutions can be expressed as products of hyperbolic and trigonometric sines and cosines. The general symmetric solution can be written as

$$y = A \sinh ax \cdot \sin ax + B \cosh ax \cdot \cos ax.$$

where $a = \sqrt[4]{k}/\sqrt{2}$, and the constants A and B can be obtained from boundary conditions. The total force on the film must sum to zero (the equilibrium condition), and the moments at the end point are zero (the free-end condition). Mathematically

these are expressed by making the third derivative vanish at the end points and by choosing the second derivative to indicate the amount of curl in the film.

Figure 2-66 shows a family of solutions to this mathematical model, and illustrates the flattening effect of increasing restoring force on a highly curved film cross section. As the platen force increases from Curve A through Curve D, the film assumes its characteristic shape with elevated ends and middle (Curve C). A 400-fold enlargement of the typical shapes is seen in Figure 2-67. Curves E, F, and G show the same soft-W shape, while Curve H begins to show an extra wave observed experimentally in highly stiff air platens.

In Figure 2-68 the deviations have been distorted by a 2000-fold scale enlargement to illustrate the tenacity of the edge problem even in extremely stiff air bearings. The nature of the problem becomes clear if we realize that a perfectly flat film could be obtained by applying the proper moments to the two ends of the film. Distributed forces are not as effective in compensating for built-in curl. Future platen designs can be more effective by concentrating greater restoring force near the edges.

89444-67
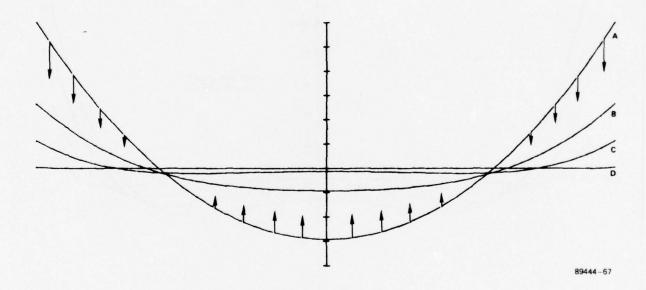
Figure 2-66.   Film Curvature Versus Restoring Force
In Double-Sided Platen
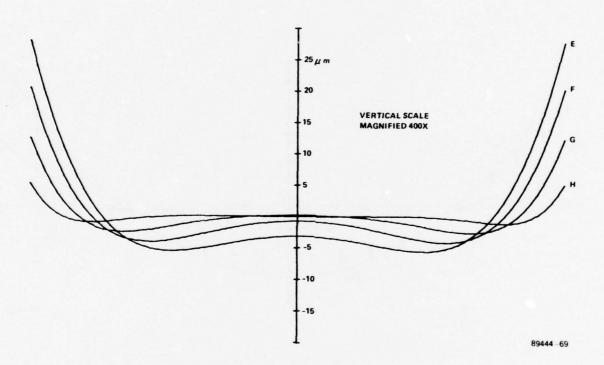
Figure 2-67. Typical Film Curvatures – 400X Expansion

VERTICAL SCALE
MAGNIFIED 2000X

5 µm
4
3
2
1

-1
-2
-3
-4

J
K
L

89444-68
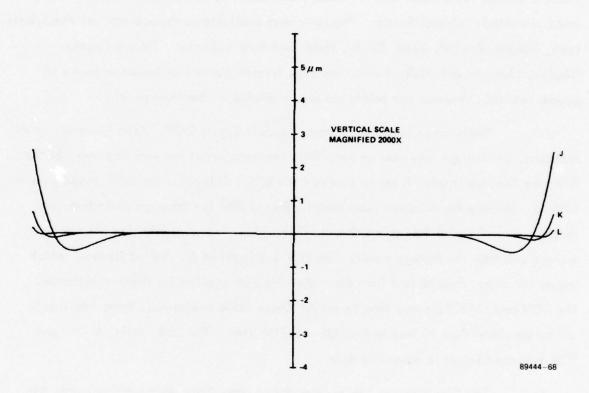
Figure 2-68. Film Curvatures in Double-Sided Platen - 2000X Expansion

2.2.7.6   Operating Procedure

The controls available to the operator of the film transport are Power Switch, Tension Switches (on Control, Remote Panel, and Transport), Loop/Spool Mode Switch, Test/Operate Switch, BOF Tab, MIN Tab, MAX Tab, EOF Tab, Stop Buttons (on controller and remote panel), Counter Zero/Preset Switch, Power Wind Switch, Mode Execute Button, Hold Mode Control, Slew Mode Control, and Record, Rewind, Read, and Cycle Mode Selector Switch. The indicators available to the operator are Phase/Rate Lock, Record, Rewind, Read, Cycle, Hold, and Slew Indicators, Takeup Footage Display, Out-of-Lock Audio Alarm, and Film Tension Meter (calibrated in tenths of pounds tension). Several test points are also available on the front panel.

These controls and indicators appear in Figure 2-37. After powering up the transport, the footage tabs must be set. With the transport at the very beginning of the film, the Footage Display is set to zero and the BOF Tab is set to the BOF stopping point desired. Because the transport takes about 5 feet of film to stop when rewinding, one should not set the BOF Tab at less than 10 feet. Next, we manually slew the film to the end and note the footage count. The EOF Tab is set at the desired footage, which should be no less than 10 feet from the end of the film to allow for stopping distance. The MIN and MAX Tabs may then be set for Cycle Mode operation. These tabs should not be set closer than 10 feet to the BOF and EOF Tabs. The BOF, MIN, MAX, and EOF Tabs must be set in ascending order.

The film transport has many modes of operation. As a starting point, the transport is in the Hold Mode (a position servoed mode where input is from a 360° rotating pot on the remote panel) any time a Stop command has been initiated. While in the Hold Mode, film advancement is made at the rate of one hologram row per turn of the Hold Mode Control. The Slew Mode is initiated from Hold Mode by simply turning the Slew Mode Control in either the forward or reverse direction; changing to the Slew Mode is automatic. When the Slew Mode Control is released, the transport returns to Hold Mode automatically. When executing Record or Read Modes, the operator selects the proper mode at the remote panel and presses the Execute Button. The transport starts running in the forward direction at a rate controlled by the main system. The Rate/Phase

2-150

Lock Indicator and Audio Alarm should show lock after a few feet of film. The transport continues running until the EOF Tab is satisfied and the transport automatically returns to Hold Mode. Re-execution of Record or Read Modes is not possible when the EOF Tab is satisfied. In order to rewind the film, the Rewind Mode is selected at the Remote Panel and executed. The transport rewinds at approximately 4 meters per second. When the BOF Tab is reached, Hold Mode is automatically executed. Further execution of the Rewind Mode with the BOF Tab satisfied is not possible. Should automatic cycling over a given area of film be desired, the MIN and MAX Tabs (inside the BOF and EOF Tabs) can be set and the Cycle Mode executed from the remote panel. The transport will sequence through Read, MAX Tab, Stop, Rewind, MIN Tab, Stop, and Read Modes in an endless automatic cycle until stopped. During the Read portion of the sequence, the lock indicators are operational. Cycle Mode is a readout mode and cannot be used with unrecorded or blank films.

When the transport is operated in the Loop Mode, either Record, Rewind, Play, or Cycle may be executed, and the transport will run until the footage tabs have been satisfied.

2.2.8 Fiber-Optic Distributor

Proper detection of the light in the 128 optical channels during the readout process is crucial to the viability of any recording system. During the design of the WBR system, various methods of detecting the data were investigated. Methods employing integrated devices were considered, and are discussed elsewhere in this report. For use in the Phase II EDM, however, an approach using discrete detectors was selected as the method offering the least risk in the developmental time frame.

The use of discrete detectors requires that the light in the linear array of optical channels be distributed to the detectors. We accomplish the distribution in the Phase II system through the use of a linear array of fiber-optic elements to intercept the channels and to conduct them individually to the appropriate detectors. In this section we provide data on the specifications, design and fabrication considerations, and achieved performance of the fiber array in use in the system. Photographs of the array as integrated

into the fiber array/detector assembly are also given. Also to supplement the text, Figure 2-69 gives a schematic view of an array of the kind under discussion in this section.

2.2.8.1   Design Considerations

During the course of the Phase II WBR program, several fiber-optic arrays were designed and tested in the system. The extensive practical information provided by these units was used in the design of the final array. Some of the key areas of investigation and experimentation are:

- Array spatial duty cycle - The design goal is to maximize the light collected by each fiber from its channel, while minimizing the light collected from adjacent channels, thus minimizing optical crosstalk. In addition, the light collected must be above some minimum to provide adequate signal-to-noise at the detector. An analysis of this situation, under some reasonable assumptions about the signal shapes involved, indicates that the optimum spatial duty cycle of the fibers depends on the expected channel spacing errors, channel jitter, and noise considerations. Using this information, we chose a spatial duty factor (64 percent) to place the contribution of optical crosstalk well below other system noise contributions.

- Transmittance fluctuations - To minimize complexity in the detector circuit design, the fibers of the array must not introduce any intensity fluctuations from channel to channel. The major obstacle to this uniformity of transmittance was found to be diameter variation in the commercially available fibers. For this reason a diameter measurement and selection procedure was used to keep transmittance fluctuations to an acceptable minimum. To achieve a transmission difference of less than ± 5% from fiber to fiber, the fiber diameter was selected to an accuracy of ± 0.0001 inches. Final refinement of transmission

2-152

DISCRETE PHOTODETECTORS

OPTICAL CONNECTOR

SINGLE FIBER-OPTIC ELEMENT

15.7 mil C-C

FIBER-OPTIC LINEAR BUNDLE

89444-83
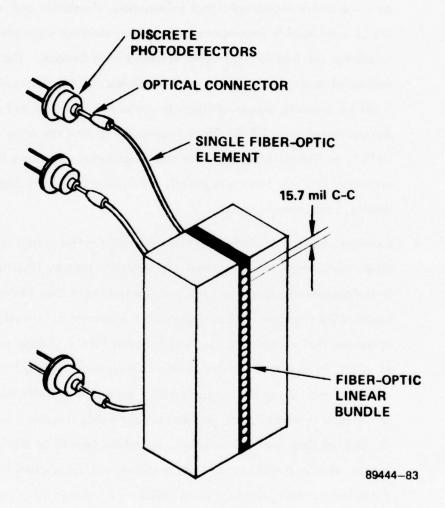
Figure 2-69. A Linear Fiber-Optic Array

uniformity was made by trimming some of the fibers slightly from their nominal length.

- Durability – Since the loss of a single channel can potentially invalidate the entire recovered signal information, durability and reliability are of considerable importance. Therefore, methods were investigated to protect the fragile fiber-optic elements from damage. The most successful method, which was used in fabricating the final unit, involved encasing groups of fibers in protective sleeving and embedding the unsleeved areas of the fibers (especially around the array head) in "RTV", a silicone compound. In test procedures, the fibers in units protected this way have successfully survived multiple flexural, tensile, and impact stresses.

- Connectorization and coupling characteristics – The output ends of the fibers were simply and inexpensively connectorized by inserting them into disposable hypodermic needle tips which were then inserted in a mechanical structure for interface with the detectors. Investigation indicated that acceptable coupling between fiber and detector could be obtained at some minimum clearance distance. The technique used, however, was to put an optically clear, non-rigid selastic material on the detector surface. This provides a deformable interface between the optical fiber and the detector. An added benefit of this procedure is that, due to the effects of light trapping and index matching within the selastic, the optical coupling efficiency between fiber and detector is increased by 25 to 30 percent.

2.2.8.2 Fabrication Methods

Production of the final unit for the Phase II EDM was accomplished using information gained from the prototype units and the technique investigations. The two major tasks in fabricating the array (after the fibers have been selected and cut to meet transmission standards) are alignment for spacing regularity and end finishing.

The alignment and spacing of the fibers of the Phase II unit was done with the aid of a threaded drum, whose thread spacing was equal to the desired fiber spacing. The fibers, having been inserted into their protective sleeving, were aligned to the drum threads and set into their plexiglass mount with epoxy glue. After the epoxy had set, the plexiglass unit was mounted between two larger blocks to form the array head. The fibers entering the rear of the head were then protected with RTV compound as described above, and the unit was ready for polishing and end finishing.

Polishing provides the best end finish for optical fibers, and is easily done on the array head where each fiber is held firmly in place. The fibers are cut close to the head, and increasingly gentle sanding, polishing, and buffing steps are completed. This technique provides a very fine finish to the ends of the fibers, although care must be taken to avoid heating and softening of the fibers during the polishing procedure.

Finishing the output ends of the fibers, where the sanding and polishing techniques are difficult or impossible, requires a different method, and several were investigated. The optimum technique, in terms of results and simplicity, was careful cutting with a razor knife. The quality of the cutting could vary the fiber transmittance by as much as ±3 dB, but little difficulty was encountered in using this technique to match fiber transmittances to within ±5% as required.

2.2.8.3   Specifications and Performance Measurements

In Table 2-8 we provide a summary of the performance parameters and specifications of the Phase II EDM fiber-optic signal distributor. The data given are primarily performance measurements, with the specifications being met or exceeded by the unit.

Finally, in Figures 2-70 and 2-71 we show photographs of the finished unit as integrated into the Phase II system. Figure 2-70 shows a front view of the unit, including the linear array of fibers, its adjustable mounting fixture and, within the plexiglass covers, the module where the interface between fibers and detector cards takes place. In Figure 2-71, a rear view of the unit, the fibers are held in groups of four by support
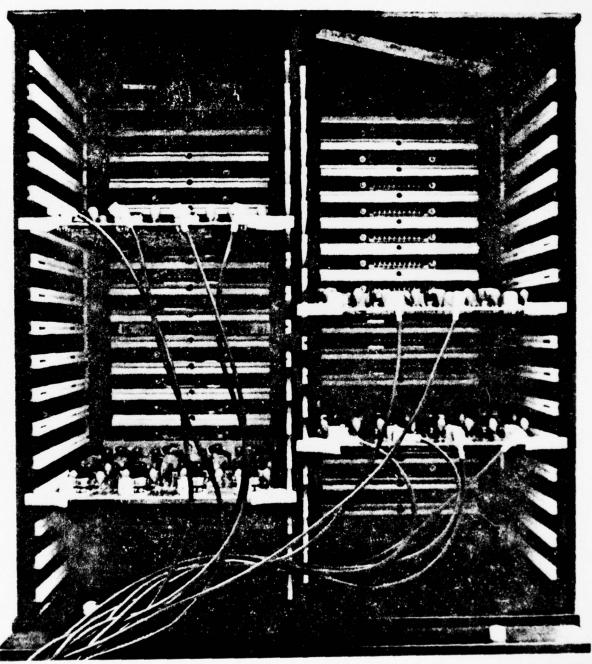
bars at the back of the enclosure. Four detector cards with four photodetectors each are shown in place, simultaneously bringing their detectors in contact with the corresponding fibers and obtaining their electrical power from sockets within the cabinet.

Table 2-8

Specifications and Performance of Fiber-Optic Distributor

Number of elements	152 (128 active)
Fiber spacing (center-to-center)	15.6 mil
Spacing uniformity	±1 mil
Transmission	≥ 64%
Transmission uniformity	±5%
Fiber diameter (nominal)	10 mil
Diameter uniformity	±0.1 mil
Crosstalk (fiber-to-fiber, max.)	– 41 dB
Crosstalk (channel-to-channel)	– 17 dB
Spatial duty factor	64%
Coupling method	Non-rigid selastic
Coupling gain	25-30%
Fiber material	CROFON (Du Pont)
Acceptance angle	64°
Stress relief method	RTV potting

Figure 2-70. Fiber-Optic Distributor and Photodetector Unit

Figure 2-71. Fiber-Optic/Photodetector Unit - Rear View

2.2.9   Photodetector Array

As described briefly in the previous section, an array of discrete photo-detectors is used to translate the optical readout information to the electrical domain for processing. In this section, we provide details of the specifications and performance of the photodetectors in use, and the associated circuits and their key design considerations.

Another feature of the Phase II EDM, which was included specifically to be evaluated for possible application to future systems, is the use of several types of thresholding circuits. In addition to the standard fixed level (or fixed function) threshold, a data-adaptive threshold, which can track slow intensity fluctuations in the data, has been included. A generalization of this idea, the group-profile threshold, applies a data-adaptive threshold to many nearby channels, as well as the one which generates it, thus possibly achieving a cost reduction at the expense of the direct correlation of threshold to data.

We present details of the implementation of these thresholding schemes in this section. The results obtained with the various thresholds will be given in the section on experimental results (Paragraph 2.3).

2.2.9.1   Photodetector Amplifier

A functional block diagram of the photodetector and amplifier used on the exploratory development model is shown in Figure 2-72. The photodetector is a hybrid photodiode/amplifier unit made by Meritt; the unit has a bandwidth of 8 MHz. The active area of the photodiode is 0.120 x 0.06 inch. The nominal responsivity of the hybrid unit is 5 mV per microwatt of incident light intensity at a 514.5 nm wavelength. This unit is ac-coupled to a Microampere 733 video amplifier providing an additional gain of 100. The output of the video amplifier is capacitively coupled to an FET input LH0032 wideband operational amplifier. An FET switch is utilized at the coupling to perform dc restoration. During known dark periods of the scan, this switch is activated to zero the input to the LH0032. The LH0032 is configured as a noninverting amplifier with a gain of 10. The output of this amplifier is low-pass filtered to provide maximum
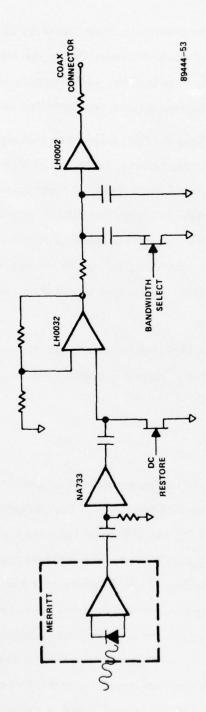
Figure 2-72. Photodetector Amplifier – Functional Diagram
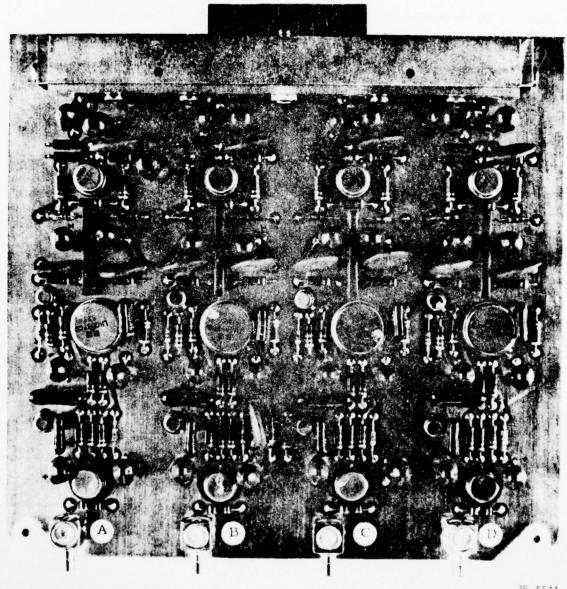
signal/noise performance of the unit. There are two filter bandwidths available to accommodate different readout speeds. The high bandwidth filter is tailored for the 6 megabits per second (Mb/s) channel data rate and is also utilized for the 3 Mb/s channel data rate. The low bandwidth position, selected by FET-switched capacitor, is optimized for the 600 kb/s channel rate and is used for the 300 kb/s channel rate. The output of the low-pass filter is buffered by an LH0002 unity gain follower to drive a 50 ohm coax cable to the remotely located bit decision electronics. The overall unit provides a responsivity of approximately 1 volt per 100 nanowatts. At the high bandwidth setting, 225 nanowatts provides an electrical signal-to-noise ratio allowing better than 10^{-6} bit error rate (BER) performance.

A photodetector card is shown in Figure 2-73. The card contains four photodetector channels. The four hybrid photodetector units are housed in the assembly at the top of the card above the electronic strip connector. Insertion of the unit into the fiber array housing completes the fiber-optic/photodetector connection as well as the power supply and control electronic connections. The Microampere 733 amplifiers are the small integrated circuits near the top of the card. The LH0032 integrated circuits are located in the center of the card. The LH0002 unity gain followers are positioned at the bottom of the card above each of the coax connectors for the analog outputs.

2.2.9.2   Bit Decision Electronics

The analog data recovered by the photodetectors must be thresholded and sampled to make bit decisions. In the exploratory development model we implemented three schemes for evaluation: channel adaptive threshold, group adaptive threshold, and manual threshold.

A functional block diagram of the channel adaptive threshold electronics is shown in Figure 2-74. The circuit operates in a bootstrapping mode. Assume the circuit has been operating and a threshold has been established. At the peak of the filtered analog data, the output of the comparator is sampled by the D-type flip-flop, yielding the digital data output for the processed bit time. If the decision is a "1," the

75-5544

Figure 2-73. Four Channel Photodetector Card
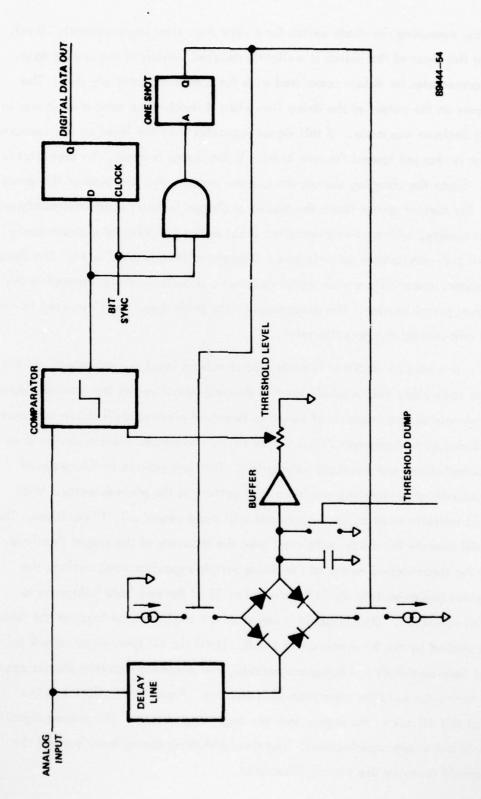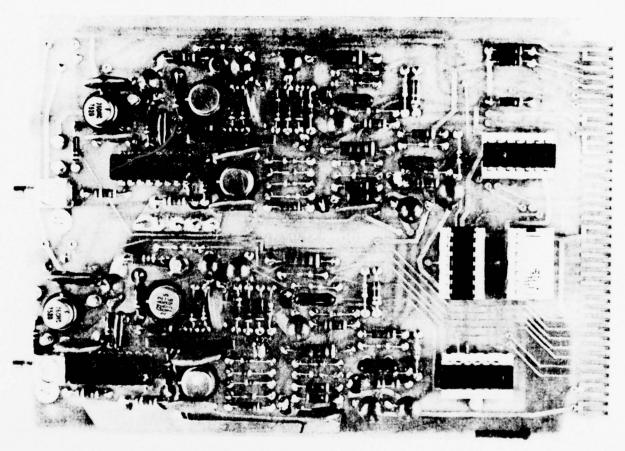
Figure 2-74. Adaptive Threshold – Functional Diagram

69444-54

ANALOG INPUT

DELAY LINE

COMPARATOR

BIT SYNC

D Q

CLOCK

DIGITAL DATA OUT

ONE SHOT

A Q

THRESHOLD LEVEL

BUFFER

THRESHOLD DUMP

one-shot fires, operating the diode switch for a very short time (approximately 20 ns). The signal at the input of the switch is a slightly delayed version of the analog data. The delay compensates for delays associated with the comparator and one shot. The switch operates on the output of the delay line when it reaches the same state it was in when the bit decision was made. If this signal is greater than the level on the capacitor, the capacitor is charged toward the new level. If the signal is lower, the capacitor is discharged. Since the charging sources are current sources, the slew rate of this process is limited. The current system limits the maximum change in level to approximately one-half volt per update, with a normal operating level at the capacitor of approximately 3 volts. This prevents radical noise-induced changes in the threshold level. The signal on the capacitor, essentially a peak signal envelope, is buffered and presented to the threshold level potentiometer. The percentage of the peak signal envelope used for the threshold is adjusted by this potentiometer.

If a zero bit decision is made, the threshold level is unaffected. At the beginning of each scan, the threshold level is dumped by activating the threshold dump switch. A picture of two channels of adaptive threshold electronics is shown in Figure 2-75. As discussed in Paragraph 2.1.3.1, the first 24 holograms contain dummy data for bit synchronization and threshold acquisition. The data pattern in this group of holograms presents an alternating one/zero data pattern to the photodetector. With the threshold initially at zero, the comparator will make almost all "1" decisions. These decisions will operate the diode switch and start the recovery of the proper threshold. Because of the slew-limited nature of the diode switch/capacitor combination, the circuit requires approximately six "1" decisions or 12 of the one/zero holograms to reach normal operation. The threshold is based on the analog signal level at the time the data is strobed by the bit synchronous clock. Until the bit synchronous clock is operational (approximately ten hologram periods), the threshold recovery process cannot converge, hence the need for more than 12 holograms. Figure 2-76 illustrates the operation of this circuit in the region near the beginning of scan. The analog signal and threshold are shown superimposed. The threshold dump during blanking and the initial threshold recovery are clearly illustrated.

75-5543

Figure 2-75. Two Channel Adaptive Threshold Card

ANALOG DATA

THRESHOLD
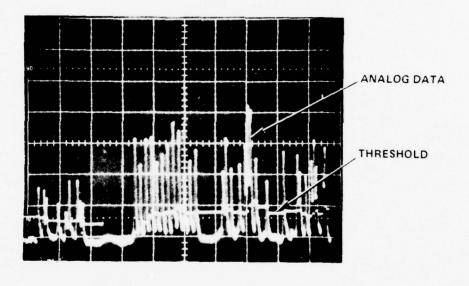
Figure 2-76. Adaptive (Threshold Acquisition Period)
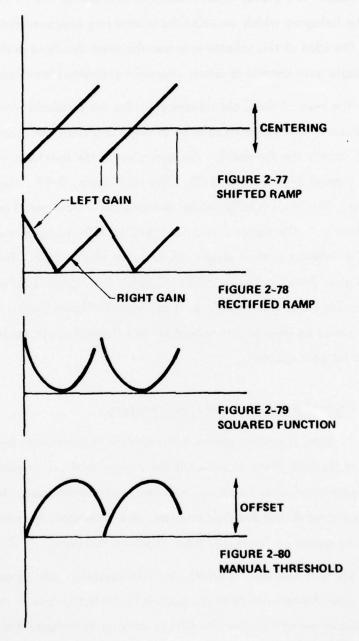
The group adaptive threshold uses the same electronics as the channel adaptive threshold. The analog input is derived from one of two special data channels recorded in the hologram which contains the alternating one/zero data pattern across the entire scan. The idea of this scheme is to use the same threshold profile for all channels with only a single gain control to adjust channel-to-channel level variations.

The manual threshold scheme provides the threshold from a special analog function generator. This scheme makes no attempt to utilize the recovered analog information to modify the threshold. The operation of the function generator is best illustrated by Figures 2-77 through 2-80. The first figure, 2-77, illustrates the shifted reference ramp. The level is adjusted by operation of a front panel potentiometer labeled "centering." The signal is rectified and the left and right sections have individual gains applied to their slopes, as shown in Figure 2-78. This signal is squared, yielding the signal shown in Figure 2-79. Finally, this signal is inverted and a front panel control allows insertion of a dc shift as shown in Figure 2-80. This generated threshold shape may be used as a threshold by any channel, with each channel again having individual gain control.

2.2.10   Recording Material and Film Processing

In terms of overall system bit-error-rate performance, one of the most crucial areas of the WBR Phase II system is the storage medium, including physical and sensitometric characteristics, handling, and processing techniques. Many of the problems encountered during the WBR program, and consequently many of the major breakthroughs in system performance, have arisen in this area.

We will now discuss briefly the film selection process and some of the specifications and characteristics of the material selected for use in the Phase II system. Also in this section we will review the film processing techniques that have evolved during the course of the program, along with some of the associated problems and their potential solutions.

CENTERING

FIGURE 2-77
SHIFTED RAMP

LEFT GAIN

RIGHT GAIN

FIGURE 2-78
RECTIFIED RAMP

FIGURE 2-79
SQUARED FUNCTION

OFFSET

FIGURE 2-80
MANUAL THRESHOLD

89444—51

2-168

2.2.10.1   Recording Material

Phase I Recordings and Phase II Film Selection

The initial material tested and used for WBR experiments during Phase I of the program was 10E56. This film provided good results from several points of view, especially, in terms of diffraction efficiency and sensitivity. Some of the relatively minor problems encountered with this film included film breakage (to which the triacetate film base initially used is highly susceptible), and delivery-schedule difficulties. The decision to look for another material, however, came as a result of two more serious difficulties associated with the 10E56 film. These were:

- Latent Image Decay – Figure 2-81 shows the results of LID tests comparing 10E56 with a replacement candidate, Kodak SO-141. The steep slope of the 10E56 curve means that highly divergent densities can result from the same exposure if only a slight change in the time interval between recording and processing is permitted. This makes the achieving of consistent results a difficult process. And it is unacceptable in future programs requiring substantial processing times for multiple-thousand-foot rolls of film. As the figure indicates, SO-141 show relatively little change in density after several hours delay.

- Film Surface Characteristics – Since WBR Phase II has high-integrity (low error-rate) readout as a major goal, potential error sources already on the film before recording are intolerable. 10E56 was found to have surface damage of two types: 1) flaws or voids in the emulsion, some as large as 500 μm in diameter; and 2) scratches parallel to the film length, imposed either during manufacturing or during the slitting process from 70 mm to 35 mm width. Both of these types of damage are potential error sources for high-density recording.
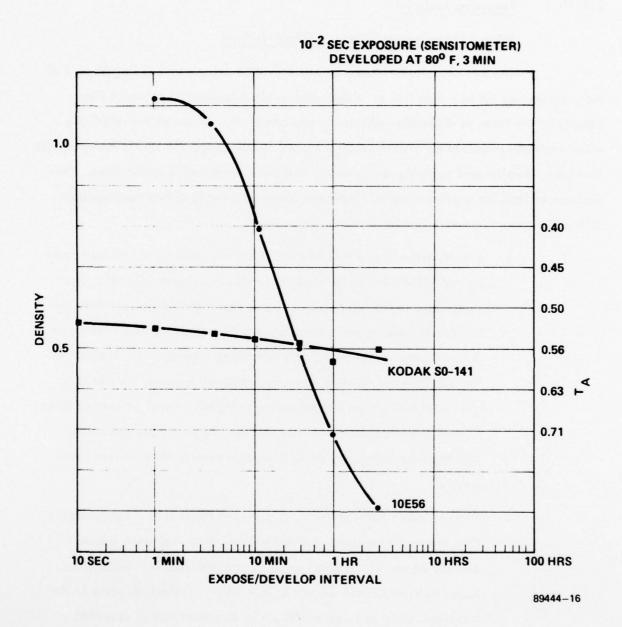
Figure 2-81. Latent Image Delay

89444-16

The candidate replacement film, SO-141, was substantially better than 10E56 in both of these important areas. It is somewhat less sensitive and has slightly less resolving capability, but was nevertheless fully able to fulfill the requirements of the Phase II WBR system.

Film Characteristics

The following nonexhaustive list presents some of the most important characteristics of SO-141 film; some from the manufacturer's data, some as measured. Emphasis is placed on those features which are of particular importance to WBR-type applications.

Table 2-9. Kodak SO-141 Film

Emulsion Properties

- Exposure Sensitivity – A typical amplitude transmittance versus exposure curve is shown in Figure 2-82. Actual record levels in the WBR system are greater than this curve would indicate due to reciprocity failure (see below).

- Spectral Response – Good sensitivity is available below 530 nm, with a peak near the WBR operating wavelength of 514.5 nm. Red insensitivity permits red safelight operation (see Figure 2-83).

- Spatial Frequency Response – Published data extends only to 200 cycles/mm (at which point the response is still 95 percent). In the WBR system application, no significant loss of response has been observed over the 300-600 cycles/mm range in use.

- Diffraction Efficiency – As shown in Figure 2-84, tests have produced DE's as high as 1 percent at 500 cycles/mm with a K-ratio of 10. The best achieved DE during the WBR Phase II program has been about 0.3 percent.
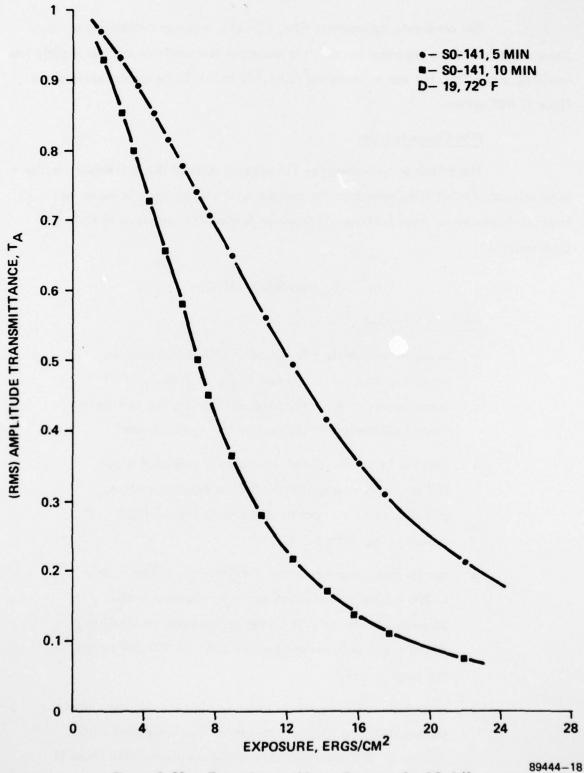
Figure 2-82. Transmittance Versus Exposure for SO-141

89444-18
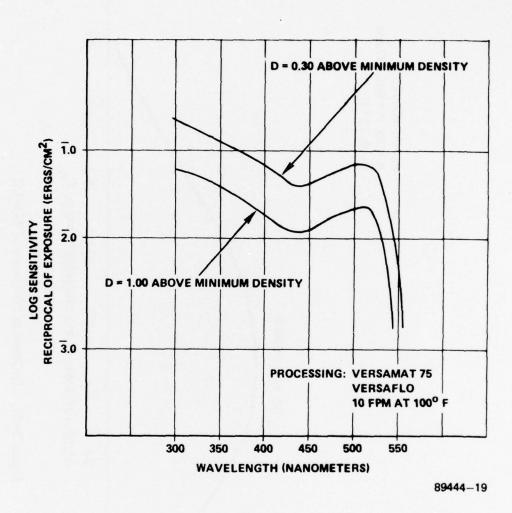
Figure 2-83. Spectral Sensitivity of SO-141

89444—19

PLANE WAVES
K = 10, ν = 500 CY/mm
D-19, 72° F

SO-141   5 MIN

AVERAGE AMPLITUDE TRANSMITTANCE, T_A

PERCENT DIFFRACTION EFFICIENCY

89444–17
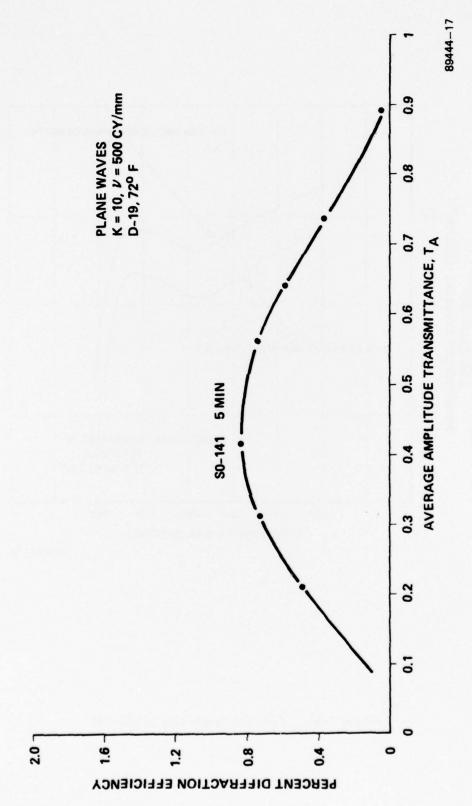
Figure 2-84.   Diffraction Efficiency of SO-141

Table 2-9. Kodak SO-141 Film (Continued)

- Packing Density – The peak packing density within the holograms is about 1.6 Mb/cm^2. On an average basis (including guardbands, etc.), approximately half this figure is currently achieved. The ultimate limit for this film may be over 2.0 Mb/cm^2.

- Reciprocity Failure – Published data is not available in the 10–200 ns range of interest. Results obtained on the Phase II system indicate about a 5X loss of sensitivity at 80 ns. Thus, to achieve a T_A value of 0.5, around 50 $ergs/cm^2$ are used, as contrasted to the 12 $ergs/cm^2$ which Figure 148B indicates is required for longer exposures.

- Latent Image, Decay – The measured values of density loss are shown in Figure 2-81, along with similar data for 10E56. As mentioned above, this was a strong consideration in the decision to choose SO-141 over 10E56 as the preferred recording material.

Base Properties

- Material – Commercial name: Estar. A high-polymer material, a thermoplastic, a member of the general class of plastics called polyesters.

- Dimensions – Width, 35 mm; thickness, 4.0 mil; length, available up to 3000 feet unspliced. Length used in Phase II WBR: 250 feet.

- Optical Properties – Refractive index, 1.5–1.65 (birefringent). Transmittance ($\lambda = 400$–700 nm): > 80%. Haze: ≤1%.

- Dimensional change due to processing: ±0.03%.

2.2.10.2   Film Processing

Having described in the previous subsection the selection of the storage medium for the WBR Phase II System - Kodak SO-141 - we will now discuss film processing. Here we describe the technique used in Phase II of the WBR program, the associated results, problems, and some actual and potential solutions.

Hand Development Procedures

Because of the exploratory nature of the WBR system, all initial experiments involved the use of hand processing techniques. Advantages of this technique include:

- Simultaneous immersion of the entire emulsion

- Use of a holographic-type developer (D-19)

- Totally untouched emulsion during entire process

Some of the disadvantages are:

- Restriction to 100-foot film lengths with current equipment

- Outer 3 mm of width unusable due to the precluding of development by film support fixture

- Inability to achieve uniform drying

The specific procedure used for hand development was as follows:

1. Develop: D-19 for 5 minutes at 68° F; or for 3 minutes at 80° F

2. Stop: 30 seconds, Kodak acetic acid stop bath

3. Fix: 4 minutes, Kodak rapid fix

4. Wash: 15 minutes, tap water

5. Wash: 15 minutes, deionized water

6. Dry: $\sim$1 hour, forced air (filtered)

Results obtained by hand processing were fairly good during the earlier portions of the program. One particularly useful improvement to the development procedure was the discovery that by adding approximately 1 gram/liter of a silver solvent (such as sodium or potassium thiocyanate) to the developer, intergrain scattering could be reduced, increasing diffraction efficiency by as much as 100 percent.

Transition to Machine Procedures

As the WBR system progressed, more and more emphasis was placed on performance measurement in terms of bit-error-rate (BER). For this reason, more uniform and repeatable processing was required. The emulsion/base shrinkage during drying is a major potential error source, and was the first area to be attacked. The attempted solution (hand processing followed by machine drying) was partially successful, but it introduced another handling and spooling operation into the processing, and net gains were small. Also, we found that forced-air drying of wet emulsion must be carefully controlled to prevent the air from locally distorting the emulsion and producing intolerable spatial frequency changes in the holograms. Because of these problems, and because machine procedures would be necessary to handle larger film lengths in the future, the Phase II System was converted to all-machine processing.

Machine Processing Procedures

The machine processor used in the WBR Phase II System is the Kodak Versamat 75. Some of the key specifications of this unit are given in the following table.

Table 2-10. Versamat 75 Film Processor Specifications

Speed	1-10 feet/minute
Film Size Acceptance	35-105mm wide, up to 200 feet long
Water Requirements	2.0 gallons/minute
Number of Racks	7
Number of Tanks	Up to 5

Since machine processing is not readily compatible with D-19 type chemistries, experiments were undertaken to identify a chemistry which would produce substantially identical sensitometric results under the speed, temperature, and environmental conditions of the machine processor. These results were achieved by configuring the processor as follows:

Table 2-11. Phase II Processing Procedures

Develop	Kodak 880 Developer, 82-1/2° F, 4 racks, 2 tanks
Fix	Kodak 22 Fixer, 1 rack
Spray Wash	Deionized water, 1 rack
Bath Wash	Deionized water + Photoflo, 1 rack
Dry	~115° F
Speed	4.2 feet/minute

An important additional step, which was found during the later portion of Phase II to significantly increase the BER performance of the system, is a rewash procedure - passing the film again through the wash and dry portions of the processor. That procedure, in spite of its introducing an additional handling/transporting step, produced typical BER gains of one order of magnitude. And, although the reason for this is not yet fully understood, we can say that the rewash appears to significantly reduce the visible "mottle" or frosty appearance of the emulsion, and may also be clearing out residual fixer not removed by the first wash.

Among the problems associated with machine processing of film, perhaps the most critical to the WBR application is scratching. Since the WBR holograms are only 16 μm wide by 1 mm long, scratches as small as 10 μm x 300 μm can significantly increase the probability of error in the holograms they affect. Larger scratches, as may be caused by improper tensioning, inadequate cleaning procedures, or sticking rollers, are, of course, more serious, but were effectively eliminated early in the optimization of the WBR processor. The smaller "microscratches" are more difficult to eliminate, and

may perhaps be attacked in the future by chemical filtration, clean-room type environments, and smoother rollers (or preferably, noncontact rollers).

Film processing for the WBR Phase II EDM has been adequately accomplished, but ranks as one of the larger error contributors in the system. We believe that increased emphasis on properly engineered film handling and processing techniques will yield significant improvement in the raw bit error rates achieved on the Phase II and future systems, with gains as great as a full order of magnitude being possible.

2.3   EXPERIMENTAL RESULTS

In addition the previously described design and development of the Exploratory Development Model, we devoted a major portion of the program to experimental evaluation of system performance. On a systematic basis, we performed an error analysis, both on the entire system and on critical components and subsystems, in an effort to extend and characterize the limits of ultimate system performance. We included in this an investigation of the sensitivity of the total system performance to small perturbations in the state of optimization of critical components, as for example light level, optical alignment, and electronic synchronization.

The EDM was implemented to afford convenience in conducting these investigations; that is, many test points and front-panel manual controls were provided, and the opto-mechanics were mounted with maximum adjustability. In addition, powerful diagnostic capabilities were provided by the electronics previously described.

In these investigations we relied upon bit-error-rate performance as the basis for determining the impact of component and subsystem parameter variations. As described earlier in this report, the recorder contains built-in data generators to provide simulated information for recording. The data generators produce the multiple channels of pseudorandom binary sequences that we recorded on the film. During readout of these films, we used the two bit-error-rate-measuring test sets and the line-sync-error test set in the EDM to measure the data errors produced under various controlled record and readout conditions. The following paragraphs discuss the nature and results of these tests.

To provide a standard for comparison, a set of record and readout procedures were developed and used during these tests. As these investigations were conducted we employed the manual flexibility of the hardware to frequently adjust the system to ensure consistent experimental results. For those readers who desire a fuller understanding of the principles of holographic recording, and for those who want a review of the recording and readout procedures followed for these tests, a synopsis of the procedures follow. A brief review of the procedures (given in Paragraph 2.3.2) should be sufficient for understanding the experiments subsequently described.

2.3.1 Record and Readout Procedures

To support experimental evaluation of EDM performance we routinely used detailed alignment and optimization procedures prior to recording and readout experiments. We wish to note, that for the most part, these procedures could be made unnecessary by the use of available servo and automation techniques. This was not done in the EDM because it would not be consistent with program goals and could have impeded certain experimental flexibility. Instead the system is brought to operational readiness by carrying out the "operator's checklists" that follow. Between recording and playback, the film is processed off-line and is reloaded on the film transport. In addition to the procedures delineated in the readout checklist, front-panel controls available to support error diagnostics are also adjusted.

2.3.1.1 Recording Checklist

1. Check laser stability. About 2 hours after turn-on, the Phase II laser reaches thermal equilibrium, making this step unnecessary.

2. Optimize beam pointing servo. This servo partially compensates for laser thermal drift. Optimize means reset to the center of its dynamic range.

3. Adjust AOMs. Bragg angle and transducer/beam position adjustments are made to maximize diffracted output power.

4. Slit jaw adjustment. Hologram vertical size is set to double-Rayleigh resolution. A different size may be used for readout.

5. Data vertical. Page composer illumination is balanced in the channel-to-channel direction.

6. Film focus. The reference beam scans a prerecorded film. The film can then be located in the exact focal plane by maximizing the induced beam modulation.

7. Temporal overlap. Simultaneous occurrence of the "hologram level" of the modulated reference beam with the "valid data" time of the signal beam is produced by adjusting transducer positions to vary the associated acoustic delay.

8. Power setting. Reference beam (hologram and guardband) and signal beam power levels are set by varying the drive power to the AOPC, beamsplitter, and modulating AOM's.

9. Parabola. The parabola AOM (the function of which is described in Paragraph 2.2.3.1) is set to proper strength for recording.

10. Scan balance. Uniformity of reference and signal exposure across the scan is adjusted.

11. Physical overlap. Reference/signal beam overlap is ensured by checking that a test slit in the film plane is transited simultaneously by both.

12. Hologram vertical uniformity. This is adjusted (on the Phase II system) with a tilting plate in the reference beam.

13. Transport lateral. The transport is adjusted to ensure centering of the scan on the film.

14. Marker beam. Alignment and power levels of the marker beam are checked.

15. Film loading. The desired footage is loaded on the transport.

16. Tab set. The transport control system is told where on the film to stop.

17. Automatic sequence recording. If all interlocks read "ready," the automatic sequencer is executed, and the following steps are performed: transport started, main shutter and marker shutter open, transport rate lock detected, AOM's enabled (and recording begun), end tab detected, AOM's disabled, shutters closed, transport stopped.

2.3.1.2   Readout Checklist

1. Film tabs. Set beginning and end of film section to be read out.

2. Beam flip. The AOMs are bypassed and all available light is used to form the readout reference beam.

3. Slit jaws. The vertical size of the read beam is set at an appropriate value for readout.

4. Film focus. Adjusted as in recording.

5. Transport lateral. The recorded scan is placed in the center of the optical aperture.

6. Scan balance. Illumination uniformity across the scan is corrected if necessary. The parabola AOM is also set for readout (see No. 9 above).

7. Reference detector. The detected signal derived from the undiffracted portion of the reference beam is checked for proper frame sync and recovered clock capability.

8. Fiber array. The array's position is optimized for the type of readout to be performed.

9. Transport phase lock. Synchronization of the scanning beam with the moving hologram rows is accomplished using the built-in transport sync delay selector switch.

10. Strobe timing. The phase relationship between the recovered clock signal and the detected data is optimized. This includes optimization of frame sync detection also.

11. Data thresholding. The detected data is sent to an appropriate thresholding circuit. The threshold level is adjusted to minimize error rate.

12. Data analysis. The various selection circuits can be used to decide which portions of the film (rows or portions of rows) are to be analyzed. Error detection, correction, and display circuits are available at this point for data verification. (More information on these systems is given in Paragraphs 2.1.6.2 and 2.2.2.4).

2.3.2 Component Evaluation

2.3.2.1 Readout Parameters and Error Rate Measurement Procedures

In the readout checklist of Paragraph 2.3.1.2, Steps 1 through 7 are constant for each film. Steps 8, 9, and 10 may be set once to read out all channels or they may be adjusted to optimize each channel separately. Steps 11 and 12 are optimized for each channel. In a final system, Steps 1 through 10 will be optimized for the entire film. Steps 11 and 12 will still be optimized for each individual channel.

The fiber-optic array was built to match the expected positions of the bits during readout. However, small autoscan misalignments or readout lens aberrations can cause some bits to shift out of the expected locations. In order to read out more than one channel at a time, the fiber array must be positioned to detect multiple channels simutaneously even though this may not result in optimal detection of any single channel. This procedure is used for the "multichannel" readout tests. In the majority of tests, each channel is individually optimized and read out. In this situation the fiber array is repositioned for each channel. The fiber in use should be centered at the focal position of the bit stream.

The film transport phase-lock sync aligns the hologram rows with the readout beam. During readout, the slit was set to provide double-Rayleigh resolution. Using the phase-lock sync control the rows of holograms can be centered in the readout beam or advanced or delayed up to the width of one row. In the current system this is normally optimized for each channel.

The strobe-delay adjustment should be orthogonal to the threshold-height adjustment. In the current system, it is not. Therefore, as threshold is optimized for each channel, the strobe delay must also be reset.

The data-threshold level is optimized for each channel in every case. The error detection and analysis circuits are described in Paragraph 2.1.6.2. The developmental model contains two such circuits; the final system will contain sufficient circuits to perform error detection and correction on all channels simultaneously.

The measurable available to compare the films is bit-error-rate, as measured on a sample size of 10^6 data bits. About 50 such samples were read out for each test and the statistical mean and standard deviation were calculated. We found that, due to the error statistics and the number of adjustable parameters available, the minimum error rate was repeatable only within 10 percent.

2.3.2.2 Light Measurements

The light efficiency of the EDM optics is an important consideration for the design of future systems. We measured the efficiency of the major components in normal record mode, normal readout mode, and with minimum light attenuation.

An intensity loss of 56.6 percent has been measured between the laser output and the input to the main AOM; this light is lost in the parabola AOM and the servo system. In the record mode, there is 1 dB of attenuation in the main AOM; 7.4 percent of the input power is diffracted. With no attenuation, 38.5 percent of the incident light is diffracted. In the record mode (with a typical beamsplitter setting of 4) eighty percent of the input light is channeled into the signal path and 13 percent is diffracted into the reference beam; the remainder is lost in reflections. With the beamsplitter set to 0, seventy percent of the light goes into the signal beam and 23 percent is diffracted into the reference beam.

During recording with 1 dB attenuation in the main AOM and 4 dB in both the beamsplitter and page composer, 0.056 percent of the laser output reaches the film plane. With no attenuation in the acousto-optic devices, 0.43 percent of the light reaches the film. Most of the loss is in the page composer which has a diffraction efficiency on the order of 0.2 percent. The system efficiency during readout is 14.5 percent. During readout, the beam bypasses the high speed modulators and most of the optics.

2.3.2.3 Exposure

To begin the determination of the proper holographic recording parameters, two special recordings were made, each of which contained 4 or 5 exposure levels. For both films, the reference beam to signal beam ratio, K, was arbitrarily fixed at 13. The exposure levels were generated by increasing the attenuation of the main AOM in 1 dB steps. The main AOM affects both signal and reference beams simultaneously, thus holding the K ratio constant. The measured quantity in this test was the intensity of the recording beams. The absolute exposure is proportional to the light intensity, the beam size and the scan rate. The effects of the exposure are also dependent on processing. For this reason the optimum recording intensity will have to be remeasured if any of the above parameters are changed. The recording intensity ranged from 408 µW to 1020 µW.

For readout, each exposure segment was channeled through a different threshold circuit. Strobe position and phase-lock sync were optimized for all exposure levels simultaneously. Each threshold circuit optimized the threshold level for a given exposure level. The detected data were directed to each threshold circuit as the different exposure levels were read out. In this way, all exposure levels were read out in a single scan, eliminating possible effects of system drift. Several page composer channels were read out.

The results are shown in Figure 2-85. The error rate is plotted as a function of the exposure intensity. For all three channels plotted, the minimum error rate occurred at about 850 µW. The error rate doubled when the intensity was changed by
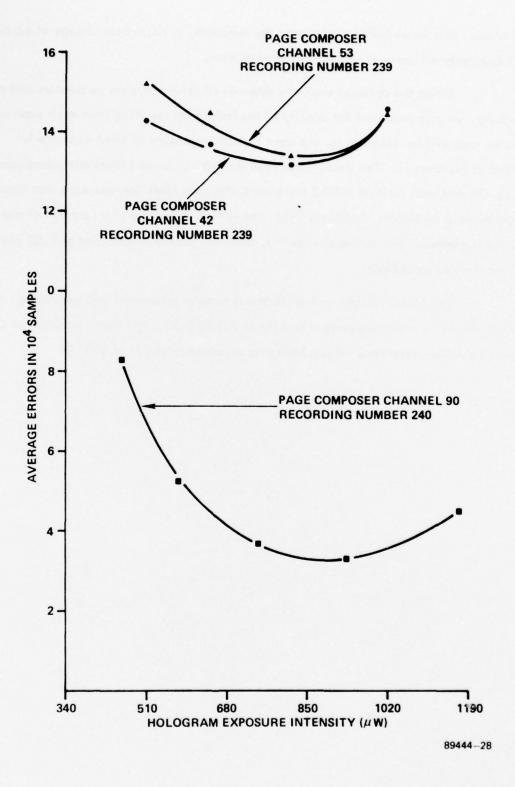
Figure 2-85. BER Versus Exposure Intensity

40 percent. In a localized region around the minimum, a 10 percent change in exposure resulted in only a 1 percent change in the error rate.

Since the optimum exposure depends on several system parameters and on processing, we also measured the density of the holograms resulting from each exposure. The error rate will be minimum for the same density regardless of what exposure is required to generate it. The density was read out with a Joyce Llobel microdensitometer. A 3 μm slit and scan ratio of 1000:1 were used; the scan direction was such that single holograms were measured. In Figure 2-86, the hologram density as a function of exposure intensity is plotted. The optimum intensity, 850 μW, results in densities of 0.52 and 0.54 for the two recordings.

For future systems with different recording parameters and processing, the exposure should be set to generate a density of 0.5 to 0.55. All films recorded for component evaluation were made with a hologram exposure intensity of 850 μW.
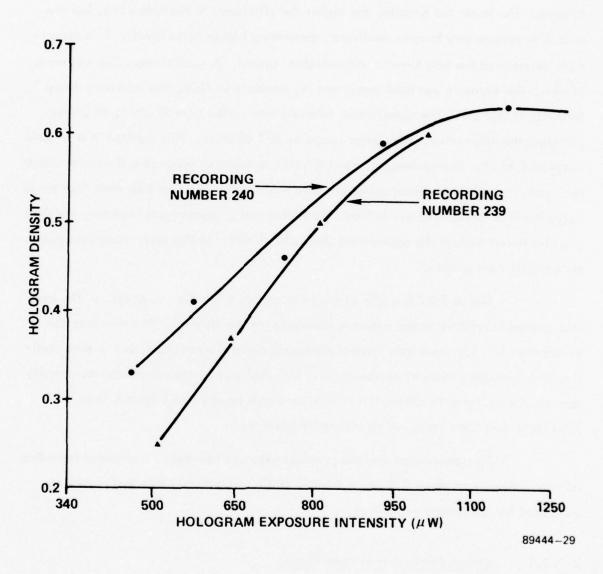
Figure 2-86. Hologram Density Versus Exposure

89444-29

2.3.2.4 K-Ratio

The ratio of reference to signal beam during recording is refered to as the K-ratio. The lower the K-ratio, the higher the efficiency of the holograms, but the recording process may become nonlinear, generating higher noise levels. This experiment determined the best K-ratio with which to record. A special recording was made, in which the exposure was held approximately constant by fixing the reference-beam intensity at 800 μW. The signal-beam intensity was varied from 27 μW to 65 μW by changing the attenuation of the page composer in 1 dB steps. This resulted in a K-ratio range of 8 to 19. During readout, each K-ratio section was assigned a threshold circuit and each threshold was optimized before data was taken. The film tabs were then set to cycle the film through the entire film. As each K-ratio segment was read out, the data was channeled through the appropriate threshold circuit. In this way, variations due to system drift were avoided.

Figure 2-87 is a plot of the error rate as a function of K-ratio. The error rate plotted is relative to the minimum error rate for the channel. The minimum BER occurred at K = 10; error rate was not symmetric about the minimum, but is more sensitive to increasing K than to decreasing it. This implies that the system can more easily tolerate the decrease in diffraction efficiency which results from higher K than the increase in nonlinear noise which occurs for lower K.

This experiment and the previous exposure test define a standard recording to have a density of about 0.5 and a K-ratio of 10. In general, standard recordings were used for component evaluation.

2.3.2.5 Effects of Number of Read Cycles

In transporting the film through the system, physical damage can occur. Such damage limits the number of times a film can be read out before the error rate becomes intolerably high. This experiment determines the sensitivity of BER to the number of readout cycles. A standard recording was divided into three sections. The
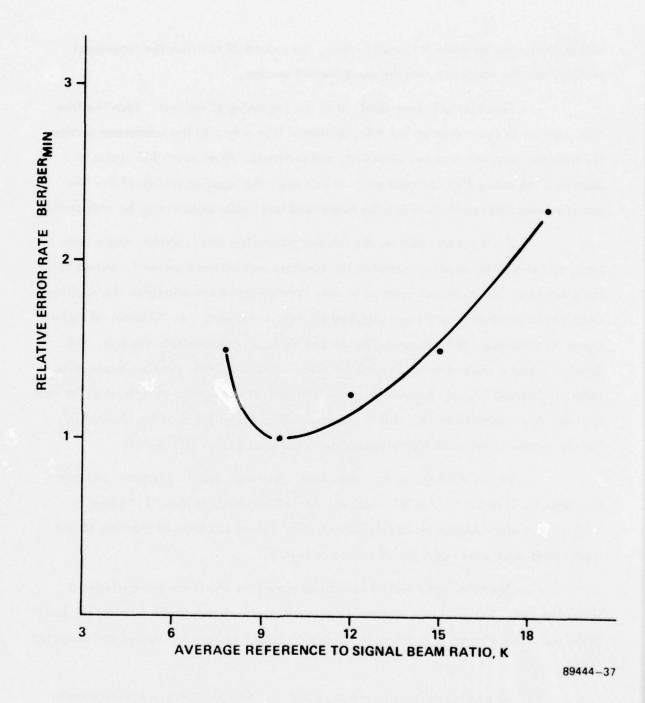
Figure 2-87. BER Versus K Ratio

89444-37

first 80 feet were set aside for baseline data, the second 20 feet was the turnaround section, and the remainder was the experimental section.

Five channels were read out at the beginning of the test. Then the film tabs were set to cycle through the third section of film only. In the turnaround section the transport stopped, reversed direction, and restarted. After every 100 cycles of Section 3 the entire film was read out. In this way, the baseline section of the film provides uncycled results to which the turnaround and cycle sections may be compared.

During each readout, the readout parameters (viz., strobe, phase lock sync, and threshold) were optimized in the baseline section and then held constant for the other two. The measured error rates were normalized by requiring that the baseline data remain constant. Five page composer channels were read out. Channel 54 had a better-than-average BER, Channels 37, 61 and 93 were approximately average, and Channel 5 had a worse-than-average error rate. In Figure 2-88, the normalized error rates of Channels 37, 54, 61 and 93 are plotted against the number of times the film was cycled. Also included on this plot is the unnormalized baseline data for Channel 37. For all channels, the error rate increased by a factor of 2 after 400 cycles.

Figure 2-89 shows the normalized cycle data and the unnormalized baseline data for Channel 5. For this channel, the BER increases to about 1.4 times its initial value after 300 cycles and then levels off. We do not know at the time of this report what causes the upper bound on the error rate.

The turnaround section contained some film which was not cycled and some that was. The error rate showed no anomalous effects due to the turnaround, but there was a sharp increase in error rate at the dividing line between cycled and uncycled film.

After the error rates were recorded, the film sections were studied under the microscope to determine the nature of the damage. The first photo in Figure 2-90 is a photograph of the uncycled film under Schlieren illumination. Point defects and microscratches of less than 1/4 mm are apparent. In comparison, the second photo of Figure 2-90 is a photograph of the cycled film. The new microscratches are 1mm and
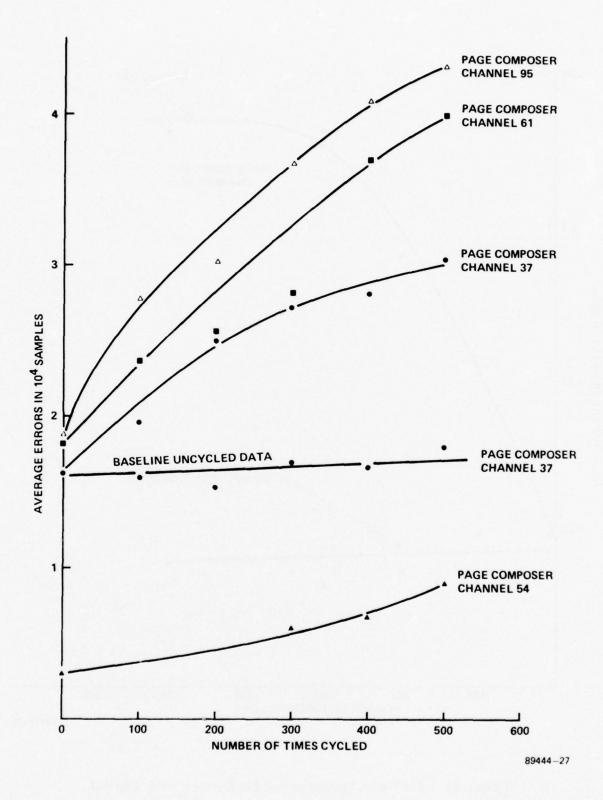
Figure 2-88.   BER Versus Number of Readout Cycles – Better Channels

89444-27
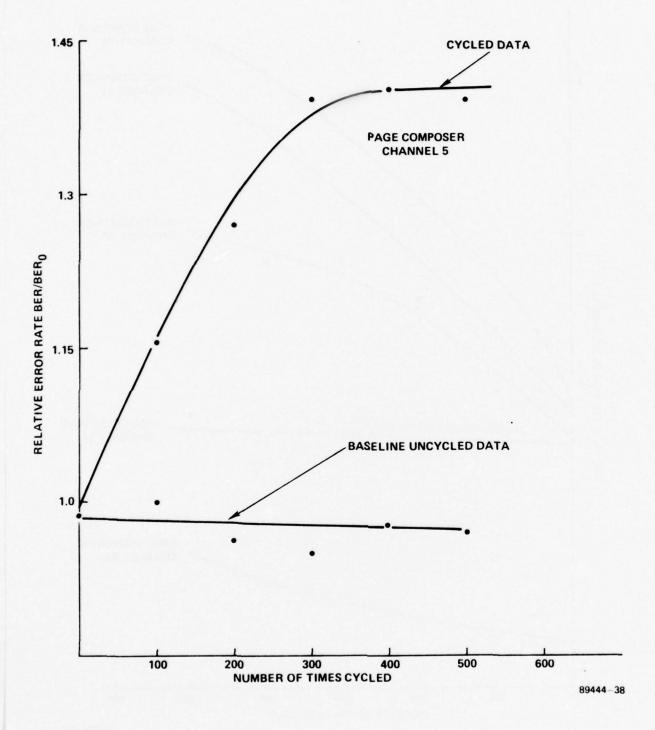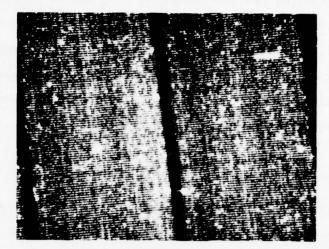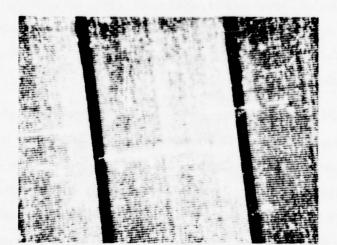
Figure 2-89. BER Versus Number of Readout Cycles — Weak Channel

89444-38

FILM SURFACE BEFORE CYCLING

TRANSPORT MOTION

FILM SURFACE AFTER CYCLING

TRANSPORT MOTION

Figure 2-90.   Effects of Transport Cycling on Film Surface

89444—65

2-195

more in length and therefore obliterate entire holograms. They are not straight line scratches, but appear to be caused by particles rolling across the film surface as the film is cinched on the spool. We conclude that the film transport and, in particular the air bearing platen are doing an excellent job of preventing scratches. The environmental conditions in the vicinity of the transport are critical. In future systems a film enclosure under positive pressure may be desirable to ensure clean conditions.

2.3.2.6   Strobe Delay

As the readout beam scans the rows of holograms, it is modulated by the different densities of the holograms and guardbands. The modulation of the throughput beam is detected and used to generate a periodic strobe pulse for readout synchronization as described in Paragraph 2.1.5.2. The purpose of the strobe is to define the time at which each data bit is sampled for comparison to the threshold level. The position of the strobe pulse can be delayed up to 2 bit widths. This experiment measures the sensitivity of the error rate to the position of the strobe pulse.

A standard recording was used. The system was optimized for each channel to be read, and only the threshold level was adjusted as the strobe delay was varied. At each strobe setting, the minimum BER was measured and photographs were taken of the strobe pulses superimposed on the data bits. From the photographs, the displacement of the strobe pulse from the bit center was measured.

In Figure 2-91, we plotted the relative error rates against the displacement of the strobe from the center of the bits. The amount of strobe displacement is in units of the percentage of one bit spacing. The error rates are plotted relative to the error rate when the bits are center-sampled. The optimum error rate occurs when the strobe is offset from bit-center by 20 to 25 percent; the optimum position is after bit center. The strobe pulse not only determines when the data bits are sampled, but also when the frame sync is sampled; frame sync is designed for center sampling. As the strobe is displaced, it begins to move off the frame sync pulses; data cannot be detected if frame sync is not detected. When the strobe is displaced 20 percent from bit center, the detection
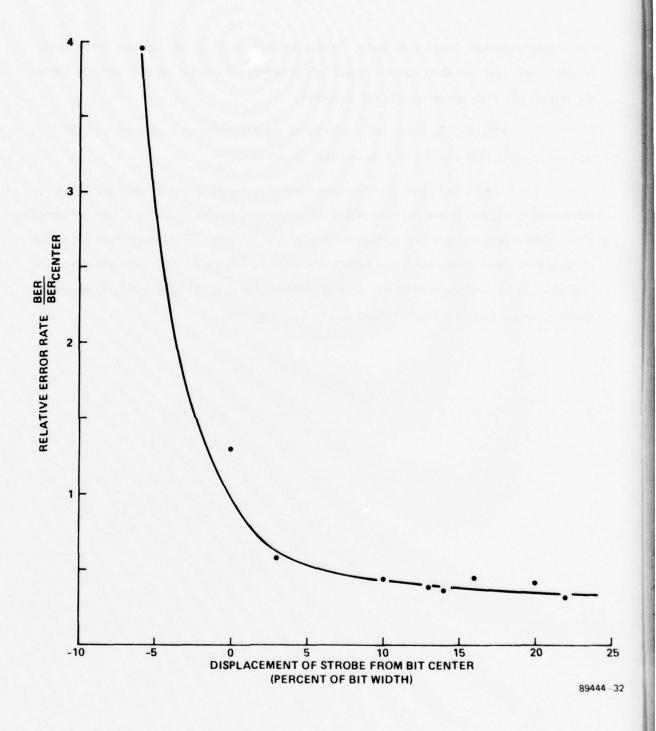
Figure 2-91. BER Versus Strobe Position

89444-32

system begins to lose frame sync data. With greater than 22 percent offset, frame sync is completely lost and data can no longer be detected. The optimum BER seems to be in the region in which frame sync is not detected.

Figure 2-92 shows the strobe pulse superimposed on a data bit with 22 percent offset. This was the best measurable strobe position.

Theory indicates that the best error rate should occur when the bits are center-sampled; this is the point at which "1" bits have maximum height. Center-sampling also provides greatest contrast between "0" bits and "1" bits. The reason that the strobe pulse is best when displaced is not fully understood at this time. It is recommended that this anomaly be investigated in the next development phase. It is desirable to separate the data strobe from the frame sync strobe in future systems.
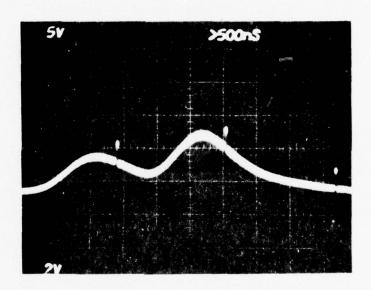
Figure 2-92. Observed Optimum Strobe Position

2.3.2.7   Readout Rate

The EDM has four readout speeds available. For final system use, the data may be read out at 750 Mb/s; for diagnostic purposes lower rates are useful; thus, three other speeds are available, 375 Mb/s, 75 Mb/s, and 37.5 Mb/s. In this experiment, we read out channels at full speed and at either 75 Mb/s or 37.5 Mb/s and compared the error rates.

Twenty-four random channels from a standard recording were used and each was read out at 750 Mb/s. Seven of the channels were read out at 37.5 Mb/s, the remainder at 75 Mb/s. At each speed and for each channel, strobe, phase lock sync, and threshold level were optimized. At this time we are not able to fully optimize the strobe position; this problem is discussed in Paragraph 2.3.2.6. At all speeds, the optimum BER occurs in the region where frame sync is not detected. The error rates were measured on the edge of frame sync loss. By considering the rate of change of BER with strobe delay, we estimate that the measured error rates are within 5 percent of the optimum error rates.

The results are given in Table 2-12. At 750 Mb/s the average error rate was about 200 percent worse than at 75 Mb/s and about 630 percent worse than at 37.5 Mb/s. For the remainder of the component evaluation experiments, readout rate was 75 Mb/s.

2.3.2.8   Spatial Frequency Effects

The recorder generates holograms from a 128-bit page composer; each page composer channel corresponds to a fixed spatial frequency determined by its degree of offset from the reference beam. Channel 1 is at 300 cy/mm, Channel 128 is at 600 cy/mm. In this experiment, we determine the effect of spatial frequency on the error rate. The fiber-optic array in the readout system has one fiber available for each page composer channel. However, the detection electronics have been implemented for only a limited number of these. For this test, four fibers and corresponding photo-detector circuits were used; they were spaced 32, 24, and 32 channels apart and each

Table 2 -12. Effects of Readout Rate

Channel Number	BER x 10^{-6} at 37.5 Mb/s	BER x 10^{-6} at 37.5 Mb/s	Percent Increase in BER at 750 Mb/s
16	35 ±8.7		730
17		482 ± 58	570
18	60 ±11		380
19		167 ±31	240
20		57 ±12	200
21		337 ±50	160
48	44 ±8		150
49		100 ±16	70
50		36 ±8	300
51		68 ±11	60
52		118 ±14	100
53		21 ±5	100
73		31 ±8	190
74	23 ±7		470
75		60 ±12	130
76		23 ±6	60
77		27 ±9	30
104	23 ±8		860
105	39 ±11		900
106	35 ±7		930
107		200 ±29	380
108		78 ±16	290
109		60 ±13	300

could be vertically translated to cover 40 channels. Therefore, Fibers 1 and 2, 2 and 3, 3 and 4 overlap in coverage, and every channel is within range or at least one of them.

Thirty-two randomly selected channels were read out and we plotted the resulting BER's in Figure 2-93 as a function of page composer channel. No obvious spatial frequency effects are apparent (the extremely bad channels are scattered throughout the frequency range). The apparent strength of a channel (i.e., bit height), depended on the photodetector with which it was read. Channels read out with Fiber 2 all partially or totally saturated the photodetector; their error rate was only slightly better than average. The fiber-to-photodetector coupling may be better for Fiber 2 than for the other three. Comparing channel strength within each photodetector group, the channels with a high error rate are not weak channels.

2.3.2.9   Scan Location

The EDM records a line of 1512 holograms across 25 mm of film. At either end of scan, the light passes through the edges of the transform lens. In general, lens resolution is best along the axis and falls off toward the edges. Therefore, theory predicts best error rate for holograms in the center of scan. In this experiment, we measure the error rate as a function of the position of the holograms in the scan.

A standard recording was used. For each channel read, the average error rate for the entire scan was first measured. The scan was then divided into 15 segments of 100 holograms each and the error rate within each segment was measured. Phase lock sync, strobe delay, and threshold level were optimized for full-scan readout and held constant for partial-scan readout. By doing this, we measure the effect each scan location has on the full scan error rate as normally measured. The results are plotted in Figure 2-94 for a typical channel. The error rates are measured relative to the average full-scan error rate. The error rate at the beginning of scan is about three times worse than average, while in the center it is about four times better than average. The first 100 holograms have an abnormally bad error rate which could be caused by resolution loss at the edge of the transform lens or by failure of the bit sync clock to come up to speed rapidly enough. Since the bad error rate of the first 100 holograms has increased

2-202
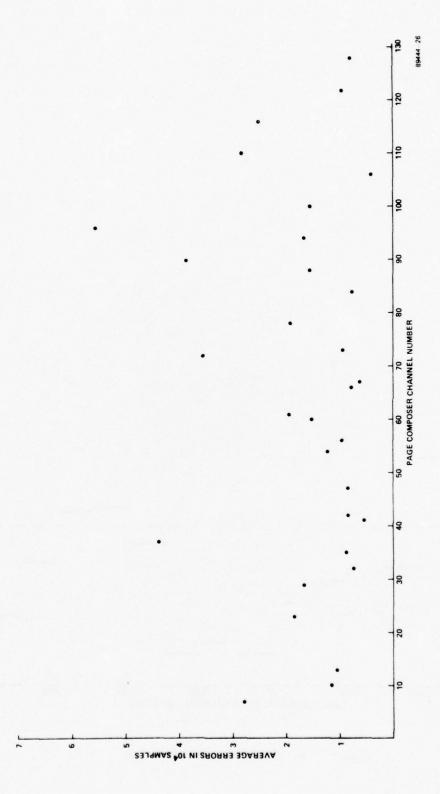
Figure 2-93. BER Versus Spatial Location

89444-26

2-203
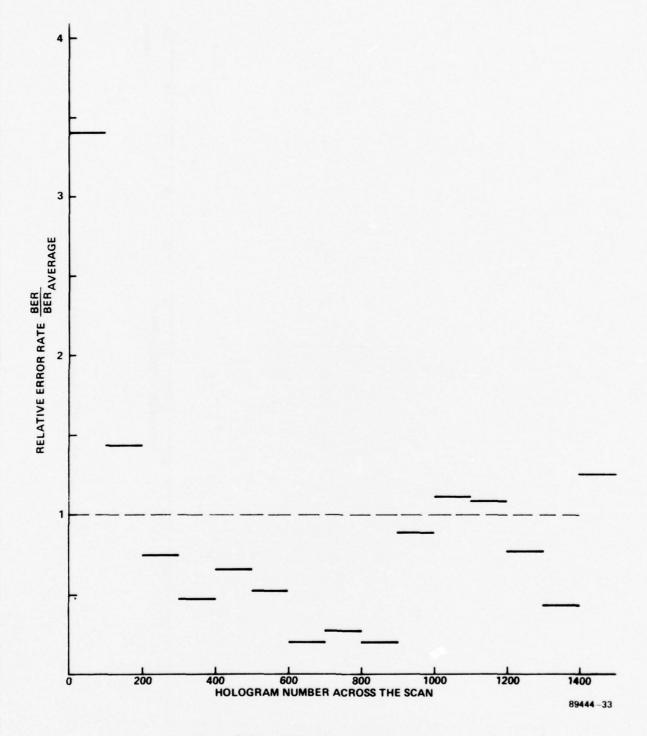
Figure 2-94. BER Versus Scan Location

89444-33

the average error rate by about 14 percent, it is recommended that the cause be found and eliminated in the next model.

2.3.2.10   Readout Illumination

In readout, a trade-off must be made between optical noise and electrical noise. As readout intensity increases, the data bits become brighter and eventually saturate the photodetectors. Theory predicts that electrical noise will increase sharply when the photodetectors are saturated. This experiment measures the sensitivity of the error rate to the readout intensity.

A standard recording was read out and the channels were optimized for an average readout intensity. Strobe delay and phase lock sync were set and held constant for all intensity levels; threshold was optimized at each intensity. The readout intensity was varied from 70 mW to 315 mW and optimum BER was measured at each intensity level. The readout intensity was measured at the film plane.

The measured error rate relative to the minimum error rate is plotted against readout intensity in Figure 2-95. At 70 mW, no bit in the data stream is bright enough to saturate the photodetector and the error rate is 4.3 times greater than the minimum. As bit intensity increases, BER decreases. At 100 mW approximately 10 percent of the data bits saturated the photodetector and the error rate was approximately halved. At 315 mW, about 80 percent of the data bits saturated the photodetector. At this illumination level the error rate is near minimum but may be improved further (315 mW was the maximum available from the system).

Theory predicts that the error rate will increase when the photodetectors saturate. The experiment has proved the opposite. Electrical noise may not be as important as predicted. One of the primary effects of optical noise is bit height fluctuations. Saturating the photodetectors eliminates bit height fluctuations and makes it easier to set the threshold. The reason why the error rate is best when the photodetector is saturated is not known, but in the future, we belive the system should be run in this mode.
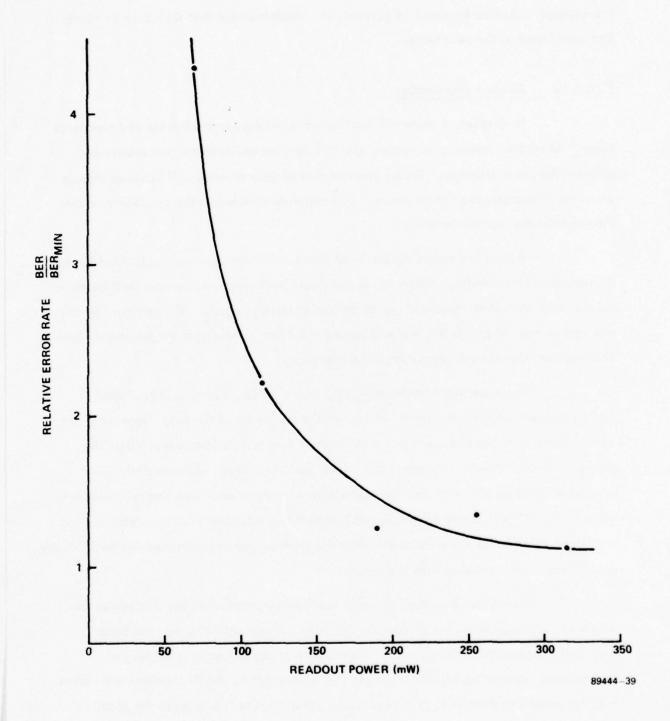
Figure 2-95. BER Versus Readout Intensity

89444-39

2.3.2.11   Film Transport Focus

Film flatness requirements are determined by the depth of focus of the transform lens. In this experiment we measure the sensitivity of the error rate to displacements of the film from the focal plane. A standard recording was used and the focal plane was determined by maximizing the modulation of the throughput beam. This modulation is caused by scanning the readout beam across the grating formed by the guardbands and the holograms. When the film is in the focal plane, the readout beam is smallest and modulation is maximized.

The readout scan was limited to holograms 300 to 1200 because the center portion of the film is flattest. Therefore we are measuring the effect of the depth of focus of the transform lens rather than the film flatness. The film was read out in the focal plane and at various positions on either side of the focal plane up to 6 μm. At each position, phase-lock sync, strobe delay, and threshold level were optimized.

In Figures 2-96 and 2-97, relative error rates are plotted as a function of film displacement from the focal plane for two page composer channels. In both cases, the minimum error rates occur in the focal plane. For page composer Channel 13, a 4 μm shift in either direction doubles the error rate. For page composer Channel 67 it requires a 6 μm displacement to double the error rate. The flatter the film, the more sharply the error rate will depend on film displacement.

2.3.2.12   Phase Lock Sync

The transport phase-lock sync delay is used to align the hologram rows with the scanning beam. Each step delays the transport 6 degrees, offsetting the hologram 1.7 percent of its width from the center of the readout slit. This experiment will determine the sensitivity of error rates to the degree of misalignment between readout beam and hologram rows.
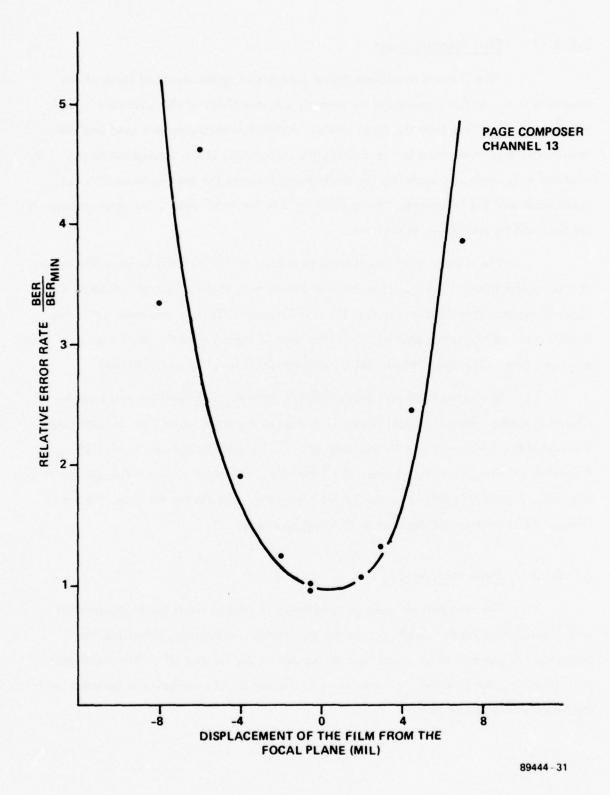
Figure 2-96. BER Versus Focus – Channel 13
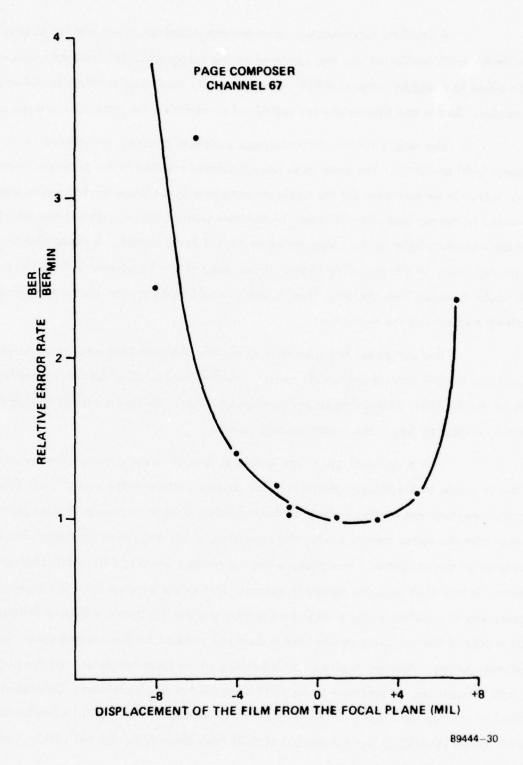
Figure 2-97. BER Versus Focus — Channel 67

89444—30

A standard recording was used and the illuminating slit was set to provide double-Rayleigh resolution and was centered on the holograms. The hologram rows were then offset in 6 degree steps and BER was measured for each step of offset on either side of center. Strobe and threshold were optimized to minimize the error rate in each case.

The results for two different page composer channels are plotted in Figures 2-98 and 2-99. The error rates are calculated relative to the minimum measured error rate. In neither case did the minimum error rate occur when the holograms were centered in the readout slit. This may be due to a nonsymmetric readout beam which centers maximum light on the hologram when the slit is off center. It could also be due to an asymmetry in the recording beam. If one edge of the holograms were more optimally recorded than the other side, readout would be best when the better side is entirely included in the readout.

The curves are not symmetric about the minimum BER; error rate increases rapidly as the hologram is shifted off center. As the row is shifted further off center, less of the hologram is illuminated and resolution is lost. When the shift is toward the center, resolution loss is not a contributing factor.

This phase-lock sync data indicates that different channels are optimum at different phase lock settings, and there is no obvious pattern to the variations. One possible explanation for this is that, if the recording is made in a near-Fourier plane rather than the exact Fourier plane, the transforms of the individual channels will not be centered in the hologram. Therefore, when the readout beam is shifted off a hologram center, it may shift onto the transform center. This would account for each channel optimizing at a different phase-lock sync setting and for the optimum setting falling on either side of the hologram center, but it does not account for the randomness of the optimum setting. Another explanation is heating of the page composer. As the page composer heats up, an arbitrary phase shift is imposed on each channel. This has the effect of shifting the focal position of the Fourier transform. The result is similar to a near-Fourier recording, but the amount of shift from channel to channel will be random (which matches observed results).
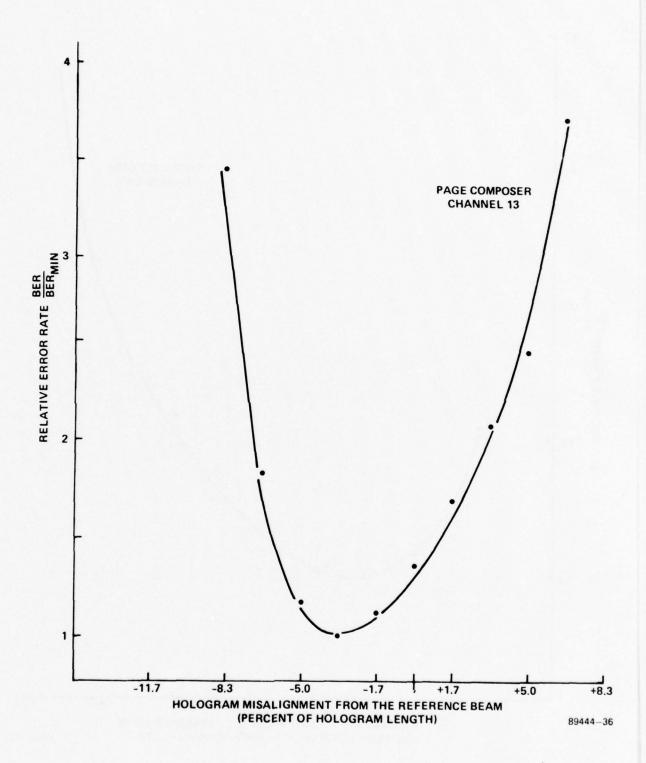
Figure 2-98. BER Versus Film/Spinner Synchronization – Channel 13

89444-36
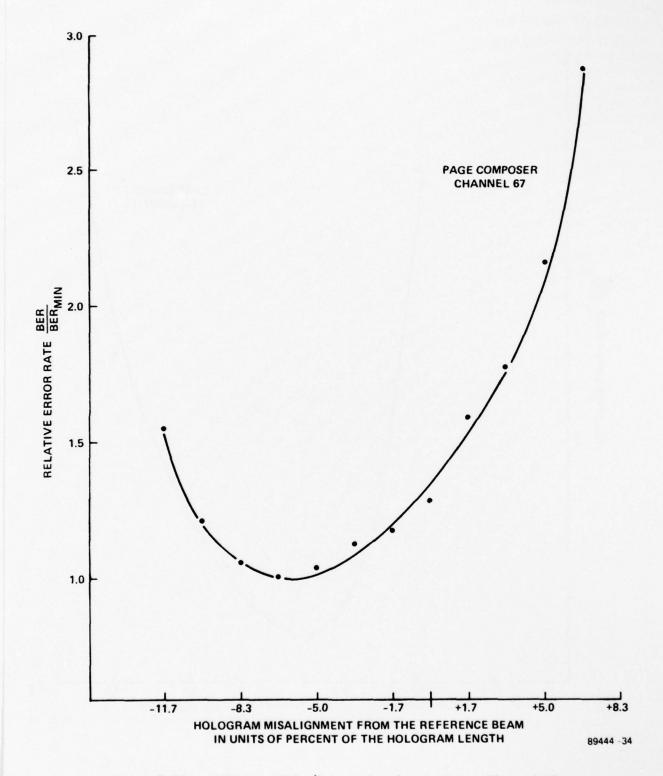
Figure 2-99.   BER Versus Film/Spinner Synchronization – Channel 67

2.3.2.13   Threshold Techniques

The EDM has four threshold sources available. The first and most commonly used is the adaptive threshold in which the threshold level adjusts to the bit height fluctuations of the page composer channel being read out. Second is the manual threshold in which a smooth curve is manually defined to track the basic envelope of the data stream. The height of this curve is then set to minimize the error rate. The last two threshold sources are the dedicated channels. Two channels are driven with a temporal pattern in which every other bit is on. Adaptive thresholds are matched to these channels. The channel which best duplicates the shape of the channel being read out provides the threshold. In this experiment we compare the performance of the four threshold sources.

A standard recording was optimized using the adaptive threshold. Full scan readout was used since we are interested in how well each threshold type handles the entire scan. Phase lock sync settings were optimized for each of the four channels read out and were held constant throughout the remainder of the experiment. Strobe and threshold levels were optimized for each threshold type. Table 2-13, Column 2 lists the measured BER for each channel read out; the error rate in each case was on the order of 1×10^{-4}.

For the manual threshold method, the strobe setting was re-optimized and the shape of the threshold curve was matched as well as possible to the envelope of the data. The shape and height of the threshold were iterated to minimize the error rate. Column 3 of Table 2-13 gives the change in error rate going to manual threshold from adaptive thresholding; error rate increased in each case. Page composer Channel 44 contained a localized dip in bit height. Since the manual threshold cannot compensate for such a dip, the error rate increased by a factor of 7.

Two special purpose channels have a bit pattern in which every other bit is on; these are the dedicated channels. Since each channel is associated with an adaptive threshold circuit, it generates a threshold which tracks the shape of its illumination intensity curve. In use, whichever of these thresholds best matches the data profile is

used to read the data. The height of the threshold is set to minimize the error rate. To use a dedicated threshold source, the fiber array must be positioned to allow both channels to be read simultaneously, but such a position may not be optimum for either channel. Columns 4 and 5 of Table 2-13 give the change in error rates when the dedicated channels were the threshold source. In each case, one dedicated channel is clearly better than the other.

Table 2-13. Effects of Threshold Technique

Page Composer Channel	BER x 10^{-6} with the Adaptive Threshold	Percent Change in BER Using Manual Threshold	Percent Change in BER Using Threshold Set from Dedicated Channel 101	Percent Change in BER Using Threshold Set from Dedicated Channel 69
50	114 ±14	+600	+581	+201
55	104 ±11	+28	+425	+70
74	114 ±25	+18	+227	+72
127	105 ±15	-3	+154	+366

Although, with the exception of Channel 44, the manual threshold was better than the dedicated adaptive, this is not expected to hold true for a fully operational system. We can not in general depend on having scan profiles which contain no localized dips. The problem here was that the two channels could not be simultaneously optimized. In this situation adaptive thresholding clearly provides the best performance. However, in a final system it would require 128 parallel threshold circuits which would be costly to implement. Since thresholding with dedicated channels requires only two threshold circuits, it will be necessary to consider the trade-offs carefully during any future design activities.

2.3.2.14   Film Base Evaluation

Film base noise sets a boundary on achievable error rate. In this experiment we determine to what extent the film base limits optimum BER. The system

was set to read the data in a back-to-back mode. For this experiment, only the signal beam is used and the data is read out as it is generated without the intermediate step of recording it on film. Since no frame sync is available, a special error detection circuit called OAF was used. This is a free-running version of the AF circuit, which is described in Paragraph 2.1.6. The OAF circuit generates up to 5 errors for every incorrect data bit, therefore, we divided the measured error rate by five. In back-to-back readout with no film, no errors were detected in 10^8 samples.

A special recording was made which contained no data. Only the reference beam was on and the film was exposed to a uniform density of 0.6. The system was then read out in back-to-back mode with the uniformly recorded film in place. Light intensity was adjusted so that the bit intensities at the fiber array were the same as previously. The resulting BER was 4.5×10^{-6} for the best channel in the system (Channel No. 1), and most likely represents the best raw error rate we can expect from any current film recording.

2.3.2.15   Line Rate Repeatability

There are two types of errors detected in wideband recording: random and burst. Each can be corrected by the use of the appropriate error correction codes, but both cannot be handled simultaneously. This test will investigate whether the majority of detected errors are of random or burst origin. Random errors caused by noise fluctuations do not come in groups and will not repeat each time the film is read out. Burst errors, on the other hand, are caused by film defects and are expected to occur in the same location each time the film is read out. The procedure used was to optimize fully a channel with average BER and then hold all readout parameters constant. Then, reducing the vertical scan window to one scan line, we cycle past that line 30 to 50 times, reading each time the number of errors in 1512 samples.

The results show that random errors exist on the order of one per row. If a row generates three or more errors, it will tend to repeat with random fluctuations added on. Therefore, burst error sources as small as three errors will repeat. One of

the channels selected was immediately adjacent to a dedicated channel recorded with a repeating one-zero-one-zero data pattern. For this case, random fluctuations did not exist. If a row contained four errors in one scan, it contained those four errors every time it was scanned. Similarly, a line containing zero errors contained zero on each scan. We expected this if the adjacent channel were inoperative, but not for an adjacent dedicated channel. The results indicate that burst errors occur and should be considered in future error correction codes.

2.3.2.16 Coded/Decoded Readout

In the EDM, eight channels have been coded for error correction. We measured the efficiency of the error correction codes used. No special experiment was run. Instead, in each of the component evaluation tests, at least one coded channel was read out. For some tests, all eight were read out. Two error detection and counting channels are available. The coded channels were read out simultaneously on both, one set to read raw error rate and the other to correct the errors and read the decoded error rate. For this experiment, we consider only the optimum readout conditions from each of the previous tests. In some cases full scan was used, in others only center-of-scan.

The results, plotted in Figure 2-100, are decoded error rate versus raw error rate. Most decoded rates fall in the rage of 10^{-6} to 10^{-7} regardless of the raw error rate. Some channels with a raw rate less than 1.3×10^{-4} decoded to better than 10^{-8}. Some channels with a raw rate greater than 1.5×10^{-4} decoded to 10^{-5} or worse. These, however, are exceptions. The average decoded rate falls between 10^{-6} and 10^{-7}.

2.3.2.17 Multichannel Readout

In an operational WBR system having a read rate of 750 Mb/s, all 128 page composer channels will be simultaneously read out. This requires 128 parallel electronic circuits and is expensive to implement in an experimental model. Therefore in Phase II we made a compromise. The 128 data bits per hologram are imaged onto a 128-unit
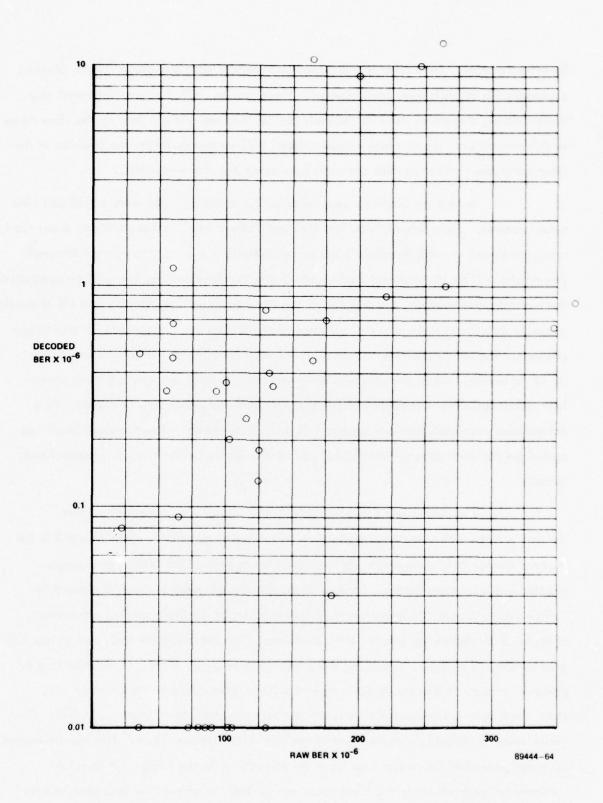
Figure 2-100.   BER Correlation – Raw Versus Corrected

fiber-optic array. Each fiber is positioned to interface with a photodetector. Sixteen photodetector circuits were implemented. These can be shifted to interface with any desired fiber, therefore, all 128 channels can be read out without moving the fiber array. In this experiment, we simulate an operational WBR system by fixing the position of the fiber array and reading random channels by moving the photodetectors.

Seventeen channels were selected for readout, eight were coded and nine were uncoded. Each channel was first read out individually. Fiber position, phase-lock sync, strobe delay, and threshold were set to optimize the error rate of each channel. The results will be the standard against which the multichannel readout will be evaluated. For multichannel readout, the position of the fiber array was adjusted so that all channels could be detected simultaneously, although that position was not optimal for any single channel. The strobe position about 20 percent to the right of the bit center was best for all channels. When the channels were individually read out, the optimum phase lock delay varied by 4 percent of the hologram width on either side of center. As a compromise, the hologram was centered in the readout beam. The threshold level was optimized for each channel individually since this would be the case in an operational system.

The results are listed in Table 2-14. Column 1 is channel number, Column 2 is the BER when each channel is individually optimized, and Column 3 is the percent change in bit-error-rate for multichannel optimized conditions over single channel optimized conditions. For raw data, the change ranges from -10 percent to +67 percent. Due to the uncertainty in determining the optimum readout parameters, changes of 10 percent or less are not significant. Ten percent show increases in raw BER greater than 10 percent. Changing the phase-lock delay by 3 percent resulted in a 67 percent increase in BER for Channel 70 and a 10 percent decrease for Channel 101. Phase-lock sync being nonoptimum is not the primary cause of an increase in BER. The major cause is probably misalignment of the data bits with the fibers. This can be caused by misalignment of the readout optics or by aberrations in the lenses. It is not a fundamental problem since the fiber array can be built to correct for lens aberrations.

The change in decoded error rate is more difficult to analyze. Since the initial error rates were low, any increase looks large. The decoded error rate under multichannel readout conditions was, on the average, about double that measured for single channel readout.

Table 2-14. Multichannel Readout

Page Composer Channel	Single Channel Optimized			Multichannel Optimized		
	Phase Lock Sync Setting	Errors in 10^6 Samples		Phase Lock Sync Setting	Percent Change in Error Rate	
		Raw	Decoded		Raw	Decoded
1	40	234 ±50		40		
13	39	526 ±64		40	+2	
18	42	264 ±22	1 ±2.5	40	+42	+90
19	39	624 ±48	35 ±17	40	+24	+323
23	37	145 ±18		40	+49	
45	40	280 ±22		40	+34	
50	40	93 ±24	0.33 ±1.3	40	+8	+9
51	37	343 ±37	0.65 ±1.5	40	+11	+26
55	40	95 ±12		40	+14	
69	42	141 ±24		40	+67	
74	40	102 ±17	0.2 ±0.9	40	+37	+75
75	40	103 ±14	0.01	40	603	+700
95	38	122 ±14		40	-1	
100	42	88 ±11		40	-10	
106	39	130 ±20	0.01	40	+6	+4000
107	40	266 ±47	14 ±11	40	-8	-29
127	39	75 ±12		40	+44	

SECTION III

ADVANCED SYSTEMS

The increasing sophistication of communication and information systems has created a need for systems capable of recording and retrieving digital data at user data rates of 2 gigabits per second (Gb/s) and higher. These readout rates are not achievable with either electron beam or direct spot recording technologies. During the course of the present contract, we have explored several approaches which have the capability of both storing and retrieving data at multigigabit per second rates.

All of the approaches are based on the holographic recording of multi-channel data on photographic film. Several advantages are inherent to this basic approach. First, the use of multichannel recording provides a significant reduction in the bandwidth requirements of individual channels. Second, the use of photographic film provides an archival storage medium for the user data. Third, the use of the holographic recording technique provides a reduction in the precision required for film position. All of these features represent significant advantages for any proposed system.

All of the approaches employ a continuous motion film transport system. The movement of the film is utilized during recording to distribute the multichannel information along the length of the film. The approaches differ in the techniques used to distribute the information across the film width and in the types of readout devices required to detect the recorded data during the readout process.

The five holographic record/read system concepts can be briefly described. The prime approach is the SP approach which is basically an extension of the present exploratory development model (EDM) that provides for higher recording rates on a 70 mm film format. The SIAM approach can be viewed as two of the present EDM systems with two parallel record/read paths, but using a common laser and film transport. The AO/SP approach is very similar to the SP approach; the significant difference is that the reference beam is directed to the film by separate optics and is scanned by an acousto-optic beam deflector. The 2D approach is a system concept

based on recording two dimensional holograms of the data pattern from an acousto-optic modulator array. The LS approach, based on an acoustic traveling wave lens, provides the necessary scanning action through unconventional acousto-optic devices.

In the remainder of this section, we provide a description of the basic requirements for the approaches considered. First, we provide a basic overview and present critical design considerations for the general case of high data rate recording systems. After the background material is covered, each of the conceptual system approaches are described. The function of the system description is to provide a basic understanding of the system operation for recording, to provide an analagous understanding for readout, to establish the requirements for major system components, and to evaluate the system potential. We conclude the section with a summary of the relative advantages and disadvantages for all of the approaches.

3.1   BACKGROUND

There are several areas of consideration for system design common to the proposed approaches. Because of the multichannel design, each of the approaches must use high-speed electronics capable of performing the demultiplexing operation for recording and the multiplexing operation for retrieving. To ensure that high fidelity information is retrieved from the system, we must use some type of error correction code during the recording process. Because each of the approaches utilizes a continuous motion film transport, we must consider a basic constraint relating the film speed and recording format to the desired system data rate. We discuss the impact on system design posed by these areas in this section.

3.1.1   Electronic Requirements

The electronic data handling requirements of a high-speed recorder/reproducer system are a major consideration for the realization of an operational system. The recorder must be capable of accepting the original high speed serial data along with a data synchronous clock. The recorder electronics must format the serial data into parallel channels for multichannel recording. Additionally, this formating operation

must be performed so that the time ordering of the serial data can be maintained between the input and output of the system. Because data is retrieved from the system in a multichannel format, we must implement a parallel-to-serial multiplexing of the output data channels. Furthermore, these operations must be performed in a manner that is compatible with the system requirements.

Previous developments have demonstrated the feasibility of performing the multiplexing and demultiplexing operations at rates corresponding to 1 Gb/s. During this phase of the development, we developed a receiver (demultiplexer) and transmitter (multiplexer) that provided error free processing of input data received at a 1 Gb/s rate. Part of the development effort was concerned with realizing techniques that maintained a time-ordered series without including prime-frame and subframe synchronization words in the data stream. Techniques to achieve this were successfully demonstrated.

The extension of these techniques to data received at rates of 2 Gb/s requires further development and refinement. A considerable effort must be devoted to this development, since proper system operation can be achieved only when the techniques are perfected. However, we are confident that the required electronic subsystems that match any of the proposed system configurations can be successfully realized.

3.1.2   Error Correction Coding

Any system used for the storage and retrieval of critical information must consider some scheme for detecting and correcting errors in that information. In particular, error correction coding (ECC) is required to achieve the high levels of fidelity that have been identified for any subsequent recorder/reproducer system. The use of ECC has two major impacts on the system performance.

The first impact is a significant improvement in system operation. When incorporated into the recorded data, ECC provides a considerable decrease in the bit-error-rate of the system. For the present breadboard system, the error corrected bit-error-rate is two orders of magnitude less than the raw bit-error-rate. A decrease in the bit-error-rate of this magnitude is significant.

The second impact is the increased recording rate that results from incorporating the error correction code. In addition to the user data that is recorded by the system, data representing both the error correction code and system-required information must be recorded. The system-required information includes sync timing, scan status, and threshold recovery signals. Overhead information must be recorded simultaneously with the user data; the extra recording that must be performed necessarily increases the system data rate.

A reasonable estimate of the required system data rate can be made based on the following assumption. To achieve the desired level of ECC improvement and to record the necessary overhead information, we require an approximate increase in the total system rate of 25 percent. Thus, for a user data rate of 2 Gb/s, the total system data rate must be 2.5 Gb/s. The system analysis performed for the various approaches is based on an aggregate system data rate of 2.5 Gb/s.

3.1.3   Recording Format Constraints

Inherent in any system that records digital data on continuous motion film is a constraint relating the data recording rate R to the film velocity V, film width W, and average information packing density δ. The constraint is summarized by the fundamental equation

$$R = VW \delta .$$

The special requirements and particular performance goals for a specific recorder/reproducer system imposed by this relation must be considered. A high data rate for recording and retrieving information is the major goal for the systems. Therefore the data rate of R = 2.5 Gb/s cannot be compromised. The film velocity V is limited by the design of the film transport system. The design for the transport system must also consider the film width W. The choice of film width is limited to those widths commercially available. The product VW, which represents the area of film used per second by the system during recording, is indicative of the cost to operate the system. From these considerations, it appears we should make the information packing density

δ as large as possible to achieve the required rate. However, limits on the value of the information packing density are imposed by system error rate considerations. The various trade-offs implied by the equation must be considered during any system analysis.

3.2 SP SYSTEM APPROACH

One method that has the capability of achieving the required user data rate of 2 Gb/s for recording and reproducing has been designated the SP system. A functional representation of the optical configuration required is given in Figure 3-1. The incoming serial stream of digital data is converted into parallel channels by the high speed demultiplexer. The approach utilizes a multichannel acousto-optic page composer to format the data in the optical domain for recording on photographic film. The channels of data are recorded in a block as one-dimensional, phase-randomized Fourier transform holograms. The information retrieval process uses the spinning mirror to descan the data and a discrete fiber-optic/photo-detector array to read the reconstructed data pattern. A subsequent multiplexing circuit converts the multichannel data into the original data stream. The SP system described here is an extension of the present Exploratory Development Model.

3.2.1 Recording Process

The recording process in the SP system is initiated by the demultiplexing of the incoming 2 Gb/s serial user data stream into parallel channels. During this demultiplexing process, the required system operation information and the necessary error correction coding are interleaved with the user data. The aggregate data rate of the 128 parallel channels is equivalent to 2.5 Gb/s. The time ordered parallel channels are used to modulate 128 signals (an RF carrier frequency). Each of the amplitude-modulated RF channels is used to control the response of one of the 128 piezoelectric transducers in the acousto-optic page composer (AOPC). The presence of a modulated RF signal, corresponding to a logical "one", causes the piezoelectric transducer to launch a compressional wave into the acousto-optic material. No compressional waves are generated at those transducer locations of the AOPC where the modulated signal was

3-5
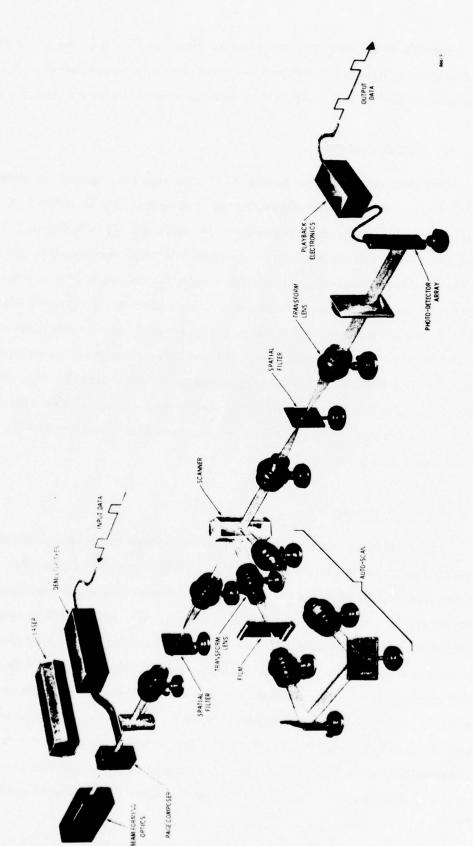
Figure 3-1. SP System Functional Diagram

absent. After the page composer has received a block of data and the compressional waves produced have propagated to fill the optical aperture of the AOPC, the laser is gated on by a single acousto-optic modulator (AOM). the AOM provides a rapid shuttering action for the laser illumination. The duration and magnitude of the gated laser pulse are chosen to properly expose the film.

The unexpanded laser beam diffracted into the system by the AOM is divided into a signal beam and a reference beam by an acousto-optic beamsplitter. The signal beam is appropriately expanded and shaped to uniformly illuminate the optical aperture of the AOPC. The cylindrically convergent signal beam is incident on the AOPC at the required Bragg angle (the convergent nature of the illumination beam provides a faster device rise time). The interaction of the reference beam illumination with the compressional waves present in the AOPC produces a diffracted pattern with an intensity profile corresponding to the electronic data pattern. This interaction provides the conversion from the electrical to the optical domain. The acoustic interaction also provides the necessary Doppler shift to the frequency of the signal beam to match the corresponding shift introduced to the reference beam. A stationary interference pattern now can be recorded since the center frequency of the signal and reference beams is the same.

The frequency-shifted reference and signal beam are brought to focus at a slit which provides a filtering and shaping function. A telescope lens pair assembly images the intensity pattern at the filtering slit onto the recording film. The first lens of the pair directs the light beams onto the spinning mirror. The spinning mirror assembly is a polygonal faceted mirror mounted to a motor. As each facet of the spinning mirror passes through the record position, the beam reflected from the mirror is scanned across the active film width in the recording plane. Thus, the spinning mirror imparts an angular motion to the beams that scan the imaged slit across the film width. The irradiance pattern imaged on the film is the one-dimensional phase-randomized Fourier transform of the input data block.

The first hologram is recorded immediately after the control logic receives a signal that the spinning mirror is in the correct position. As the spinning mirror rotates, the one-dimensional interference patterns, gated by the initial AOM, are scanned across the film surface. After the first hologram, corresponding to the Fourier transform of the input data block, is exposed, the recording process is repeated. Another data block enters the AOPC, the laser is gated on, and the next Fourier transform is recorded. Data records are in this fashion continuously recorded across the film until a complete row of holograms has been recorded. The incoming data is then buffered until the next signal from the spinning mirror, signifying it is in the correct position, is received. The recording process is then repeated for the next row of holograms.

A continuous motion film transport system is used to distribute the recorded data patterns along the surface of the film. The film velocity is chosen to be consistent with the recording rate and film format. A separate and independent sequence of exposures is provided at the beginning of each row. These marker exposures are used as an indexing control to signal the presence of recorded data. After the entire supply of film is recorded, the film is removed from the transport system and is processed to provide archival storage of the data records.

3.2.2   Readout Process

The system configuration used for the readout process is similar to that used for recording. The primary difference in the system configuration is the diversion of all the available laser power into the reference beam; this allows the holograms to be reconstructed at maximum power levels. For readout, the exposed film, which has been processed to provide an archival data store, is replaced in the film transport system.

The film transport and spinning mirror provide functions during readout similar to those in the record process. The additional complication that arises during readout is the need to synchronize the film transport motion with the spinning mirror. This synchronization allows the scan line of the reference beam to coincide with the row of recorded holograms. To determine when a row of holograms is in the proper location

for readout, a separate beam, which senses the presence of the marker exposures, is used to establish closed-loop control of the spinner and transport during readout. When the necessary control is established, the readout process begins. The concentrated-power reference beam is scanned across the row of recorded holograms. At each hologram location the reference beam reconstructs an irradiance profile that corresponds to the original Fourier transform that was recorded.

A telescope assembly images the reconstructed signal pattern in a separate plane for readout. In this plane, the signal pattern is scanned through a distance corresponding to the active width of the film. A separate telescope assembly reimages the reconstructed signal pattern after reflection from a second facet of the spinning mirror. Data descan is accomplished by utilizing the reflection from the spinning mirror to cancel the angular motion of the signal patterns.

The space invariant image of the reconstructed signal pattern is formed on a fiber-optic/photodetector array by the telescope assembly. Each fiber of the 128 element array samples one bit position of the imaged signal pattern. Each optical fiber is terminated at a discrete photodetector which provides the reconversion from the optical to the electrical domain. Electronic processing is provided at this stage to ensure that proper thresholding and synchronization have been performed. The processed outputs from the array are connected to an error correction module. The error correction module outputs a signal pattern that is the most probable pattern for the input pattern received. The module corrects for random errors that occur during the recording or readout process. The channelized data from the error correction module are connected to a multiplexing circuit that provides a serial data pattern corresponding to the original high-speed digital data.

3.2.3 Component Requirements for the SP Approach

The user data rate of 2 Gb/s in the SP system imposes specific constraints on the components used to perform the specialized functions within the system; any system trade-off study for the SP approach must consider these constraints. The major components required to realize an operational system can be grouped into four separate categories: the acousto-optic devices, the optical components, the spinner and film transport subsystems, and the detection subsystem. We discuss the requirements for the components in each category in this section.

3.2.3.1 Acousto-Optic Devices

Two acousto-optic devices are required for the SP approach: one is the acousto-optic page composer (AOPC) used to format the data for recording; the other is the acousto-optic modulator (AOM) used to provide rapid intensity modulation of the laser power. The operation of both devices is based on the Bragg interaction between the incident optical beam and the acoustic wave inside the device. The Bragg interaction provides both higher efficiency during operation and more angular separation between output beams than other interaction types.

The physical characteristics of the acousto-optic device determine the modulation performance achieved for a given digital data rate. The important acousto-optic interaction parameters are illustrated in Figure 3-2. The optical beam is incident on the acousto-optic device (AOD) at the Bragg angle θ_B and has an angle of convergence $2\delta\theta_o$. An acoustic wave is induced in the device by the piezoelectric transducer driven at a frequency v_o. The acoustic beam propagates in the material with a velocity V_a and an angular divergence $\delta\theta_a$. The Bragg interaction of the optical beam and acoustic beam causes a frequency-shifted beam to be diffracted.

Several requirements for the acousto-optic devices arise from the Bragg interaction of the convergent optical beam with an acoustic beam. First, in order for the device to operate in the Bragg regime, the geometrical factor Q for the device must be larger than 2π. The factor Q is related to the device parameters by

3-10

DIFFRACTED OPTICAL SIGNAL

THROUGHPUT OPTICAL BEAM

$2 \theta_B$

$\delta \theta_a$

d_w

L

V_a

PIEZOELECTRIC TRANSDUCER DRIVEN AT FREQUENCY ν_o

$2 \delta \theta_o$ $\delta \theta_o$ θ_B

ACOUSTIC WAVE IN MATERIAL WITH A REFRACTIVE INDEX n

INCIDENT OPTICAL BEAM WITH WAVELENGTH λ

89444—5
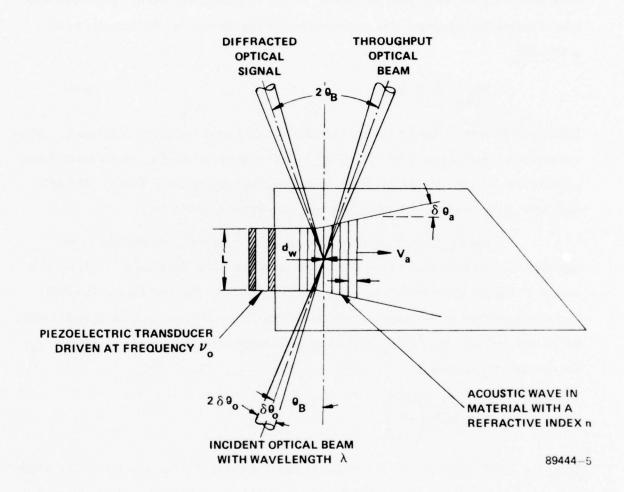
Figure 3-2. Acousto-Optic Interaction Parameters

$$Q = \frac{2\pi\lambda L}{\Lambda^2 n} \geq 2\pi$$

where λ is the optical wavelength, L is the transducer length, Λ is the acoustic wave-length, and n is the index of refraction. Second, for the Bragg diffraction condition to be satisfied over the angular range $\delta\theta_o$ for the optical beam, the acoustic beam must have a corresponding range; this is summarized by the relation for the acoustic beam spread $\delta\theta_a$

$$\delta\theta_a = \frac{\Lambda}{L} \geq 2\delta\theta_o. \qquad (3-1)$$

The acoustic beam spread $\delta\theta_a$ arises from diffraction by the transducer aperture L. When the acoustic beam spread is less than $2\delta\theta_o$ due to a large value of L, an elliptical beam is diffracted, which is acceptable for some modulation applications. Finally, the AOD must have a rise time τ_R consistent with the data rate requirements.

The rise time τ_R required for an AOD is typically determined by the application. For NRZ data under worst-case conditions, the rise time τ_R is simply the inverse of the per-channel data rate R_c, i.e., $\tau_R = 1/R_c$. The rise time of the AOD is also proportional to the time that the acoustic wave requires to cross the optical beam. For an optical beam of width d_w and an acoustic material with an acoustic velocity V_a, the rise time τ_R is given by

$$\tau_R = 0.75 \left(\frac{d_w}{V_a} \right).$$

Thus, the width of the optical beam must be small to achieve a fast rise time. The width of the optical beam d_w is also related to the optical beam spread $\delta\theta_o$, since the minimum spot diameter d_w of a lens is related to the convergence angle; this relationship is given by

$$2\delta\theta_o = \frac{1}{F} = \frac{2\lambda}{d_w} ,$$

where F is the f-number of the incident light cone and λ is the optical wavelength.

3-12

Several device characteristics are required for the fabrication of any AOD. Of course, the material considerations are important, since they determine the effort necessary to work the material. They also affect the performance levels the device is capable of achieving. Typically, the application provides information on the wavelength, data rates, and rise times of the device. The remaining parameters are the operating frequency ν_o and the transducer length L. These constraints are:

$$\nu_o \geq \frac{3n}{\tau_R} \; ;$$

and

$$L \leq \frac{\tau_R V_a^2}{3\lambda \nu_o} \; .$$

The first constraint is necessary to maintain the geometrical factor Q larger than 2π to ensure operation in the Bragg regime. The second constraint arises from the relation of the acoustic beam spread to the optical beam spread to ensure a minimum ellipticity of the diffracted beam. Thus, the maximum piezoelectric transducer width and minimum operating frequency are determined when the acoustic velocity V_a, optical wavelength λ, the per-channel rate R_c, and rise time τ_R are specified.

The remaining design parameter is the transducer height H. For multichannel applications the channel-to-channel spacing ΔH is also required. Practical limitations on these dimensions exist because of fabrication difficulties. For single channel devices the minimum practical height H is near 50 μm. For multichannel devices, the minimum height H and spacing ΔH are approximately 100 μm. The transducer dimensions should be maintained as small as practical to reduce the RF drive power requirement.

The diffraction efficiency of the AOD can be calculated when the transducer geometry and the acousto-optic material are specified and the RF drive power is given. The maximum level of RF power density that can be used to drive multichannel devices without requiring water cooling for the transducers is 20 W/cm^2. Much higher RF drive power levels can be used with single channel devices because the removal of
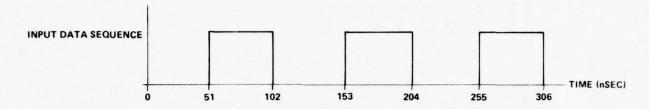
thermal energy is accomplished through the use of special transducer bonding techniques not applicable to multichannel devices. The maximum drive power levels for single channel devices can be as high as 1,000 W/cm^2. When the device geometry and the RF drive power levels are established, the diffraction efficiency η of the AOD can be calculated using the relationship:

$$\eta = \sin^2\left[\frac{\pi}{2} \quad \sqrt{\overline{\frac{2}{\lambda^2} M_2 \frac{L}{H} \eta_a P_e}}\right],$$
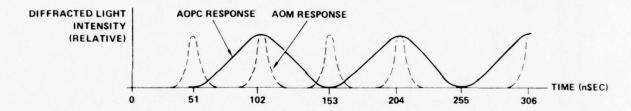
where M_2 is the acoustic figure of merit for the material selected.

The fabrication details and operational characteristics of the AOPC can now be determined. For a user data rate of 2 Gb/s, a total system data rate of 2.5 Gb/s is required to account for the error correction coding and system operation information. For an AOPC design that user 128 channels, the required per-channel data rate is 19.5 MHz, corresponding to a device rise time of 51 ns. The input data and the required response for each channel of the AOPC and the shutter AOM are shown in Figure 3-3. For an illuminating optical wavelength λ of 514.5 nm, an RF drive power density of 20 W/cm^2, and a transducer conversion efficiency η_a of 0.4, the device parameters can be calculated. Table 3-1 lists the device parameters for several candidate materials. In the table the material parameters (acoustic velocity, refractive index, and figure of merit) are presented for the AOPC design as well as the required transducer geometry, the minimum operating frequency ν_o, and diffraction efficiency per channel. The optical beam width required for the device to achieve the required 51 ns rise time is also given.

It is important to note that the efficiencies listed in Table 3-1 are the efficiencies per channel. These efficiencies can be converted to a device efficiency by accounting for the active transducer area. For a transducer spacing equal to the transducer height, only one-half of the incident light can interact with the acoustic beams. Thus, the device efficiency, representing the fraction of total incident light that is diffracted by the AOPC, is one-half of the per channel efficiency.

INPUT DATA SEQUENCE

```
            ┌─────┐        ┌─────┐        ┌─────┐
            │     │        │     │        │     │
────────────┘     └────────┘     └────────┘     └────────── TIME (nSEC)
  0    51   102      153   204      255   306
```

A. INPUT DATA SEQUENCE FOR NRZ DATA (WORST-CASE)

DIFFRACTED LIGHT
INTENSITY
(RELATIVE)

AOPC RESPONSE   AOM RESPONSE

```
                                                    TIME (nSEC)
  0    51   102      153   204      255   306
```

B. MINIMUM REQUIRED CHANNEL RESPONSE FOR THE 128-CHANNEL
     AOPC AND THE HIGH DATA RATE AOM

89444–7

Figure 3-3. Input Data Sequencer and Required Channel Response for 2.5 Gb/s
Page Composer (Per-Channel Rate 19.5 Mb/s)

Table 3-1. Device Parameters For 128 Channel Acousto–Optic Page Composer For Different Material Selections

Material	Acoustic Velocity V_a (mm/μs)	Refractive Index n	Figure of Merit M_2 (S³/g)	Transducer Length L (mm)	RF Drive Power P_e (mW)	Operating Frequency v (MHz)	Efficiency η (%)	Spot Diameter d_w (mm)
SF–8	3.89	1.69	6.3	5.03	101	99	21.9	0.26
SF–58	3.26	1.91	11.9	3.13	63	112	16.4	0.22
SF–59	3.20	1.94	17.3	2.96	59	114	21.0	0.22
PbMoO$_4$	3.63	2.39	36.1	3.10	62	141	43.3	0.25
TeO$_2$	4.20	2.26	34.5	4.38	88	133	70.3	0.29
TiO$_2$	10.30	2.58	1.52	23.10	462	152	79.4	0.70
Quartz	5.94	1.46	1.59	1.36	271	86	37.7	0.40

Aggregate Data Rate	R	= 2.5 Gb/s
Per Channel Data Rate	R_c	= 19.5 Mb/s
Rise Time (10–90%)	τ_R	= 51 ns
Transducer Height	H	= 100 μm
Transducer Spacing	ΔH	= 100 μm

The characteristics of the AOPC devices summarized in the table vary significantly from one acousto-optic material to another. The transducer length L required ranges from 2.96 mm for SF-59 glass to 23.1 mm for titanium dioxide (TiO_2). The maximum RF drive power at 156 MHz ranges from 59 mW for SF-59 glass to 462 mW for the TiO_2 crystal. The maximum diffraction efficiency per channel of the device ranges from 16 percent for SF-58 glass to 79 percent for TiO_2. The recommended material for fabricating the device is crystalline tellurium dioxide (TeO_2), which would require 87 mW of RF drive power to achieve a diffraction efficiency per channel of 70 percent.

Each of the designs summarized in the table is capable of an aggregate data rate of 2.5 Gb/s. However, other factors affect the final design. The effect of thermal degradation of the material must be considered. A thermal gradient in the acousto-optic material can seriously degrade the optical quality of the diffracted beams. Another consideration is the size in which the materials are obtainable. For the 128 channel AOPC design presented previously, a rectangular material sample that is 26 mm high, 10 mm wide and 5 mm thick is required. The cost to obtain high quality materials of this size is high. Finally, the difficulty of fabrication must be considered. Some crystalline acousto-optic materials, although capable of providing high performance levels, require delicate care during the fabrication process.

The requirements for the AOM that performs the shuttering control can be determined similarly. To achieve a shuttering action consistent with the data rates, the response time of the AOM must be at least five times faster than the 51 ns rise time of the AOPC. For the design analysis, the rise time τ_R of the AOM is chosen as 10 ns. The transducer height H is chosen to be 50 μm to provide the lowest RF drive power levels. Because special bonding techniques can be used to provide excellent heat transfer characteristics, the allowed power density for the single channel AOM is 1 kW/cm^2. Transducer conversion efficiency η_a is typically 0.4. The AOM device parameters are calculated for two conditions. The first is the case in which the acoustic beam spread $\delta\theta_a$ satisfies Equation (3-1); the diffracted optical beam for this condition is

circular. The second is the case in which $\delta\theta_a = 1.5\delta\theta_o$; the intensity profile of the diffracted beam in this case is elliptical (elongated in one dimension by approximately 15 percent). The results of the calculations for several different materials are summarized in Table 3-2 for two beam-spread ratios. A comparison of the cases shown indicates the effect of the beam-spread ratio. The decreased acoustic beam spread allows the use of a larger transducer length. This results in increased drive power levels, which correspondingly raise the device efficiency. The optimum material for the AOM device is the tellurium dioxide (TeO_2) crystal. A drive level of 1.12 W produces an efficiency of 83 percent; this efficiency is acceptable for the application.

Table 3-2.   Design Parameters for a High Speed Acousto-Optic
Modulator with 10 ns Rise Time

a)   Circular Diffracted Beam $(\delta\theta_a = 2\delta\theta_o)$

Material	Transducer Length L (μm)	Operating Frequency f (MHz)	Drive Power P_e (W)	Spot Size d_w (μm)	Efficiency η (%)
SF-8	193	507	0.97	19.7	16.6
SF-58	120	573	0.60	16.6	12.3
SF-59	113	582	0.57	16.2	15.8
$PbMoO_4$	119	717	0.60	18.4	33.5
TeO_2	169	678	0.84	21.3	56.9
TiO_2	888	774	4.44	52.3	65.7
Quartz	522	438	2.61	30.2	29.0

b)   Elliptical Diffracted Beam $(\delta\theta_a = 1.5\delta\theta_o)$

Material	Transducer Length L (μm)	Operating Frequency f (MHz)	Drive Power P_e (W)	Spot Size d_w (μm)	Efficiency η (%)
SF-8	258	507	1.29	1.97	28.1
SF-58	150	573	0.81	16.6	21.1
SF-59	152	582	0.76	16.2	27.0
$PbMoO_4$	159	717	0.79	18.4	53.8
TeO_2	225	678	1.12	21.3	82.6
TiO_2	1184	774	5.92	52.3	90.7
Quartz	696	438	3.48	30.2	47.2

3.2.3.2   Optical Components

A basic analysis of the requirements for the optical components necessary to perform the recording and retrieving operation for the SP system concept is presented in this section. The analysis is based on the design requirements obtained for the AOPC and practical limits imposed by the recording process. The optical components considered can be grouped into three classifications according to the primary function they perform. These classifications are the AOPC illumination optics, the transform optics, and the reconstruction optics. The performance needed for each of these groups can be determined by examining the particular requirements of the group.

The AOPC illumination lens group provides the beam shaping necessary for the proper illumination of the AOPC. This lens group is indicated schematically in Figure 3-4. The unexpanded laser beam with a 1.5 mm diameter is expanded by microscope objective S1 and subsequently filtered by a pinhole. A cylindrical lens C1 located *a focal length* from the spatial filter collimates the expanding beam is one direction. The spherical lens L1 collimates the beam in the orthogonal direction and provides a line focus at the AOPC plane in the other direction. A filter located at lens L1 truncates the beam height to provide a uniform intensity at the AOPC. The dimensions of the illumination beam in the AOPC correspond to the Bragg acceptance angle of the AOPC. To illuminate all of the 128 channels (100 µm transducers on 200 µm centers), the beam height must be 25.6 mm. To achieve the required rise time of 51 ns with a TeO_2 device, the horizontally focussed illumination line width in the AOPC plane must be 285 µm or less.

The Gaussian intensity profile of the unexpanded laser beam requires truncation to achieve an illuminating beam uniform within 10 percent over a distance of 25.6 mm. The unexpanded incident beam has a 1.5 mm diameter to the 1/e points. The Gaussian beam must be expanded to a 36 mm diameter and truncated to a 25.6 mm diameter to achieve the uniformity condition. The ratio of focal lengths of the microscope objective
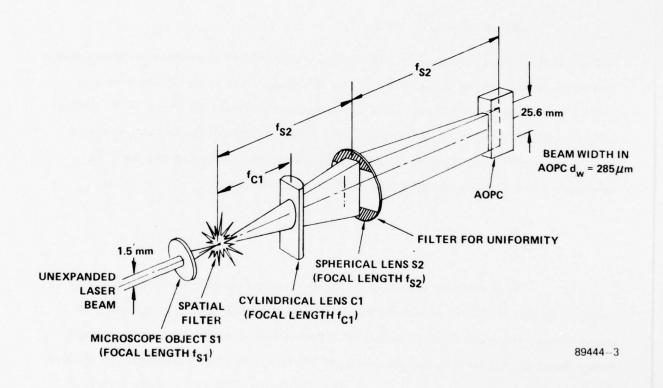
Figure 3-4. AOPC Illumination Optics - SP System

89444-3

S1 to the spherical lens S2 determines the magnification. To achieve the desired magnification, the focal length ratio is:

$$\frac{f_{S1}}{f_{S2}} = \frac{1.5}{36} = \frac{1}{24}$$

The spot width d_w formed in the AOPC is determined by the spherical lens S2 and the width d of the beam at the lens entrance. The relation may be expressed as:

$$285 \; \mu m \geq \frac{2\lambda f_{S2}}{d} = d_w \quad ,$$

where λ is the optical wavelength. This relation determines the minimum width d allowed that achieves the desired line width d_w. For this design, the value of d is chosen to yield a spot width d_w of 140 μm. This choice reduces the rise time of the AOPC, allows full usage of the Bragg acceptance angle, and poses no difficult optical requirements. The focal length f_{C1} of the cylindrical lens determines the width d at the lens. To achieve a width d at the entrance to lens S2 requires that:

$$\frac{F_{S1}}{F_{C1}} = \frac{1.5}{d} \quad .$$

These relations specify both the focal lengths and F-numbers of the lenses required for the AOPC illumination when the microscope objective is specified. For convenience, the microscope objective S1 is designated as a 10X, 16 mm focal length lens. Based on this choice, the parameters of the lenses may be calculated. To achieve the desired performance the focal lengths of the cylindrical lens C1 and the spherical lens S2 are 29.6 mm and 384 mm, respectively. The corresponding F-numbers required for these lenses are 10.7 and 15.0. The relatively low performance required of the AOPC illumination lenses can be obtained with standard, off-the-shelf lenses. No problems are anticipated in realizing the required performance.

The transform optics provide the necessary imaging properties to record the one-dimensional Fourier transform hologram of the AOPC data sequence. The transform optics which follow the AOPC are shown schematically in Figure 3-5. Spherical lens S3,
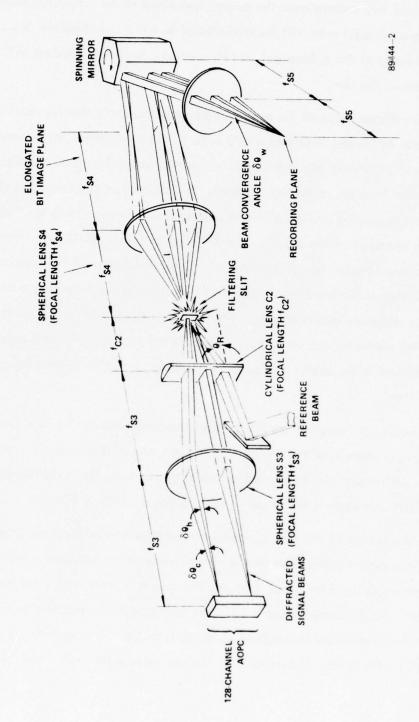
Figure 3-5. Transform Optics – SP System

89444-2

located one focal length f_{S3} from the AOPC, intercepts the 128 data beams diffracted by the AOPC. The lens collimates the beams in one direction and converges them in the other. The cylindrical lens concentrates the energy contained in the diffracted beam into a single line focus at a filtering slit located a focal length f_{C2} behind the lens. The reference beam, directed to the cylindrical lens by a mirror, is also coincident with the focused signal beams at the slit.

The incidence angle of the reference beam is chosen so that the maximum fringe frequency recorded in the hologram is 600 cy/mm. This frequency range provides a substantial decrease in Wiener spectrum noise, while still achieving good modulation transfer characteristics from the recording material. The irradiance pattern in the slit aperture represents a magnified version of the one-dimensional Fourier transform hologram of the 128-bit data sequence of the AOPC. The filtering action of the slit prevents unwanted light from reaching the recording material. The telescope assembly consisting of lenses S4 and S5 images the irradiance pattern in the slit onto the recording material. The first lens of the telescope assembly images the bit pattern just prior to the spinning mirror. The spinning mirror imparts an angular motion to the bit pattern which causes the Fourier transform formed in the back focal plane of the second lens S5 to scan laterally in the recording plane.

The basic configuration for the transform optics group can be used to generate the design parameters for the lenses. For the purpose of this analysis, we assume that the recording material has an active width of 50 mm in the recording plane. This active film width corresponds to the use of film having a width of 70 mm.

The dimensions of the lens apertures for the Fourier transform optics are determined to a large extent by the divergence of the beams diffracted by the AOPC. These beams are anamorphic, which means that the divergence of each diffracted beam in the plane defined by the diffracted beam is different than that in the perpendicular direction. These divergences are determined by the optical beam incident on the AOPC and the dimensions of the AOPC channels. The divergence of a beam in a direction

perpendicular to the plane defined by the diffracted beam is denoted by $\delta\theta_c$. This divergence $\delta\theta_c$ is equal to the divergence of the illumination beam incident on the AOPC and is given by:

$$\delta\theta_c = \frac{d}{f_{S2}} = 7.24 \text{ mrad},$$

where d and f_{S2} refer to dimensions in Figure 3-4. The divergence $\delta\theta_h$ in the orthogonal direction is caused by diffraction spreading of the incident AOPC beam by the finite acoustic aperture. Experimental evidence indicates that the divergence angle $\delta\theta_h$ is nominally 6 mrad.

The dimensions of the hologram that is recorded on the photographic film must allow compact storage of the 128 elements of the AOPC. Typical high resolution, high contrast recording materials suitable for holography can support an information packing density of 10^6 bits/cm^2 with an associated signal-to-noise ratio of 20 dB. This packing density provides both compact storage and high quality retrieval characteristics for digital data. The hologram dimensions used in this design analysis are a hologram width w of 12.8 µm and a hologram height h of 1 mm. These dimensions allow a packing density of 10^6 bits/cm^2 and are comparable to the dimensions used in the present EDM system.

The hologram dimensions establish certain requirements on the transform lens S5. The transform lens S5 must provide double-Rayleigh resolution of the hologram width w, while maintaining a collimated beam height h of 1 mm in the other direction. The minimum convergence angle $\delta\theta_w$ (as indicated in Figure 3-4) that can achieve the double-Rayleigh resolution of w is:

$$\delta\theta_w = \frac{2.44\lambda}{w}.$$

The corresponding beam width W at the lens entrance is $f_{S5}\, \delta\theta_w$. The lens aperture must also be sufficient to cover the active film width W_o of 50 mm. The lens must also form an interference pattern between the reference beam and signal beams with a maximum fringe frequency v of 600 cy/mm. To accomplish this, the full angle θ_R between the two beam sets is:

$$\theta_R = \lambda \upsilon = 308.8 \text{ mrad} \quad .$$

The height H at the lens entrance required to provide the convergence angle θ_R is f_{S5} θ_R. In addition, the aperture must also be sufficient to pass the beam height h of 1 mm. The requirements for the lens are established by the above conditions; for these conditions, the F-number (defined as the ratio of focal length to aperture diameter) can be calculated. The minimum F-number, F, that provides the necessary aperture is given by:

$$F = \frac{f_{S5}}{\sqrt{(W_o + W)^2 + (H + h)^2}} \quad . \tag{3-2}$$

An indicator of the feasibility of the transform lens S5 is the F-number. The minimum practical F-number, of the transform lens is F = 2.0. Incorporating this restriction into Equation (3-2) and solving the resultant quadratic equation for f_{S5} yields:

$$f_{S5} = \frac{\sqrt{\left(W_o \, \delta\theta_w + h\theta_R\right)^2 - \left(\delta\theta_w^2 + \theta_R^2 - \frac{1}{F^2}\right)\left(W_o^2 + h^2\right)} + \left(W_o \, \delta\theta_w + h\theta_R\right)}{\delta\theta_w^2 + \theta_R^2 - \frac{1}{F^2}}$$

or,

$$f_{S5} = 172.1 \text{ mm} \quad .$$

The corresponding lens aperture D_{S5} is 86.1 mm. For the focal length f_{S5} of 172.1 mm, the width W of the data pattern at the lens entrance is 16.88 mm. The height H required for the data pattern is 53.14 mm.

The width W of the data pattern reflected from the spinning mirror is only half the width of the incident beam. This arises because of the continuous recording cycle obtained with the spinning mirror. Thus, in order to double-Rayleigh resolve the desired hologram width, the illumination optics preceding the spinning mirror must provide an incident data pattern illumination which has a 33.76 mm beam width at the mirror. The optics must also scale the height of the elongated image of the signal and reference beams prior to the spinning mirror to the proper height H of 53.14 mm. These conditions are sufficient to determine the remaining elements of the transform group,

once a focal length is assigned to one lens of the group. A reasonable choice would be to assign a focal length to lens S3, the spherical lens following the AOPC. The approximate aperture required for the lens is known from the AOPC design parameters. A practical choice for the focal length f_{S3} is 380 mm. This choice does not pose any high performance imaging requirements. The remaining focal lengths can now be determined.

The telescope formed by lenses S3 and S4 must image the signal and reference pattern just prior to the spinning mirror. The focal length of S4 must be chosen to form the image at the correct scale. The required height H of the image has been previously determined and is 53.14 mm. The nominal extent of the signal and reference patterns in this direction is simply twice the AOPC height H_A, or 51.2 mm. Thus, to provide the proper scaling, the focal length f_{S4} is given by:

$$f_{S4} = \frac{H}{H_A} \, f_{S3} = 394.4 \text{ mm} \quad ,$$

where the focal length f_{S3} is 380 mm.

The anamorphic telescope formed by the cylindrical lens C2 and the spherical lens S4 must provide a beam width 2W of 33.76 mm. This is required because the spinner directs only half of the total beam width to the transform lens. To find the focal length f_{C2} of the cylindrical lens, the width of the pattern incident on the lens must be determined. The data pattern incident on the cylindrical lens has a constant width. The width W_c is related to the divergence angle $\delta\theta_c$ of the page composer beam and the focal length $_{S3}$ of the spherical lens S3. The divergence angle $\delta\theta_c$, corresponding to the Bragg acceptance angle of the AOPC, is 7.24 mrad. For the anamorphic telescope to provide the proper width W, the focal length f_{C2} is:

$$f_{C2} = \frac{W_c}{W} \, f_{S4} = \frac{f_{S3} \, \delta\theta_c}{W} \, f_{S4} = 32.14 \text{ mm} \quad .$$

The focal lengths for each lens of the transform optics group are now defined. The apertures and corresponding F-numbers required for the lenses can be determined from similar considerations.

The aperture D_{S3} required for the spherical lens S3 must be adequate to accept the incident signal beam pattern from the AOPC. The optical beam divergences $\delta\theta_c$ and $\delta\theta_h$, indicated in Figure 3-5, are 7.24 mrad and 6 mrad, respectively. The minimum aperture D_{S3} for the lens is given by:

$$D_{S3} = \left[(H_A + f_{S3}\,\delta\theta_h)^2 + (f_{S3}\,\delta\theta_c)^2 \right]^{1/2} = 28.0 \text{ mm,}$$

where H_A, the height of the AOPC, is 25.6 mm.

The cylindrical lens C2 must have an aperture sufficient to collect and concentrate the incident signal and reference beams. The width of these beams is determined by the spherical lens S3; thus, the required aperture D_{C2} is:

$$D_{C2} = f_{S3}\,\delta\theta_c = 2.9 \text{ mm,}$$

where θ_c is the angular beam divergence from the AOPC.

The aperture D_{S4} of the spherical lens S4 must accommodate the extent of the signal and reference beams as enlarged by the cylindrical lens. The aperture D_{S4} is given by:

$$D_{S4} = \left[(f_{S5}\,\theta_R)^2 + \left(\frac{\delta\theta_c\, f_{S3}\, f_{S4}}{f_{C2}} \right)^2 \right]^{1/2} = 62.7 \text{ mm,}$$

where the first term is equivalent to the height of the reference and signal pattern at the entrance to lens S4.

The focal lengths, lens apertures, and F-numbers for the transform optics group are summarized in Table 3-3. Of these lenses, the spherical lens S5 providing the final imaging of the slit has the strictest requirements. It must provide flat field imaging over a large field of view. A significant amount of design and fabrication effort is required to realize the desired lens performance.

Table 3-3. Optical Requirements for the Fourier Transform Lens Group

Lens	Focal Length (mm)	Aperture (mm)	F-Number
S3 (Spherical)	380	28.0	13.6
C2 (Cylindrical)	32.1	2.9	11.1
S4 (Spherical)	394.4	62.7	6.3
S5 (Spherical)	172.1	86.1	2

The format of the holographic recording can be calculated from the dimensions of individually recorded holograms. The hologram recorded on the film has a width w of 12.8 μm and a height h of 1.0 mm. These dimensions correspond to a packing density in the hologram of 1 Mb/cm^2. With a guardband that is 20 percent of the hologram width, approximately 2951 holograms are recorded across the active 50 mm film width. The parameters determined for the holographic storage can be used to establish the requirements for both the scanning system and the film transport. These requirements are discussed in a later section.

The requirements for the reconstruction optics are analogous to those of the transform optics. The functions performed by the reconstruction optics are indicated schematically in Figure 3-6. For reconstruction of the recorded data pattern, all available power is diverted into the reference beam, which is scanned across the film by the spinning mirror. The film transport motion must be synchronized with the scanning motion. As the reference beam addresses each hologram location, the recorded Fourier transform is reconstructed. Spherical lens S6 provides the inverse Fourier transform to form an image of the original data sequence in the back focal plane of lens S6. However, the data sequences and the reference beam leaving the film are not stationary. To compensate for the movement, an autoscan configuration is utilized. Spherical lenses S7 and S8 form a unity power telescope and reimage the data sequence. During the reimaging process, an angular motion is added to the beams by the spinning mirror that cancels the scanning motion; thus, a stationary image is formed in the back focal plane of lens S8. Since the

FIBER-OPTIC ARRAY TO DETECTORS

REFERENCE BEAM MONITOR FOR SYSTEM TIMING

STATIONARY DATA IMAGE

READOUT REFERENCE BEAM

PATTERN TRANSLATION

AUTOSCAN LENSES

f_{C3}

f_{S10}

$f_{S9} + f_{S10}$

f_{S9}

f_{S8}

f_{S8}

f_{S7}

C3

S10

S9

S8

S7

S6

89444-11
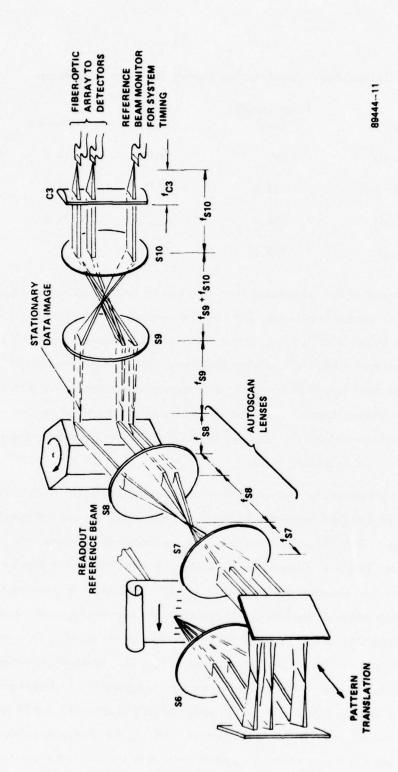
Figure 3-6. Reconstruction Optics – SP System

data bits are elongated in one dimension, a telescope assembly (lenses S9 and S10) reimages the data pattern and the cylindrical lens C3 concentrates the light into a line focus for the fiber-optic array.

The performance required of lenses S6, S7, and S8 is equivalent to that of the original transform lens S5. Thus, for the unity power configuration chosen, the focal lengths and apertures of these lenses are identical to the requirements for S5. The requirements for the spherical lenses S9 and S10 are equivalent to lenses S4 and S3, respectively. The cylindrical lens C3 performs a function similar to C2. Thus, the imaging lenses after the spinning mirror perform conventional roles and are easily specified. No difficulty in obtaining these lenses is anticipated.

The strictest optical requirements for the reconstruction optics are those of the inverse transform lens and the autoscan lenses. Since these lenses must provide high precision imaging over wide angular fields, the design and fabrication of these lenses must be given critical attention. Also, the optical configuration chosen for the system analysis is not an absolute one. Physical sizes may impose limitations not considered in this discussion. In these instances, image scaling may be performed by choosing different focal length lenses.

The laser required for the record operation must also be considered. Since the temporal intensity modulation is accomplished by an acousto-optic device, a continuous wave laser is suitable. The power level required for the laser can be determined by estimating the exposure level required during recording, the recording format, and the optical system efficiency. For an exposure time τ of 20 ns, typical high sensitivity recording materials suitable for holographic applications require an exposure of $10 \ \mu J/cm^2$. For a recorded hologram area A_h of $1.29 \times 10^{-5} \ cm^2$ and an estimated system efficiency η_i of 1.3 percent, the required laser power P is:

$$P = \frac{E \ A_h}{\tau \eta_i} = 4.6 \ \text{Watts} \quad .$$

The anticipated power levels present in the output plane of the recorder/reproducer can be similarly estimated. Since the AOPC is not used during data retrieval, the optical

3-31

efficiency η_o is higher for readout than for record. The readout efficiency is estimated as 3 percent. The expected diffraction efficiency for the hologram is 0.5 percent. Assuming an input reference beam power of 0.4 watt, the energy per bit, E_b, in the reconstructed data pattern is:

$$E_b = \frac{(0.03)(0.005)}{128}(0.4 \text{ watt}) = 500 \text{ nW}$$

The power levels required for the laser can be achieved by commercially available argon-ion lasers. The laser in the present exploratory development model has the necessary power for both exposure and readout at data rates of 2.5 Gb/s.

3.2.3.3   Spinner and Film Transport Subsystems

The dynamics of information recording in the SP system are provided by the spinner and film transport. During the record process, the spinner and the film transport are used to distribute the information across and along the film, respectively. For the readout process, the situation is more complex. To correctly sample data, the holograms must be in the proper spatial location when addressed by the scanning reference beam. This requires that the position of each hologram row be sensed correctly and the spinner and film transport operate under closed-loop control. A common clock derived from the hologram row locations provides timing for both the spinner and transport. Once the synchronization is established the readout process becomes straightforward.

The spinner performs the scanning action for both the record and reproduce processes. The characteristics of the spinner are easily established by considering the hologram format and the data rate. The spinner is an N-faceted polygonal mirror. For convenience we assume that there are 40 spinner facets. The height required for the spinner facets corresponds to the height of the imaged data pattern as indicated in Figure 3-6; this height is 53.14 mm. The angular speed of the spinner can be determined by considering the data rates. To achieve a data rate of 2.5 Gb/s, a row of 2951 holograms must be recorded in 151 μs. Since each hologram row recorded corresponds to a facet, the angular velocity V_m of the mirror is 166 r/s. This angular rate, although fairly high, is certainly achievable.

The velocity required for the transport system can be determined from the constraint relating the recording format and information packing density. The recording rate R of 2.5 Gb/s is the key design goal and cannot be compromised. The active recording width W has already been established as 50 mm. The average information packing density $\bar{\sigma}$ must account for the area taken up by guardbands. Typical dimensions of guardbands are 10 percent of the associated hologram dimension. For this choice the average packing density is

$$\bar{\sigma} = \frac{128 \text{ bits}}{(1.1)^2 \text{ hw}} = 0.82 \text{ Mb/cm}^2 \quad ,$$

where h and w are the hologram dimensions. For these parameters, the required film velocity V can be determined by

$$V = \frac{R}{W\bar{\sigma}} = 6.1 \text{ m/s} \quad .$$

This required film velocity is achievable using present technology coupled with further engineering development.

While the transport is moving at the required film velocity of 6.1 m/s, the surface of the film must be constrained close to the back focal plane of lens S5. The amount of displacement allowed from the back focal plane is related to the depth of focus of the lens. The total depth of focus for lens S5 during the recording process is nominally 10 μm. Thus, the transport must constrain the surface of film moving at 6.1 m/s within an allowable range of ±15 μm.

The two dynamic components required for the SP system represent challenges to achieve. The challenges are certainly within attainment range; however, careful design and engineering development are necessary to achieve the desired performance goals.

3.2.3.4   Detection Subsystem

The reconversion of the optical signals to the electronic domain is performed by the detection subsystem. The detection subsystem is comprised of two major elements: the fiber-optic/photodetector array and the preprocessing electronics. The fiber-optic array distributes the optical signals to the discrete photodetectors. The preprocessing electronics provide the thresholding decisions and error correction prior to the demultiplexing operation.

The linear array of optical fibers is located in the output plane of the SP recorder/reproducer. Each fiber of the 128-element array samples the intensity at one bit location. The coverage area of the fiber is chosen to maximize both optical gathering efficiency and stray noise immunity. Each optical fiber is terminated at a discrete photodetector, which provides an electrical signal proportional to the sampled intensity. The technique of distributing the optical signals with optical fibers is used to minimize electrical crosstalk. The per-channel readout rates required of the photodetectors are equivalent to the per-channel record rate of 19.5 MHz. Per-channel readout rates of 19.5 MHz are difficult to achieve with solid-state detectors for the anticipated optical power levels. However, the rapid advancements in detector technology offer much encouragement that these data rates can be achieved.

The preprocessing electronics provide the thresholding decisions and error corrections for the detected data. The demonstrated success of these electronics on the present development model provides a firm basis for further effort. The design and fabrication of the necessary electronics are not considered technical risks.

3.3   SIAM SYSTEM APPROACH

An alternate concept possessing the capability for recording user data at rates of 2 Gb/s is designated the SIAM approach; the operation of the SIAM system is indicated in Figure 3-7. The approach, based on a dual recording path technique, utilizes two acousto-optic page composers operated in parallel to format the electronic data for recording. Two high speed spinning mirrors mounted on a common shaft perform the scanning operation. The two sets of optical data are recorded simultaneously as pairs of one dimensional Fourier transform holograms on a 70 mm film format. Information retrieval from the system is accomplished by scanning the two distinct reference beams across the recorded hologram rows. The reconstructed data patterns are descanned by the spinning mirror and imaged onto two distinct fiber-optic/photodetector arrays. Subsequent multiplexing reconverts these two data blocks into the original high speed bit stream. The SIAM system as described is essentially two SP systems operating in parallel at reduced data rates.

3.3.1   Recording Process

The recording process for the SIAM system is similar to that for the SP approach. The major differences arise because two distinct recording channels are used. The recording process for the SIAM approach begins with the high speed demultiplexing operation where the serial data are converted for input to the two acousto-optic page composers. The parallel bit streams, each of which is 128 bits wide, control the modulation of the AOPC devices. When both AOPC devices are ready, a single channel acousto-optic modulator (AOM) is energized, which allows a pulse of laser power to enter the system.

The unexpanded laser beam is divided into two equal intensity beams. These beams are directed along two paths which provide identical recording geometries. Both recording paths have the same optical components as the single recording path of the AOPC. Each of these beams is appropriately expanded by beam shaping optics to form the reference beams and to uniformly illuminate the optical aperture of the respective AOPC. Each AOPC provides a diffracted intensity pattern corresponding to
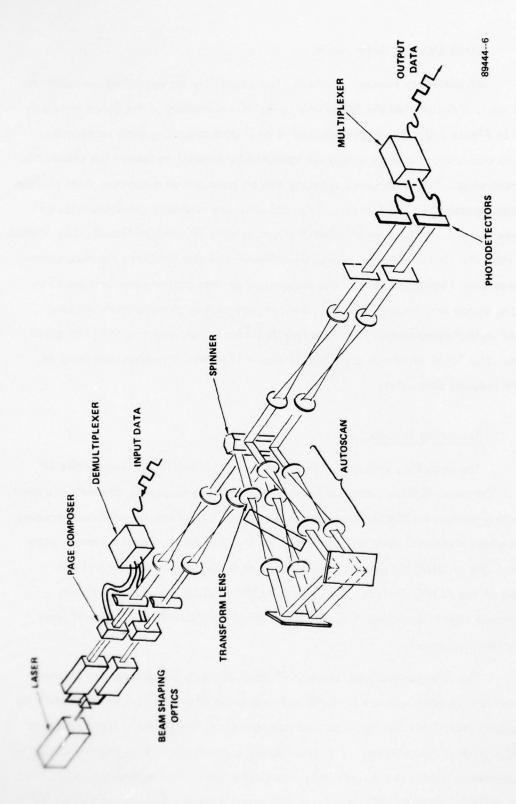
Figure 3-7. SIAM System – Functional Diagram

89444-6

3-36

the 128 bit sequence containing both user and system data. In each leg of the recorder system, a spherical lens and cylindrical lens display the one dimensional Fourier transform at the filtering slit. The reference beam is also incident at the slit, where an interference pattern is formed. Identical telescope assemblies image the irradiance distribution at each of the slits onto the recording plane, where the transform hologram is recorded. During the image formation by the telescope, a spinning mirror in each path imparts to the pattern an angular motion which causes the imaged slit pattern to scan laterally across the film. The rate of scanning is chosen to format the recorded patterns in hologram rows.

A transport moves film past the recording areas as indicated by Figure 3-8. The film is oriented at an angle to provide a distinct recording area on the film for each of the optical paths. As in the SP system, a signal from the spinning mirror is used to control when a row of holograms is recorded until the film supply of the transport is exhausted. The exposed film is then removed and processed.

3.3.2   Readout Process

The functions performed during the readout process for the SIAM approach are analogous to those for the SP approach. Two identical sets of readout optics are provided; each set is used for one of the recording paths. For readout, the processed film is replaced in the transport system. Maximum power is diverted into the reference beams to allow the maximum intensity for the reconstructed data images.

To sample properly the reconstructed data images, the spinner and transport must work in unison. Once this synchronization is established, the readout for each channel proceeds in the same manner as in the SP system. Data descan is accomplished with the autoscan technique. The space invariant image produced for each recording leg is sampled by a discrete fiber-optic/photodetector array. The array output signals are processed by thresholding electronics, and the resulting signals from each of the arrays are properly interleaved and multiplexed to provide a serial data pattern corresponding to the original data sequence.

RECORDING PATH 1

RECORDING PATH 2

DUAL POLYGONAL SPINNERS

H

S5a

FILM MOTION

S5b

θ

SCAN DIRECTION

H = DISTANCE BETWEEN OPTICAL AXES OF THE TWO RECORDING PATHS

θ = RELATIVE ANGLE BETWEEN FILM DIRECTION AND PLANE CONTAINING THE OPTICAL AXES

89444–9
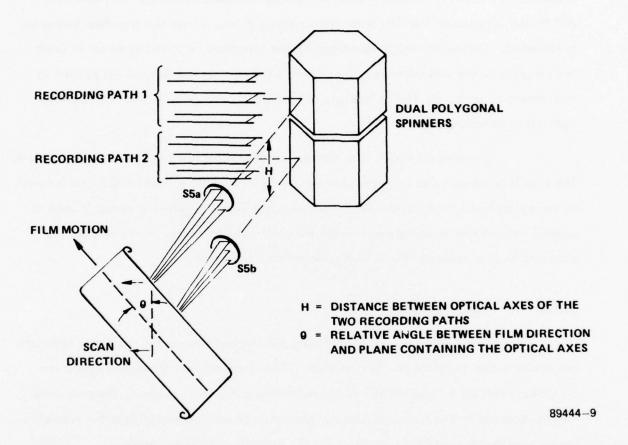
Figure 3-8. Recording Plane Details – SIAM System

3.3.3 Component Requirements for the SIAM Approach

The component requirements for the SIAM approach can be determined from an analysis similar to that of the previous section. The components required for the SIAM system can be segmented into four categories: acousto-optic devices, optical devices, the scanning devices, and the detection subsystem. The requirements for the major components of these categories are established in this section.

One important design aspect that merits consideration in the actual realization of a SIAM system is the opto-mechanical stability of the components. The dual recording paths must have fixed and precise positions with respect to each other to provide proper operation. The positional stability of the individual components is a critical requirement of the readout process. A relative shift of the SIAM system components between the times of recording and reproducing would prevent proper readout. Any system realization of the SIAM approach must contend with this stability constraint. We feel that practical solutions can be reached. However, the details for such solutions are dependent on specific components and, therefore, are not discussed here.

3.3.3.1 Acousto-Optic Devices

Two acousto-optic device types are required for the SIAM system. One is the acousto-optic page composer (AOPC) necessary to properly format the incoming data. The second is the acousto-optic modulator (AOM) necessary to control the duration and intensity of the laser pulses. The physical parameters necessary for these devices to be consistent with the desired performance goals are determined.

Two acousto-optic page composers are used in the SIAM system. Each utilizes a 128 channel design to perform the conversion to the optical domain. The aggregate data rate required for the pair of AOPC devices is 2.5 Gb/s. This data rate is necessary to account for the burden caused by overhead and error correction information. To reach this data rate, the per-channel data rate of each AOPC channel is 9.8 Mb/s; the corresponding rise time is 102 ns. The AOPC design assumes an illuminating wavelength of 514.5 nm, a maximum RF drive power density of 20 W/cm^2, a

transducer height and spacing of 100 μm, and a piezoelectric transducer conversion efficiency of 0.4. These are the same assumptions made in the AOPC design for the SP device. Several different acousto-optic materials are considered. The device parameters for these are summarized in Table 3-4. The device parameters calculated for the candidate materials are the transducer length L, the maximum RF drive power P_e, and operating frequency ν. In addition, the maximum per-channel efficiency η at maximum drive levels and the optical spot diameter d_w to achieve the desired rise time are presented. Each device design summarized in the table is capable of a per-channel efficiency greater than 99 percent for drive power levels below the maximum limit. This increase in efficiency from the AOPC design for the SP system is attributable to the change of both the required rise time and operating frequency. The change provides similar acoustic interaction geometries at greatly increased transducer lengths. The larger transducers can support a higher RF drive power, resulting in higher device efficiency.

Since good modulation performance is achieved from all of the candidate materials, the material selection is based on the ease of fabrication. The crystalline materials, although providing good performance, are extremely fragile, making device fabrication difficult. The recommended material is the SF-58 glass, providing both fabrication ease and low drive power requirements.

The acousto-optic modulator (AOM) for the SIAM system also has a relaxed rise time compared to that for the SP system. The AOM for the SIAM approach must produce a light pulse with a rise time τ of 20 ns. The transducer height H is chosen as 50 μm to require low electrical drive power P_e; the maximum allowed power density for the RF signal is 1 kW/cm^2. The transducer conversion efficiency is 0.4. For these design constraints, the performance levels achieved with several acousto-optic materials are summarized in Table 3-5. These device parameters include the RF drive power, operating frequency, transducer geometry, and per-channel diffraction efficiency. The beam-spread ratio assumed for the calculation satisfies the equality expressed by Equation (3-1).

3-40

Table 3-4. Device Parameters For 128 Channel Acousto-Optic Page Composer For Selected Candidate Materials

Per Channel Data Rate R_c = 9.8 Mb/s
Rise Time τ (10-90%) = 102 ns
Transducer Height H = 100 μm
Transducer Spacing ΔH = 100 μm

Material	Transducer Length L (mm)	Operating Frequency ν (MHz)	RF Drive Power P_e (mW)	Maximum Efficiency η (%)	Spot Width d_w (mm)
SF-8	20.1	49.7	402	99 *	0.53
SF-58	12.5	56.2	250	99 *	0.44
SF-59	11.9	57.1	238	99 *	0.44
$PbMoO_4$	12.4	70.3	248	99 *	0.49
TeO_2	17.5	66.5	350	99 *	0.57
TiO_2	92.4	75.9	1848	99 *	1.40
Quartz	54.4	42.9	1088	99 *	0.81

*All the devices achieve an efficiency greater than 99 percent at less than the maximum drive power P_e.

Table 3-5. Device Parameters And Performance Levels For SIAM Acousto-Optic Modulator With a 20 ns Rise Time

Material	Transducer Length L (mm)	Operating Frequency ν (MHz)	RF Drive Power P_e (W)	Efficiency η (%)	Spot Diameter d_w (μm)
SF-8	0.77	254	0.385	25	39
SF-58	0.48	287	0.240	19	33
SF-59	0.46	291	0.230	25	32
$PbMoO_4$	0.48	359	0.240	50	37
TeO_2	0.67	339	0.335	77	43
TiO_2	3.55	387	1.775	87	105
Quartz	2.09	219	1.045	43	60

Satisfactory performance is obtained with either the titanium dioxide (TiO_2) or tellurium dioxide (TeO_2) crystalline materials. Both of the devices offer a per-channel efficiency greater than 75 percent. However, because the proposed TiO_2 modulator requires high RF drive levels, the tellurium dioxide is the preferred material for the AOM.

3.3.3.2   Optical Components

The optical configuration for the SIAM approach is based on the use of two separate, although completely equivalent, recording and readout paths. The requirements for the optical components in these paths are determined by the AOPC geometry, information packing density considerations, and certain holographic parameters. Since the individual AOPC devices required for the SIAM system have dimensions equivalent to the SP AOPC, the requirements for the AOPC illumination optics are also equivalent. The requirements imposed by the information packing density and the holographic parameters are identical to those of the SP system. However, the recording film width for each channel in the SIAM system is nominally 25 mm, as opposed to the 50 mm width for the SP approach. The smaller film width allows a slight reduction in the optical apertures of the transform and autoscan lenses. The optical aperture required for these SIAM lenses is 69 mm, corresponding to an F-number of 2.5 (compared to the F-number of 2 required for the equivalent SP lenses, S5, S6, S7, and S8 indicated in the previous Figure 3-6). The remaining optical components required for each channel of the SIAM approach duplicate those of the single channel SP optical train. The laser power required for the SIAM system to record at an aggregate data rate of 2.5 Gb/s is also equivalent to that of the SP approach.

The final configuration of the SIAM approach would then consist of two identical recording and readout paths operating in parallel. The optical components required for each of the paths would be essentially the same components needed to implement the single channel SP system. The additional complexity of the SIAM approach lies in achieving the necessary mechanical stability of the two optical paths.

3.3.3.3   Spinner and Film Transport Subsystems

As for the optical components, the requirements and performance levels for the spinner and film transport subsystems are very similar to those for the SP design. However, the SIAM approach offers an advantage. The effective increase in the number of channels for the SIAM system provides a decrease in the data rates and bandwidths required on the per-channel level. The reduced data rates allow a slight reduction in spinner and transport speeds.

The dual spinners for the SIAM system provide the scanning action for both the record and reproduce phases of operation. The height of the mirror must be adequate to completely accept the incident data and reference patterns. As in the SP approach, this spatial extent is 53.14 mm. The spinning mirror must deflect a pattern of this height at a rate consistent with the overall 2.5 Gb/s recording rate, and the velocity of the transport must also be consistent with this recording rate.

The particular recording format used for the SIAM approach determines the rates required for both the spinner and transport. As indicated in Figure 3-8, the optical axes of the two recording paths are separated by a distance H. The distance H must be sufficient to provide an adequate separation between the optical components in each path. The minimum separation occurs at the positions of the spherical transform lenses S5a and S5b, as indicated in Figure 3-8. Each of these lenses have an optical aperture of 69 mm (corresponding to an F-number of 2.5). Allowing an additional 11 mm for mounting supports, the minimum separation H is 80 mm. The corresponding angle θ between the direction of film motion and the plane containing the optical axes is 318 mrad (18.2 degrees). The length L of each row of recorded holograms for these recording conditions is nominally 26.3 mm. As in the SP system, the hologram dimensions (allowing for guardband regions) are 14.2 μm by 1.1 mm for each SIAM channel. These dimensions correspond to an average information packing density σ of 0.82 Mb/cm^2.

The angular speed required for the spinner can now be determined. To achieve the desired data rates, two rows, each containing approximately 1850 holograms, must be recorded in 190 μs. Since each pair of hologram rows correspond to one of the

40 facets on the dual spinner, the angular velocity needed is 132 r/s. Angular velocities of this order are achievable with present spinner technology.

The velocity required for the film transport can be determined similarly. The average packing density of the stored information is 0.82 Mb/cm^2. The active film width used for recording is 50 mm. For these recording conditions, the film transport velocity required is 6.1 m/s. This is the same film speed required for the SP approach. The dynamic stability provided by the film transport must be adequate for holographic recording. The allowable displacement for the surface of the film is the ±15 μm depth of focus of the recording transform lens. However, this stability must be maintained at two recording stations separated spatially by 80 mm. This requirement emphasizes the high degree of opto-mechanical stability for the SIAM system.

3.3.3.4   Detection Subsystem

During the information retrieval process, each optical path produces a reconstructed image of the data block with 128 bit positions. Two discrete fiber-optic/photodetector arrays, located in the stationary bit image plane, sample the resulting intensity pattern. After suitable electronic preprocessing which performs the thresholding operation, the parallel bit streams are reconverted to the original serial bit stream.

The detection subsystem has two major areas of concern. One is the positional integrity required of the optical components to achieve proper readout. The other is the per-channel data rates at which the detection system must work.

The positional integrity required for system components is related to the relative displacement that the readout process can tolerate. The maximum relative shift between the two reference beams allowed in the recording (or film) plane is 7.1 μm, which corresponds to a displacement of one-half a hologram position. The reference beams must be aligned to maintain a shift no greater than 7.1 μm over the 80 mm distance between their respective optical axes. This criterion corresponds to a required angular stability of 89 μrad; this extremely tight angular tolerance is another indication of the high degree of stability required for the SIAM system.

The per-channel data rates required for the SIAM readout system are equivalent to those necessary for recording. This per-channel detection rate of 9.8 Mb/s is significantly lower than that for the SP approach. Presently available discrete detectors can achieve the desired performance level at this information rate.

3.4 AO/SP SYSTEM APPROACH

The optical performance required for the SP and SIAM approaches demands high-quality, low F-number lenses. The AO/SP approach has relaxed demands for the optical system. The AO/SP approach is based on the synchronous scanning of a reference and signal beam across the film width as in the first two approaches. In the AO/SP approach, the data-carrying signal beam is still scanned across the film by the spinner subsystem. The significant change is that the reference beam, directed to the film by separate optics, is scanned with an acousto-optic beam deflector. A system layout for the AO/SP approach is given in Figure 3-9. Since the optical apertures for the lenses in the signal path need only be large enough to pass the signal pattern, the lens requirements are reduced. To alleviate strict tolerances on the acousto-optic beam deflector, the reference beam is defocused at the recording plane. This allows several adjacent holograms in the along-scan direction to overlap, thus recording incoherent additions. Information retrieval from the system is accomplished by the acousto-optic scanning of the reference beam across the one-dimensional Fourier transform holograms. The signal beam reconstructed at each hologram location is appropriately processed to form a stationary bit pattern at a fiber-optic/photodetector array.

3.4.1 Recording Process

The recording process for the AO/SP approach is similar to the recording process in the SP approach. The AO/SP approach represents a modification to the recording method of the SP approach that decreases the optical apertures of the lenses required. An incoming high-speed serial bit stream is demultiplexed into separate channels and interwoven with system operation information. The aggregate data rate of the demultiplexed signals is 2.5 Gb/s to account for the increased burden posed by the system operation information. The 128 demultiplexed signals are mixed with a single frequency RF carrier, and the resulting signals are routed to the acousto-optic page composer (AOPC). The piezoelectric transducers of the AOPC convert the electrical signals received into variations of refractive index within the optical apertures of each channel. When the optical apertures have filled, the mode-locked, cavity-dumped

OTUPUT DATA

89444-8

ERROR CORRECTION AND
MULTIPLEXER NETWORK

PHOTODETECTOR
ARRAY

INPUT DATA

DEMULTIPLEXER

LASER

AOPC

SPINNER

AUTOSCAN

AOBD AND
SCANNER

FILM PLANE
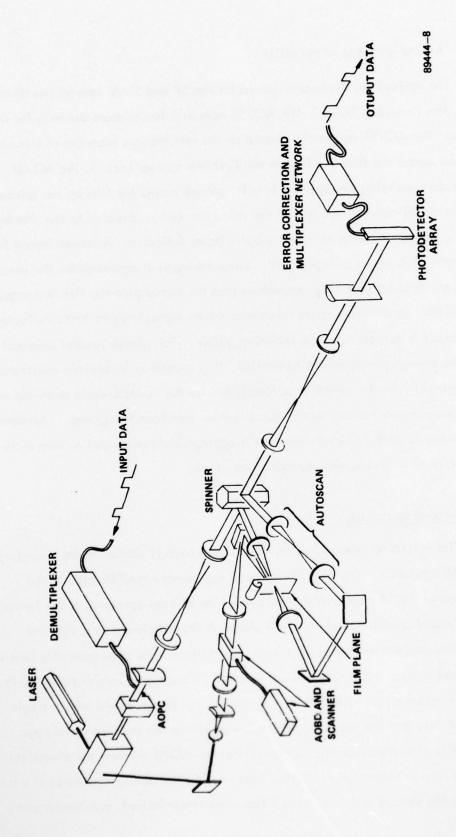
Figure 3-9. AO/SP System Functional Diagram

(MLCD) laser supplies a short duration light pulse. The MLCD laser, providing a rapid shuttering action for the laser illumination, supplies a light pulse whose duration and magnitude are chosen to properly expose the film. The laser is also required to supply pulses short enough (2 ns) to record a stabilized fringe pattern.

The unexpanded laser beam entering the recording system is divided into appropriate signal and reference beam illuminations. The signal beam undergoes the same beam shaping as in the SP system. After illuminating the AOPC channels, the signal beam has an intensity profile corresponding to the input data pattern. Appropriate optics display the one-dimensional Fourier transform of the data pattern in the film recording plane. A spinning polygonal mirror, situated in the signal beam path, imparts a lateral scanning motion to the Fourier transform. The rate of the scanning is chosen to allow the recording of transforms consistent with the required system data rates.

Concurrent with the scanning of the Fourier transform is the reference beam scanning. The reference beam illumination is scanned across the film surface by an acousto-optic beam deflector (AOBD). The spatial extent of the reference illumination at the film surface is larger than that of the data transform. The size difference allows a reduction in the time-bandwidth product for the AOBD. The scanning rate of the AOBD corresponds to that of the polygonal spinner. When the reference and signal beams are combined at the recording plane, a one-dimensional Fourier transform hologram is recorded. The oversized reference beam causes an increase in the background exposure level at neighboring locations.

As in the SP recording process, the first hologram of a row is recorded after control logic receives a signal that the spinning mirror is in the proper orientation. When this signal is received, holograms are recorded across the film by the simultaneous scanning of the spinner and AOBD. When the recording of a row is completed, the control logic waits for the next spinner signal. A continuous motion film transport moves the film at velocities consistent with the recording rate and format. The row recording process continues until the film supply is exhausted. At this point the exposed film is removed from the transport and processed to provide archival storage of the data records.

3.4.2   Readout Process

For readout, the processed film containing the data records is replaced in the system transport. The optical system used to reconstruct the stored data patterns is equivalent to that used for recording. All available power is diverted into the reference illumination in order to read out the recorder patterns with maximum intensity. For the readout process, the actions of the spinner, AOBD, and film transport must be synchronized. The synchronization between the film transport and AOBD is necessary to allow the line scanned by the AOBD to coincide with a row of recorded holograms. The synchronization with the spinner is required to form a stationary image of the data pattern at the fiber-optic/photodetector array. When this control has been established, the readout process begins. The reference beam is scanned across the recorded hologram rows. At each hologram location, the recorded signal waves are reconstructed.

The focal lengths of the optical components required for the AO/SP readout system are identical to those of the corresponding lenses in the SP system. However, since the lenses must pass only the signal beams, the aperture requirements are relaxed. A telescope assembly images the data bit sequence into a separate plane. In this plane the signal pattern is scanned through a distance corresponding to the active film width. Another telescope assembly reimages the data pattern after reflection from the spinning mirror. Data descan is accomplished by utilizing the reflection from the spinning mirror to cancel the scanning motion.

A stationary data pattern is imaged onto the fiber-optic/photodetector array. Each fiber of the 128-element array samples one bit location. The necessary thresholding decisions are performed on the output signals from the array. Error correction is performed, and the resulting digital signals are routed to the multiplexer network. The channelized data is reconverted into a high-speed serial bit stream by the network.

3.4.3   Component Requirements for the AO/SP Approach

Four different component categories are required to realize an AO/SP recorder/reproducer system. Acousto-optic devices are required to perform the intensity

modulation and the data conversion processes. Optical components that perform the proper imaging and transforming operations are necessary. A spinning mirror and film transport that distribute information across and along the film are required and the detection subsystem is necessary to provide the reconversion to the electrical domain. The major requirements for these categories are discussed in this section.

3.4.3.1   Acousto-Optic Components

Three acousto-optic device types are required for the AO/SP approach. An acousto-optic page composer (AOPC) is used to convert from the electrical to the optical domain. An acousto-optic beam deflector (AOBD) is used to scan the reference beam during both the record and readout processes. The use of a mode-locked, cavity-dumped (MLCD) laser, providing rapid high intensity light pulses, is necessary to successfully record holograms.

The AOPC for the AO/SP approach has the same requirements as that in the SP approach. The AOPC design summarized for the SP description possesses all the proper characteristics. The AOPC design is based on 128 individual channels on 200 μm center spacings. The design parameters of the AOPC are summarized for several candidate materials in Table 3-1. The recommended material for the device is the tellurium dioxide (TeO_2) crystal.

The acousto-optic beam deflector (AOBD) is used to scan the reference beam across the film width. To reduce the performance levels required for the device, the scanned reference beam does not individually address each of the recording locations in the film plane. The reference beam is sized to overlap four recording locations. Thus, the number of single-Rayleigh resolved spots the AOBD must achieve is one-fourth of the hologram locations. Since the number of holograms per row is approximately 3000, the AOBD must resolve only 750 locations. The number of single-Rayleigh resolved spots from an AOBD is identical to the time-bandwidth product P of the device. The recording format of the AO/SP system is the same as that of the SP system: 2951 holograms, each containing 128 bits, are recorded in a time T of 151 μs. Since the time-bandwidth product P is 750, the device bandwidth B required is P/T, or 5 MHz.

These conditions do not impose any significant difficulties. The relatively low time-bandwidth product and bandwidths involved can be achieved within the existing state of the art of AOBD technology.

The use of the AOBD to deflect the reference beam does introduce one complication. The frequency of the reference beam is Doppler shifted by the acousto-optic interaction. The amount of shift is dependent on the scanning position. The time-varying frequency shift of the reference beam does not allow the formation of a stationary interference pattern during the recording process. A short (2 ns) exposure is necessary to freeze the fringe motion. These short pulses at the required energy levels can be obtained only with a mode-locked, cavity dumped laser. The mode-locking provides a very pure illumination wavelength, while the cavity-dumping allows the extraction of high energy pulses for exposure.

The mode-lock, cavity-dump process is performed by a single acousto-optic device inside the laser cavity. The laser cavity is used in a storage resonator configuration. The acousto-optic device periodically diverts the circulating power within the cavity so that an extremely high spectral purity pulse is achieved. The requirements for the MLCD laser are discussed further in the next section.

3.4.3.2   Optical Components

The optical layout for the AO/SP system is essentially identical to the layout for SP system approach. There are only two primary differences between the systems. First, the reference beam illumination is scanned, not by the spinning mirror as in the SP approach, but by an AOBD with separate optics. Second, because the signal beam optics do not have to pass the reference illumination, the corresponding F-numbers can be reduced from those required in the SP approach.

The AOBD and its associated optics must be capable of scanning the reference beam across the 50 mm active film width in the recording plane. The angle relative to the plane defined by the film surface should be 154.4 mrad. This angle forms an interference pattern with a maximum fringe frequency of 600 cy/mm. The

optics associated with the AOBD are conventional and are easily specified when the particular system geometry is chosen; they will not be considered further here.

The use of separate optics to direct the reference beam to the film recording plane decreases the optical apertures of the lenses required in the signal path. The amount of decrease is dependent on the particular optical layout. The optical components after the AOPC now need be only large enough to pass the signal illumination. Thus, the apertures of the spherical lenses after the AOPC can be decreased by a factor of two from those of the SP case. The cylindrical lenses and the optics prior to the AOPC should remain unchanged. No change in focal lengths is required from the SP configuration.

The holographic recording format is also unchanged from that of the SP approach. There are 2951 one-dimensional Fourier transform holograms recorded across the 50 mm active film width W. Each hologram, containing 128 bits has a height h of 1.0 mm and width w of 12.9 μm. The recording format allows a guardband corresponding to 10 percent of the respective hologram dimension. To achieve the desired recording rate of 2.5 Gb/s, the holograms must be recorded at a repetition rate R of 19.5 MHz.

The average power of the laser can be estimated using the hologram recording format and the film sensitivity. The exposure requirement S_f for the film is estimated as 10 μJ/cm^2. The hologram area A_h is 1.29×10^{-4} cm^2. For an estimated system efficiency η of 0.03 the average laser power P_ℓ required is:

$$P_\ell = \frac{S_f A_h R_c}{\eta} = 0.84 \text{ Watt}.$$

Thus, the energy required per 2 ns pulse for the exposure is approximately 40 nJ. This energy per pulse is somewhat higher than the level typically achieved. Further engineering development is required to achieve the necessary power levels from a MLCD laser.

3.4.3.3   Scanner and Film Transport

The film transport required for the AO/SP approach must move film past the recording station at a velocity consistent with the 2.5 Gb/s recording rate. The required

film velocity V is determined by the average packing density $\bar{\sigma}$, the active film width W, and the data recording rate R. The average information packing density $\bar{\sigma}$, allowing for a 10 percent guardband, is 0.82 Mb/cm^2. The AO/SP approach records on an active film width W of 50 mm. The system data rate R must be 2.5 Gb/s. For these conditions, the film velocity V is:

$$V = \frac{R}{\sigma W} = 6.1 \, m/s \quad .$$

While moving film at these rates, the transport must also maintain the film surface within the depth of focus of the transform lens. For the AO/SP system, this depth of focus criterion allows a film jitter of ±15 μm. To successfully achieve the performance levels required for the film transport will require significant design and fabrication effort. However, based on our success with the present EDM transport, we feel the film transport requirements can be achieved.

The rate requirements for the spinner can be similarly determined. The spinner facet height can be reduced from that of the SP spinner, since it must handle only the signal pattern. The facet height for the spinner for the AO/SP approach is nominally 26 mm. For a polygonal spinner with 40 facets, the angular velocity to achieve a 2.5 Gb/s recording rate is 166 revolutions per second. We feel that this angular rate, although high, is achievable.

3.4.3.4   Detection Subsystem

The 128-channel fiber-optic/photodetector array located in the output plane of the AO/SP system performs the conversion from the optical domain to the electrical domain. Each channel of the array samples the intensity at one bit location. The per-channel readout rate is 19.5 Mb/s. Readout rates of this magnitude are difficult to achieve with presently available solid-state detectors for the anticipated optical power levels. However, the rapid advancements in detector technology offer much promise.

3.5   2D APPROACH

The approaches to achieve the 2.5 Gb/s data rates considered thus far are based on recording one-dimensional Fourier transforms. A different concept based on a two-dimensional recording technique is the 2D approach. A functional representation of the required optical recording and readout system is given in Figure 3-10. One of the significant differences involved in the 2D approach is that many bits are recorded simultaneously by projecting the laser beam through a multichannel, multiposition modulator instead of a single position modulator. Information retrieval from the system utilizes a two-dimensional array of photodectors to sense the reconstructed data pattern. The resulting signals from the detectors are processed and fed in parallel to the multiplexing system to generate a reproduction of the original input data sequence. The 2D approach summarized here is similar to the two-dimensional hologram recording approach investigated both theoretically and experimentally under a previous phase of the wideband recording program, but is extended to enable utilization of 70 mm photographic film.

3.5.1   Recording Process

As in the previous approaches, the recording process for the 2D approach is initiated by the demultiplexing operation. Here, the input data to be recorded is demultiplexed into several low-rate data streams. These parallel bit streams modulate RF carrier signals, which drive the various channels of a multichannel acousto-optic modulator array (AOMA). In the AOMA, acoustic waves are generated which correspond to the input electronic data sequence. Thus, the various data-modulated acoustic waves propagate parallel to one another through the acousto-optic material. When the aperture of the AOMA has filled, a short pulse of light is generated and projected through the system by a mode-locked, cavity-dumped (MLCD) laser. An MLCD laser is required to produce a short duration, high energy laser pulse to maintain acceptable fringe contrast during the recording process. Suitable beam-shaping optics provide both reference and signal beam illuminations. The signal beam incident on the AOMA is a uniform, collimated wave.
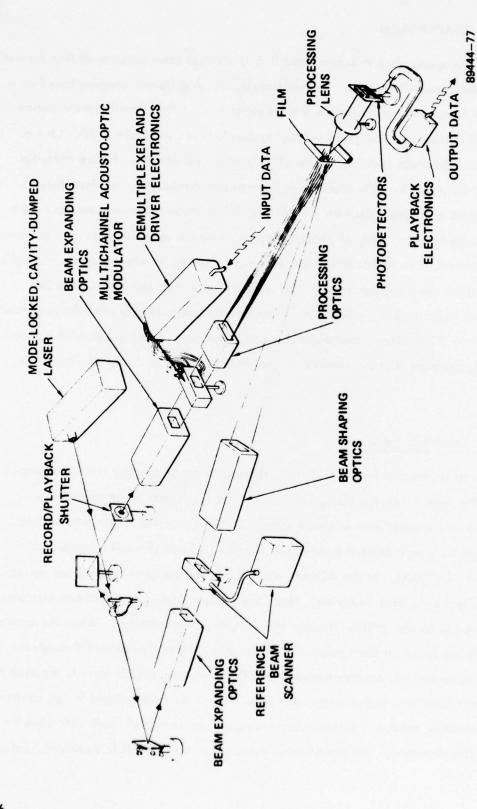
Figure 3-10.   2D Functional System Diagram

MODE-LOCKED, CAVITY-DUMPED LASER

BEAM EXPANDING OPTICS

MULTICHANNEL ACOUSTO-OPTIC MODULATOR

DEMULTIPLEXER AND DRIVER ELECTRONICS

RECORD/PLAYBACK SHUTTER

BEAM EXPANDING OPTICS

REFERENCE BEAM SCANNER

BEAM SHAPING OPTICS

PROCESSING OPTICS

INPUT DATA

PROCESSING LENS

FILM

PHOTODETECTORS

PLAYBACK ELECTRONICS

OUTPUT DATA

89444–77

As a result of passing through the multichannel AOMA, the signal beam is spatially modulated by the data block pattern superimposed on the acoustic beams. This modulated light is accepted by the processing optics. A cylindrical lenslet array, one component of the processing optics, is positioned in an image plane of the AOMA. The lenslet array performs as a high efficiency phase grating and produces 15 multiple, equal intensity diffraction orders. A spherical lens accepts the 15 diffracted orders containing the data block and displays 15 corresponding identical Fourier transforms of this data block in its back focal plane. Two-dimensional Fourier transform holograms of successive data blocks are recorded by sequentially combining the reference beam and each of the 15 spatially separated Fourier transforms at the film plane. The intensity distributions of the nonaccessed Fourier transforms are not mixed with the reference beam; this intensity causes only a low level exposure of the film and makes a small contribution to the background noise in the reproduced data images. However, this noise contribution is tolerable for several practical sets of system parameters.

After a hologram is recorded, the recording process is repeated. Another block of data is accepted by the AOMA. Another pulse of laser energy from the MLCD laser is generated. An acousto-optic beam deflector in the reference beam path is used to deflect the reference beam to the next storage location along the continuously moving film strip. The process continues until the film supply has been exhausted.

3.5.2 Readout Process

After the film supply has been recorded, the exposed film is processed and repositioned in the recording plane. All available energy from the laser is diverted to form the reference beam. As the film moves through the system, the acousto-optic beam deflector (AOBD) directs the reference beam to the various holograms recorded on the film. Each time a hologram is illuminated by the reference beam, an irradiance pattern corresponding to the Fourier transform of the original recorded data block is reconstructed. A spherical lens performs the inverse transform operation and displays an image of the data block on the two-dimensional array of photodetectors. The electrical signals obtained from the photodetector array are fed in parallel to a preprocessing network which provides

bit decision thresholding. The multiplexing electronics accept the processed signals and generate a single high-rate bit stream, which is a replica of the original input data to the recorder.

3.5.3 Components Requirements for the 2D Approach

The major components required to implement a 2D recorder/reproducer system can be categorized in a manner similar to the other systems considered. Various acousto-optic devices are required to modulate the laser power and format the data block for recording. Optical components are necessary to provide beam shaping and processing functions. The scanning system is comprised of only the continuous motion film transport, which provides for the distribution of information along the film length. The detection electronics must be capable of converting the reconstructed intensity patterns at rates consistent with program goals.

3.5.3.1 Acousto-Optic Devices

Several types of acousto-optic devices are required for the realization of the 2D approach. To format data in two dimensions requires an acousto-optic modulator array (AOMA). The deflection of the reference beam to access desired film positions requires an acousto-optic beam deflector (AOBD). The short duration of the laser pulse necessary for recording requires a mode-locked, cavity dumped (MLCD) laser. Some considerations for these devices are presented in this subsection.

The design parameters of the AOMA impact the optical efficiency of the system, the data storage format on the film, and the requirements of the optical components. The AOMA is to be a multichannel array of acousto-optic modulators. The modulators are grouped in two columns, each with the same number of channels. Practical design considerations for both efficiency and acoustic attenuation properties limit the acousto-optic material selection to lead molybdate (Pb Mo O_4). Several additional constraints are imposed on the design parameters of the AOMA by the device geometry. First, the device must work in the Bragg regime. Thus, the acoustic interaction parameter Q must be at least 2π. Second, the per-channel device efficiency η must be high. The design

goal is an efficiency of 0.8. Third, the device must attain the efficiency with a transducer power density P_d that is no more than 20 W/cm^2. Finally, the electrical impedance of the transducer must be approximately 50 Ω for compatibility with the device electronics. This places a constraint on the transducer geometry (length L and height H) and the drive frequency. The constraint is expressed by

$$LH = \frac{4K}{f^2} = \frac{4(3.191 \times 10^4 \text{ MHz}^2 \text{ mm}^2)}{f^2} \ ,$$

where f is the device operating frequency and the constant K is given for lithium niobate (LiNbO$_3$) transducers.

The constraints expressed above can be used to determine the operating parameters for each channel of the AOMA. These operating parameters include the length L and height H of the transducer, the device operating frequency f, and the drive power P_e required to achieve an efficiency of 0.80. The design equations assume the use of lithium niobate transducers bonded to a lead molybdate crystal. The illumination wavelength λ is 514.5 nm, and the transducer conversion efficiency η_a is 0.4. For these parameters, the design relations may be manipulated to yield the operating parameters as follows:

Transducer Length: $L = \frac{1}{\pi} \sqrt{\frac{2\lambda^2}{\eta_a P_d M_2}} \text{ arc sin } \sqrt{\eta} = 4.77 \text{ mm }$;

Transducer Height: $H = \frac{4K\lambda}{n V_a^2} = 2.09 \text{ mm }$;

Operating Frequency: $f = \sqrt{\frac{n V_a^2}{\lambda L}} = 113.3 \text{ MHz }$;

and

RF Drive Power: $P_e = P_d L H = 1.99 \text{ W }$;

where n is the index of refraction and V_a is the acoustic velocity of the lead molybdate crystal.

The remaining parameters necessary to completely specify each channel of the modulator array are the channel length D and the transducer spacing H. The number of bit locations per channel is chosen to be 128. The channel length D is the length of acousto-optic material necessary to contain the 128 spatial bit locations. Each of these bit locations corresponds to the distance travelled by the acoustic wave during the time of one RF signal packet which is nominally twice the rise time τ_R (10 to 90 percent response) of the transducer. Thus, the distance D is given by

$$D = 128 \, V_a \, (2\tau_R) = 2 \, (128) \, V_a \, \frac{2.2}{f} = 18.04 \text{ mm} \quad .$$

The transducer spacing δH must be adequate to prevent interference between adjacent acoustic channels. Interference is prevented if adjacent acoustic beams broadened by the diffraction spreading from the finite transducer height H are spatially separated at a distance D from the transducer; this is achieved for a transducer spacing δH given by

$$\delta H = \frac{2 \, V_a \, D}{H \, f} = 0.55 \text{ mm} \quad .$$

Each channel of the AOMA is now completely specified. To specify the array, we need to determine the total number of channels required for the device. The number of channels N required is determined by the recording rate R of 2.5 Gb/s, the time T required for an acoustic wave to propagate across the aperture D, and the number m of bits per channel. The number of channels is given by

$$N > \frac{R}{mT} = \frac{R \, D}{m \, V_a} = 97.06 \quad .$$

Since N must be an even integer, the obvious choice is N = 98 channels.

Thus, the AOMA is composed of two columns, each containing 49 acousto-optic channels. The total height required for the AOMA is 129.4 mm, while the width of the array (allowing a 5-mm space between columns for acoustic absorbers) is 41 mm. The dimensions of one bit location in an AOMA channel is 140 μm by 2.09 mm. The time required to fill the AOMA to its 12.544K-bit capacity is 4.97 μs. Each channel of

the AOMA has an efficiency of 0.8; the device efficiency, which accounts for the inactive area of the AOMA, is 0.56.

The acousto-optic beam deflector (AOBD) scans the reference beam to the 15 Fourier transform locations in the recording plane. The low resolution and low access times required for the AOBD represent no significant problems. The major effect of the AOBD is to introduce a position dependent frequency shift to the reference beam. This frequency shift cannot be completely compensated and requires the use of a mode-locked, cavity-dumped (MLCD) laser to provide useful holographic recordings.

An MLCD laser is capable of providing extremely brief light pulses. The short duration times (typically 2 ns) are necessary to freeze the interference pattern between the signal and frequency-shifted reference beam of the 2D system. The techniques for achieving MLCD laser action with acousto-optic devices are well established for low laser power levels. However, to achieve the desired laser action for a high output power level requires further advancement in the present state of the art. Significant engineering effort will be required to overcome the anticipated problems.

3.5.3.2   Optical Components

The optical layout required to implement the 2D system approach is indicated in Figure 3-11. The multichannel acousto-optic modulator array is uniformly illuminated by an expanded laser beam. The diffracted bit pattern, corresponding to the data block in the AOMA, is separated from the throughput beam by the spatial filter P2 located in the back focal plane of spherical lens S3. Sperical lens S4 reimages the AOMA data pattern on the cylindrical lenslet array C1. The action of the cylindrical lenslet array is to diffract 15 equal intensity diffracted orders, each of which corresponds to the AOMA data block. The spherical lens S5 displays the Fourier transform of these diffracted orders in its back focal plane. One of these 15 identical Fourier transforms is illuminated by the deflected reference beam to record the Fourier transform hologram of the AOMA data block.
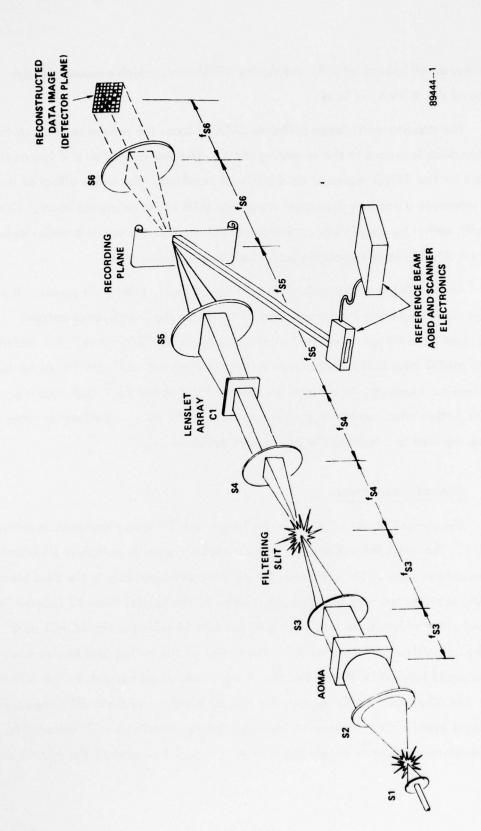
Figure 3-11. Optical Layout – 2D System

During the readout process, the reference beam is sequentially scanned across each of the hologram locations. At each location, a signal beam corresponding to the originally recorded Fourier transform is reconstructed. Spherical lens S6, located a focal length f_{S6} from the film plane, performs the inverse transform operation and images the original data sequence onto the photodetector array.

The requirements of the reference beam optics and the optics prior to the AOMA are conventional and are not considered here. The performance levels for the optics subsequent to the AOMA are determined for a specific otpical layout in which the focal lengths of the spherical lenses after the AOMA are equal, i.e., $f_{S3} = f_{S4} = f_{S5} = f_{S6}$. All the significant features of the 2D approach are derivable from this assumption. However, it is noted that this is not a system requirement. To achieve better system operability, these focal lengths may be made unequal; the extension of the analysis for unequal focal lengths represents only a minor modification.

Spherical lens S3 must have an aperture D which is sufficient to pass the diffracted data pattern of the AOMA. In one direction, the dimensions of the lens must be large enough to pass the combined distance of the hologram width w and AOMA width. In the other, the aperture of the lens must be larger than the combined hologram height h and the AOMA height H. For all practical system designs, the AOMA geometry is much larger than the hologram dimensions. With this simplifying assumption, the aperture D_3 of the lens is

$$D_3 \approx \sqrt{H^2 + W^2} \approx 135.7 \text{ mm}, \qquad (3-3)$$

where H and W, the AOMA dimensions, are 129.4 mm and 41 mm, respectively. The aperture D_4 required for the spherical lens S4 is also given by Equation (3-3).

The use of the cylindrical lenslet array C1 to generate multiple signal patterns requires the diameter D_5 of lens S5 to be larger than that of S3 or S4. The Diameter D_5 is increased to provide coverage across the active film width W_o of 50 mm. For hologram dimensions much smaller than the AOMA dimensions, the minimum lens diameter D_5 is

$$D_5 \approx \sqrt{H^2 + (W + W_o)^2} \approx 158.2 \text{ mm}. \qquad (3-4)$$

The minimum diameter D_6 for lens S6 that images the reconstructed bit pattern on the photodetector array is also given by Equation (3-4). Once the focal lengths of the lenses are specified, the remaining system parameters can be determined. Thus far, the choice of focal length is completely arbitrary.

One consideration for a lens specification is the F-number (ratio of focal length to aperture) of the lens. In practice, a reasonable choice for the F-number of the lens for a wide field application such as that of lens S5 or S6 is 2.8. For this condition, the focal length of S5 and S6 can be determined from Equation (3-4) and is

$$f_{S5} = f_{S6} = 2.8 \, D_5 = 443.0 \text{ mm}.$$

For the particular optical system chosen, the focal lengths of the remaining spherical lenses S3 and S4 are also 443.0 mm. However, the tolerances for these lenses are relaxed slightly, since they work at the higher F-number of 3.3.

The dimensions of each hologram must be sufficient to allow the reconstruction lens S6 to achieve double-Rayleigh resolution of a bit location in the AOMA. A single bit location in the AOMA has a height h of 2.09 mm and a width w of 140 μm. The hologram height $\overline{h}$ and width $\overline{w}$ are then specified by

$$\overline{h} = \frac{2 \lambda f_{S6}}{h} = 0.218 \text{ mm} ;$$

and

$$\overline{w} = \frac{2 \lambda f_{S6}}{w} = 3.26 \text{ mm} .$$

The active film width required to record 15 holograms is 53.3 mm, allowing a guardband spacing between holograms of 10 percent the hologram width $\overline{w}$.

Thus, the cylindrical lenslet array C1 must produce 15 equal intensity signal distributions separated by 3.59 mm in the film plane. For the cylindrical lenslet array in the front focal plane of the transform lens S5, the center spacing S between the lenslets forming the array is given by

$$S = \frac{\lambda f_{S5}}{3.59 \text{ mm}} = 63.7 \text{ } \mu m \text{ .}$$

Cylindrical lenslet arrays consistent with these requirements are commerically available.

The laser power requirements for the 2D system can be determined from system geometry and estimated optical efficiencies. The MLCD laser used for recordings must provide pulsed operation at rates consistent with the fill time of the AOMA. The laser supplies a train of 2 ns duration light pulses separated by 4.97 µs, corresponding to a repetition rate of 201.2 kHz. The hologram recording area A_h is 0.716 mm^2. The esimated efficiency of the reference beam optics is 0.18. The estimated efficiency of the signal beam optics, including the AOMA, is 0.25. To achieve acceptable holographic performance in the presence of the incoherent addition, the intensity of the reference beam at the film recording plane must be a factor of ten larger than the signal beam intensity. For these conditions, the efficiency η of the total optical system from the laser to the recording plane is approximately 0.25. For these parameters and a film sensivity S_f of 10 µJ/cm^2, the energy per laser pulse E_ℓ is

$$E_\ell = \frac{S_f A_h}{\eta} = 0.30 \text{ } \mu J \text{ .}$$

This is a high output power level to achieve for a mode-locked, cavity-dumped argon ion laser. Typical power levels achieved are approximately two orders of magnitude less than the required energy level. Further engineering development is required to achieve mode-locked, cavity-dumped operation in such high output lasers.

3.5.3.3   Film Transport

The film transport in the 2D approach must move the recording film through the recording station at a velocity consistent with the recording rate of 2.5 Gb/s. The

film velocity V required for the transport is determined by several recording parameters: recording rate R, active film width W, and average information packing density $\overline{\sigma}$. The recording rate R is 2.5 Gb/s. The active film width W has been established as 53.3 mm. The average packing density $\overline{\sigma}$ for the 12.544 k-bit capacity of the AOMA is 1.46 Mb/cm^2. (The 10 percent guard band region is included in the hologram area.) For these values, the film speed V required is

$$V = \frac{R}{W\,\overline{\sigma}} = 3.2 \text{ m/s} .$$

While moving the film at rates of 3.2 m/s, the transport must maintain the film surface within the depth of focus of the transform lens S5. The depth of focus for the lens allows a film jitter of ±10 μm. Although the film velocity required for the 2D film transport is not excessively high, the depth of focus requirement is relatively difficult to achieve in practice.

3.5.3.4   Detection Subsystem

The reconstructed data image of the 2D system is a two-dimensional array of more than 12×10^3 bit locations over a field covering 129.4 mm × 41 mm. One bit location in the image field is 2.09 mm × 140 μm. For arrays of this size and complexity, discrete detectors are totally impractical, and an integrated approach, such as the use of a CCD array, must be taken. CCD arrays for high data rates, but with fewer elements than discussed above, have been proposed. However, even though the per-element data rate is nominally only 200 kb/s, the task of fabricating a 12,000-element array to the geometry necessary appears formidable.

3.6 LS APPROACH

An unconventional method to achieve data recording rates of 2.5 Gb/s is the LS approach. The heart of the LS system is the acoustic traveling wave lens (ATWL), which eliminates the need for a mechanical scanning device. A functional layout for a system based on the LS concept is presented in Figure 3-12. Incoming serial data is formatted for input to an acousto-optic page composer by a demultiplexing circuit. The page composer imparts a spatial modulation to the illumination. The diffracted bit pattern from the AOPC is shaped for recording by the recorder optics and is incident on an acousto-optic beam deflector (AOBD). The AOBD, in conjunction with transform optics, deflects the transformed bit pattern at a rate identical to that of an acoustic compressional pulse traveling through the ATWL. The acoustic pulse performs a cylindrical lensing action and provides a smaller spot width for recording. Information retrieval is accomplished with a similar scheme. A second acoustic traveling wave lens, the readout ATWL (in conjunction with an AOBD) is used to provide a stationary image at a linear array of detectors. Subsequent multiplexing networks reconstruct the original high rate, serial data stream.

3.6.1 Recording Process

The demultiplexing operation is the starting point for the recording process in the LS system. During this stage, the incoming serial data is demultiplexed into channelized data streams compatible with the page composer format. The piezoelectric transducers of the acousto-optic page composer (AOPC), driven by signals corresponding to the channelized data, launch acoustic waves in the AOPC channels corresponding to the data. When the laser illumination is passed through the AOPC cell, a diffracted pattern corresponding to the bit pattern results. Appropriate optics expand the diffracted beam pattern for input to the AOBD. The AOBD imparts to the bit pattern an angular deflection, which subsequent optics convert to a positional movement of the transformed pattern that tracks the acoustic compressional wave in the ATWL. The ATWL compressional wave, acting as a cylindrical lens, further reduces the width of the one-dimensional Fourier transform for recording a hologram on the film. Because the
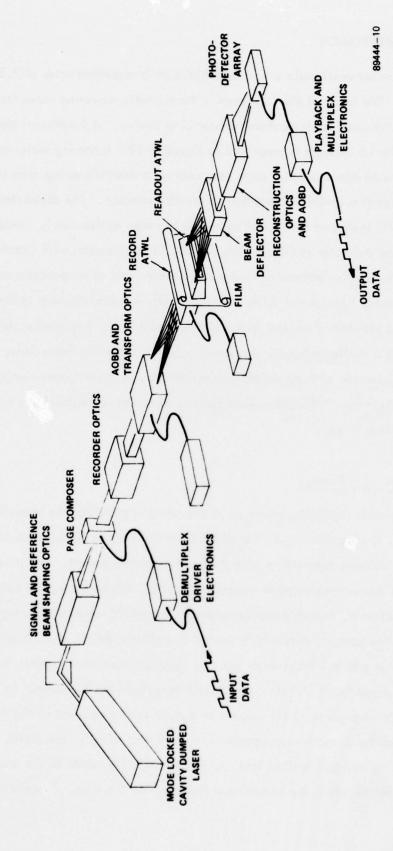
Figure 3-12. LS System Functional Diagram

89444-10

frequency shift between the reference beam diffracted by the AOBD and the signal data pattern cannot be completely compensated, short duration high intensity exposures are required. These exposure conditions require a mode-locked, cavity-dumped laser. To accommodate the inactive dead time between scanning operations, the data record rate is higher than that of the other systems. The instantaneous record rate will be taken to be 3.2 Gb/s. This rate provides a 70 percent duty factor for the beam deflector system. We note, however, that current investigations aimed at increasing the duty factor of the ATWL system offer hope of reducing this overhead requirement.

Critical timing requirements exist for the recording process of the LS approach. The actions of the page composer, acousto-optic beam deflector, and traveling wave lens must be precisely synchronized for successful system operation. In addition, the deviation from scan linearity for the acousto-optic beam deflector must be less than 0.04 percent to achieve the tracking accuracy required for the traveling lens. To achieve these requirements over the environmental changes expected is a challenge.

The mode-locked, cavity-dumped laser pulses must occur at the proper time to ensure that synchronization is achieved. The film at the recording station is exposed, recording a one dimensional Fourier transform hologram. The process is repeated until a hologram row is completed. At this time, another acoustic pulse is launched into the traveling wave lens material. Another row of holograms is then recorded across the 12-inch film. The process is continued until the film supply is exhausted.

3.6.2   Readout Process

The readout process for the LS system is similar to the recording process. All available laser power is diverted into the reference beam so that holograms are read out at maximum levels. The reference beam, shaped by anamorphic optics, is incident on the AOBD. The beam deflector deflects the reference beam in synchronism with the acoustic pulse propagating in the ATWL. The ATWL scans the focused

reference beam at a constant velocity across the recorded hologram row; at each holo-
gram location, the recorded signal wave is reconstructed.

To provide a stationary image of the data pattern, an optical system that
reverses the function of the record system is used. Two ATWL devices working synchro-
nously with a scanning AOBD are required. The AOBD scans the concentrated-power
readout beam at a rate which tracks the traveling lens of the first ATWL. At each
hologram location, the recorded signal beams are reconstructed. The second readout
ATWL captures these beams and expands them. The remaining components of the optical
system are analogous to those of the record system. The reconstructed signal beams from
the hologram are collimated in one direction by a cylindrical lens. Subsequent optics
and a beam deflector form a stationary image of the original page composer bit pattern
on a fiber-optic/photodetector array. Processing electronics multiplex the multichannel
data into a replica of the original serial bit stream.

3.6.3   Component Requirements for the LS Approach

Of all the system approaches considered, the LS approach requires the
most precise timing controls for operation. The synchronous operation of the AOPC,
AOBD, and ATWL with the mode-locked, cavity-dumped laser requires device drivers
of a highly sophisticated nature. The realization of the necessary control electronics
demands a high level of concentrated development effort. The electronics required are
beyond the scope of the present work and are not considered further. The remaining
components may be separated into acousto-optic devices, optical components, film
transport, and detection subsystem. The requirements for these components are
investigated in this section.

3.6.3.1   Acousto-Optic Devices

Four different types of acousto-optic devices are required in the LS system.
An AOPC is necessary to spatially modulate the laser illumination. The acousto-optic
beam deflector provides the angular deflection of the signal and reference illuminations.

The acoustic traveling wave lens provides a significant decrease in the recorded hologram dimension. A mode-locked, cavity-dumped laser also requires acousto-optic devices.

The AOPC operates in a similar fashion to the page composer of the other systems. The design relations previously summarized may be used to determine the operating parameters of a tellurium dioxide (TeO_2) AOPC having 64 separate channels. The relevant parameters are presented in Table 3-6. The configured TeO_2 page composer has a per-channel efficiency of 0.95 for an input drive power level of 300 mW. The overall device efficiency, accounting for inactive or dead areas of the AOPC, is 0.47. The rise time requirement for the AOPC requires that the incident optical cone angle is 3.33 mrad, corresponding to an optical spot width of 43 µm. The overall operating data rate for the AOPC is consistent with the required recording rate.

Table 3-6. Operating Parameters for 64 Channel Tellurium Dioxide
Page Composer

Parameter	Value
Acoustic Wavelength, Λ	20 µm
Operating Frequency, f	210 MHz
Transducer Length, L	6 mm
Transducer Height, $\bar{d}_{pc}$	250 µm
Transducer Spacing, Δ	250 µm
Maximum Drive Power, P	300 mW
Per Channel Efficiency, η_c	0.95
Rise Time, τ	13.5 ns
Optical Cone Angle, θ_{pc}	3.33 mrad

Three different acousto-optic beam deflectors are needed. For recording, one AOBD scans the reference and signal beams through an angle corresponding to the length of the traveling wave lens. For readout, the reference beam only is scanned. However, an additional AOBD is used to cancel the angular motion of the reconstructed

signal beams. The AOBD that sweeps the reference and/or signal beams must allow tracking of the traveling acoustic pulse in the ATWL. The number of resolvable spots produced by the AOBD must be large to take full advantage of the spot width demagnification by the traveling wave lens. The AOBD must similarly provide high-efficiency operation. The time-bandwidth product required for the AOBD is 1800, corresponding to the number of single-Rayleigh resolution elements that the AOBD can produce. The bandwidth (to ±3 dB points) required for the device is 151.3 MHz. To achieve operation in the Bragg regime, the device center operating frequency ν_o must be at least 1.5 times the bandwidth, or $\nu_o \geq 227$ MHz. A practical choice for ν_o would be 250 MHz. The corresponding length of the optical aperture for the AOBD is 50 mm. The acoustic attenuation in the material creates additional problems; the attenuation for a 50 mm length of TeO_2, the prime candidate material, ranges from 2.3 dB at the low end of the band (174 MHz) to 8.0 dB at the high end (325.7 MHz). The envelope of the chirp waveform, which drives the AOBD, must be tapered to account for this changing attenuation. The height of the AOBD must be sufficient to pass both the signal and reference beams. Overall, the development of an AOBD with acceptable performance levels represents a considerable advancement in state of the art technology. Significant funding would be necessary to support the highly concentrated research and development activity required.

The ATWL devices provide a reduction in spot width for recording. The reduction in spot width increases the effective intensity of the exposure pulse and provides a higher information packing density. During the recording process, one ATWL is used; the high resolution AOBD discussed above must scan the recording beams in unison with the acoustic pulse traveling at the acoustic velocity of the ATWL material. For readout, two ATWL devices are required. One device provides the necessary beam shaping of the playback reference beam, while the other, working in synchronism with the first, provides reshaping for the reconstructed signal beams. The acoustic pulse, generated by rapidly discharging the piezoelectric transducer, causes an acoustic compressional pulse to propagate. The acoustic traveling wave lens makes use of the portion of a traveling acoustic stress wave that has an increase in the index of refraction. This

area of the pulse has an index profile that is approximately parabolic and possesses a focusing power. The focal length of the ATWL is proportional to the square root of the index of refraction modulation, and thus proportional to the square root of the input power.

The relevant parameters for the ATWL are summarized in Table 3-7. The ATWL configuration has been chosen to allow recording in a 300 mm film format. The ATWL spatially compresses the 1800 resolved spots from the AOBD into 22,390 possible recording locations on the film. A significant consideration is the acoustic velocity of the material. This velocity must be matched to within 0.04 percent by the scanned AOBD beam to derive the spatial compression advantages of the ATWL.

Table 3-7. Operational Parameters for SF-59 Acoustic Traveling Wave Lens for LS Approach

Parameter	Value
Material Length, L_s	300 mm
Acoustic Velocity, V_s	3.2 mm/µs
Static Refractive Index, n_s	1.96
Induced Refractive Index, Δn_s	$1.23 \times 10^{-4} n_s$
Transducer Height, D_s	24.1 mm
Transducer Width, W_s	24.1 mm
Incident Spot Reduction Ratio, G	12.4
Material Height, H	40 mm
Resolved Spots per 300 mm scan, N_s	22,390

The acoustic velocity of the material determines the AOBD scan rate, and thus the recording or readout data rate. Readout rates which differ from record rates require that the two ATWL devices used for readout have a different acoustic velocity than the device for the recording process. Since the acoustic velocities available are discrete, a continuous range of recording (and readout) rates is not available.

An additional problem with the ATWL approach is the interference caused by back-reflected acoustic pulses. These pulses reflected from the end of the acoustic material interfere with the next pulse launched into the cell. The amplitudes of these two pulses add constructively in some locations and destructively in other locations. The effective focal length of the acoustic lens is then changes. The effect of this interference must be eliminated during the ATWL design stage.

3.6.3.2 Optical Components

The optical layout from the page composer to the ATWL for the LS approach is shown in Figure 3-13. The type of optics required for illumination of the AOPC are similar to the illumination optics of the other system approaches and are not considered here. Their primary effect is to produce an output beam divergence θ_{pc} from the page composer of 3.33 mrad; this divergence is necessary to achieve the required device rise time.

The signal beams from the page composer and the reference beam are combined by spherical lens L1 to form an interference pattern in its back focal plane. The remainder of the optical system provides three separate functions: 1) to provide suitable illumination for the scanning AOBD; 2) to reimage the interference pattern in the back focal plane of lens L1 at the recording plane; and, 3) to match the scanning rate of the AOBD to the traveling lens in the ATWL.

The optical system between the AOPC and AOBD must provide a uniform illumination of the AOBD aperture. For an AOBD height H_{bd} and a width L_{bd}, the required focal lengths are given by

$$L_{bd} = \frac{f_{L1}\, f_{C2}}{f_{C1}}\ \theta_{pc} \quad ,$$

and

$$H_{bd} = 2N\bar{d}_{pc}\, \frac{f_{L2}}{f_{L1}} \quad ,$$
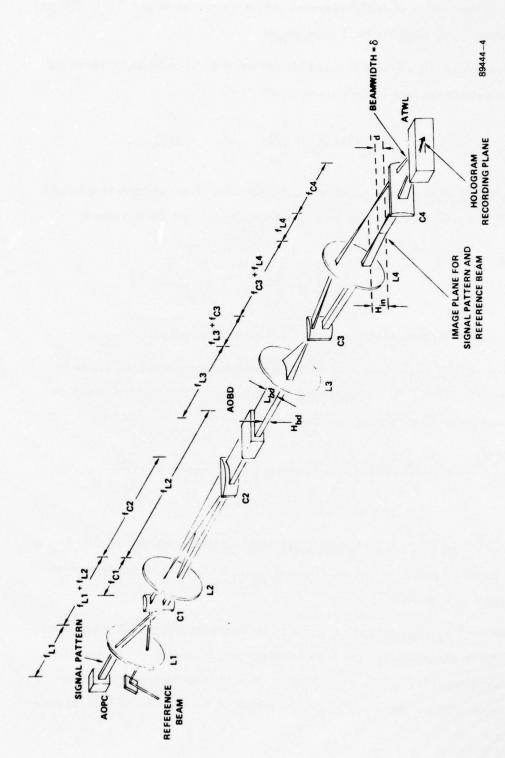
Figure 3-13. Optical Layout – LS System

89444-4

3-75

where N (= 64) is the number of AOPC channels with a transducer height $\bar{d}_{pc}$ (= 250 μm) and θ (= 3.33 mrad) is the output optical cone angle.

The height H_{in} of the diffracted bit pattern and signal beam in the image plane before the cylindrical lens is similarly given by

$$H_{in} = (2N\bar{d}_{pc}) \frac{f_{L4}}{f_{L3}} \frac{f_{L2}}{f_{L1}} = 2N\bar{d}_c \quad ,$$

where $\bar{d}_c$ is the height in the image plane of the transducers. The corresponding height h_{in} of the signal and reference beam pattern at the cylindrical lens C4 is given by

$$h_{in} = H_{in} \left[1 - \frac{2f_{C3}}{f_{L4}} \right] + \frac{2f_{C4}\lambda}{d_c} \quad .$$

The required F-number for the cylindrical lens C4 is given simply by f_{C4}/h_{in}.

The optical system must also match the angular scan of the AOBD to the traveling wave in the ATWL. This requirement establishes an additional constraint on the optical components. The velocity-matching constraint can be expressed as

$$\frac{V_s V_{bd}}{\lambda} = \left(\frac{f_{L4} f_{L3}}{f_{C3}} \right) \left(\frac{B_{bd}}{\frac{L_s}{V_s} + \frac{L_{bd}}{V_{bd}}} \right) = \frac{f_{L4} f_{L3}}{f_{C3}} \frac{B_{bd}}{t_{fm}} \quad .$$

In this equation, V_s and V_{bd} are the acoustic velocities of the ATWL and AOBD, B_{bd} is the bandwidth (to –3 dB points) of the AOBD, and t_{fm} is the total time duration of the chirped FM signal into the AOBD.

Several parameters must be specified to determine the optical components. The relative magnification between the page composer and its image must be specified. The materials and geometries for the acousto-optic devices (and their corresponding acoustic velocities) must be specified. The focal length of the cylindrical lens C3 must

be chosen. In addition, the ratio f_{C2}/f_{C1} of the focal lengths of the other cylindrical lenses must be specified. When these items are specified, the remaining parameters can be determined.

To simplify the optical design, we choose the relative magnification between the page composer and its image to be unity, i.e., $\bar{d}_{pc} = \bar{d}_c$. The AOBD is fabricated from tellurium dioxide with an acoustic velocity V_{bd} of 4.2 mm/μs; the device bandwidth is 151.3 MHz. The ATWL, fabricated from SF-59 glass, has an acoustic velocity of 3.2 mm/μs. The focal length f_{C3} is chosen as 32 mm. The ratio f_{C2}/f_{C1} is set equal to five. For these conditions, the remaining optical parameters may be calculated.

The time t_{fm} required to complete the frequency scan through the AOBD bandwidth is 105.7 μs. The sweep duration time is related to the geometry and characteristics of the ATWL. The requirements for the optical system are summarized in Table 3-8. Only two lenses have critical imaging tasks. They are the spherical lens L2, performing the AOBD illumination task, and the cylindrical lens L4, performing the transforming task. In particular, the long (300 mm) cylindrical lens, which must provide high quality transforms in a flat focal plane, will require considerable design and fabrication effort.

Table 3-8. Optical Component Requirements for the LS System Concept

Lens	Focal Length (mm)	F-Number
L1	3000	93.8
C1	40	4
L2	234.4	2.5
C2	200	4
L3	244.6	4.5
C3	32	10.4
L4	3131.5	10.4
C4	126.5	5.2

The components required for the readout system are equivalent to those of the record system. Critical imaging requirements exist for the counterparts to L2 and C4 in the readout path. The overall system optical path length is extremely long, approaching twenty meters. A high degree of opto-mechanical stability is required to achieve proper synchronism of the acousto-optic devices.

The laser requirements for the LS system can also be estimated. The use of the acousto-optic devices introduces a relative frequency shift between the two beams interfering at the hologram. Since the shift cannot be compensated, short exposures (~2 ns) must be used. This requires the use of a mode-locked, cavity-dumped laser. The energy E_ℓ for each recording pulse can be determined, assuming a film exposure requirement S_f of 10 $\mu J/cm^2$ and a system optical efficiency η_o of 0.01. The average power P_ℓ of the laser is related to E_ℓ by the per-channel recording rate R_c of 50 Mb/s for the LS system. The hologram area is 1.1×10^{-2} mm^2 (521 μm × 22 μm). The recording format allows a guardband between hologram rows of 20 percent and a guardband of two hologram widths between holograms. The high guardband area indicates that the 300 mm wide recording film is being used inefficiently at these recording rates. For these conditions, the average laser power requirement is

$$P = \frac{S_f A_h R_c}{\eta_o} = 5.5 \text{ W}.$$

This level of average power for a MLCD laser at a pulse rate of 50×10^6 Hz is not presently achieved by state-of-the-art technology. Since the film resolving power is modest (≈500 cy/mm), the use of higher sensitivity films is possible. The increased film sensitivity will allow a corresponding reduction in laser power requirements.

3.6.3.3   Film Transport

The critical timing and optical requirements of the LS approach allow a large guardband between holograms. In fact, the guardband region is equivalent to two hologram locations. These guardband regions are utilized by a staggered recording

format. To accomplish this the system clock must operate three times faster than the per-channel recording rate, and holograms are recorded every third clock pulse. However, the hologram rows are formatted into groups of three. In the first row of the group, a hologram is recorded on every third clock pulse. For the second row, the clock pulses are selected so that the holograms of that row are recorded in one of the vacant locations of the first row. Thus, a relative shift of one clock pulse occurs between the first and second row. For the third row of the group, the holograms are recorded in the remaining vacant locations of the first row. Recording on continuous motion film displaces the hologram rows relative to each other, resulting in a staggered recording format. This format imposes no additional constraints on the recording system components and provides a significant increase in the average packing density achieved.

The film transport in the LS system must move the recording film at a velocity V consistent with the average information recording rate R of 2.5 Gb/s. (The instantaneous recording rate is 3.2 Gb/s). The active film width W is 300 mm (12 in.). The packing density within the hologram is 0.58 Mb/cm^2; the average packing density for each hologram row is 0.16 Mb/cm^2. However, the staggered recording format provides an average information packing density $\bar{\sigma}$ that is three times higher, or 0.48 Mb/cm^2. This density allows a 20% guardband region between each three-row group. For these conditions, the film velocity V required is

$$V = \frac{R}{W\bar{\sigma}} = 1.4 \text{ m/s}$$

The development of a film transport capable of achieving these rates for 300 mm film is a challenge. The difficulty is further increased by the depth of focus constraint. The film surface across the 300 mm width must be constrained to a ±15 μm depth of focus.

The readout subsystem includes the scanning acousto-optic devices, readout laser, and film transport, as well as the fiber-optic/photodectector array. To correctly read the information recorded on the film, the simultaneous synchronization of two AOBD devices, two ATWL devices, the pulsed laser, film transport, and

photodetector array must be achieved. Departure from linearity of these elements by more than one part in 10^4 would prevent synchronization. The fabrication of electronics to accomplish the desired performance will require significant design consideration.

The rate requirements of the fiber-optic/photodector array are also severe. At a readout data rate of 3.2 Gb/s, the required per-channel rate for the array is 50 Mb/s. The high per-channel data rate demands increased readout power to achieve an acceptable signal-to-noise ratio. No discrete hybrid photodectector units are available which operate at these high data rates. Presently, only photomultiplier tubes can operate in this regime. The photodetector array will require significant development.

3.7   SYSTEM TRADE-OFFS AND RECOMMENDATIONS

Each system approach presented in this chapter has the potential for recording and reproducing user data at rates of 2 Gb/s. The design considerations for each system are highly dependent on the recording concept used. However, there are several baseline parameters that are common in each system design. These are summarized in Table 3-9. The table lists the hologram recording format, the per channel data rates, the film speeds, and the laser requirements for each system concept.

The key trade-off factors for each system are listed in Table 3-10. These factors include both the merits and disadvantages involved in any particular system implementation. The areas requiring special consideration are also summarized in the table. The present development state of the components necessary for each system approach is also addressed. These major components and their present development state are assessed in Table 3-11. Four different developmental states are used in the table. "Engineering" means that straightforward techniques can be used to produce a component. "Engineering Development" means that new and creative designs based on proven techniques must be generated. "Technology Development" means new designs using state-of-the-art techniques must be generated. "Technology Risk" means that new techniques must be researched and developed before the component can be built.

A trade-off study, based on the successful development of the major components of each system, can be performed to rank the systems in terms of operability and reproducibility. The ranking gauges the overall performance levels and maintainability that each system can attain once configured. The ranking, in order of the most to least promising approach is:

- SP

- SIAM

- AO/SP

- 2D

- LS

Table 3-9. Baseline Design Parameters for 2 Gb/s User Data Record Rate

	SP	SIAM	AO/SP	2D	LS
Holograms/Scan	2951	2x1850	2951	15	4688
Scan Time (μs)	151	185	151	75	94
Scan Length (mm)	50	2x25.7	50	53.3	300
Bits/Scan	0.38×10^6	0.46×10^6	0.38×10^6	0.19×10^6	0.30×10^6
Average Packing Density (bits/cm^2)	0.82×10^6	0.82×10^6	0.82×10^6	1.5×10^6	0.2×10^6
Bits/Hologram	128	128	128	12.5×10^3	64
Input Per Channel Rate (Mb/s)	19.5	9.8	19.5	25.5	50
Detector Per Channel Rate (Mb/s)	19.5	9.8	19.5	0.20	50
Film Speed (m/s)	6.1	5.9	6.1	3.2	1.7
Film Format (mm)	70	70	70	70	300
Energy Per Laser Pulse (μJ)	0.010	0.020	0.010	0.30	0.11
Repetition Rate (MHz)	19.5	9.8	19.5	0.02	50
Argon Ion Laser Type	CW	CW	MLCD	MLCD	MLCD

Table 3-10. Summary of Key Trade-Off Factors for User Data Rate Recording of 2 Gb/s

SP

- Most technologies well developed.

- Opto-mechanical stability readily maintained.

- Transform lenses (50 mm field) require special attention.

- Per-channel photodetector rates (19.5 Mb/s) require engineering development.

SIAM

- All technologies well developed.

- Opto-mechanical stability requires special design procedures

AO/SP

- Transform lenses do not transmit reference beam (smaller apertures).

- Reverse readout provides aberration compensation.

- Zero guardband wastage.

- Readout at 2.5 Gb/s requires very powerful laser (6-12 watts) and fast photo-detectors (20 Mb/s each).

- Incoherent additions must be balanced within film dynamic range.

- Stronger contender at further reduced readout rates.

2D

- Nonmechanical scanning, but AOBD requires high time-bandwidth with constrained time.

- Highest data packing density, but SNR and BER impact merits special consideration.

- 98 channel 2D photodetector array and page composer at 0.2 Mb/s per channel require technology development.

Table 3-10. Summary of Key Trade-Off Factors for User Data Rate
Recording of 2 Gb/s (Continued)

- Mode-locked, cavity-dumped laser with 3 watts average output requires technology development.

- Transform lenses (50 mm field) require special attention.

- Lenslet array requires engineering development.

LS

- Nonmechanical scanning, but extremely critical timing is required.

- Development of ATWL and control electronics merits special consideration.

- Per channel photodetector rates of 50 Mb/s require technology development.

- Mode-locked, cavity dumped laser requires technology development.

- Film transport requirements for 300 mm film widths are severe.

- Capability for extremely high data recording rates.

Table 3-11. Design Trade-Offs for Component Development
System Approach

Component	SP	SIAM	AO/SP	2D	LS
Page Composer	E	E	E	TD	ED
Spinner	E	ED	E	–	–
ATWL	–	–	–	–	TD
AOBD	–	–	ED	E	TD
Transform Lenses	TR	E	E	TD	ED
Film Transport	ED	ED	ED	ED	TD
Record Laser	ED	ED	ED	TD	TD
Photodetectors	TD	ED	TD	TR	TR
Lenslet Array	–	–	–	ED	–

Code: E = Engineering Effort

        ED = Engineering Development

        TD = Technology Development

        TR = Technology Risk

The ranking is preliminary in the sense that minor variations of performance could interchange the order of any two systems adjacent in the list. However, the list does provide an overall comparison of the difficulties posed by the system concepts.

The SP approach represents a potential solution to achieve a user data recording rate of 2 Gb/s in the near term. Both the SIAM and AO/SP approaches are qualified alternate approaches that take advantage of all successes achieved with the SP approach. The remaining approaches, the 2D and LS systems, have an ultimate potential for very high recording rates (perhaps 5 Gb/s). However, the components required represent large technical risks and will require significant developmental effort.

SECTION IV

ADVANCED COMPONENT INVESTIGATIONS

The WBR program significantly advanced several technologies necessary to wideband digital data recording. Some of these developments were applied to the EDM approach and, we believe, may be extended to realize the 2 Gb/s SP system described in Section III. Others were aimed at realization of one or more of the alternative system concepts, presented in the previous chapter, that also promise the capability of storing and retrieving digital data at multigigabit per second rates.

Several components are common to all system concepts. A laser system capable of providing mode-locked, cavity-dumped operation is essential for several of the approaches. Similarly, acousto-optic devices operating as beam deflectors and page composers are required for the deflection and modulation of the optical data stream. The optical components, notably the transform lens system, are critical for the information recording process. A film transport system capable of velocities consistent with the aggregate data rates is required during the record and retrieval process. The readout devices, either discrete or CCD types, are required for the recovery of the recorded digital data.

These components comprise the major elements in the system designs, and their current developmental status is a major factor in determining the practical performance levels of a system concept. Following, we present various trade-off considerations and practical device limitations that affect the performance levels of the components. We conclude each discussion by comparing current performance levels with the performance levels required to realize recording and readout rates of 2 Gb/s using one or more of the conceptual systems presented in Section III.

4.1   MODE-LOCKED, CAVITY-DUMPED LASERS

The mode-locked, cavity-dumped (MLCD) laser is a controlled source of short time duration pulses having a high spectral purity. Several of the system designs presented in the previous chapter require such a light source during the optical

recording process. Any continuous wave (CW) laser can be converted into a pulsed light source through the use of fast acousto-optic modulators internal to the laser cavity. Energy in the form of circulating photons is stored within the optical cavity of the laser and periodically "cavity-dumped" by the acousto-optic modulator. Even shorter optical pulses can be obtained by combining the cavity-dumping operation with laser mode-locking. The remainder of the section describes the conditions necessary to obtain mode-locked, cavity-dumped operation.

A CW laser, when examined over a broad frequency range (e.g., 0-1 GHz), exhibits significant amplitude fluctuations. A major cause for the high-frequency amplitude fluctuations observed in a CW laser is intermode noise which consists of beat frequencies between the various longitudinal modes of the laser. A CW laser exhibiting intermode noise is generally referred to as free-running because its longitudinal modes are undergoing independent fluctuations in both amplitude and phase. These fluctuations result in random amplitude fluctuations in the laser output power which typically amount to 40 percent of the average power.

A condition opposite to the free-running condition can be created by forcing the longitudinal modes to maintain a constant amplitude and fixed phase relationship with respect to one another. Under this condition, the laser is said to be mode locked and the light output consists of a well-controlled, periodic train of pulses. The noisy fluctuations in a free-running laser are thus organized into a train of pulses that exhibit good amplitude stability. For high-frequency applications the mode-locked laser holds two advantages over a free-running laser. First, optical pulse durations of much less than a nanosecond can be obtained; and second, the intermode noise that is very difficult to overcome in a free-running laser is organized into a useful output.

These advantages of a mode-locked laser are independent of the modulating operation that is used to impose a signal on the optical output. However, the modulation technique of laser cavity dumping holds several unique advantages which, in combination with the advantages of mode-locking, yield a laser system that is an excellent, controlled source of short light pulses. The advantages of a cavity dumping

4-2

arrangement stem from the fact that the laser cavity is used to store the energy that is not being used in the output beam building up a large, circulating optical power within the cavity that can be diverted into the output beam to form a high-peak-power optical pulse.

A major component to be considered is the mode-locking modulator. The effect of this modulator is to cause the longitudinal cavity modes to maintain a fixed phase relationship with respect to one another. In this condition, the amplitudes of the cavity modes add constructively at a particular point that is propagating within the laser; this has the effect of converting the continuous beam circulating within the laser into a small, intense bundle of light that reflects back and forth between the mirrors.

Mode locking may be produced by modulating the cavity loss at a frequency equal to the frequency difference between adjacent longitudinal modes. These modes are separated by a frequency, $\Delta \nu$, given by

$$\Delta \nu = \frac{C}{2L} ,$$

where C is the speed of light and L is the laser length.

An acousto-optic modulator can be used to produce the required loss modulation. The modulator is constructed so that an acoustic standing wave is generated transverse to the optical beam. The standing wave will grow and collapse at a rate equal to twice the drive frequency. Thus, the cell is driven by a piezoelectric transducer at a frequency of C/4L. In effect, the modulator acts as a shutter that opens and closes once during a round trip transit time of the laser. The light within the laser tends to adjust itself so that an intense bundle of light arrives at the shutter just as the shutter fully opens. The circulating light will arrange itself to accommodate higher frequency loss modulations equal to integer multiples of the fundamental frequency, C/2L. In this case, more than one pulse exists within the laser and the resulting pulse train that could be coupled out of the laser would have a repetition rate of nC/2L where n is a small integer.

An aspect of the argon-ion laser that must be taken into account during mode-locking experiments is the short lifetime of the upper state of the lasing transition. Because this lifetime ($\sim$7.5 x 10^{-9} s) is shorter than the round trip transit time of a light pulse within a typical optical resonator ($\sim$10 x 10^{-9} s), the ratio of the light lost due to spontaneous emission to the light contributed to the stored cavity energy by stimulated emission increases when the laser is mode locked. This occurs because the light pulse is in the vicinity of a particular argon ion for only a fraction of a nanosecond. The rest of the time, which will be on the average about 5 nanoseconds, the ion is free to undergo spontaneous emission. Because of this extra loss due to spontaneous emission and some smaller losses associated with the modulator, the average power obtained from a mode-locked, argon-ion laser may be as low as 30 percent of the free-running power.

Laser cavity dumping is a technique that makes use of a fast light deflector to periodically remove some of the light from an optical resonator that serves as a temporary storage device. Ideally, the cavity dumper should be able to divert a large fraction of the circulating light within a time less than the round trip travel time of light within the cavity. In addition, the dumper must exhibit very low optical losses when in an "off" state; this requirement eliminates a large class of devices that rely on an electro-optic effect to divert the circulating light. Most electro-optic crystals introduce more than 1 percent additional loss in a resonator whose total loss is 1 percent or less. Thus, these devices would reduce the circulting power by more than 50 percent and are, therefore, usually unacceptable.

Acouto-optic devices, on the other hand, can be fabricated on high-quality substrates such as fused quartz, which introduce less than 0.2 percent loss in the cavity. The acousto-optic cavity dumper shown in the MLCD system in Figure 4-1 uses Bragg diffraction to deflect light from the cavity. The deflection angle of the light diffracted is determined by the frequency of the acoustic wave, whereas the amount of light diffracted depends on the amplitude of the acoustic wave. Finally, the rise time is determined by the transit time of the acoustic wave across the diameter of the light beam.

M₁ - REFLECTIVITY ≃ 100%, RADIUS 10 cm

M₂ - REFLECTIVITY ≃ 100%, RADIUS 20 cm

M₃ - REFLECTIVITY ≃ 100%, FLAT

P - COMBINATION WAVELENGTH SELECTOR AND MODE-LOCKING MODULATOR

———— CIRCULATING LIGHT PATH

- - - - - DEFLECTED LIGHT PATH

89444-74
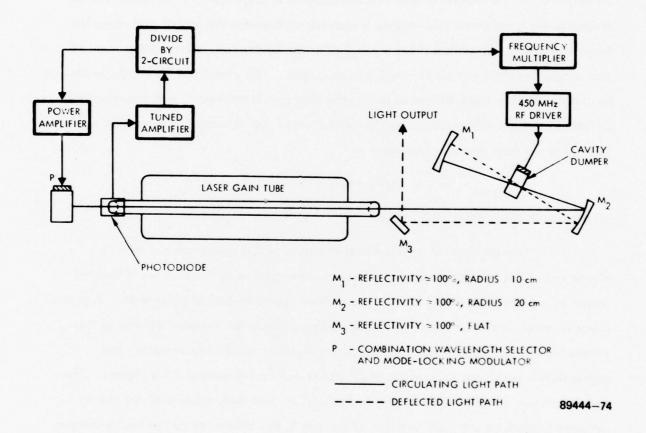
Figure 4-1.   Mode-Locked, Cavity-Dumped, Laser System

During each round trip the circulating light passes through the dumper twice and is partially diffracted each time. The light that is diffracted during the first pass returns to the dumper after being reflected by mirror M_1 and is partially rediffracted into the circulating beam. Because of this rediffraction during the second pass, no more than 50 percent of the circulating light within a free-running laser can be diverted into an output when the dumper is used in a double-pass arrangement. If the laser is mode-locked and a fixed phase relationship is maintained between the laser's mode-spacing frequency and the electrical drive signal to the cavity dumper, nearly 100 percent of the circulating light can be diverted into an output. This effect can be briefly explained by stating that the light diffracted during the first pass is coherently and constructively added to the light diffracted during the second pass. For this case, the fraction of the light diverted from the laser is given by

$$\eta_{total} = \frac{I}{I_o} = 4 \eta (1 - \eta)$$

where η is the single pass diffraction.

An example of a system that produces MLCD operation is shown in Figure 4-1. The laser achieves the coherent, constructive addition in the diffracted output by deriving the cavity dumper signal from the mode-locked pulse train. A photo-diode is arranged to receive a light signal reflected from the Brewster window of the plasma tube. The fundamental frequency of the pulse train is thus extracted and appropriately processed to form the mode locker and cavity dumper drive signals. These two signals are coherent with respect to each other, and their relative phase can be adjusted to produce coherent addition of the two beams diffracted by the cavity dumper. This addition allows the extraction of high power output pulses.

A mode-locked, cavity-dumped laser is an excellent source of regulated, fast, intense light pulses. The typical performance levels for a Spectra-Physics Model 166/366 Combo, a commercially available MLCD laser system, are listed in Table 4-1. Also included in the table is the laser performance required for the LS system approach.

Table 4-1. MLCD Argon Ion Laser Parameters for an
Operating Wavelength $\lambda = 514.5$ nm

Performance Parameter	Spectra-Physics Model 166/366	LS Systems Requirements
Peak Power Output (50% Coupling Efficiency)	200 W	50 W
Pulse Width	1.5 ns	2 ns
Repetition Rate	1 MHz	50 MHz
Long Term Amplitude Stability	5%	5%

The LS system, discussed fully in Chapter 3, presents the most demanding laser require-
ments of the conceptual designs considered. The Model 166/366, operating with an
argon-ion plasma tube nominally capable of only 1 watt of CW power, satisfies all the
power requirements for the LS system at a reduced repetition rate.

The primary difficulty involved in achieving the high output power pulses
at a 50 MHz repetition rate is the laser recovery time T_R. This time represents the
minimum time required between pulses to achieve the maximum peak pulse level. The
recovery time T_R is given by

$$T_R = \frac{L}{fC} \ln \frac{\eta}{0.1} \qquad (4.1)$$

where L is the cavity length, f represents the internal loss level of the laser, C is the
speed of light, and η is the output coupling efficiency. The cavity length L is fixed
for a given laser and is typically 1.5 m. The internal losses f of an MLCD laser generally
amount to 0.01. For these typical parameters and a 50 percent coupling efficiency, the
laser recovery time T_R is nominally 0.8 μs; this is the time required for the laser output
power to rise from 10 to 90 percent of maximum power. Thus, the laser cannot be
pulsed faster than once every 0.8 μs without a significant loss in the peak output power.

One approach to reduce the recovery time is to decrease the output coupling efficiency. In fact, for the above parameters, the coupling efficiency η must be less than 10 percent to achieve full power at a 50 MHz repetition rate corresponding to a 20 ns recovery time. However, the decreased efficiency reduces the peak output power available below the required levels. To offset this power reduction, a laser tube with a higher CW power rating could be used. Such tubes are presently available.

The design and fabrication of the high power MLCD laser would require further technology development. The effect of plasma density fluctuations occuring at the higher current densities should be considered. The thermal and mechanical problems involved in mounting the MLCD unit within the optical resonator must be solved. A low-loss material for the acousto-optic device capable of operating at the high optical and drive power levels anticipated must also be produced. However, we are optimistic that a successful development could be accomplished.

4.2 ACOUSTO-OPTIC BEAM DEFLECTORS

Several of the system concepts presented earlier use an acousto-optic beam deflector (AOBD) to accomplish a scanning operation. This scanning (or angular positioning) may be required for addressing the recording locations as in the AO/SP approach, or for tracking a travelling acoustic lens as in the LS approach. The design considerations for the AOBD must be based on the major elements comprising the device: the acousto-optic material and the piezo-electric transducer. However, other considerations must also be included to establish the device performance. In particular, the properties of the transducer bonding and heat sinking techniques must be examined.

Several characteristics of the acousto-optic material must be considered in the selection of a device material. To obtain high diffraction efficiency at low drive power levels requires the choice of a material having a high figure of merit. However, materials with a high figure of merit typically suffer high acoustic attenuation. The selection of a material with a low acoustic velocity favors obtaining an AOBD capable of a large number of resolvable spots. The low acoustic velocity, however, adversely affects the rise and access times of the device. The thermal properties of the material must also be included in the design analysis to ensure that thermal degradations are within acceptable bounds.

Considerations of the transducer and its bonding must be included. The transducer design greatly affects the efficiency with which the acoustic energy excited in the transducer is coupled into the cell. Acoustical and electrical impedance matching must be accomplished to prevent reflected waves from degrading performance. The transducer bonding process must also be selected. Three types of transducer bonding procedures are commonly used: epoxy, indium, and ultrasonic. Epoxy bonding is suitable for low frequency applications and is easily performed; however, device characteristics achieved with epoxy bonding are not easily reproduced. Indium bonding, although suitable for medium frequency applications, requires pressures of several hundred kilograms per square centimeter during bonding. Ultrasonic bonding provides the best high frequency characteristics, but requires highly specialized equipment.

The AOBD is typically operated at high drive power levels. The high power densities create undesirable temperature profiles within the device. The increased temperatures are caused by the conversion losses of the transducer and the acoustic attenuation in the cell. Fluctuations in the temperature gradient are a major cause of device instability. Proper heat sinking is critical in minimizing the thermal degradation.

The performance of an AOBD as a deflector is determined by the device bandwidth and diffraction efficiency. Generally, a good AOBD possesses a large bandwidth and high diffraction efficiency. The major objective of an AOBD design is to achieve the largest bandwidth with the smallest drive power requirements; however, the device power consumption is proportional to the square of the bandwidth. In addition, a broadband AOBD requires small dimensions for the transducer geometry. These parameters and their interaction must be considered to achieve an optimum AOBD design.

As the AOBD drive frequency is varied over a frequency range, the beam diffracted by the device is swept through a corresponding angular range. Since the Bragg condition cannot be satisfied over the entire angular range, the diffracted light intensity does not remain constant. The amount of intensity falloff is determined by the interaction length and the operating frequency of the device. As these parameters are increased, the intensity falloff over the angular range becomes significant. To minimize the amount of intensity falloff, an acoustic beam steering technique utilizing a phased acoustic transducer array is employed. The acoustic beam steering effectively changes the Bragg angle of the device, thereby reducing the amount of intensity falloff. The beam steering provides two added advantages: the interaction length can be increased without a corresponding increase in bandwidth; and the cross-section of the acoustic beam is increased. Both of these features reduce the power density of the device.

We presently have the capability to fabricate acousto-optic beam deflectors employing the phased acoustic transducer array. The performance levels that we have achieved with this type of device are listed in Table 4-2. Also listed in the table are the corresponding parameters required for the tracking AOBD in the LS system approach. The Phased Array AOBD, using a lead molybdate crystal, gives state-of-the-art performance. Significant refinements of crystal handling and preparation techniques are required to achieve comparable performance levels with the tellurium dioxide crystal.

Table 4-2. A Comparison of the Operational Parameters for the Phased Array and LS Tracking Acousto-Optic Beam Deflectors

Parameter	Phased Array AOBD	LS Tracking AOBD
Acoustic Material	$PbMoO_4$	TeO_2
Cell Length (mm)	30	50
Resolved Spots	2000	1800
Center Frequency (MHz)	265	250
Half Power Bandwidth (MHz)	250	150
Access Time (μs)	8.5	10

4.3   ACOUSTO-OPTIC PAGE COMPOSERS

In a multichannel optical system, several operations must be performed to allow successful recording. First, the information carried by the high data rate electronic signals must be demultiplexed, allowing a reduction in the required per channel data rates. Second, a formatting operation to prepare the data for recording must be performed. Last, a conversion of the channelized data from the electronic to the optical domain must be accomplished. The key component in performing this conversion is the acousto-optic page composer (AOPC). The AOPC imparts a temporal and spatial modulation to the optical beam; thus, the information of the electronic signals is impressed on the optical beam.

Several factors must be considered during the design of an acousto-optic page composer. The AOPC must be capable of efficiently modulating the optical signals. Since the diffraction efficiency is directly related to the RF drive levels, higher efficiencies are obtained by increasing the drive power. However, high drive power levels can cause significant heating effects which degrade system performance. A thermal gradient in the acousto-optic material can seriously degrade the optical quality of the diffracted beams or even fracture the acousto-optic material. A trade-off to provide high efficiency with tolerable thermal degradation must be performed.

The AOPC should also provide a rise time consistent with user data rates. Short rise times require a high RF carrier frequency, a large bandwidth, and a short transit time. The increases in carrier frequency and bandwidth raise the level of electronic channel-to-channel crosstalk and correspondingly reduce the extinction ratio that the AOPC can achieve. Another trade-off must be made to ensure that these parameters are within acceptable bounds.

The characteristics of the AOPC device can also vary significantly from one acousto-optic material to another. Several factors determine the choice of an acousto-optic material. The material should have a high figure of merit; good efficiency can then be obtained at low RF drive levels. The optical quality of the material must be high; this ensures that any aberrations introduced by the crystal are minimal. The difficulty of fabrication for a given material must also be considered. Some acousto-optic materials, although capable of providing high performance levels, require delicate care during the polishing and coating stages of fabrication. Thus, these materials pose a high risk of breakage which must be considered.

The AOPC performance is also affected by the transducer design. The transducers must provide good heat transfer characteristics to minimize thermal degradations. The RF switching characteristics and rise times of the AOPC are determined by the drive electronics and tranducer circuitry; their design must provide a frequency response that satisfies the performance goals. The geometry of the transducer array

influences the resolution achieved with subsequent imaging optics. Thus, the effect of the transducer size and spacing on optical performance must also be considered during the design stage.

The illumination conditions for the AOPC must be determined to satisfy the Bragg incidence angle and angular bandwidth requirements. The convergence angle of the incident optical beam must be chosen to provide rise times (i.e., acoustic transit times) consistent with system requirements. These parameters interact to determine both the efficiency and shape of the diffracted beams obtained in the final AOPC device.

The final design should represent a combination of acousto-optic material and transducer geometry that yield the optimum operational parameters. The fabrication of the AOPC device should then proceed with both care and cleanliness to ensure that the design goals are achieved.

During an earlier phase of the WBR program, two types of acousto-optic page composers were developed and tested; these were one-dimensional and two-dimensional AOPC devices. The one-dimensional AOPC is composed of a linear array of transducers attached to an acousto-optic material. The illumination is provided by a line source, and the diffracted data is a linear array of optical channels, whose intensity corresponds to the demultiplexed data. The two-dimensional AOPC is also an array of transducers on an acousto-optic material. But in this case, each channel of the array is driven by demultiplexed data to load a two dimensional array into the device. To freeze the bit motion and to minimize the effects of an uncompensatable frequency shift between reference and signal beams, a short exposure pulse is required. A two-dimensional array of data is then diffracted by the AOPC.

Aggregate data rates of 800 Mb/s have been achieved with both the one-dimensional linear AOPC (LAOPC) and the two-dimensional matrix AOPC (MAOPC). The characteristics and specifications for these devices are summarized in Table 4-3. Also included for comparison are the nominal requirements presented by the AOPC devices in the SP and 2D system concepts. The requirements for the AOPC in the SP

system represent a significant advancement in performance levels. However, based on our past experience in acousto-optic technology, we feel that these design goals are achievable. The requirements for the AOPC in the 2D system are beyond the current state of the art. Considerable technology development would be required to achieve the required performance levels.

Table 4-3. Characteristics and Requirements for One- and Two-Dimensional Acousto-Optic Page Composers
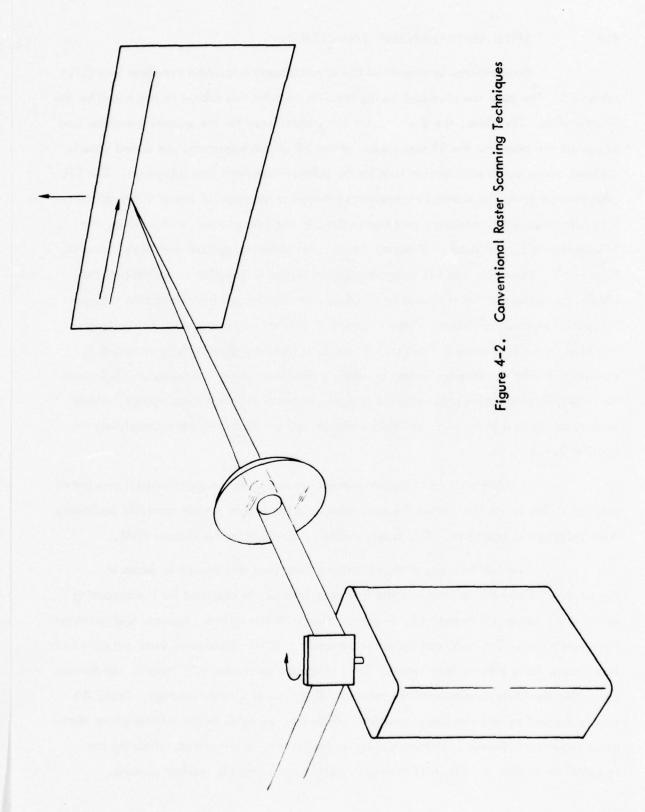
| AOPC Characteristics | Device | | | |
	LAOPC	MAOPC	SP AOPC	2D AOPC
Material	SF-8	SF-8	TeO_2	TeO_2
Number of Channels	136	15	128	98
Maximum Per Channel Data Rate (Mb/s)	6	50	19.5	50
Aggregate Data Rate (Mb/s)	800	750	2500	2500
Device Diffraction Efficiency (%)	30	24	35	50
Drive Power Levels (Watts)	0.1	0.5	0.1	2.0
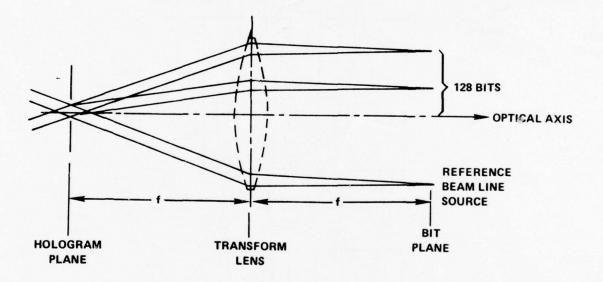
4.4   SPINNER-TRANSFORM LENS DESIGN

Fundamental to several of the approaches is a spinner-transform lens (STL) subsystem. The most complex and taxing requirements for this subsystem are posed by the SP approach. Therefore, the design constraints considered for the spinner transform lens subsystem are based on the SP approach. In the SP system approach, the coded data is scanned across continuous motion film by the spinner-transform lens subsystem. The STL subsystem performs the scanning operation by mapping the angular sweep of the spinner, a multifaceted rotating mirror, into translations in the film plane. In this sense, the STL subsystem is analogous to a conventional raster scanning optical system as shown in Figure 4-2. However, the STL subsystem differs since, in addition to generating the image translations at the film as a result of spinner rotation, it also transforms a linear bit spatial intensity distribution (see Figure 4-3) into a Fourier transform intensity distribution at the film plane. The Fourier transform intensity distribution, recorded in conjunction with a reference beam, provides a one-dimensional hologram; the hologram has highly advantageous properties for low bit-error-rate archival data storage. These properties, spatial invariance and data redundancy, are discussed more completely in Section 2.1.2.

A refinement of hologram scanned recording is the synchronized descanned readout. This technique allows the recovered data pattern to remain spatially stationary from hologram to hologram. This is referred to as autoscan in the current EDM.

The full STL subsystem comprising both scan and descan is shown in Figure 4-4. Only the spinner and the first scan lens L2 are required for the recording operation. Lenses L2 through L5, in conjunction with the spinner, provide full autoscan implementation. The autoscan system is basically two 1:1 telescopes, each composed of two lenses, for a total of four lenses. Each telescope generates a left-right, top-bottom inversion; the inversions reverse the apparent direction of spinner rotation. Thus, the two telescopes restore the image polarity, while the two folds in the spinner plane introduce one more inversion. Therefore, the spinner motion is cancelled, allowing the resultant reconstructed data bits to remain stationary during the readout process.

Figure 4-2. Conventional Raster Scanning Techniques

128 BITS

OPTICAL AXIS

REFERENCE
BEAM LINE
SOURCE

BIT
PLANE

f   f

HOLOGRAM
PLANE

TRANSFORM
LENS

89444-57

Figure 4-3.   Bit to Hologram Fourier Transform

INPUT
PLANE P_1

P_2

P_5

SLIT
FILTER

INPUT
LENS

L_1

L_4

FILM
PLANE

P_3

L_1-L_4: AUTOSCAN
LENSES

M_1, M_2: TURN-AROUND
MIRRORS

L_2
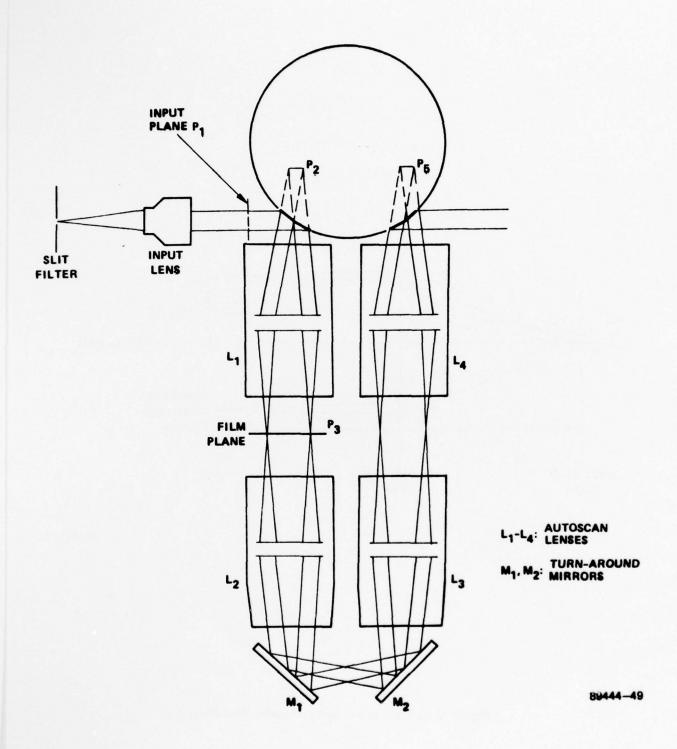
L_3

M_1

M_2

89444—49

Figure 4-4. STL Autoscan Subsystem

Any future system configured to record and read out data at 2 Gb/s will certainly contain an autoscan implementation. The initial WBR autoscan implementation closely followed that shown in Figure 4-4. The spinner was a 40 faceted polygonal spinner manufactured by Speedring Corporation. The four commercially available transform lenses were Super Baltar 4-inch focal length projection lenses. In order to improve system performance, the WBR program undertook a custom lens design with the Ferson Division of the Bausch and Lomb Corporation for a 25 mm wide scan lens to accommodate 35 mm film. A summary of those design parameters is provided in Paragraph 2.2.6.

Critical demands are made on the spinner and transform lens in a high-speed optical recorder/reproducer system. Recording data records on film relies on the high linear and flat field scanning of the STL subsystem. To provide stationarity of the reconstructed data image, the performance demands on the spinner and autoscan lenses are even more stringent. Several design areas for the spinner-transform lens subsystem must be considered. These are as follows:

1. Telecentricity. The transform lens must be a telecentric lens. This implies that the scanning beam must remain perpendicular to the film plane during scan; this condition occurs when the virtual pivot point of the spinner deflection is at the front focal plane of the scan lens. This configuration minimizes the aperture requirements and enables us to utilize four identical lens assemblies, thereby reducing the design and fabrication costs.

2. Duty Cycle. The spinner-transform lens subsystem must be designed to operate at 100 percent duty cycle. In order to achieve the near synchronous operation required for a very high data rate system, the auto-scan system must operate without time loss at a 100 percent duty cycle. This implies that the transform lens must be able to handle a full 720/N degrees of scan without vignetting, where N is the number of spinner facets. Therefore, the recording bundle from the first hologram and the last hologram in a scan line (50 mm apart) must be present in the lens at the same time.

3. <u>Field Size</u>. The required field size is 50 mm, corresponding to the active scan length of the SP system approach. The system approach utilizes 50 mm of the total film width of 70 mm for data recording.

4. <u>External Entrance Pupil</u>. The transform lens entrance pupil is the location of the effective pivot plane which is inside the spinner. The entrance pupil must, of course, be located external to the lens with as large a clearance as possible in order to accommodate the spinner.

5. <u>Field Coverage</u>. The field coverage in the scan direction, represented by L, is a function of both the lens focal length, F, and the optical scan angle, θ. For a distortion corrected lens, the field coverage L is given by $L = F \tan \theta$. However, for scanning applications, a negative (barrel) distortion equal to $\theta/\tan \theta$ is introduced by design, so that the lens performs as $L = f \cdot \theta$. This negative distortion allows the linear angular velocity of the spinner to produce linear spot velocity at the film and, hence, provides uniform controllable exposure.

6. <u>Resolution Requirements</u>. The transform lens for the SP system scans holograms rather than pixels onto the film and presents some unusual requirements in terms of resolution. Since these requirements are different for the along scan direction as opposed to the orthogonal cross scan direction, they are presented separately.

   a. <u>Along-Scan (Hologram to Hologram) Resolution</u>. In the along-scan direction, the transform lens is required to resolve the 12.8 μm wide holograms with double-Rayleigh resolution across the full 50 mm hologram row (see Figure 4-5). The 12.8 μm wide hologram image has a $(\sin x/x)^2$ or $\text{sinc}^2(x)$ intensity profile which results from the uniformly illuminated

Figure 4-5. Along Scan Optical Schematic

89444-55

finite aperture. The convergence angle $\delta\theta_w$ required to produce a double-Rayleigh resolved spot width W of 12.8 μm is given by

$$\delta\theta_w = \frac{2\,(1.22)\,\lambda}{w} = \frac{2\,(1.22)\,(0.5145\ \mu m)}{12.8\ \mu m} = 98.1\ \text{mrad},$$
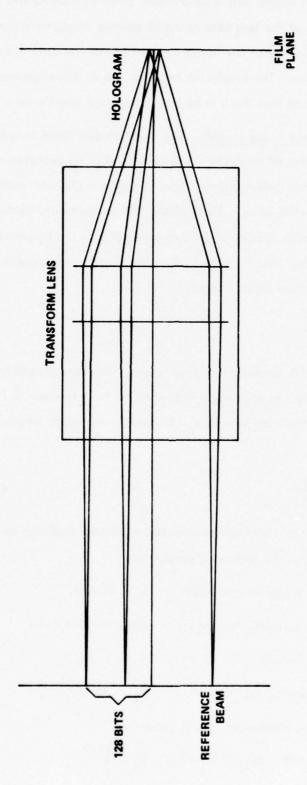
where an illumination wavelength λ of 0.5145 μm has been assumed. This convergence angle is not to be confused with the scan angle which sweeps the spot described by the convergence angle. The 12.8 μm spot must be resolved across the entire 50 mm flat field scan to the double-Rayleigh diffraction limit. An immediate implication of this is that the transform lens must scan a flat field. The resolution requirements are further compounded since the resolution must be maintained throughout the entire autoscan system of four transform lenses. The exact requirements for the transform lenses should be considered in an autoscan analysis prior to future system development.

b. Cross Scan (Bit-to-Bit) Resolution. In the cross scan direction, the output of the 128-element page composer and the reference beam are Fourier tranformed to generate a hologram (see Figure 4-6). The hologram length has been specified as 1 mm, and the maximum recorded spatial frequency is specified as 600 cycles/mm. The full angle, θ_R, then, between the reference beam and the highest data bit is given by

$$\theta_R = \lambda \nu$$

where ν is the spatial frequency and λ is the recording wavelength. For a recording wavelength λ of 0.5145 μm and a spatial frequency ν of 600 cy/mm, the full angle θ_R is

$$\theta_R = 0.309\ \text{rad} = 17.69°.$$

Figure 4-6. Cross Scan Optical Schematic

89444-58

The transform lens maps a linear array of spots at the front focal plane of the lens into an equal number of planar wavefronts pivoting about the hologram aperture at the back focal plane of the lens. The resolution requirements in this direction result from the need that the bits be equally spaced and lie on a flat plane.

7. Aperture and Focal Length. The aperture and focal length requirements for the SP transform lenses can readily be calculated based on the available information. There are only a discrete number of focal lengths available as a result of the 100 percent duty cycle requirement and the finite number of spinner configurations. This implies that the active sweep length, or hologram row length, corresponds to exactly one facet scan angle θ where

$$\theta = \frac{4\pi}{N}$$

and N is the number of spinner facets. The scan length to scan angle relationship, as previously described, $L = f \cdot \theta$ where f is the focal length of the transform lens. Therefore, the focal length is constrained to be

$$f = \frac{L \cdot N}{4\pi} \qquad . \qquad\qquad\qquad (4\text{-}2)$$

The minimum aperture can also be calculated from the hologram information. For the following parameters

Recorded hologram row width $L = 50$ mm,

Hologram convergence angle $\delta\theta_w = 98.1$ mrad,

Hologram height $h = 1$ mm,

Bit to reference full angle $\theta_R = 0.309$ rad,

the minimum aperture, A, is given by:

$$A = \left\{ \left[L + (f \cdot \delta\theta_w) \right]^2 + \left[h + (f \cdot \theta_R) \right]^2 \right\}^{1/2} .$$
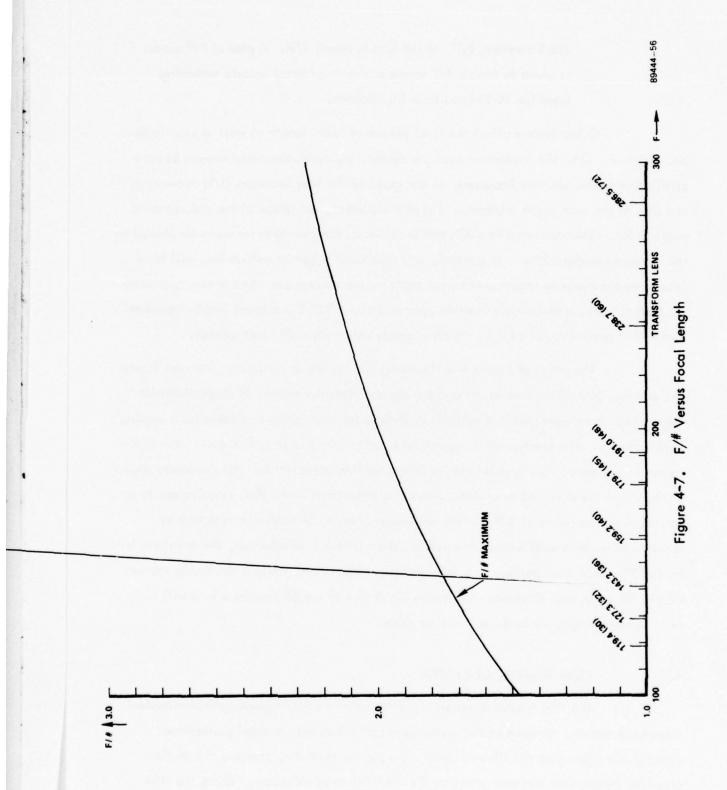
The f-number, $F/\#$, of the lens is simply f/A. A plot of $F/\#$ versus f is given in Figure 4-7 where a number of focal lengths satisfying Equation (4-2) have been highlighted.

Other factors affect the final choice of focal length as well as scan angle and aperture. From the implementation standpoint, the resolution requirements become prohibitive as the aperture increases, as the speed of the lens increases (f/H decreases), and also as the scan angle increases. Equally important, the image plane and entrance pupil to lens clearances must be sufficient to allow all the transform lenses to be placed in the autoscan configuration. In general, a longer focal length transform lens will have greater image plane to lens and entrance pupil to lens clearances. At this time and without further work, a reasonable solution appears to be a 159.2 mm focal length transform lens with a maximum $F/\#$ of 2.2, which is compatible with a 40 facet spinner.

The graph of Figure 4-8 illustrates the "curve of difficulty" for scan lenses. The ordinate plots field size in mm and the abcissa plots the number of single-Rayleigh spots. The curve represented is taken from designs for scan lenses available from leading manufacturers. The position of the proposed scan lens for the SP system gives some indication of the complexity involved in its design and implementation. All the lenses shown on the curve are designed to operate within the diffraction limit; this is equivalent to an optical wavefront error of $1/4\,\lambda$. We anticipate that the SP transform lens may be required to perform with wavefront error less than $1/16\,\lambda$. In addition, the transform lens for the SP system must perform in a telecentric configuration, while maintaining resolution in the cross scan direction. Although the design of the SP transform lens will truly be state-of-the-art, we believe it can be done.

4.5 FILM TRANSPORT SYSTEM

The film transport has an important role in a high-speed optical recorder/reproducer system. In each of the system concepts examined, critical performance demands are placed on the film transport. During the recording process, the motion produced by the film transport provides the distribution of information along the film
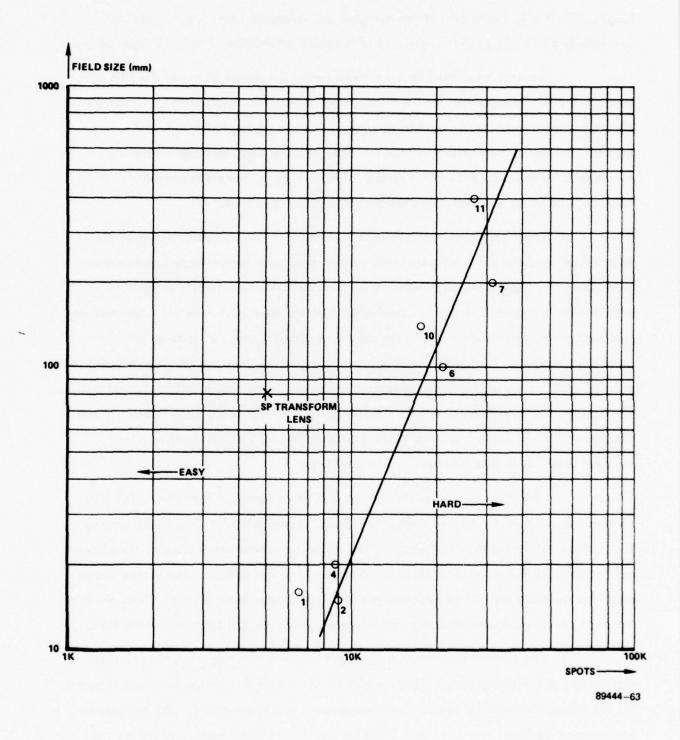
Figure 4-7. F/# Versus Focal Length

Figure 4-8. Curve of Difficulty for Scan Lenses

89444-63

length. Similarly, the motion of the transport and reference beam scanner must be synchronized to accomplish the retrieval of recorded information from a film data record.

Several areas must be considered during the design stages of the film transport. The drive requirements for the transport motors must be established. The motors chosen for the transport must be able to supply adequate torque at the required running speeds. The reel acceleration, viscous friction, bearing drag, and film tensioning torque must be offset by peak motor torque to allow smooth, balanced operation. In addition, the motor size and power dissipation must be specified.

Servo loops must be incorporated to ensure transport stability under all operational conditions. A separate servo loop must be used for the record and readout procedure. During the record process, a velocity or tachometer loop is utilized to provide base speed control and to smooth the motor response nonlinearities. The tachometer loop parameters determine both the degree of stability and the response time for velocity commands. During the readout process, a position loop must be incorporated to provide synchronization between the reference beam scanner and the film transport motion. The performance of the position loop determines the transport positioning errors. In addition, both of these servo loops must have a bandwidth wide enough to allow proper response times while still maintaining film stability.

The film transport platen design is a major factor in determining the film flatness achieved in the record/readout station. The platen must constrain the moving film surface within the depth-of-focus of the recording lenses. Furthermore, the platen must accomplish this constraint while not damaging the film surface. The platen design must also maintain the lateral positioning within acceptable error bounds. Thus, the film transport system must provide stable, precise positioning and guidance of moving film.

The performance levels achieved with the film transport in the present exploratory development model (EDM) are listed in Table 4-4. The performance required for the transports in the SP and LS system approach are also presented. The increase in performance between the EDM and SP transports is not significant. Based on our past experience, we believe that the necessary performance for the SP transport can be

readily achieved through a straightforward engineering effort. However, the LS transport has several difficult requirements. In particular, the depth-of-focus constraint over a 300 mm film width is extremely demanding. Considerable development effort would be necessary to implement the desired hardware.

Table 4-4. Performance Characteristics for
Film Transport Systems

Characteristic	EDM	SP	LS
Film Width (mm)	35	70	300
Film Velocity (m/s)	4.0	6.1	1.7
Depth-of-Focus Constraint (μm)	±15	±15	±15
Lateral Positioning Tolerance (μm)	±50	±50	±50
Velocity Linearity (%)	±0.2	±1.0	±1.0

4.6   PHOTODETECTOR TECHNOLOGIES

All of the systems presented require conversion of multiple optical signals to electrical signals. Two major approaches to the optical detection requirement may be taken: discrete devices and monolithic detector arrays. In the discrete device approach, the optical channels are separated and the optical signals are routed to discrete detectors by a fiber-optic array. The array approach utilizes a monolithic array of detectors; one detector for each optical signal. Each of these detectors is sequentially accessed to produce a temporal signal representing the light intensities incident on the elements of the array. The two approaches have various advantages and disadvantages depending on the readout speed and configuration of the system.

4.6.1   Discrete Detector Technologies

The discrete technologies require a fiber array to separate and distribute the optical signals. Fiber technologies provide insertion losses of less than 2 dB for the fiber-optic interface between the readout plane and the discrete detector. The discrete device technologies applicable to wideband recorders may be separated into three major groups: silicon photodiodes, avalanche photodiodes, and photomultipliers. Silicon photodiodes are easy to use, have excellent gain stability, and typically require low operating voltages. Avalanche photodiodes have higher sensitivities and bandwidths than silicon photodiodes, but have several operational problems. They have relatively poor gain stability and require well-regulated, low noise, high-voltage bias supplies. Photomultipliers offer a small sensitivity improvement over avalanche devices, but have even higher voltage requirements than the solid-state devices. Because the quantum efficiency of the photomultiplier is much lower than that of a silicon device, it is also possible that a photomultiplier could become photon shot-noise limited in some applications. Photomultipliers are fragile and occupy a much larger volume than other device technologies. Figure 4-9 illustrates the optical power necessary for an electrically noise-limited BER of 10^{-9} for silicon photodiodes. The upper and lower curves
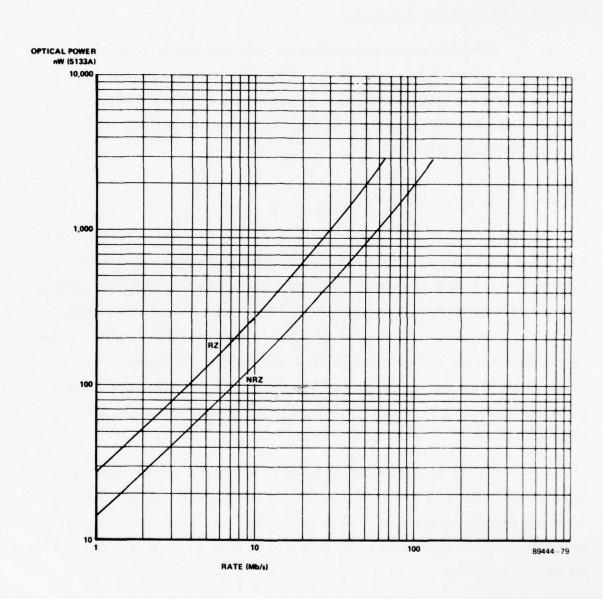
OPTICAL POWER
nW (5133A)

RATE (Mb/s)

89444-79

Figure 4-9. Optical Power Required as a Function of Bit Rate – PIN Photodiode

illustrate the approximate state of the art for detection of data in return-to-zero (RZ) and nonreturn-to-zero (NRZ) formats, respectively. Figure 4-10 illustrates the same information for avalanche photodiodes.

Although avalanche photodiodes provide more than an order-of-magnitude gain in sensitivity over silicon photodiodes, difficulties in implementing stable designs preclude their use in many systems. At higher channel rates (above 10 Mb/s), or where readout illumination is limited, the sensitivity and speed advantages may outweigh these implementation difficulties.

4.6.2   Array Detector Technologies

The array technologies allow the photodetector elements to be placed in the readout plane, eliminating the losses of a fiber-optic interface, and somewhat reducing the mechanical requirements for the photodetectors. Two major technologies are applicable to wideband recorders: self-scanned arrays and charge-coupled devices (CCD). Both technologies utilize an array of silicon photodetectors, but differ in the method used to access each sensor. The signal obtained from the detector is generally not an instantaneous light intensity, but related to the integral of the light intensity over a user-defined time period. This integration can provide much of the electrical filtering required.

The self-scanned array uses multiplexed analog switches to interrogate each detector and reset the value to zero. Present self-scanned array technology limits the sample period to approximately 100 ns per detector. This does not include the integration period required; hence, this technology is limited to systems having very low per channel data rates.

Charge coupled devices show much greater promise for higher speed systems. A typical CCD device integrates light intensity in the detector cell for user-defined period of time, and then dumps the accumulated charge into a light-isolated CCD shift register. The information in this register may then be shifted out while the detector integrates the next sample. Shift periods as low as 600 picoseconds may be
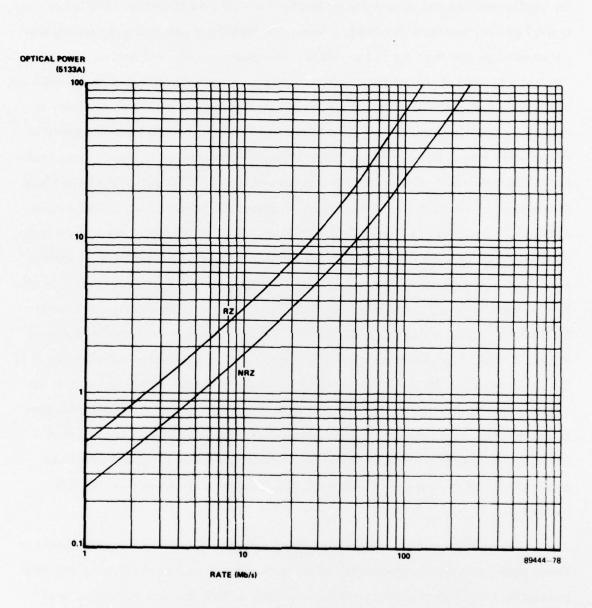
OPTICAL POWER
(5133A)

Figure 4-10. Optical Power Required as a Function of Bit Rate –
Avalanche Photodiode

possible, allowing instantaneous data rates well in excess of 1 Gb/s. However, there are implementation and complexity trade-offs that must be considered. The use of this type of device requires a thresholding technique capable of processing the analog signal at rates greater than the full system rate (as opposed to discrete devices, whose thresholds operate at the lower per-channel rates). Error correction coding, if required, would have to operate at speeds above the system rate. Elastic buffers, necessary to make the system transparent to required overhead functions, would have to operate at these higher rates. Some work has been performed in an attempt to reduce these implementation problems.* One technique uses several smaller CCD shift registers in place of one long output register. This approach increases the number of electrical outputs, but allows a reduction in the required shift rates. Another approach uses a fiber-optic bundle to distribute the light signal to several CCD arrays. One end of the bundle is positioned in the readout plane and samples the reconstructed light signal. This bundle is subsequently fanned out to simultaneously illuminate the photodetectors of several CCD arrays. Only one of the CCD arrays is allowed to sample the intensity during a given bit time. This provides an effective demultiplexing operation and allows each of the CCD arrays to shift at a lower rate. A major disadvantage of this approach is the decrease in effective signal intensity due to the fanning out process. These considerations are fully applicable to SP type system configurations. The 2 D type system configurations would be handled better by array technologies, since multiple linear arrays would not require each linear subsection to operate at speeds near the full system rate.

Discrete technologies are mature and may be used in all systems based on linear page composition. Monolithic array technology is rapidly developing and holds promise for reduction of detector array complexity in both one and two dimensional systems.

---

*Gandolfo, D. A., A. Boorhard, and L. J. Nicastro, "Charge Coupled Devices For Gigabit Recording Applications," Proceedings of the Electro-Optical Systems Design Conference - 1975, Anaheim, California, November 1975.

SECTION V

CONCLUSIONS AND RECOMMENDATIONS

5.1   CONCLUSIONS

The design, implementation and experimental evaluation of the Wideband Recorder Exploratory Development Model has proven the viability of high-speed digital data storage and playback using holographic techniques and photographic film. This development program has made available a new, high-speed, high-capacity information storage approach offering significant operational advantages over more conventional recording approaches (e.g., magnetic-tape recording) for some applications. Many of these advantages are apparent in the following synopsis.

1. Archivability – Using Photographic film as the recording medium provides archival storage properties. Therefore, very long term storage (i.e., years) is possible without concern for environmental influences such as shock, vibration and natural or man-made magnetic fields.

2. High Recording Speed – Augmented by a multichannel optical modulator, the laser line-scanning technology developed under this contract has been demonstrated at 600 Mb/s and appears to be extendable to rates up to 2 Gb/s.

3. High Capacity – The high packing density (nearly 5000 Kb per linear inch of 35 mm film) provides an extremely high capacity memory capability using only a single roll of film. For example, at 5000 Kb/inch, over 6×10^{10} bits can be stored on 1000 feet of film.

4. Multiple and Variable Speed Playback – Holographic data reproduction offers several operational advantages over magnetic tape. First, we have shown that readout can be done over a broad range of speeds with about equal performance. Unlike magnetic recording, the signal strength of reproduced bits does not decrease as a function of speed

reduction. Therefore, not only is full speed readout available, but time-expanded readout necessary to some applications can be provided. Secondly, because the film is transported through a noncontacting read station (i.e., it does not contact a read head), the same data can be read many times without significant degradation of the original recording.

5. Machine-to-Machine Compatibility - Recording on one machine with playback on any of a number of readers can be a significant requirement in some applications. This capability can enhance data distribution capabilities and may be essential to meeting system reliability and maintainability requirements. This capability has been, for the most part, demonstrated with the EDM. Because spinner facets used during readout were randomly related to facets used for recording, because most of the critical optics involved during readout were not the same as those used to record, and finally because the film was removed from and replaced on the transport between recording and readout, all of the recording and playback experimental evaluations were conducted as if two machines were involved.

6. Digital Data Handling - Digital recording in the format developed for the EDM offers system and operational advantages. Reconstruction of raster scanned holograms can be accomplished with relaxed mechanical tolerances. Time-base errors are removed with only nominal buffering, and the need for deskew electronics does not exist. Accommodations for both error correction coding and some data rate variations, such as may be created by Doppler effects, are readily implemented. Finally, long unit records and long record times are possible by recording on roll film.

With this overview of some of the EDM's operational advantages, let us now summarize our conclusions relative to critical components, subsystems, and technologies investigated. These are considered below in the sequence in which they are documented in Section II.

1. Error Correction Coding - In the direction of film movement, the redundancy properties of a hologram provide inherent coding. Electronic coding was provided horizontally along given channels in the hologram row. We found that coding typically provided a BER improvement in the reproduced data from the 10^{-4} to 10^{-5} range for raw data to 10^{-6} to 10^{-8} for corrected data. Thus, the codes we implemented are adequate for most applications.

2. Electro-Optics Synchronization - Providing markers corresponding to each row of holograms on the film and reestablishing bit and frame sync on a per row basis provides operational advantages and significantly reduces spinner and film transport tolerances. The markers also could be used for high-speed data block search without data readout.

3. System Operability - Although the implementation was an Exploratory Development Model, we made progress toward implementing operability and maintainability features - further work remains to be achieved in this area. Stability of the illumination beam was significantly enhanced between Phase I and Phase II implementations. The optics were configured to improve mechanical stability and ease of adjustment, and the laser illumination directional stability was improved by servo controlling a two-axis mirror. Alignment test modes were implemented, including automatic light-level monitors throughout the system. Electronic techniques for optical system alignment were also developed.

4. Data Handling and Control Electronics - Because multichannel recording and playback is used, only moderate-speed digital electronics is required to achieve the high-speed throughput rates. Some additional

development of the mux/demux electronics may be required to support multispeed operation or to track variations in the incoming clock from a data source.

5. Auto-Scan — This technology has now been developed; it has been demonstrated for scan widths up to 25 mm as used with the 35 mm film in the EDM, and should be readily extendable to implementation in the 50 mm scan width formats of the conceptual systems described in Section III.

6. Page Composer — A high-risk component at the start of the program, its development is considered to be a significant achievement. Fully populated, 128-channel units providing up to 780 Mb/s throughput are now established technology.

7. Spinner — The EDM has demonstrated that the system approach does not require a sophisticated spinner in terms of speed and facet pointing precision. We did learn that the impact of facet figure precision on focal depth constraints requires close attention, and techniques for achieving this necessary accuracy were developed and implemented.

8. Transform Lens — A high-risk technology at the beginning of the program, the design and fabrication of lenses with a 25 mm field are now within existing technology.

9. Film Transport — The film transport implemented for the EDM met all of the basic requirements necessary for successful system demonstration. For example, the recorded housekeeping tracks and associated servo design met the speed and phase lock accuracies required. The film transport provided the necessary lateral tracking. The unique air-bearing platen ensured proper focus and film flatness without damaging the emulsion or film base. Whereas the transport met all the program requirements, long record times (e.g., 20 minutes) will

require the implementation of an inertially isolated transport capable of handling long reels of film.

10. Fiber-Optic Distribution - While this represented an important technology development at the beginning of the program, devices similar to those required are now commercially available. The fiber-to-photodetector interface will require some additional development.

11. Photodetection - The discrete photodetectors implemented for the EDM are adequate for the demonstration of the technology. Ongoing developments promise to reduce illumination requirements (and thus prime power) for future systems.

12. Thresholding - Three threshold algorithms were implemented and evaluated. Two of these, the adaptive and the group adaptive, showed merit for future systems. Cost, implementation complexity, and performance trade-offs remain to be done.

13. Recording Material - Of the currently available films, Kodal SO-141 was determined to have the most suitable properties for demonstrating EDM performance. Depending upon specific requirements, an alternative film may be more applicable; for example, thinner base films may be used to increase volume packing density, and to support longer recording periods.

14. Film Processing - Within the scope of this contract, development of automatic film processing techniques necessary to demonstrate system performance goals was achieved. However, significant limitations were imposed on system performance in the areas of processing speed and read-out bit error rate. Therefore, the realization of the performance capabilities of wideband holographic recording will require the use of more sophisticated techniques for film processing.

15. Component Evaluation – We performed a series of system performance measurements for different operational modes while varying the parameters of key components. The results of these measurements will form a basis for optimizing the design of future systems. Details of these experiments along with associated conclusions may be found in Paragraph 2.3.

A significant part of this program was the consideration of the potential for higher rate recording systems. To achieve this, we synthesized advanced system concepts and component specifications for recording at rates up to 2 Gb/s. It is noteworthy that each of these systems was based upon a common technology base which was addressed as part of this and related programs. Within this technology base, we have assessed the state of the art and have identified the critical areas for further development. These advanced concepts and component investigations are documented in Sections III and IV. From these investigations, we have concluded that the SP approach is currently best for most systems *that must support user data rates up to 2 Gb/s*. Alternative systems may be applicable for some system requirements. Two of the alternative systems show promise for achieving data rates up to 5 Gb/s. Thus, it is evident that a significant growth potential exists within the wideband holographic recording technology.

5.2   RECOMMENDATIONS

While the SP approach using 35 mm film has been demonstrated to be a solution to recording rates up to 600 Mb/s and appears applicable up to about 1 Gb/s, we recommend that 70 mm technology be developed. At all recording speeds, raster scanning of the holograms over a 50 mm scan in lieu of a 25 mm aperture will double the effective record time for a given film reel length, and will halve the film transport speed. Table 5-1 compares the capability of a 70 mm optical recorder operating at 600 Mb/s and 300 Mb/s to that of a typical magnetic recorder operating at 80 Mb/s. For all cases, the effective recording densities of user-supplied input data have been determined and have been used to synthesize system performance. For the optical recorder, the effective packing densities achieved with the EDM have been calculated under the assumption that

all channels are error-correction coded. The magnetic recorder provides no error-correction coding, but codes the user data with one overhead bit for every seven user bits. For record speeds above 1 Gb/s, the 70 mm format may be essential. Realization of the 70 mm format optical recording will require further development of spinner-transform lens and film transport technologies.

Table 5-1. Comparison of Laser and Magnetic Recorders

Design Parameters	Laser Recording 600 Mb/s	Laser Recording 300 Mb/s	Magnetic 80 Mb/s
Channel Packing Density	60.96 kb/In.	60.96 kb/In.	24.8 kb/In.
Number of Channels	128	128	24
Total Linear Packing Density	7.8 Mb/In.	7.8 Mb/In.	0.6 Mb/In.
Film or Tape Width	2.76 In. (70 mm)	2.76 (70 mm)	1 (25.4 mm)
Packing Density	2.83 Mb/In.^{2}	2.83 Mb/In.^{2}	0.6 Mb/In.^{2}
Film or Tape Speed	79 IPS	39 IPS	135 IPS
Recording Media Reel	5000 Ft of 0.004 In. on 18 In. Reel	5000 Ft of 0.004 In. on 18 In. Reel	10,800 Ft of 0.001 In. on 15 In. Reel
Record Time (Approx)	12.5 Min	25 Min	16 Min
Total Data Capacity	450 Gb	450 Gb	76.8 Gb

Second, we recommend that thin-base photographic recording materials be investigated. Available emulsions, transporting, handling, and high-speed processing of thin base film should all be addressed. Such films promise longer record times and improved volume packing density for archival storage.

The bit-error-rate performance of the EDM is currently limited by page composer crosstalk and film processing and handling. It is also dependent upon optimization of readout threshold settings. Therefore, our third recommendation is that development of page composer technology be continued with the goal of reducing cross-

talk while maintaining or enhancing other performance parameters. The development of page composers with faster channel data rate capability is recommended.

Fourth, <u>we recommend that investigations continue to perfect techniques for optimum, high-speed processing of holographically recorded films.</u> Techniques for handling latent image decay during long record periods should also be investigated.

Because our experimental investigations have verified that bit-error-rate performance is dependent upon optimization of readout threshold, <u>we recommend that experimental investigations of threshold performance continue and that appropriate hybrid or integrated circuits be developed.</u> Further, <u>we recommend that the performance of recordings at higher packing densities be studied.</u> Higher packing densities will provide longer record times for given film lengths and will reduce the volume necessary to store information.

Finally and most significantly, we believe that the success of this program makes optical recording attractive for all future high-speed, high-capacity recording applications.

POTENTIAL HAZARDS

The Wideband Digital Recorder/Reproducer Exploratory Development Model developed under this contract is a nondeliverable item and, as such, presents no hazard to any Government employee.

There are two areas in a deliverable Wideband Recorder/Reproducer that will require a conscious effort to minimize possible hazards: the Laser/Optics subsystem and the Film Transport subsystem.

The Laser/Optics subsystem will contain beams of intense, collimated light which could cause serious eye damage. This danger can be easily reduced to a Category II hazard level by proper baffling and shielding of the subsystem and by educating all system personnel to the potential hazards present. The Laser subsystem high voltage, high power supply would be a safety critical area. Proper installation, checks for proper grounding, and servicing by qualified personnel can reduce this hazard to Category I. The probability of occurrence for accidents of this nature would be remote. The resulting real hazard index would be 2.

The second area, the Film Transport subsystem, will contain hazards common to all rotating mechanical systems. Proper design, safety shielding, and interlocks would reduce the hazards to Category II. The probability of occurrence for accidents involving this subsystem would be occasional yielding a real hazard index of 8.

REFERENCES AND BIBLIOGRAPHY

1. Kozma, A., A. Vanderlugt, R. M. Montgomery, and C. J. Palermo, Proceedings of the Electro-Optical Systems Design Conference, New York, NY, September 1971.

2. Montgomery, R. M. and Watkins, J. W., Proceedings of the Electro-Optical Systems Design Conference, New York, NY, September 1972.

3. Bardos, A. M., Montgomery, R. M., and Roberts, H. N., "Gigabit/Second Recording with Holography," Proceedings of the Technical Program of the Electro-Optical Systems Design Conference, New York, NY, September 1973, pp. 90-101.

4. Bardos, A. M., Nelson, R. H., and Shuman, C. A., "High Data Rate Holographic Recording," Proceedings of the Technical Program of the Electro-Optics Systems Design Conference, San Francisco, Calif., November 1974, pp. 126-133.

5. Roberts, H. N., Watkins, J. W., and Johnson, R. H., "High Speed Holographic Digital Recorder," Applied Optics, Vol. 13, N. 4, April 1974, pp. 841-856.

6. Bardos, A. M., "Wideband Holographic Recorder," Applied Optics, Vol. 13, No. 4, April 1974, pp. 832-840.

7. Palermo, C. J., Montgomery, R. M., and Young, E. H., Jr., "Applications of Acousto-Optics to Laser Recording," Presented at the SPIE Conference, San Diego, Calif., August 1974.

8. Bardos, A. M., Nelson, R. H., Roberts, H. N., and Shuman, C. A., "Multigigabit per Second Digital Data Recording," Proceedings of the Technical Program of the Electro-Optics International Laser '75 Conference, Anaheim, Calif., November 1975.

9. Bardos, A. M., Nelson, R. H., Roberts, H. N., and Shuman, C. A., "Electro-Optic Components for Wideband Recording and Reproduction," Proceedings of the Electro-Optics Systems Design Conference, Anaheim, Calif., November 1975, PP. 293-300

REFERENCES AND BIBLIOGRAPHY (CONTINUED)

10.   Nelson, R. H., "Wideband Digital Recording System," National Security
Agency, Wideband Recording Symposium, April 1976.

11.   Nelson, R. H., and Shuman, C. A., "Design and Performance of a Wideband
Digital Recorder," Proceedings of the Electro-Optics Systems Design Conference,
New York, NY, November 1976.

METRIC SYSTEM

BASE UNITS:

Quantity	Unit	SI Symbol	Formula
length	metre	m	...
mass	kilogram	kg	...
time	second	s	...
electric current	ampere	A	...
thermodynamic temperature	kelvin	K	...
amount of substance	mole	mol	...
luminous intensity	candela	cd	...

SUPPLEMENTARY UNITS:

Quantity	Unit	SI Symbol	Formula
plane angle	radian	rad	...
solid angle	steradian	sr	...

DERIVED UNITS:

Quantity	Unit	SI Symbol	Formula
Acceleration	metre per second squared	...	m/s
activity (of a radioactive source)	disintegration per second	...	(disintegration)/s
angular acceleration	radian per second squared	...	rad/s
angular velocity	radian per second	...	rad/s
area	square metre	...	m
density	kilogram per cubic metre	...	kg/m
electric capacitance	farad	F	A·s/V
electrical conductance	siemens	S	A/V
electric field strength	volt per metre	...	V/m
electric inductance	henry	H	V·s/A
electric potential difference	volt	V	W/A
electric resistance	ohm		V/A
electromotive force	volt	V	W/A
energy	joule	J	N·m
entropy	joule per kelvin	...	J/K
force	newton	N	kg·m/s
frequency	hertz	Hz	(cycle)/s
illuminance	lux	lx	lm/m
luminance	candela *per square* metre	...	cd/m
luminous flux	lumen	lm	cd·sr
magnetic field strength	ampere per metre	...	A/m
magnetic flux	weber	Wb	V·s
magnetic flux density	tesla	T	Wb/m
magnetomotive force	ampere	A	...
power	watt	W	J/s
pressure	pascal	Pa	N/m
quantity of electricity	coulomb	C	A·s
quantity of heat	joule	J	N·m
radiant intensity	watt per steradian	...	W/sr
specific heat	joule per kilogram-kelvin	...	J/kg·K
stress	pascal	Pa	N/m
thermal conductivity	watt per metre-kelvin	...	W/m·K
velocity	metre per second	...	m/s
viscosity, dynamic	pascal-second	...	Pa·s
viscosity, kinematic	square metre per second	...	m/s
voltage	volt	V	W/A
volume	cubic metre	...	m
wavenumber	reciprocal metre	...	(wave)/m
work	joule	J	N·m

SI PREFIXES:

Multiplication Factors	Prefix	SI Symbol
1 000 000 000 000 = 10^{12}	tera	T
1 000 000 000 = 10^9	giga	G
1 000 000 = 10^6	mega	M
1 000 = 10^3	kilo	k
100 = 10^2	hecto*	h
10 = 10^1	deka*	da
0.1 = 10^{-1}	deci*	d
0.01 = 10^{-2}	centi*	c
0.001 = 10^{-3}	milli	m
0.000 001 = 10^{-6}	micro	μ
0.000 000 001 = 10^{-9}	nano	n
0.000 000 000 001 = 10^{-12}	pico	p
0.000 000 000 000 001 = 10^{-15}	femto	f
0.000 000 000 000 000 001 = 10^{-18}	atto	a

* To be avoided where possible.